UAB
Universitat Autònoma de Barcelona

Reading sediments: anthropogenic impacts on coastal wetlands

Irene Alorda Montiel

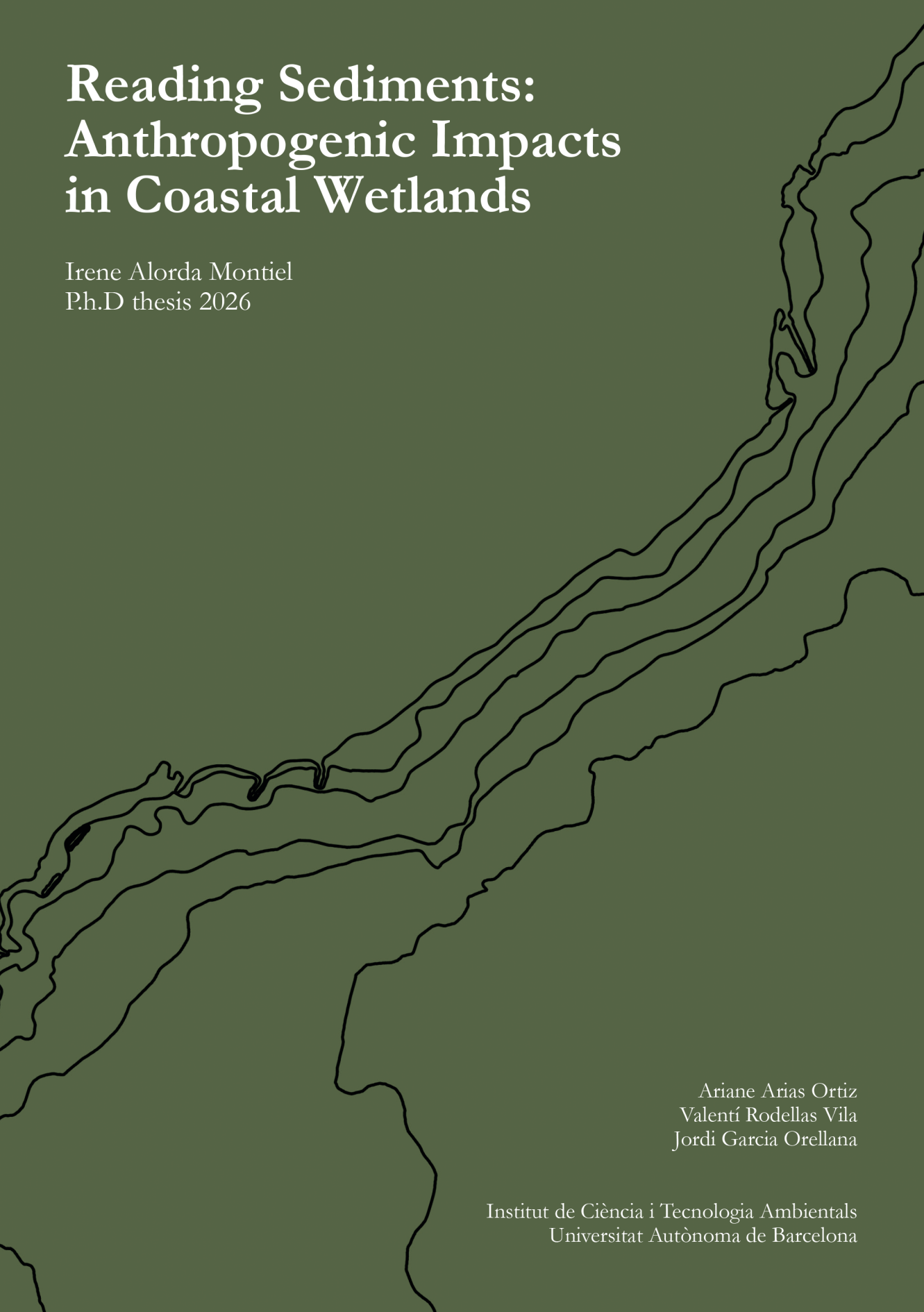
ADVERTIMENT. L'accés als continguts d'aquesta tesi queda condicionat a l'acceptació de les condicions d'ús establertes per la següent llicència Creative Commons: https://creativecommons.org/licenses/?lang=ca

ADVERTENCIA. El acceso a los contenidos de esta tesis queda condicionado a la aceptación de las condiciones de uso establecidas por la siguiente licencia Creative Commons: https://creativecommons.org/licenses/?lang=es

WARNING. The access to the contents of this doctoral thesis it is limited to the acceptance of the use conditions set by the following Creative Commons license: https://creativecommons.org/licenses/?lang=en

Reading Sediments: Anthropogenic Impacts in Coastal Wetlands

Irene Alorda Montiel
P.h.D thesis 2026



Ariane Arias Ortiz
Valentí Rodellas Vila
Jordi Garcia Orellana

Institut de Ciència i Tecnologia Ambientals
Universitat Autònoma de Barcelona

UNIVERSITAT AUTÒNOMA DE BARCELONA

INSTITUT DE CIÈNCIA I TECNOLOGIA AMBIENTALS

TESI DOCTORAL

Doctorat en Ciència i Tecnologia Ambientals

Juliol 2026

Reading sediments: anthropogenic impacts on coastal wetlands

Irene Alorda Montiel

Directors:

Dra. Ariane Arias Ortiz
Dr. Valentí Rodellas i Vila
Dr. Jordi Garcia Orellana

Tutor:

Dr. Valentí Rodellas i Vila

This thesis was supported by the Spanish Ministry of Science and Innovation through the FPI doctoral fellowship PRE2020-092343, from September 2021 to September 2025.

Additional funding was provided by the Marine and Environmental Biogeosciences Research Group (MERS; grant 2021-SGR-00640), ICTA-UAB Unidades de Excelencia María de Maeztu (CEX2024-001506-M) and by the following research projects funded by the Agencia Estatal de Investigación (AEI) of the Spanish Ministry of Science and Innovation:

- OPAL (PID2019-110311RB-C21): *Origins and Pathways of Anthropogenic solutes into coastal Lagoons: groundwater, sediments and episodic events.*
- WINDERS (TED2021-130710B-I00): *The role of wind-induced sediment resuspension in the eutrophication processes of the Mar Menor.*

Agraïments /Ackowledgments

No man is an island,
Entire of itself,
Every man is a piece of the continent,
A part of the main.

John Donne

Cap persona és una illa i res que costi es fa sol. Aquesta tesi és el resultat de l'ajuda que m'ha brindat tanta gent des de la banda acadèmica, i del suport que m'ha ofert tanta altra des del costat personal.

El Jordi era el primer que deia que la tesi era meva i que seria el que jo volgués. He començat aquests agraïments contradient-lo, perquè així era una mica la nostra relació. I és que aquesta tesi no existiria si ell no m'hagués ofert l'oportunitat de començar-la, allà pel 2021. Existeix perquè un dia el Jordi va confiar en mi i va obrir-me una porta, i forçosament el primer nom en aquesta pàgina havia de ser el seu. Gràcies, Jordi. T'escriuria una pàgina sencera d'agraïments i de moltes altres coses, però em limitaré a dir que sovint, quan treballo, em passa rabent pel cap un "Què pensaria el Jordi, d'això?" i el que abans feia mal ara em fa somriure.

Valentí, moltes gràcies per tot el suport tan professional com personal durant tots aquests anys. De tu he après maneres de mirar-me la ciència i la vida que espero que segueixin amb mi molt de temps. Trobo que la teva perspectiva com a director d'una tesi que et quedava prou a prop però a vegades força lluny sempre ens ha portat a millores i a preguntes que els que hi estàvem massa endins no ens hauríem fet.

Ari, et vas incorporar a la tesi en circumstàncies complicades i n'ets, de lluny, la persona que hi ha contribuït més. Gràcies per la paciència i el suport infinits personal i professionalment, per ensenyar-me tant a nivell científic, per les oportunitats que han estat possibles durant la tesi gràcies a tu, i per l'esforç en ser una supervisora present, exigent i dedicada.

Gràcies al Marc i l'Aaron, per fer-me de referents i confidents al laboratori, i per recolzar-me de formes tan diferents cadascun i necessàries totes. A l'Anna i el Roberto, per ser tan lluminosos que il·lumineu tot el *lado oscuro*, i per totes les estones fora del lab. Heu estat una font inesgotable de suport i amor tots aquests anys i aquesta tesi seria molt pitjor sense la vostra contribució diària a la meva felicitat. Al Joan Manuel, pel mentoratge al laboratori, i pels milers de converses sobre tants temes interessants. Espero ser una digna bruixa del teu regne. Carlos, me encantó compartir contigo un año lleno de campañas y risas después de un momento tan complicado. Gracias por enseñarme que ir en calidad de bulto no es lo más deseable, pero que a veces es lo que toca. A la Muntsa, per l'alegria encomanadissa que transmets sempre i l'optimisme que a mi a vegades em falta. A la Sophie, per les campanyes i tots els cops que ens hem pixat de riure juntes explicant-nos coses al despatx. A la Maria Sierks, et dec un viatge a Menorca i tantes altres plans! Quina sort que la tesi ens hagi permès trobar-nos. Angèlica, has portat una energia tan dolça i maca al grup! Les converses de costat al despatx sempre em fan el dia una mica millor. María Muñoz, tu has portat una mica d'energia més canyera, que també ens fa falta. Meryem, you amaze me everyday with your knowledge and wit! Alejandro, has llegado hacia el final pero no te negaré que verte en la puerta del despacho con una taza en la mano y una interrogación en la mirada no me alegre bastante el día. Martina, el mateix! Molts ànims amb el sensecrostó! A la resta de gent del GRAB (i GRAB+), gràcies per ser-hi tots! Sembla que algú faci passar un examen de persona maca a tothom que s'incorpora al grup. I per últim i sobretot sobretot, gràcies a la Júlia, amb qui vaig començar aquesta aventura, amb qui n'he compartit els moments més complicats i els més feliços, i de qui no sabré com desenganxar-me després de ser cadascuna la mà dreta de l'altra tots aquests anys.

Als OPALINES, gràcies per tants moments divertits de campanya i per ser un grup tan estupendo. Dani, *hermanito*, qué genial haver compartido este viaje de años contigo. Siempre transmites una energia preciosa.

Javier, Carolina y todo el equipo de la UPCT: esta tesi no habría sido possible sin vuestra colaboración y disponibilidad con los muestreos. Muchas gracias!

A really big thanks to all my collaborators, for endlessly improving the works that constitute this thesis.

To everyone that helped during my stay at Durham, specially Darren and Cat. Darren, it was (and still is) a pleasure to learn from you, and it was great to be hosted by you and to get to know Sarah, and the girls: Jet, Leyla, Ruby, Sady and Misty. Thanks, Cat for your friendship and companionship! It was great to be at Witton Gilbert with you. Big thanks also to everyone else that made my work there easier and my time more enjoyable: Freya, Jack, but also the Archaeological people: Joanna, Juan and Ele (that hike at Hadrian's wall was amazing!).

To the Berkeley crew, a special thanks to Dennis for hosting me and for those great talks in the trip to Santa Cruz. Daphne and Joe, none of my work there would have been possible without your great ideas and endless willingness to help, so thanks a lot. Arman, it was great to share so many lunches and insights with you during that summer. Robert, thanks for your support inside and outside of the lab. Koong, thanks for your kindness and your help at Hill Slough! Eddie and Dim, thanks for your help during our hard wetland Barbie sampling day ("like walking through a knee-deep ball pit, except the balls are also covered in glue", as Daphne said). Leti, fue un placer compartir ese tiempo contigo en Oakland, gracias por acogerme! Carlos, thank you for hosting me as well! Huachao, Irina, Efekan, and David, thanks for such short but beautiful friendships!

Agraïment infinit també a la gent de Doctorands en Lluita, al CARES group de l'ICTA i a la CGT de la UAB, pel suport mutu i els objectius aconseguits aquests anys. Si la recerca és més digna avui que ahir és gràcies a qui s'ha organitzat en el passat, i a gent com vosaltres. També a tot el personal de la UAB, perquè cada tesi que s'acaba a aquesta universitat no seria possible sense cada persona que posa un granet de sorra per a què les coses funcionin en aquesta institució tan complexa i gegantina.

Ara toca escombrar cap a casa: a tota la família i especialment al Martí, a l'Eva i al Cisco, per ser els meus tres pilars més importants. Al Rai, per la comprensió, a l'Aina per la tendresa, a la Miri per ser la germana que mai he tingut, i a l'Ester per treure'm de tots i cadascun dels pous. A la Laura B., per voler ser la meva amiga allà pel 2016 i per cada experiència plegades que m'ha donat oxigen aquests anys (i que m'ha hidratat el cervell haha). A l'Iris per ser una constant font d'inspiració i la tia més

valenta que conec. A la Júlia O., perquè les hores i dies que hem viscut aquests anys són quasi de la mida de les muntanyes que ens falten per pujar juntes. T'admiro infinit! Al Miguel, per una amistat incomparable, i per ser la persona que més em fa pensar en el món. A le Lu, per cuidar-me igual quan estàs a l'altra punta del planeta que quan estàs aquí. A l'Eva S. per ser refugi. A l'Anna L., i la Laura A. pels bocins de vida que seguim compartint després de tants anys. Al Sergi, per estimar-me sobretot quan jo mateixa no sé fer-ho. A tanta altra gent que m'ha estimat, cuidat i recolzat durant aquesta tesi: Jack, James, Pau, Toni, Marc, Clàudia, Núria, Eloi, Ben, Laia, ...i tants altres que em deixo. Gràcies es queda curt.

I a la Celes, com tot i per sempre.

I a on tu veus lo desert
eixams de mons formiguegen.

Jacint Verdaguer

Abstract

Coastal wetlands are among the most productive and crucial ecosystems on Earth, providing essential ecosystem services such as carbon sequestration, nutrient burial, contaminant retention, shoreline protection and biodiversity support. At the same time, these environments have been exposed to multiple anthropogenic pressures, including agriculture, urbanization, mining, hydrological modifications, species introduction, and climate change. Due to their nature as land-sea interfaces, coastal wetlands integrate material inputs from different sources in their sediments, and in this context, sedimentary archives constitute powerful tools to reconstruct past environmental changes and evaluate how human activities have altered ecosystem functioning through time. This thesis deepens the understanding of anthropogenic impacts on coastal wetlands through i) the reconstruction of historical metal contamination, fluxes, and sources in the Mar Menor coastal lagoon (Spain); ii) the assessment of long-term changes in sedimentary carbon and nitrogen dynamics, organic matter sources, and nutrient burial associated with agriculture and hydrological modifications in the same lagoon; and iii) the evaluation of sedimentary carbon and nitrogen responses and greenhouse gas evolution to tidal wetland restoration in Hill Slough marsh (California, USA). The results demonstrate that sediment records provide reliable reconstructions of environmental changes and their drivers. In the Mar Menor lagoon, sedimentary metal concentrations reflected the historical influence of mining activities in the nearby mining mountain range and the more recent influence of urban metal sources. Anthropogenic nutrient loading due to agricultural intensification and urbanization, hydrodynamic alterations, and the expansion of allochthonous macroalgae increased nutrient burial and changed organic matter sources to the sediment in the same lagoon. Finally, this work shows how tidal wetland restoration rapidly modifies sediment carbon and nitrogen cycling and greenhouse gas dynamics, highlighting the importance of combining sediment-based measurements with other techniques such as eddy covariance to achieve a more complete understanding of ecosystem functioning. Overall, this thesis underpins the value of sedimentary archives for understanding the evolution of anthropogenic impacts on coastal wetlands and provides new insights into the interactions between human pressures and ecosystem buffering mechanisms.

List of articles

- Chapter 3 is based on Alorda-Montiel, I., Rodellas, V., Arias-Ortiz, A., Palanques, A., Bravo, A. G., Rodriguez-Puig, J., Alorda-Kleinglass, A., Green-Ruiz, C., Diego-Feliu, M., Masqué, P., Gilabert, J., & Garcia-Orellana, J. (2025). A century of sediment metal contamination of Mar Menor, Europe's largest saltwater lagoon. *Marine Pollution Bulletin*, *220*, 118347. https://doi.org/10.1016/j.marpolbul.2025.118347

- Chapter 4 is based on Alorda-Montiel, I., Arias-Ortiz, A., Rodellas, V., R, Gröcke, D., Palanques, A., Rodriguez-Puig, J., Alorda-Kleinglass, A., Diego-Feliu, M., Masqué, P., Gilabert, J., & Garcia-Orellana, J.. Land-use change and hydrodynamic alteration reshape sediment carbon and nitrogen burial in a coastal lagoon. This work will be soon submitted to *Limnology and Oceanography*.

- Chapter 5 is based on Alorda-Montiel et al. Response of soil carbon, nitrogen and greenhouse gas fluxes to tidal marsh restoration. This is ongoing work.

Related papers not included in this thesis:

Lavergne, C., Rodriguez-Puig, J., Ruiz-González, C., Montero-Curiel, M., Casas, G., Romano-Gude, D., Alorda-Montiel, I., Dordal-Soriano, J., Alorda-Kleinglass, A., Diego-Feliu, M., Gilabert, J., Campillo-de La Maza, A., Romera-Castillo, C., Torres-Rodriguez, N., Heimbürger-Boavida, L.-E., García-Orellana, J., Rodellas, V., & G. Bravo, A. (2025). Unveiling Hidden Mercury and Methylmercury Sources: The Role of Submarine Groundwater Discharge in Coastal Lagoons. *Environmental Science & Technology*. https://doi.org/10.1021/acs.est.5c07191

Romano-Gude, D., Dordal-Soriano, J., Rodriguez-Puig, J., Bravo, A. G., Alorda-Montiel, I., Alorda-Kleinglass, A., Diego-Feliu, M., Romera-Castillo, C., Mallenco-Fornies, R., Gilabert, J., Garcia-Orellana, J., Rodellas, V., & Ruiz-

González, C. (2025). Impact of Submarine Groundwater Discharge on Microbial Communities in a Highly Anthropized Coastal Lagoon (Mar Menor, SE Spain). *Molecular Ecology*, *34*(24), e70201. https://doi.org/10.1111/mec.70201

Rodriguez-Puig, J., Rodellas, V., Diego-Feliu, M., Alcolea, A., Jiménez-Martínez, J., Alorda-Montiel, I., Alorda-Kleinglass, A., Pereira, F., Manzano, M., Gilabert, J., & Garcia-Orellana, J. (2025). Seasonality of submarine groundwater discharge pathways in a coastal lagoon revealed by radium isotopes: The importance of porewater exchange in summer. *Journal of Hydrology*, *661*, 133616. https://doi.org/10.1016/j.jhydrol.2025.133616

Rodriguez-Puig, J., Ruiz-González, C., Diego-Feliu, M., Alorda-Montiel, I., Alorda-Kleinglass, A., Romano-Gude, D., Bravo, A. G., Dordal-Soriano, J., Gilabert, J., Bergeler, S., Lavergne, C., Casas, G., Manzano, M., Garcia-Orellana, J., & Rodellas, V. (2026). Recirculated submarine groundwater discharge dominates nutrient inputs and enhances eutrophication risk in a coastal lagoon. *Limnology and Oceanography*, *71*(4), e70371. https://doi.org/10.1002/lno.70371

Table of contents

Agraïments / Ackowledgments 3

Abstract 6

List of articles 7

Table of contents 9

List of tables and figures 13

Thesis structure 17

1. Introduction 4

1.1 Coastal wetlands 6

1.1.1 Definition and diversity 6

1.1.2 Coastal wetlands as land-sea interfaces and biogeochemical hotspots 7

1.1.3 Global loss and vulnerability of coastal wetlands 13

1.2 Anthropogenic pressures as perturbations to element fluxes in coastal wetlands 15

1.2.1 Hydrological and sediment flux alterations 15

1.2.2 Trace metal flux alterations 16

1.2.3 Carbon, nitrogen, and organic matter flux alterations 18

1.2.4 Perturbations of biological fluxes and ecosystem engineering 20

1.2.5 Fluxes of other pollutants 21

1.3 Conservation and restoration after coastal wetland degradation 22

1.4 Sediments as archives of ecosystem change 23

1.4.1 Sediments as time-integrated environmental records 25

1.4.2 Geochronology and historical reconstruction 26

1.4.3 Geochemical proxies in sediment studies 28

1.5 General and specific objectives 29

2. General Methods 31

2.1 Sediment core sampling and subsampling 33

2.2 ^{210}Pb dating 34

2.2.1 Principles of the method 34

2.2.2 Dating models, inventories, and sedimentation rates 35

2.2.3 Radiochemical analysis of ^{210}Pb and ^{226}Ra 38
2.3 Sedimentological analysis 39
2.4 Metal analysis 39
2.5 Carbon and nitrogen analysis 42
2.6 Stable isotope results and mixing models 43
2.7 Estimation of stocks and accumulation rates 45
3. A Century of Sediment Metal Contamination of Mar Menor, Europe's Largest Saltwater Lagoon 46
3.1 Introduction 48
3.2 Methods 49
3.2.1 Study site 49
3.2.2 Sampling and sample processing 53
3.2.3 Analytical and dating methods 53
3.2.4 Enrichment factors 54
3.2.5 Interpolation and statistical analysis 55
3.3 Results 56
3.3.1 Sediment grain size and dry bulk densities 56
3.3.2 Lead-210 dating 56
3.3.3 Depth profiles of metal concentrations and accumulation rates 58
3.3.4 Spatial distribution of metals 62
3.3.5 Correlation and Principal Component Analysis (PCA) 64
3.4 Discussion 65
3.4.1 Last century sedimentation patterns in Mar Menor are driven by inputs from streams and mining materials 65
3.4.2 Metal contamination is caused by industrial mining and recent anthropogenic contributions 67
3.4.3 Metal concentrations surpass sediment quality guidelines 72
3.4.4 Mar Menor sediments present some of the highest metal concentrations in coastal enclosed ecosystems 74
3.4.5 Enhanced resuspension could remobilize accumulated metals to the water column 76
4. Land-use change and hydrodynamic alteration reshape sediment carbon and nitrogen burial in a coastal lagoon 78

4.1 Introduction 80
4.2 Methodology 81
4.2.1 Study site 81
4.2.2 Sampling and sample processing 86
4.2.3 Analytical methods 87
4.2.4 Mixing model setup for source contribution to nutrients 87
4.2.5 Spatial Interpolation and statistical analysis 88
4.3 Results 89
4.3.1 Depth profiles of C_{org} (%) and TN(%) 89
4.3.2 Carbon and nitrogen stocks and accumulation rates 92
4.3.3 Depth profiles of $\delta^{13}C$ (‰) and $\delta^{15}N$ (‰) 97
4.3.4 Stable isotope mixing models 99
4.4 Discussion 103
4.4.1 Human activities and derived stressors have reshaped nutrient sources and sediment organic matter composition 103
4.4.2 Sediment nutrient stocks and accumulation rates reflect different facets of nutrient storage and burial efficiency 106
4.4.3 Multiple stressors drive nutrient dynamics and ecosystem transitions 108
5. Response of soil carbon, nitrogen, and greenhouse gas fluxes to tidal marsh restoration 111
5.1 Introduction 113
5.2 Methods 114
5.2.1 Study site 114
5.2.2 Soil sampling and analyses 117
5.2.3 Wetland-Atmosphere Carbon Exchange 118
5.3 Results 119
5.4 Discussion 130
5.4.1 Sediment carbon and nitrogen dynamics reflect early-stage biogeochemical changes after restoration 130
5.4.2 Greenhouse gas fluxes indicate a system functioning as a carbon source the first years after restoration 133
5.4.3 Sediment and atmospheric carbon dynamics are partially aligned across spatial scales 136

6. Conclusions and future perspectives 139
6.1 Conclusions 141
6.2 Future perspectives 144
7. Appendices 148
7.1 Supplementary Information for Chapter 3 148
7.1.1 Specific activity profiles of ^{210}Pb 149
7.1.2 Grain size and dry bulk density 150
7.1.3 Summary of metal concentrations 152
7.1.4 Results for statistical tests 153
7.1.5 Metal concentration profiles for all cores 153
7.1.6 Sequential T-test Analysis of Regime Shifts (STARS) results 159
7.1.7 Metal correlations with dry bulk density and grain size 161
7.1.8 Accumulated Pb stocks 162
7.2 Supplementary Information for Chapter 4 163
7.2.1 Spatial patterns of C_{org}, TN, $\delta^{13}C$ and $\delta^{15}N$ for all sediment data by region 164
7.2.2 C_{org} (%), TN (%), $\delta^{13}C$ (‰) and $\delta^{15}N$ (‰) depth profiles 166
7.2.3 C:N ratios depth profiles 171
7.2.4 Mixing model without concentration dependence and 5 endmembers 172
7.2.5 Mixing model with concentration dependence and 3 endmembers 173
7.3 Supplementary Information for Chapter 5 174
8. References 180

List of tables and figures

List of figures

Figure 1.1 Schematic representation of nitrogen transformations within coastal wetlands. 9
Figure 1.2 Schematic representation of carbon cycling showing storage of carbon. 10
Figure 1.3 Reconstructed global (total, coastal and inland) wetland loss between 1700 and 2020. 13
Figure 1.4 Effect of sedimentation rate on the temporal resolution of sediment records. 26
Figure 2.1 Sediment coring and processing workflow. 34
Figure 3.1 Location of the sampled sediment cores and surrounding land uses based on the CORINE land cover (2018) in the Mar Menor coastal lagoon 52
Figure 3.2 Concentration profiles of Pb, Hg, As, Cu, Zn, and Ag of selected cores representative of the different lagoon sectors. 60
Figure 3.3 Pb, Hg, As, Cu, Zn, and Ag accumulation rates during the last century. 61
Figure 3.4 Spatially interpolated sediment metal stocks of Pb, As, Hg, Cu, Zn, and Ag 63
Figure 3.5 Principal Component Analysis biplots 65
Figure 3.6 Pb surface concentrations ($mg \cdot kg^{-1}$) at different periods 71
Figure 3.7 Enrichment factor values. 73
Figure 4.1 (a) Location of the Mar Menor coastal lagoon within Europe. (b-c) Land uses according to the CORINE land cover dataset for 1990 (b) and 2018 (c) from all the hydrological basins discharging to the Mar Menor lagoon. 85
Figure 4.2 C_{org} and TN concentration profiles (%) of selected cores 91
Figure 4.3 Spatial distribution of sediment C_{org} and TN stock maps ($Mg \cdot ha^{-1}$) across the study area. (a, c) Stocks integrated over the upper 30 cm of sediment; (b,d) stocks accumulated over the last 100 years. 94

Figure 4.4 $\delta^{13}C$ profiles and $\delta^{15}N$ (‰) of selected cores 98
Figure 4.5 Crossplots of $\delta^{13}C$ and $\delta^{15}N$ values for sediment samples and sampled endmembers. 100
Figure 4.6 Spatially interpolated C_{org} and N source contributions to the sediments 102
Figure 5.1 a) Location map of the Hill Slough wetland in the Sacramento-San Joaquin Delta system, California, USA. b) Sediment core sampling sites within the wetland and the location of the eddy covariance tower (US-Hsm). 116
Figure 5.2 a) Sediment organic carbon content (C_{org}, %) and (b) total nitrogen content (TN, %) as a function of cumulative dry mass (g cm^{-2}) 121
Figure 5.3 Profiles of sediment dry bulk density (g cm^{-3}) as a function of cumulative dry mass (g cm^{-2}) 122
Figure 5.4 Sediment a) C_{org} and b) N stocks (kg m^{-2}) down to 20 cm depth 123
Figure 5.5 $\delta^{13}C$ and $\delta^{15}N$ biplot 125
Figure 5.6 Principal Component Analysis biplots. 126
Figure 5.7 Daily sums of net ecosystem exchange a) (NEE; g C-CO_2 m^{-2} d^{-1}) and methane fluxes b) (CH_4; g C–CH_4 m^{-2} d^{-1}) across the period 2021-2025. 128
Figure 5.8 a) Atmospheric C balance for the growing season of all studied years. b) Increment of the growing season atmospheric C balance with respect to 2021 values. 129
Figure 7.1 Total ^{210}Pb (in black) and ^{226}Ra (in orange) specific activity profiles for all cores. 149
Figure 7.2 Grain size percentage distribution by depth for all sampled cores. 150
Figure 7.3 Dry bulk density (g·cm^{-3}) profiles. 151
Figure 7.4 Pb concentration (mg·kg^{-1}) profiles for cores. 153
Figure 7.5 Hg concentration (mg·kg^{-1}) profiles for cores 154
Figure 7.6 Arsenic concentration (mg·kg^{-1}) profiles for cores. 155
Figure 7.7 Cu concentration (mg·kg^{-1}) profiles for cores 156
Figure 7.8 Zn concentration (mg·kg^{-1}) profiles for cores 157
Figure 7.9 Ag concentration (mg·kg^{-1}) profiles for cores. 158

Figure 7.10 Pb accumulated stock for cores 162
Figure 7.11 Boxplots for C_{org}, TN, $\delta^{13}C$ and $\delta^{15}N$ grouped by lagoon sector (North, Center, South) 164
Figure 7.12 Mass-weighted mean boxplots for C_{org}, TN, $\delta^{13}C$ and $\delta^{15}N$ grouped by lagoon sector (North, Center, South). 165
Figure 7.13 C_{org} concentration profiles (%) of the cores not shown in the main text. 166
Figure 7.14 TN concentration profiles (%) of the cores not shown in the main text. 167
Figure 7.15 $\delta^{13}C$ profiles (‰) of the cores not shown in the main text. 168
Figure 7.16 $\delta^{15}N$ profiles (‰) of the cores not shown in the main text 169
Figure 7.17 C:N ratio profiles of selected cores. 171
Figure 7.18 C:N ratio profiles of of the cores not shown in the main text 171
Figure 7.19 Spatially interpolated nutrient contributions for model configuration without concentration dependence and 5 endmembers 172
Figure 7.20 Spatially interpolated nutrient contributions for model configuration with concentration dependence and three endmembers 173
Figure 7.21 Cumulative dry mass (g cm^{-2}) profiles by depth. 174
Figure 7.22 a) $\delta^{13}C$ (‰) and (b) $\delta^{15}N$ (‰) as a function of cumulative dry mass (g cm^{-2}) in cores. 175
Figure 7.23 Relationship between organic matter (OM, %) and organic carbon content (C_{org}, %) 176
Figure 7.24 Relationship between sediment organic carbon (C_{org}, %) and total nitrogen (TN, %) 176
Figure 7.25 Relationship between sediment C:N ratio and $\delta^{13}C$ values 177
Figure 7.26 a) Net ecosystem exchange (g C-CO_2 m^{-2} d^{-1}) and b) CH_4 (g C-CH_4 m^{-2} d^{-1}) flux evolution over the period 2021-2025. 178
Figure 7.27 a) Annual atmospheric C balance for years 2021-2025. b) Increment of the annual atmospheric C balance with respect to 2021 179

List of tables

Table 1.1 Global comparison of main characteristics for coastal wetland habitats. Values are global ranges or medians, except for underlined references, which were chosen when global estimates were unavailable. 7
Table 2.1 Certificate and measured concentrations for standard reference materials and recovery factors. 41
Table 3.1 Sediment mass accumulation sediment rates (MAR in $g \cdot cm^{-2} \cdot yr^{-}$) for the dated cores in the lagoon. 57
Table 3.2 Reported metal concentration ranges ($mg \cdot kg^{-1}$) for coastal lagoons and bays. 75
Table 4.1 Carbon (CAR) and nitrogen (NAR) accumulation rates ($g\ m^{-2} \cdot yr^{-1}$) since 1900 for dated cores in the lagoon. 95
Table 4.2 Carbon (CAR) and nitrogen (NAR) accumulation rates ($g\ m^{-2} \cdot yr^{-1}$) for different historical periods in dated sediment cores from the Mar Menor lagoon. 96
Table 7.1 Lowest and highest metal concentration value for each circulation sector. 152
Table 7.2 H values and Z values ($p < 0.01$) for Kruskal-Wallis and Dunn tests for differences between lagoon regions. 153
Table 7.3 RSI and p-values. for cores OPC1 (North), OPC6 (Center) and OPC8 (South). 159
Table 7.4 R correlation coefficient (Spearman) between dry bulk density, grain size, and metal concentrations in sediments. 161
Table 7.5 Accumulated Pb by periods and core for each area. 162

Thesis structure

This thesis is organized into six chapters:

Chapter 1 constitutes a general introduction to **coastal wetlands as dynamic land-sea interfaces** and to their role in regulating sediment, nutrient, carbon, and contaminant fluxes, and how anthropogenic impacts alter said fluxes. The chapter is divided into five main sections:

i) A general description of coastal wetlands, including their definition, diversity, biogeochemical functioning, ecosystem services, and global vulnerability.
ii) An overview of anthropogenic pressures as perturbations to element fluxes in coastal wetlands, with emphasis on hydrological and sediment alterations, trace metal inputs, carbon and nitrogen cycling, biological fluxes, and other pollutants.
iii) A description of conservation and restoration strategies after coastal wetland degradation.
iv) A summary of sediments as archives of ecosystem change, including their use as time-integrated environmental records, the application of geochronological tools, and the interpretation of geochemical proxies.
v) A description of the general and specific objectives of the thesis.

Chapter 2 focuses on the **general methodologies** employed throughout this thesis, particularly those applied across multiple chapters or central to their development. More specific methodological details are provided within each chapter.

Chapter 3 analyzes the **spatial distribution and decadal variability of sedimentary metal concentrations, fluxes, and sources in a Mediterranean coastal lagoon, the Mar Menor, during the last century.** This work was published in *Marine Pollution Bulletin* in 2025.

Chapter 4 assesses the **anthropogenic nutrient inputs and ecosystem responses in the Mar Menor coastal lagoon.** This includes **quantifying organic carbon (C_{org}) and total nitrogen (TN) stocks and burial rates, evaluating their spatial and temporal variability, and identifying changes in sedimentary nutrient sources using stable isotope mixing models.** This work will be submitted to *Limnology & Oceanography*.

Chapter 5 examines **biogeochemical changes in soils and greenhouse gas fluxes following wetland restoration at Hill Slough, a tidal wetland in the Sacramento-San Joaquin Delta, California (USA).** This work is currently in preparation.

Finally, Chapter 6 synthesizes the **main findings related to this thesis and provides perspectives to develop future work related to it.**

1. Introduction

Living in the earth-deposits of our history.

Adrienne Rich

1.1 Coastal wetlands

1.1.1 Definition and diversity

Wetlands, as defined under the Ramsar Convention on Wetlands (UNESCO, 1971), are "areas of marsh, fen, peatland or water, whether natural or artificial, permanent or temporary, with water that is static or flowing, fresh, brackish or salt, including areas of marine water the depth of which at low tide does not exceed six meters". While this definition focuses on physicochemical characteristics, wetlands are increasingly recognized as complex social-ecological systems (Newton et al., 2020), shaped by long-standing interactions between biophysical processes and human activities. This perspective is particularly relevant in coastal zones (<100 km from the coast), where more than one third of humanity lives (Reimann et al., 2023). Wetlands include a broad range of ecosystems and habitats, such as inland peatlands, unvegetated mudflats, coastal vegetated ecosystems, macroalgal beds, lagoons, river mouth systems, and shallow bays. Coastal vegetated ecosystems, often referred to as *blue carbon ecosystems*, include mangrove forests, tidal marshes, and seagrass meadows. Macroalgal beds, coastal lagoons, and bays can be considered wetlands when they fall within the depth limits defined above. In total, wetlands occupy approximately 6% of the global land surface (Junk et al., 2013).

Coastal wetlands are estimated to occupy 1.42×10^6 km^2 (N. C. Davidson & Finlayson, 2019), which represents approximately 9% of wetlands worldwide. Coastal wetlands function as transitional zones between land and sea, where exchanges of sediments, nutrients, and pollutants are central to ecosystem functioning. The diversity of coastal wetland types supports a wide range of primary producers that structure ecosystem functioning, including microbial mats, herbaceous plants, shrubs, mangroves, seagrasses, and macroalgae, with different characteristics in terms of productivity, nutrient burial, and global area lost (Table 1.1). These habitats have been identified as areas of global importance for biodiversity, constituting key areas for migratory routes of bird populations and critical breeding habitats for fisheries (Ghosh et al., 2024; Hamza et al., 2024).

Table 1.1 Global comparison of main characteristics for coastal wetland habitats. Values are global ranges or medians, except for underlined references, which were chosen when global estimates were unavailable.

	Area (km^2)	Net primary production ($Tg\ C\ yr^{-1}$)	C_{org} sediment stocks ($Mg\ ha^{-1}$)	N sediment stocks ($Mg\ ha^{-1}$)	C_{org} burial rates ($g\ C\ m^{-2}\ yr^{-1}$)	Lost area ($\%\ yr^{-1}$)
Tidal marshes 	32,000 – 60,000 (a)	21 (b)	270 (c)	3 – 23 (d, e)	200 (f)	0.28 (g)
Mangroves 	150,000 (h)	54 (b)	500 (i)	50 (j)	140 (k)	0.14 (l)
Seagrass meadows 	160,000 – 270,000 (m)	83– 140 (n)	78 (o)	4.7 – 11 (p, d)	27 (q)	7 (r)
Macroalgal beds 	6.1 million (s)	1,300 (s)	23 – 62 (t,*)	3 - 7.2 (t, *)	5 – 45 (t, u, *)	-
Tidal flats 	128,000 (v)	11 (w)	86 (x)	14 (y)	130 (x)	0.5 (v)

(a) (Worthington et al., 2024) (b) (Alongi, 2025) (c) (Maxwell et al., 2024) (d) (Martins et al., 2022) (e) (Jiménez-Ramos et al., 2025) (f) (Martinetto et al., 2023) (g) (Campbell et al., 2022) (h) (Jia et al., 2023) (i) (Alongi, 2020a) (j) (Alongi, 2020b) (k) (Breithaupt & Steinmuller, 2022)(l) (Bunting et al., 2022) (m) (McKenzie et al., 2020) (n) (Gomis et al., 2025) (o) (Krause et al., 2025) (p) (Apostolaki et al., 2024) (q)(Arias-Ortiz et al., 2026) (r) (Waycott et al., 2009) (s) (Duarte et al., 2022) (t) (de los Santos et al., 2022) (u)(Moreda et al., 2024) (v) (Murray et al., 2019) (w) (Lin et al., 2020) (x) (Z. L. Chen & Lee, 2022) (y) (Jatobá-Junior et al., 2026) & *this thesis.

1.1.2 Coastal wetlands as land-sea interfaces and biogeochemical hotspots

Coastal wetlands are located at the interface between terrestrial and marine environments, where they integrate fluxes and process materials transported from both land and ocean. This transitional position makes them hotspots of biogeochemical activity, characterized by intense transformations and by the regulation of nutrients, carbon, metals, and other contaminants fluxes and storage. Inputs from river discharge, groundwater fluxes, atmospheric deposition, and tidal exchange converge in these systems, linking catchment processes with coastal biogeochemistry.

Among these processes, nutrient cycling —particularly nitrogen cycling—is especially important. Coastal wetlands receive large inputs of nitrogen from natural sources and anthropogenic activities. In this context, nitrogen refers to reactive nitrogen, which includes biologically available inorganic forms such as ammonium (NH_4^+) and nitrate (NO_3^-) and organic compounds (Galloway et al., 2003). Once in the system, nitrogen undergoes multiple microbial transformations (Fig. 1.1), including assimilation by primary producers, nitrification, denitrification, and mineralization.

Under the anoxic conditions that dominate coastal wetlands' waterlogged soils, this organic nitrogen is continuously recycled through mineralization (Mishra et al., 2005), producing NH_4^+, which can accumulate through adsorption to sediment particles (Liang et al., 2024), taken up by plants and microorganisms, or released to the water column (Ratmaya et al., 2022), thus sustaining internal nitrogen cycling even when external inputs are low.

Coupled nitrification-denitrification processes regulate nitrogen losses from the system. While nitrification is restricted to oxic microsites, denitrification dominates under anoxic conditions, converting NO_3^- into gaseous nitrogen (N_2), thereby removing nitrogen permanently from the ecosystem (Martínez-Espinosa et al., 2021; Newton et al., 2020) and contributing to eutrophication mitigation (Fig. 1.1). However, denitrification is a stepwise process in which nitrous oxide (N_2O) is produced as an intermediate product (Fig. 1.1). This behavior is often conceptualized using the "hole-in-the-pipe" model (E. A. Davidson & Verchot, 2000), where N_2O can escape during nitrogen transformations depending on environmental conditions.

A large fraction of nitrogen is stored in wetland sediments as organic nitrogen derived from plant production, microbial biomass, and external inputs (Schulten & Schnitzer, 1997). This sedimentary storage represents an important, though often overlooked, pathway for long-term nitrogen retention in coastal wetlands, linking nutrient cycling to sediment accumulation. The balance between nitrogen removal through denitrification, temporary retention in biomass, and long-term burial ultimately determines the capacity of coastal wetlands to regulate nutrient loads and mitigate eutrophication.

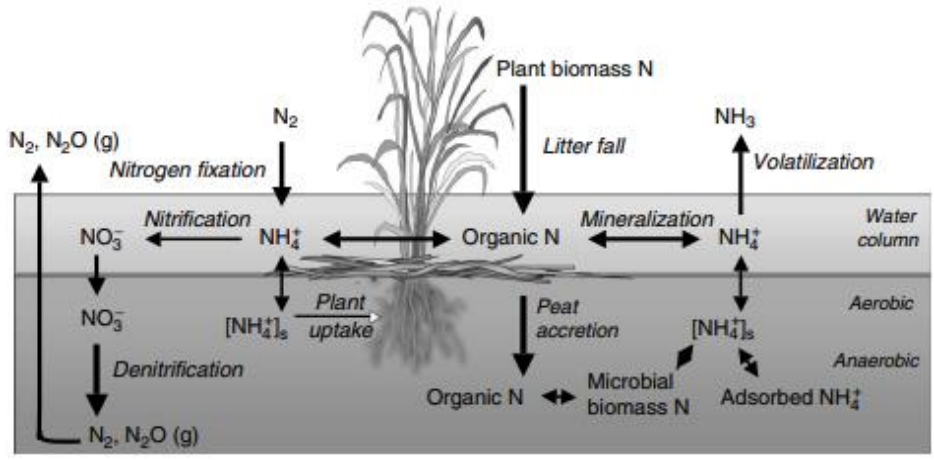


Figure 1.1 Schematic representation of nitrogen transformations within coastal wetlands (Reddy & DeLaune, 2008).

Carbon cycling in coastal wetlands is tightly linked to primary production and the fate of organic matter within the system (Fig. 1.2). Coastal wetland ecosystems rank among the most productive on Earth (Millennium Ecosystem Assessment (Program), 2005) due to high water, nutrient, and light availability that promote atmospheric CO_2 fixation through photosynthesis by plants, algae, and microphytobenthos. The balance between gross primary production (GPP) and respiratory losses determines net primary production (NPP), which represents the excess amount of organic matter available for accumulation, export, or decomposition.

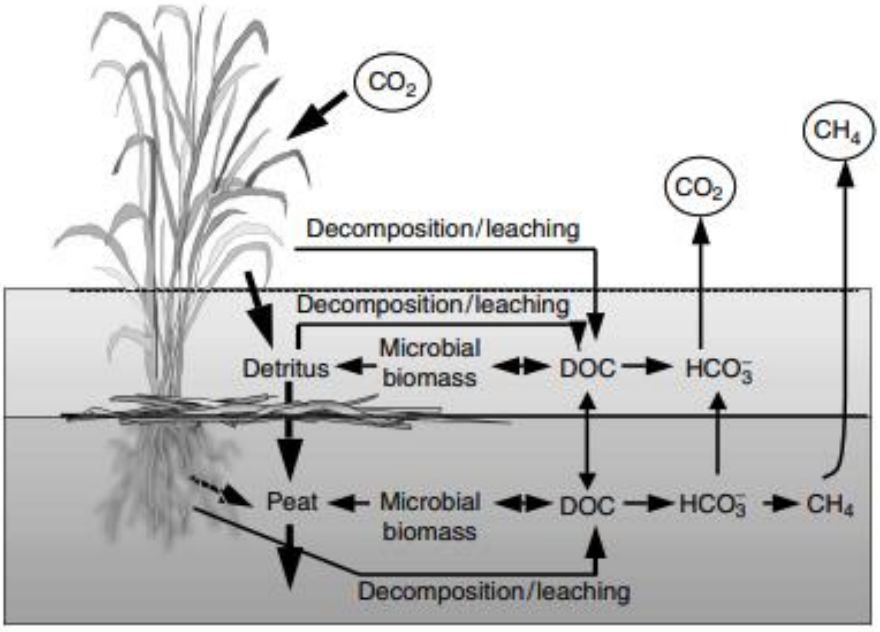


Figure 1.2 **Schematic representation of carbon cycling showing storage of carbon (Reddy & DeLaune, 2008).**

In waterlogged wetland soils, persistent anoxic conditions limit decomposition and enhance organic matter preservation, leading to the accumulation and burial of organic carbon in sediments over long timescales. Additionally, coastal wetlands import and export carbon from and to hydrologically connected surrounding environments and this is an important component of the carbon cycle within these ecosystems (Bogard et al., 2020; Yao et al., 2022). As a result, coastal wetlands act as efficient carbon sinks, burying autochthonous and allochthonous organic carbon (H. Kennedy et al., 2010; J. Zhang et al., 2024), with important implications for long-term carbon sequestration and climate change mitigation (Mcleod et al., 2011). This burial is evidenced by organic deposits that can reach several meters deep, representing thus continuous carbon burial for centuries to millennia (Mateo et al., 1997; McKee et al., 2007) when ecosystems remain undisturbed. Notably, seagrasses, tidal marshes, and mangroves contribute to 8-13% of the global carbon burial in the oceans (Arias-Ortiz et al., 2026) despite occupying a relatively small global area.

However, not all produced organic carbon is buried. A substantial fraction is returned to the atmosphere through microbial and abiotic processes, which are also strongly regulated by oxygen availability. Under oxic conditions, organic matter is primarily mineralized to CO_2 through autotrophic and heterotrophic respiration and photooxidation. In contrast, under anoxic conditions, microbial metabolism shifts towards methanogenesis, leading to the production of methane (CH_4). Methane can be emitted through diffusion, ebullition, or plant-mediated transport. As a result, coastal wetlands, while acting as long-term carbon sinks, are also the largest natural source of atmospheric methane, contributing approximately to 30% of global emissions (Saunois et al., 2020). Indeed, the increase in global atmospheric CH_4 concentrations observed since 2007 has been partly attributed to enhanced emissions from tropical wetlands (Nisbet et al., 2016; Saunois et al., 2020).

The net exchange of carbon between wetlands and the atmosphere can be expressed as net ecosystem exchange (NEE), which integrates the balance between carbon uptake through photosynthesis and multiple pathways of carbon loss, including respiration and methane emissions (Chapin et al., 2006). Unlike NPP, which reflects only biological production, NEE captures the combined effects of biotic and abiotic processes and ultimately determines whether a wetland functions as a net carbon sink or source at a given time. In this context, carbon accumulation rates can be interpreted as a proxy of NEE integrated over time (Arias-Ortiz et al., 2021).

The balance between carbon burial and atmospheric carbon losses in coastal wetlands is controlled by multiple interacting environmental factors, including hydrology, oxygen availability, temperature, salinity, organic matter availability, vegetation type, and nutrient loading. These drivers regulate both primary production and the pathways of organic matter decomposition, thereby influencing whether carbon is stored in sediments or returned to the atmosphere as CO_2 or CH_4. For example, higher salinity conditions tend to suppress methanogenesis, as sulfate-reducing bacteria outcompete methanogens for common substrates (Maltby et al., 2018; Poffenbarger et al., 2011), resulting in lower CH_4 emissions in tidal and saline wetlands compared to freshwater systems (Arias Ortiz et al., 2024; Vizza et al., 2017). Overall, the interplay between carbon sequestration and atmospheric carbon emissions ultimately determines whether coastal wetlands act as net carbon sinks or sources.

In parallel, coastal wetland sediments play a key role in the retention of metals and other contaminants. Metals delivered from terrestrial and marine sources can be immobilized in sediments through adsorption to organic matter, precipitation under reducing conditions, and physical burial. These processes allow wetlands to act as effective sinks that integrate natural and anthropogenic inputs over long timescales. However, the mobility and bioavailability of these elements (Chapman et al., 2011) are strongly influenced by environmental conditions such as salinity (Förstner et al., 1986), redox state (Williams, 1992), and sediment disturbance, meaning that changes in these factors can promote the remobilization of previously stored contaminants (Caetano et al., 2003; Santos-Echeandía et al., 2023).

All these biogeochemical functions underpin many of the ecosystem services provided by coastal wetlands, which support human well-being at local and global scales. Following the Millennium Ecosystem Assessment (2005), these services can be grouped into four main categories: i) supporting services, including fundamental ecosystem processes such as nutrient cycling, oxygenation of seawater by seagrasses (Ward et al., 2022), and the provision of habitat for diverse fauna (Malone & Newton, 2020); ii) provisioning services, derived from the direct use of wetland resources, such as fisheries, timber, fuelwood, pharmaceutical and natural compounds; iii) regulating services, including water quality improvement through nutrient and contaminant retention, global and microclimate regulation (Lima & Galvani, 2013) , and coastal protection via attenuation of storm surges (Möller et al., 2014); and iv) cultural services, encompassing recreational, aesthetic, scientific, and spiritual values associated with these ecosystems, such as birdwatching and ecotourism in saltmarshes, navigation in lagoons and bays, or the religious practices closely related to the largest mangrove forest in the world, the Sundarbans (Bangladesh and India) (Friess et al., 2020).

Among these, regulating services are particularly linked to the biogeochemical functioning described above, as they are directly derived from processes such as carbon burial, nutrient removal, and sediment accumulation. This has led to increasing recognition of coastal wetlands as nature-based solutions for climate change mitigation and adaptation, as well as for coastal protection and water quality improvement (S. F. Jones et al., 2024; Temmerman et al., 2023). More broadly, this

highlights their role as socioecological systems in which ecosystem functioning and human well-being are tightly interconnected.

1.1.3 Global loss and vulnerability of coastal wetlands

An estimated 50% of coastal wetlands have disappeared globally since 1900 (Q. Wang et al., 2015), due to a combination of human pressures, sea level rise, warming, and extreme climate events (Fig. 1.3). Their intrinsic characteristics and proximity to highly populated areas render them particularly vulnerable to both climatic and anthropogenic disturbances (Fitzgerald et al., 2008). Coastal development, land reclamation, and land-use conversion have historically been the primary causes of wetland loss (Fluet-Chouinard et al., 2023). Large extensions of coastal wetlands have been transformed into urban zones, agricultural fields, aquaculture ponds, and other infrastructure. Although resident population size around a wetland can provide a useful indication of human pressure, it does not fully capture the magnitude of anthropogenic impacts. In many systems, tourism significantly amplifies these pressures and should therefore also be considered (Petrişor et al., 2020). This is the case of the Venice lagoon, where a relatively small resident population (around 85,000) is accompanied by an exceptionally high number of visitors (20 million per year) (Newton et al., 2020).

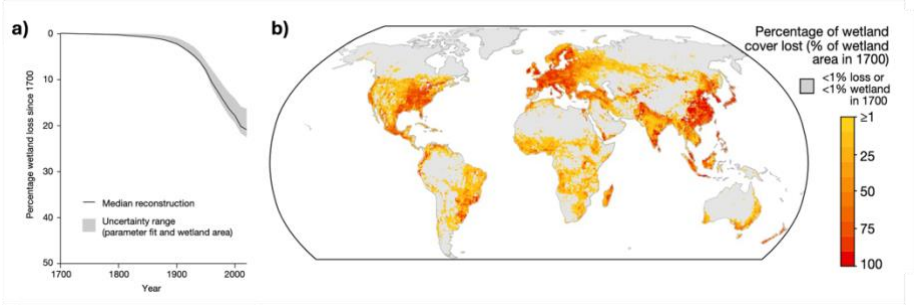


Figure 1.3 **Reconstructed global (total, coastal and inland) wetland loss between 1700 and 2020. a) Percentage of wetland loss since 1700. b) Map of cumulative percentage wetland loss as a fraction of wetland cover in 1700. Adapted from Fluet-Chouinard et al., (2023).**

The location of coastal wetlands strongly shapes the type and intensity of the anthropogenic pressures they are subjected to. Boreal and tropical regions host the largest global extents of wetlands (Martínez-Espinosa et al., 2021). Within boreal regions, polar coastal wetlands are typically characterized by low population densities and predominantly traditional land uses, resulting in comparatively limited direct pressures. However, they are highly vulnerable to rapid environmental changes driven by high-latitude amplification of climate warming (Forbes, 2019; Martini et al., 2019) due to the presence of thawing permafrost. Additionally, the progressive reduction of sea ice, which is increasing navigation and economic investment in the area, is expected to further intensify environmental changes (Forbes, 2019). Wetlands located in temperate and tropical areas, more densely populated, are subject to greater direct anthropogenic pressures.

Rising sea levels represent one of the most significant threats to coastal wetlands, as these ecosystems often occupy narrow elevation ranges relative to tidal levels (Törnqvist et al., 2021). Wetlands can respond to gradual sea-level rise through vertical accretion and landward migration (Enwright et al., 2016). However, these adaptive mechanisms are often limited by anthropogenic barriers or naturally rising land, and lead to the phenomenon known as coastal squeeze (Doody, 2004). Rising sea levels may also promote saltwater intrusion into coastal wetlands, altering salinity regimes and affecting vegetation composition (M. Yu et al., 2019).

Additional pressures further contribute to the degradation of coastal wetlands. Hydrological alterations such as river regulation through dam construction (Jin et al., 2016), channelization (Nakamura et al., 1997), and groundwater extraction (Mancuso et al., 2020) can modify freshwater inputs and sediment delivery. Nutrient enrichment derived from agricultural runoff and wastewater inputs represents another major pressure, altering biogeochemical cycles and promoting eutrophication in many coastal systems (Ballut-Dajud et al., 2022; S. R. Conrad et al., 2019). Biological invasions can also modify ecosystem structure and functioning, sometimes leading to large shifts in dominant vegetation and organic matter sources (I. C. Davidson et al., 2018).

These pressures ultimately act by modifying sediment, nutrient, and contaminant fluxes that control coastal wetland functioning.

1.2 Anthropogenic pressures as perturbations to element fluxes in coastal wetlands

Coastal wetlands are systems governed by fluxes of water, sediments, and elements such as carbon, nutrients, and contaminants, as described above. Anthropogenic activities alter the magnitude, composition, and direction of these fluxes. These anthropogenic pressures can be both direct (e.g. the direct point source release of sewage effluents into the wetland) or indirect (e.g. sea level rise, derived from anthropogenically-induced climate change) (Mengel et al., 2016).

Alterations of this kind are particularly evident in highly impacted coastal wetlands. Within this context, this thesis examines alterations in metal and nutrient fluxes to coastal wetlands, as well as the changes in carbon cycling associated with ecosystem shifts, the spread of non-indigenous species, and hydrological restoration. The thesis is based in two coastal wetlands subject to significant anthropogenic pressures that have altered their ecological functioning and chemical cycling: i) Mar Menor (Spain), a Mediterranean coastal lagoon that has historically received long-term inputs of trace metals and nutrients from anthropogenic activities (mainly agriculture and mining), has been affected by the introduction of the macroalgae *Caulerpa prolifera*, and that has suffered recurrent eutrophic crises; ii) the Sacramento-San Joaquin Delta (California, USA), another historically impacted system, where subsidence and land use transformations have significantly altered sediment and carbon dynamics, including greenhouse gas (GHG) emissions.

1.2.1 Hydrological and sediment flux alterations

Changes in the hydrological land-ocean connectivity –either to the terrestrial (e.g. rivers, streams, groundwater) or the marine part– alter flows of water, nutrients, and sediment to wetlands. Alterations to sediment dynamics include modifications to the quantity and type of sediments reaching coastal wetlands, coastal erosion, and wetland subsidence and drowning. One of the main drivers of reduced sediment delivery to coastal wetlands is the construction of dams. River damming has existed

for millennia, but the first hydroelectric dam appeared in 1882 in Wisconsin, and since then, their implementation across the globe has escalated quickly (Sternberg, 2006). As a consequence, the flux of sediments reaching the world's coasts has been reduced by 20% (a reduction of 1.4 ± 0.3 x 10^{12} kg yr^{-1}) through retention within reservoirs (Syvitski et al., 2005). Reduced sediment delivery can limit the capacity of wetlands to maintain elevation relative to rising sea levels and therefore lead to wetland loss. Wetland drowning occurs when rates of sea-level rise exceed the speed of vertical accretion driven by mineral sediment and organic matter accumulation, as well as because of drainage and impoundment (Mount & Twiss, 2005). Many deltas and coastal wetlands in the world have been drained for agriculture, resulting in subsidence and soil C_{org} oxidation (Drexler et al., 2009). Several feedback mechanisms have been identified between plant growth and geomorphology that make wetlands resilient to sea level rise (Kirwan & Megonigal, 2013). However, under many climate change scenarios, numerous coastal wetlands are expected to cross sensitivity thresholds within the coming decades, potentially leading to widespread wetland loss (Osland et al., 2024). Climate change can also increase the frequency of extreme precipitation events (Kyselý et al., 2012; Myhre et al., 2019) and thus impact the magnitude of sediment loads to some coastal wetlands through surface runoff and erosion (Cahoon, 2006; Tweel & Turner, 2014).

Another important anthropogenic pressure affecting sediment dynamics is dredging, which impacts sediment composition and perturbs benthic habitats (Cox et al., 2021; Mielck et al., 2020). Changes in wetland vegetation can also strongly influence sediment fluxes, as shifts in plant cover or root systems modify particle trapping and accretion processes. In addition, coastal erosion can decrease sediment budgets (Cahoon, 2006), and may be exacerbated under scenarios of increased storm frequency and severity, contributing to the loss of coastal wetlands (Michener et al., 1997). Finally, land use and land cover changes can further modify sediment dynamics by increasing sedimentation rates and inducing siltation, an increase in the fine-grained proportion of sediments (Farias et al., 2024).

1.2.2 Trace metal flux alterations

Trace metal fluxes to coastal wetlands have increased since the 19th century with the evolution of several human activities such as mining, industry, and urban

development (Paul et al., 2024). Although metal contamination is not as dominant as other drivers of coastal wetland degradation at the global scale, it can be highly significant locally and regionally, particularly in areas influenced by intensive industrial or mining activities (Newton et al., 2020).

Metal mining was among the first human activities to significantly enhance the release and accumulation of metals in coastal environments. Although earlier exploitations, such as those during the Roman Republic and Empire (5th – 4th c. BC - 3rd c. AD), also contributed to increased metal fluxes (Larsen et al., 2012; Silva-Sánchez & Armada, 2023), modern and contemporary mining has had a far greater global impact. Between 1959 and 1990, while the world population doubled in size, the production of the six major non-ferrous metals (zinc, copper, lead, tin, nickel, and aluminium) increased eightfold, exceeding the total minerals extracted from the Earth during previous human history (Sheoran & Sheoran, 2006). Mill and mining tailings represent a major associated issue to this (Aswathanarayana, 2003). Water infiltration through these materials can generate acid drainage that mobilizes metals and other toxic substances used in mineral processing, often persisting long after mine closure (Modis et al., 1998). Indeed, constructed wetlands have been used as biogeochemical systems to treat acid mine drainage in some cases of contemporary mining (Mays & Edwards, 2001).

In addition to mining, a wide range of anthropogenic sources contribute to metal inputs in coastal wetlands. Industrial emissions from processes such as smelting, battery manufacturing, and iron and steel production have contributed substantially to metal inputs (Aiello et al., 2025; Dang et al., 2021; Valette-Silver, 1993). Infrastructure such as airports, ports, and roads, as well as antifouling boat paints and vehicle emissions, also represent significant sources of metals to wetlands (Costa et al., 2016; Fang et al., 2018; J. W. Readman, 2006). Urban development contributes to both point source and diffuse inputs of metals through sewage discharge and runoff (Rouff et al., 2013; Xu et al., 2019). Environmental protections and new regulations, such as the ban of leaded gasoline in 2000 in Europe, have contributed to the decline in contamination in coastal ecosystems (Palanques et al., 2017).

Once delivered to wetlands, metals are often efficiently retained in sediments, where they can accumulate over time. This accumulation has important ecological

implications, and the resuspension of sediments containing legacy pollution has been identified as an additional source of metals to the water column, especially in systems with permanent water cover (Santos-Echeandía et al., 2023). Metal contamination can have potentially toxic effects on biota (Jordi et al., 2012), and elements with widely known harmful effects such as mercury (Hg), cadmium (Cd), copper (Cu), and lead (Pb) have been the most studied in coastal wetlands (C. Li et al., 2022). Metals can bioaccumulate and biomagnify through the trophic web, potentially affecting human health as well (Sharifuzzaman et al., 2016). Their toxicity depends not only on their concentrations, but also on their speciation and bioavailability (Bayen, 2012), as well as the organism affected (Langston, 1990).

1.2.3 Carbon, nitrogen, and organic matter flux alterations

Anthropogenic pressures can modify carbon and nitrogen cycling in coastal wetlands, either by altering the regime of production and cycling of autochthonous organic matter or by modifying the inputs of nutrients or allochthonous organic matter from the surrounding catchment. Agriculture and urban development have substantially increased nutrient fluxes to coastal ecosystems through fertilizer runoff, livestock production, wastewater discharges, and stormwater inputs (Amaral et al., 2023; Clarke et al., 2003; Fong et al., 2020; McKergow et al., 2012; Savage, 2005). An important fraction (~25%) of the anthropogenic nitrogen released in coastal watersheds is estimated to reach coastal ecosystems (Purvaja et al., 2008), primarily as nitrate (NO_3^-). The increased availability of nutrients, especially nitrogen, can lead to higher primary production in coastal wetlands, where this nutrient is often limiting (Purvaja et al., 2008). Enhanced phytoplankton growth and biomass production by primary producers can generate higher loads of organic matter, both to the sediments and the water column.

This increase in organic matter, which can be internally produced or imported, stimulates microbial respiration and remineralization of the organic matter, increasing oxygen consumption in the water column and sediments (Xie et al., 2023). When driven by excessive nutrient inputs, this sequence of processes is referred to as eutrophication, originally defined as an increase in the rate of supply of organic matter to an ecosystem (Nixon, 1995), which can result from an excessive nutrient

supply (mainly labile, inorganic nitrogen and phosphorus) (Malone & Newton, 2020). As oxygen demand exceeds supply, hypoxic or anoxic conditions may develop, and different states of oxygen depletion, like hypoxia and anoxia, can cause massive die-off of fish and macrophytes, including benthic seagrasses and macroalgae (Bernardeau-Esteller et al., 2023; Riedel et al., 2012). The loss of vegetated habitats can promote sediment resuspension and limit the burial of organic matter (Dieter, 1990; Lovelock et al., 2017), while promoting the release of nutrients back to the water column, reinforcing eutrophic conditions (C. Tang et al., 2020).

In addition, higher microbial respiration increases CO_2 emissions, particularly when sediments are exposed to oxygen through drying, drainage, disturbance, or resuspension (Kasak et al., 2026; Martinsen et al., 2019). The degradation of coastal vegetated ecosystems has been identified as a source of greenhouse gas emissions (Pendleton et al., 2012). For example, heatwaves that can increase the mortality of seagrasses can cause an increase in emissions from their previously accumulated carbon stocks (Arias-Ortiz, Serrano, et al., 2018). Any activity that disturbs sediments can cause a release in the form of GHG emissions of the carbon stored in them. These processes can shift coastal wetlands from net carbon sinks to net sources (Pendleton et al., 2012).

Enhanced primary production and organic matter inputs, whether autochthonous or allochthonous, can increase carbon accumulation in sediments if they exceed decomposition (Watanabe & Kuwae, 2015). However, the net effect on carbon storage depends on the balance between primary production, heterotrophic respiration, and sedimentation rates, as well as environmental conditions such as oxygen availability and hydrology (Gattuso et al., 1998).

Under anoxic conditions, increased organic matter availability or flooding can stimulate methanogenesis, important in low-sulfate-concentration environments (Maltby et al., 2018; Poffenbarger et al., 2011). Enhanced methanogenesis can lead to increased CH_4 emissions, potentially offsetting the climate benefits of carbon burial and reinforcing the role of coastal wetlands as sources of greenhouse gases (Hemes et al., 2018).

Alterations in organic matter cycling also modify microbially mediated processing of nitrogen within wetland sediments. Increased microbial respiration can promote ammonium release during decomposition. This can alter the balance between key nitrogen transformation processes such as nitrification and denitrification, which are typically strongly coupled in wetland sediments. For example, in the case of limited nitrification, nitrogen removal through later denitrification can be compromised. (Galloway et al., 2003). If nitrogen removal capacity is exceeded, the ecosystem can shift from a nitrogen sink to a nitrogen source, exporting reactive nitrogen to adjacent coastal waters such as the open ocean (Alongi, 2020). Alterations in nitrification and denitrification can also increase N_2O production (E. A. Davidson & Seitzinger, 2006), further contributing to greenhouse gas emissions. Elevated N_2O emissions are generally associated with anthropogenically impacted systems receiving high nitrogen inputs (Seitzinger & Kroeze, 1998), where excess nitrate and fluctuating redox conditions promote incomplete denitrification.

1.2.4 Perturbations of biological fluxes and ecosystem engineering

The introduction of non-indigenous species represents an important biological flux perturbation in coastal wetlands. When these species are primary producers, differences in organic matter production relative to native communities can significantly alter organic matter inputs, nutrient cycling, and greenhouse gas emissions (I. C. Davidson et al., 2018; A. Fuchs et al., 2025).

Moreover, species-specific traits such as root architecture, growth form, and canopy structure can modify sediment redox conditions and influence dominant biogeochemical pathways (Yamuza-Magdaleno et al., 2024). These traits also modify hydrodynamic conditions by altering flow and turbulence, thereby impacting sediment deposition, transport, resuspension, and erosion processes (Gacia et al., 2002). Beyond primary production, introduced species may also restructure trophic interactions and have effects on consumer organisms and broader ecosystem functioning (Ning et al., 2021).

A well-documented example is the introduction of macroalgal species in seagrass-dominated ecosystems, which are often better adapted to eutrophic or disturbed

conditions (Robertson & Savage, 2021). In the Mediterranean Sea, species of the green macroalgal genus *Caulerpa* have extensively colonized coastal environments (Belando et al., 2021). Three species of the genus are relevant here: *C. prolifera* (Forsskal) J.V. Lamouroux, 1809, native but opportunistic, *C. taxifolia* (M. Vahl), and *C. racemosa* (Forsskal) J. Agardh, which are invasive in the Mediterranean basin (Hendriks et al., 2010) and have negatively affected native seagrasses like *Posidonia oceanica* (Villèle & Verlaque, 1995). Although some *Caulerpa* species (*C. racemosa* and *prolifera*) can form dense canopies, like those of seagrasses, with a high capacity for flow attenuation and particle trapping, important functional differences exist. Particularly, *C. racemosa* and *C. taxifolia* exhibit a marked reduction of their biomass in winter without a pronounced rhizome structure, which increases sediment susceptibility to erosion and resuspension (Hendriks et al., 2010). The native *C. prolifera* presents a gross primary productivity and a sediment stabilization capacity 40% lower than native seagrass *Cymodocea nodosa* (Tuya et al., 2014). These species typically thrive at temperatures between 20 and 30 ºC (Komatsu et al., 1997; Ukabi et al., 2013), and salinities above 20 (West & West, 2007). The expansion of *C. prolifera* has been notable in the Mar Menor coastal lagoon, where it coexists with *C. nodosa*, although the latter has experienced substantial declines after hypoxic events (Belando et al., 2021). Outside the Mediterranean, it has expanded into several regions of the North Atlantic (Alexandre & Santos, 2020; Brewton & Lapointe, 2023; Cacabelos et al., 2019).

1.2.5 Fluxes of other pollutants

In addition to the alterations described above, other contaminant fluxes to coastal wetlands have increased in recent decades. Oil and gas extraction activities have increased the delivery of toxic polycyclic aromatic hydrocarbons (PAHs) and saline drilling fluids (Thienpont et al., 2013). In polar regions, these wastes were historically stored in permafrost sumps, which are now collapsing due to rising temperatures and increasing contaminant release (Thienpont et al., 2013). Other persistent organic pollutants, such as polychlorinated biphenyls (PCBs), tend to accumulate in wetland sediments due to their degradation resistance and affinity for organic matter and have been proven to have negative effects on wetland organisms (Girones et al., 2021). In addition, emerging contaminants like pharmaceuticals, personal care

products, and pesticides and herbicides are increasingly detected in these systems, reaching them mainly through wastewater inputs and runoff (Clark et al., 1993; Moreno-González et al., 2015; Pinto et al., 2016). Overall, the accumulation of these contaminants can affect organism survival and ultimately alter ecosystem functioning (Soriano et al., 2024). Macro- and microplastics have also been widely found in coastal wetlands, with very diverse sources and exerting negative effects on biota (Ouyang et al., 2022).

1.3 Conservation and restoration after coastal wetland degradation

Global wetland conservation efforts have been internationally recognized since the 1971 Ramsar Convention, and further reinforced under Indicator 6.6.1 of the United Nations' Sustainable Development Goals (Fluet-Chouinard et al., 2023). In parallel, countries like the United States of America have implemented a "no net loss of wetlands" policy (Maron et al., 2018), while the European Union has multiple pieces of legislation (including the Water Framework Directive, the Habitats and Birds Directive, and the EU Nature Restoration law) that protect and aim to maintain good ecological status of wetlands (Ignar & Grygoruk, 2015).

The widespread modifications of coastal wetland functioning have led to increasing efforts to restore these ecosystems. Ecosystem restoration has been defined as an intentional activity that initiates or accelerates the recovery of an ecosystem that has been degraded as a result of human activities, with respect to its health, integrity, and sustainability (Society for Ecological Restoration International, 2004). Over the last 20 years, restoration projects have expanded globally, culminating in the United Nations Decade on Ecosystem Restoration (2021-2030) (Cadier et al., 2020).

Restoration measures in coastal wetlands often consist of levee breaching or building, sediment dredging, tidal inundation, and/or autochthonous revegetation (X. Li et al., 2018). Historically, most restoration projects have been implemented to recover habitat for birds and fish, reverse subsidence, or improve flood regulation (Murphy, 2021), with carbon sequestration emerging more recently as an additional objective. As a result, climate change mitigation has often been considered a co-

benefit rather than the primary driver of restoration efforts, although its importance is increasingly recognized in the context of natural climate solutions (Fennessy & Lei, 2018; S. F. Jones et al., 2024). To be considered effective in that framework, restoration projects need to provide climate cooling benefits that otherwise would not have occurred (additionality), be implementable (feasibility), and persist over management-relevant time periods (permanence) (S. F. Jones et al., 2024). However, restoration actions can involve trade-offs among desired and unwanted outcomes. For example, wetland reflooding usually increases carbon accumulation in the sediments, but concurrently it can increase CH_4 emissions (Hemes et al., 2018). Additionally, restoration does not necessarily lead to a return to pre-disturbance conditions (H. P. Jones et al., 2018), as ecosystems may follow alternative trajectories, especially under omnipresent stressors like climate change (Hobbs & Cramer, 2008).

The evaluation of the success of restoration strategies has been widely discussed, but general consensus indicates that long-term records are needed to assess the success of restoration efforts (Cadier et al., 2020). Reconstructing past or reference conditions is therefore essential to determine the trajectory and extent of ecosystem degradation and recovery. These conditions can be inferred from records that preserve information on previous wetland functioning, including sediments, historical data, images, and traditional and local ecological knowledge (Biró et al., 2019; Ståhl & Weimann, 2022).

1.4 Sediments as archives of ecosystem change

Ecosystem changes can be assessed by multiple methods. Contemporary ecological observations and monitoring are often limited by their short temporal coverage (Estes et al., 2018). For example, remote sensing observations and water quality monitoring can only provide datasets that began once the necessary infrastructure and technology for them were developed. Additionally, present-day ecosystem shifts may be influenced or driven by legacy contamination if it becomes available through new onset processes (Santos-Echeandía et al., 2023). Furthermore, time lags may exist between current anthropogenic pressures and ecosystem responses (X. Chen et al., 2023), complicating the interpretation of current observations. These

limitations can be particularly relevant in coastal wetlands, where many ecological processes operate over long timescales and responses to disturbance or restoration may take decades to fully manifest. For instance, *Posidonia* seagrass meadows can require nearly two decades to develop the structural and functional characteristics of mature ecosystems (Marbà et al., 2015).

Overall, the determination of baseline conditions before anthropogenic impacts or restoration is a very important process for advancing ecological knowledge. This includes, for instance, a detailed understanding of past metal, nutrient, and carbon stocks and fluxes. In this context, sediments are a valuable tool to assess ecosystem changes that overcomes many of the above-mentioned limitations. Sediments act as a reservoir for metals, nutrients, and other chemicals, accumulate layer by layer and have the capacity of preserving physical, chemical, biological, and genetic signals of past environments (Ellegaard et al., 2020). Therefore, they are long-term, continuous, and integrative records of ecosystem change, allowing the reconstruction of past environmental conditions, such as past biogeochemical fluxes and ecosystem functioning (Canuel et al., 2017), and in some cases, they can help define a baseline predating major anthropogenic pressures (O. Serrano et al., 2016). Their interpretation relies on understanding the processes governing sediment deposition and preservation, as well as the use of geochemical proxies and geochronological tools.

Sediments accumulate in wetlands, from both autochthonous sources, such as in situ primary production, and allochthonous inputs delivered from the surrounding catchment (Komada et al., 2022). Wetland vegetation plays a key role in sediment accumulation by enhancing particle trapping and reducing hydrodynamic energy (Hendriks et al., 2010; Mudd et al., 2010). In addition, the accumulation and partial preservation of organic matter further contribute to sediment accretion.

The preservation of sedimentary signals is influenced by a combination of physical, chemical, and biological processes. Burial, presence of fine sediments, and anoxic conditions can limit the decomposition of organic matter and protect deposited materials from degradation (Howard, 2018; Hulthe et al., 1998). However, post-depositional processes such as early diagenesis, including microbial decomposition

and redox-driven transformations, can alter the original composition of sediments (Reimers et al., 2013).

Despite their advantages, sedimentary records are not free from limitations. Processes such as physical mixing, bioturbation, erosion, and resuspension can disturb stratigraphic integrity, potentially obscuring or altering the temporal signal of ecosystem change (Arias-Ortiz, Masqué, et al., 2018). The fidelity of sedimentary records depends on several conditions, including relatively low-energy settings that allow for the deposition of fine-grained sediments, sedimentation rates that are compatible with the temporal resolution of the processes under study, and limited disturbance by bioturbation or physical mixing (Bentley et al., 2006; Edwards, 2007). Together, these processes determine the extent to which environmental signals are preserved or modified within the sediment column.

1.4.1 Sediments as time-integrated environmental records

Sediments serve as time-integrated records of ecosystem functioning, capturing changes in material fluxes from both the surrounding watershed and in situ physicochemical and biological processes. When stratigraphic integrity is preserved, vertical sediment profiles can be interpreted as temporal sequences of environmental change, with each layer partially recording the conditions at the time of its deposition. The temporal resolution of these records depends largely on sedimentation rates, with higher rates allowing finer resolution of short-term events (Larson et al., 2018) (Fig. 1.4).

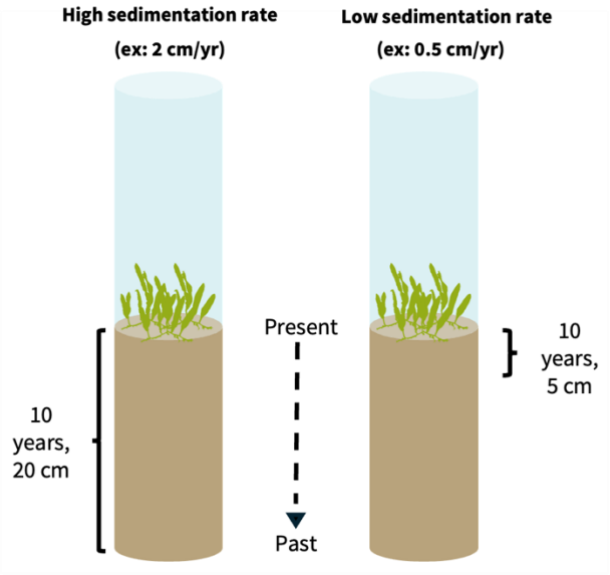


Figure 1.4 **Effect of sedimentation rate on the temporal resolution of sediment records.**

When combined with geochronological tools, these stratified materials enable the reconstruction of environmental changes over time. A range of dating approaches can be applied, including radiometric methods (such as ^{210}Pb and ^{14}C), marker horizons (^{137}Cs) or event stratigraphy (i.e. volcanic ash deposits from explosions). The temporal resolution of reconstruction depend on the method employed, spanning from recent decades to millennia. Within these dated records, concentrations and accumulation rates of substances can reflect long-term fluxes. Mass accumulation rates (MAR) reflect material inputs, while elemental accumulation rates (CAR for carbon, NAR for nitrogen) reflect biogeochemical fluxes.

1.4.2 Geochronology and historical reconstruction

Sediment dating converts depth profiles into chronological timelines, enabling the reconstruction of temporal trends and the calculation of accumulation rates.

Geochronological tools are thus essential for linking sedimentary signals to specific time periods and environmental changes.

In this context, ^{210}Pb dating constitutes a key approach for reconstructing environmental change over the last 100-150 years, a period that includes the intensification of most anthropogenic pressures affecting coastal wetlands. Because ^{210}Pb is efficiently scavenged from the atmosphere and water column and incorporated into settling particles, its distribution in sediments reflects the balance between atmospheric supply, sediment deposition, and post-depositional processes. As a result, ^{210}Pb profiles provide not only a chronological framework but also insights into sedimentary dynamics, including variations in accumulation rates, sediment focusing, and erosion. Beyond providing age-depth relationships, ^{210}Pb-based chronologies enable the quantification of sediment accumulation rates, which then allow for converting geochemical concentration profiles into fluxes and accumulation rates of the analyzed variable (Velandia-Aquino et al., 2023). This is particularly important in coastal wetlands, where changes in sedimentation are closely linked to anthropogenic drivers such as land-use change or hydrological alteration. By resolving decadal-scale variability, ^{210}Pb allows the identification of shifts in material inputs and ecosystem responses that cannot be captured by short-term monitoring records. Moreover, the use of ^{210}Pb-derived accumulation rates provides a framework for distinguishing between changes driven by variations in sediment supply and those resulting from changes in geochemical composition. This distinction is critical when interpreting sedimentary records, as increases in contaminant or nutrient concentrations may reflect either enhanced inputs or reduced dilution due to lower sedimentation rates.

Other radionuclides, such as ^{137}Cs can be used as complementary dating marker to ^{210}Pb (Arias-Ortiz, Masqué, et al., 2018). Cs-137 is an artificial radionuclide that appeared in the 1950s following atmospheric nuclear weapons testing, with a well-defined global fallout peak corresponding to 1963. These atmospheric production and fallout events are transferred to aquatic systems and become recorded in sediments, where they are preserved as distinct activity peaks corresponding to specific time periods. In the Northern Hemisphere, an additional peak is associated with the Chernobyl disaster in 1986. These distinct chronological markers are commonly used to validate and constrain ^{210}Pb-derived age models (Foucher et al.,

2021). However, its use as a tracer has become increasingly challenging because approximately 2.5 half-lives have elapsed since peak fallout, meaning that more than three quarters of the original activity has decayed. This limitation is particularly relevant in the Southern Hemisphere and in environments with low sediment accumulation rates.

In contrast, radiocarbon (^{14}C) dating enables the reconstruction of longer-term environmental changes over much longer timescales, from centuries to millennia (until 55,000 years ago) (Hajdas et al., 2021). However, its applicability in coastal wetland systems is often constrained by the relatively recent formation of many depositional environments following post-glacial sea-level rise, as well as by potential reservoir effects that can complicate age interpretations.

By combining geochronological tools with geochemical proxy data, sediment records can be used to reconstruct the timing, magnitude, and drivers of ecosystem change, providing a robust basis for understanding long-term environmental dynamics.

1.4.3 Geochemical proxies in sediment studies

Sediments preserve a wide range of geochemical signals (i.e. proxies) that provide insights into past environmental conditions and ecosystem functioning. In sedimentary research, a proxy is a measurable physical, chemical, or biological variable that provides indirect information about an environmental process that cannot be observed directly from the past. The interpretation of these proxies requires careful consideration of how these elements are produced, transported, deposited and altered after burial.

Among the most widely used geochemical proxies in sediment studies are elemental concentration, elemental ratios, and stable isotope ratios (Algeo & Liu, 2020; Rothwell & Croudace, 2015). Elemental concentrations of metals like Pb, Zn, and Hg, can serve as indicators of pollution derived from anthropogenic activities, including mining, urbanization and industrial processes. Likewise, the concentration of redox-sensitive elements such as molybdenum and rhenium can be used to infer hypoxic or anoxic conditions in depositional environments (Gooday et al., 2009). Nutrient concentrations (C, N, P) can also provide information on sources and

cycling of organic matter, while nutrient elemental ratios of these elements can also inform on productivity and broader ecosystem change (Rumolo et al., 2011).

Stable isotopes of elements of interest can be powerful proxies because they record variations in the isotopic composition of the materials incorporated in the sediment. Stable isotopes do not decay over time, and their relative abundance is expressed using delta (δ) notation as the deviation, in parts per thousand (‰), from an international standard. Stable isotope ratios of nutrients, such as $\delta^{13}C$ and $\delta^{15}N$ are particularly used in the study of biogeochemical transformations (Hadas et al., 2009; Torres et al., 2012). For example, $\delta^{13}C$ values are widely used to distinguish among different sources of organic matter, such as terrestrial plants, phytoplankton, seagrasses, or macroalgae, because these producers often differ in their carbon acquisition pathways and isotopic signatures. For example, terrestrial $\delta^{13}C$ values for C3 plants range from -31.5 to -23 ‰ (Kohn, 2010), while marine phytoplankton range from -26 to -19 ‰ (Magozzi et al., 2017). Similarly, $\delta^{15}N$ values can provide information on nitrogen sources and transformations, helping to identify the relative influence of wastewater, fertilizers, atmospheric deposition, or in situ biogeochemical processing such as nitrification and denitrification (Vizzini et al., 2005). When interpreted together with elemental concentrations and ratios, these isotopic proxies can offer a more robust understanding of shifts in ecosystem functioning and organic matter origin (Yamamuro, 2000). To quantitatively interpret these signals, isotopic compositions of potential sources –commonly referred to as endmembers—are first characterized, and a mixing model is applied to estimate the proportional contribution of each endmember to the sedimentary organic matter (Parnell et al., 2013).

However, since geochemical proxies are not direct measurements, their interpretation requires caution, as sedimentary signals may be altered by diagenetic processes and influenced by multiple, overlapping environmental drivers.

1.5 General and specific objectives

Coastal wetlands are increasingly exposed to multiple anthropogenic pressures that alter sediment, nutrient, and contaminant fluxes, with important consequences for ecosystem functioning, resilience, and climate regulation. In highly impacted coastal

lagoons such as Mar Menor (Spain), long-term inputs of nutrients and contaminants from agriculture, mining, and urban development have led to severe ecosystem degradation, including eutrophication and hypoxia events. Despite the general awareness of these processes, important uncertainties remain regarding the historical evolution of fluxes, their sources, and the extent to which they have driven observed ecosystem changes.

At the same time, wetland restoration is increasingly implemented in coastal wetlands to recover ecosystem functioning and enhance carbon sequestration. However, the biogeochemical responses of restored wetlands remain insufficiently understood, particularly with respect to greenhouse gas fluxes and soil carbon and nitrogen dynamics. This is especially relevant in highly impacted deltas such as the Sacramento-San Joaquin in California (USA), where tidal restoration may simultaneously promote carbon accumulation and increase methane emissions, leading to uncertain net climate outcomes.

Within this context, sediment records provide a unique opportunity to reconstruct past environmental changes and disentangle the effects of multiple stressors over decadal to centennial timescales. The overall objective of this thesis is to **reconstruct and quantify the impact of anthropogenic pressures (including mining, agriculture and urban expansion) on sediment, nutrient and metal fluxes to coastal wetlands and how these changes are linked to shifts in ecosystem functioning.**
The main goal is divided into three specific objectives:

1. To reconstruct the spatial and temporal variability of sedimentary metal concentrations, fluxes, and sources in a coastal lagoon sediments and link them to the development of mining industry and other anthropogenic activities.
2. To evaluate how anthropogenic nutrient inputs derived from agriculture and urban expansion alter carbon and nitrogen cycling, including organic matter sources, stocks, and burial rates in coastal lagoon sediments.
3. To assess the effects of wetland restoration on biogeochemical functioning, focusing on soil carbon and nitrogen dynamics and greenhouse gas fluxes.

2. General Methods

Time may change me
But I can('t) trace time.

David Bowie

2.1 Sediment core sampling and subsampling

Sediment coring was the primary sampling method used in this thesis (Fig. 2.1). PVC tubes of different lengths (30 cm to 1 m) and diameters (6.5 to 8.5 cm) were driven into the sediment using a mallet by researchers or a collaborating diving team. A vacuum was created by sealing the upper end of the tube to create a vacuum, and the sediment core was slowly extracted and covered with a lower lid. Coring was conducted carefully to ensure that the sediment column remained as vertical as possible and to minimize sediment disturbance and compaction. Cores were subsampled by using a vertical core extruder into sections of varying thickness, typically 1 in lagoon sediments and 2.5 cm in marsh sediments. The choice of the subsampling resolution was based on the expected sedimentation rates, typically higher in marshes than in seagrass habitats (Duarte et al., 2013), and the sediment was sliced using knives or spatulas. The samples were later stored in sealed plastic bags and dried at 65ºC until constant weight was achieved.

Before geochemical analyses, identifiable plant remains and shell fragments were removed from the samples. In lagoon sediments, a portion of each sample was preserved for grain size analysis, while visible shell fragments larger than approximately 0.2 cm were manually removed. Smaller shell fragments were common throughout the samples and were retained, as their complete removal would have been impractical given the similar size of coarse lithological fractions. In marsh sediments, plant remains larger than 0.5 cm were removed by hand and sediment samples were then passed through a sieve with the same mesh size to remove any extra coarse plant debris before grinding. These materials generally represented a small fraction of the total sample volume and were excluded to focus analysis on the finer sediment matrix. While this procedure may influence carbon stock estimates in sediments containing large quantitities of macro-remains, the abundance of removed material was generally low and is not expected to substantially affect the interpretation of carbon burial patterns in this study.

Keeping a minimally disturbed, continuous sediment record is particularly important for geochronological analyses such as ^{210}Pb dating. The superficial layers, where most recent changes and anthropogenic impacts are recorded, are especially prone

to collapse or disturbance during sampling. However, even when cores are carefully collected, natural processes such as bioturbation, physical mixing, erosion, or resuspension can disrupt sediment deposition, potentially limiting the reliability of the geochronological reconstruction and the interpretation of past environmental changes.

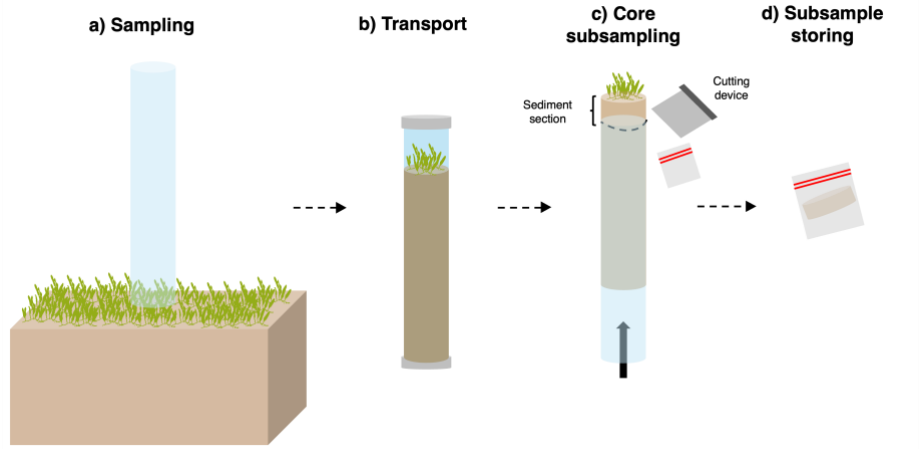


Figure 2.1 Sediment coring and processing workflow. (a) Sediment sampling using PVC tubes inserted into the substrate under downward pressure. (b) Transport of sediment cores with sealed ends to preserve stratigraphy. (c) Core subsampling using a vertical extruder, where pressure is applied from below to extrude the sediment from the tube, and sediments are sectioned into discrete intervals for further analysis (dark, bold arrows represent the direction of exerted pressure). (d) Storage of subsamples in sealed bags.

2.2 ^{210}Pb dating

2.2.1 Principles of the method

^{210}Pb, a naturally occurring radioisotope in the ^{238}U decay chain, has a half-life ($t_{1/2}$) of 22.3 years (i.e., the time required for half of an initial quantity to decay). In aquatic environments, ^{210}Pb readily adsorbs onto particles and is transported and deposited with sediments (Baskaran & Santschi, 1993). Therefore, it constitutes a valuable tracer of sedimentary processes during the last century, particularly for reconstructing patterns of sediment deposition and erosion.

The ^{210}Pb present in sediments has three sources: i) the in-situ decay of ^{226}Ra ($t_{1/2}$ = 1600 years) in the geological matrix, ii) atmospheric deposition (both dry and wet), and iii) ^{210}Pb produced in the water column from dissolved ^{226}Ra. In coastal systems, the contribution from the water column is generally negligible. These sources can be grouped into two fractions. The first is supported ^{210}Pb ($^{210}Pb_{sup}$), which is continuously produced in situ from the decay of ^{226}Ra and is therefore in secular equilibrium with it in sediments. The second is excess or unsupported ^{210}Pb ($^{210}Pb_{xs}$), which corresponds to the fraction supplied primarily through atmospheric fallout and subsequently delivered to the sediments via particle scavenging.

The time span over which a radionuclide can be used for dating is approximately seven half-lives. After that, the remaining activity is considered negligible. In the case of ^{210}Pb, with a half-life of 22.3 years, this corresponds to a theoretical dating range of approximately 150 years. This is because unsupported ^{210}Pb decays progressively after deposition, eventually leaving only supported ^{210}Pb activity. In practical terms, the effective dating range depends on the magnitude of unsupported ^{210}Pb relative to supported ^{210}Pb and analytical uncertainty. As unsupported ^{210}Pb activities decrease with depth, they eventually become too low to be reliably distinguished from background levels. In coastal environments, where surface ^{210}Pb activities may be low, this often limits the method to the most recent decades to a century.

A key step in ^{210}Pb dating is the determination of $^{210}Pb_{sup,}$ to constrain $^{210}Pb_{xs.}$ Supported ^{210}Pb can be estimated in two ways. First, it can be directly quantified through the measurement of ^{226}Ra, once secular equilibrium between the two isotopes has been reached. Alternatively, supported ^{210}Pb can be inferred from the deeper sections of the sediment core, where $^{210}Pb_{xs}$ has decayed to negligible levels, and total ^{210}Pb activity approaches a constant background value. This approach assumes relatively homogeneous sediment composition at depth and is less reliable. In both cases, the unsupported ^{210}Pb fraction is obtained by subtracting supported ^{210}Pb from total ^{210}Pb activity.

2.2.2 Dating models, inventories, and sedimentation rates

Several models have been developed to use ^{210}Pb for dating sediments, which are based on modelling the accumulation and decay of the unsupported ^{210}Pb. They derive the age-depth relationships from the temporal change of Pb activity with depth, the Pb flux, and the sediment accumulation rate. The main assumption of the models is that the sediment is a closed system without post depositional ^{210}Pb mobility. The models most commonly used, which are also the ones applied in this thesis, are the Constant Flux: Constant Supply (CF:CS) (Krishnaswamy et al., 1971) and the Constant Rate of Supply (CRS) (Appleby & Oldfield, 1978). The Bayesian model Plum has also been increasingly used in recent years, and it is also applied in this thesis as a comparison (Aquino-López et al., 2018). The models usually allow to calculate a sediment mass accumulation rate (MAR; g cm^{-2}), from which a sediment accumulation rate (SAR; cm or mm yr^{-1}) can be calculated.

Constant Flux: Constant Supply (CF:CS) is one of the simplest and most widely used ^{210}Pb dating models (Eq. 2.1). It assumes a constant flux of $^{210}Pb_{xs}$ to the sediment and a constant sediment mass accumulation rate (MAR) over time. Under these conditions, the vertical distribution of $^{210}Pb_{xs}$ in the sediment follows an exponential decrease with cumulative mass depth. This relationship can be described as:

$$C_m = C_0 \cdot e^{-\lambda m/MAR};\ t = \frac{m}{MAR} \qquad \text{(Eq. 2.1)}$$

where C_m is the specific activity of $^{210}Pb_{xs}$ at a specific depth (Bq kg^{-1}), C_0 the $^{210}Pb_{xs}$ specific activity at surface sediments (Bq kg^{-1}), λ is the decay constant of ^{210}Pb (0.0311 yr^{-1}), m the cumulative mass (g cm^{-2}) and t the time since that layer of sediment was deposited (yr). The MAR can be estimated by fitting this exponential decay to the measured $^{210}Pb_{xs}$ profile. For convenience, this relationship is often linearized by taking the natural logarithm of $^{210}Pb_{xs}$ activities and regressing them against cumulative mass depth using least-squares fitting. Once the average MAR is obtained, sedimentation rates (cm yr^{-1}) can be calculated using dry bulk density (DBD) (g cm^{-3}), and ages can be assigned to each sediment layer based on cumulative mass depth. In cores showing changes in slope in the ^{210}Pb profile, separate fits can be applied to different intervals, yielding distinct MAR values for different depositional regimes.

The **Constant Rate of Supply (CRS)** model (Appleby & Oldfield, 1978) (Eq. 2.2) assumes a constant flux of $^{210}Pb_{xs}$ to the sediment surface, but does not require a constant sediment accumulation, and therefore allows for calculations of variable MARs. The basis of the CRS model is the inventory of $^{210}Pb_{xs}$, that is, the total amount of $^{210}Pb_{xs}$ accumulated per unit area in the sediment. If the atmospheric supply of $^{210}Pb_{xs}$ to a site is constant, an expected total inventory can be defined, which is equal to the $^{210}Pb_{xs}$ flux divided by the decay constant (λ). This reference flux can be estimated in different ways, for example, from regional atmospheric fallout data (Baskaran, 2011)or from well-preserved sediment cores that are assumed to retain the full $^{210}Pb_{xs}$ inventory. At any given depth, the remaining inventory below that horizon (Im) decreases as a function of time due to radioactive decay. This relationship is described by:

$$I_m = I \cdot e^{-\lambda t};\ MAR = \frac{\lambda I_m}{C_m} \qquad \text{(Eq. 2.2)}$$

Where I_m is the inventory of $^{210}Pb_{xs}$ below a specific depth (Bq m^{-2}), I the initial inventory of $^{210}Pb_{xs}$ at surface sediments (Bq m^{-2}), λ the decay constant of ^{210}Pb (0.0311 yr^{-1}), t the time since that layer of sediment was deposited (yr), and C_m the specific activity of $^{210}Pb_{xs}$ at that depth (Bq kg^{-1}). Thus, layer ages are obtained from the proportion of the total inventory that remains beneath each horizon, and MAR can then be calculated for each interval. Because the CRS model relies on them, measured $^{210}Pb_{xs}$ inventories can also be compared with the expected one. If the measured inventory is lower than expected, this may indicate sediment erosion or incomplete recovery of the dated sequence. Conversely, inventories higher than expected may reflect sediment focusing or enhanced local deposition.

Plum is a Bayesian ^{210}Pb dating model that shares the same core assumptions as the CRS model, namely a constant flux of $^{210}Pb_{xs}$ but not necessarily a constant sediment accumulation rate (Aquino-López et al., 2018). Unlike CF:CS and CRS, which are deterministic models that provide a single best-fit age-depth relationship, Plum creates a probabilistic framework in which ages and sedimentation rates are estimated as probability distributions. A key advantage of Plum is that it does not require the explicit identification of an equilibrium depth where unsupported ^{210}Pb

reaches supported levels. Instead, supported ^{210}Pb is estimated as part of the modelling process. This is particularly relevant near the practical dating limit, where unsupported ^{210}Pb activities approach background levels, and the identification of an equilibrium depth becomes uncertain. By estimating supported ^{210}Pb within the model and propagating this uncertainty, Plum can provide more robust age estimates for deeper sediment layers. (Aquino-López et al., 2020).

The selection of the most appropriate ^{210}Pb dating model depends on the characteristics of the sedimentary record and the validity of model assumptions. In this thesis, both the CF:CS and CRS models were applied and compared where appropriate. The CF:CS model was used for cores exhibiting an approximately exponential decrease of $^{210}Pb_{xs}$ with depth, consistent with constant sedimentation rates. In contrast, when deviations from exponential decay suggested variable sediment accumulation or when age estimates appeared inconsistent at depth, the CRS model was preferred, as it allows for temporal variability in sedimentation rates.

2.2.3 Radiochemical analysis of ^{210}Pb and ^{226}Ra

The specific activity of ^{210}Pb in the sediments was determined by alpha spectrometry of its granddaughter isotope ^{210}Po ($t_{1/2}$ = 138 days), assuming that secular equilibrium had been reached between the two radionuclides. ^{210}Po is analysed following the method described in Sanchez-Cabeza et al., (1998). Briefly, sediments were previously homogenized with a mortar and pestle or a coffee grinder, and major shell structures and plant remains were removed. Between 150 and 300 mg of dry sediment was added to 100 mL Teflon liners with 9 mL of HNO_3, 3 mL of HF, and a known amount of ^{209}Po as an internal tracer, with an activity of 0.373 Bq g^{-1} (1 Dec 2013). These aliquots were microwave digested. Following the first digestion step, after the addition of 15 mL of H_3BO_3, complex fluorides were broken down in the analytical microwave. Samples were then transferred to Teflon beakers after rinsing the liners with 1 M HCl, and evaporated. 1 mL of HCl (37%) was added to the beakers three times, and the samples were evaporated again. Before plating, 100 mL of 1 M HCl was added to the beakers and heated while stirring. Solutions were transferred to glass beakers after rinsing, and heated and stirred again before adding ascorbic acid ($C_6H_8O_6$) to reduce Fe^{3+} to Fe^{2+}. Silver disks, with one side lacquered with urethane, were suspended in the solution by a nylon string. Po isotopes were

plated onto the silver disks at approximately 90 ºC while stirring, for 6-8h. Disks were then air-dried.

Alpha spectrometry was conducted to analyse ^{210}Po and ^{209}Po on the silver disks using Passive Implanted Planar Silicon (PIPS) detectors (CANBERRA, Mod. PD-450.18 A.M.) and a GenieTM data acquisition software. Analytical blanks, reference materials (IAEA315 and IAEA447), and replicates were recurrently measured alongside the samples for quality control.

The specific activities of ^{226}Ra were determined in selected samples from each core by gamma spectrometry of its daughter ^{214}Pb at 295 and 351 keV using calibrated geometries in a well-type high-purity germanium gamma detector (CANBERRA, Mod. GCW3523). A homogenized subsample was placed and weighed inside a sealed vial and measured a minimum of 21 days after sealing, to ensure that secular equilibrium between ^{226}Ra and its daughters is reached.

2.3 Sedimentological analysis

Dry bulk density (g cm^{-3}) was assessed by drying the whole core slices (either 1 cm or 2.5 cm-thick) and dividing the net dry weight by the sample volume. Sediment grain size fraction in each sediment core section was determined in unground samples using a Horiba Partica LA-950v2 particle-size analyzer from the Institut de Ciències del Mar (ICM-CSIC) in Barcelona, with an accuracy of 0.6 % and precision of 0.1 %. The contents of gravel (>2 mm, including shell fragments), sand (2 mm–63 μm), silt (63–4 μm) and clay (<4 μm) were obtained for each sample.

2.4 Metal analysis

Metal analyses were conducted by two-step microwave total digestion using the same acid additions as for ^{210}Pb, in acid-cleaned Teflon liners. The digestate was then filtered by 0.45 μm nylon filters and analysed by inductively coupled plasma mass spectrometry (ICP-MS; Agilent 7900 model), in the Servei d'Anàlisis Químics in the Science Faculty of Universitat Autònoma de Barcelona. Analysed metals comprised Na, Al, Si, Ca, Ti, Cr, Fe, Ni, Cu, Zn, As, Sr, Ag, Cd, and Pb. Standard reference

materials (NIST 2702 and IAEA 457) were analysed for metal concentration recovery factors (Table 2.1).

Table 2.1 Certificate and measured concentrations for standard reference materials and recovery factors.

Metal (mg·kg^{-1} or %*)	NIST 2702			IAEA457		
	Reference	Measured average (n=3)	Recovery factor (%)	Reference	Measured average (n=3)	Recovery factor (%)
Ag	-	-	-	1.9 ± 0.4	2.1 ± 0.1	110
Al	8.4 ± 0.2*	4.5 ± 1.3*	54	83,000 ± 3,000	45,000 ± 12,000	54
As	45 ± 2	40.5 ± 0.1	90	10 ± 1	10.5 ± 0.1	110
Cd	0.817 ± 0.011	1.3 ± 0.2	160	1.09 ± 0.08	1.2 ± 0.1	110
Cr	350 ± 20	290 ± 10	83	144 ± 8	120 ± 1	83
Cu	-	-	-	370 ± 20	350 ± 4	95
Fe	7.9 ± 0.2*	6.4 ± 0.3*	81	41,000 ± 2,000	38,000 ± 1,100	93
Ni	75.4 ± 1.5	60.6 ± 2.7	80	53 ± 3	48 ± 1	91
Pb	132.8 ± 1.1	130 ± 2	98	105 ± 7	110 ± 2	100
Sr	120 ± 3	48 ± 17	40	137 ± 10	50 ± 20	36
Ti	0.8267 ± 0.006	0.7 ± 0.1	85	-	-	-
Zn	485 ± 4	350 ± 13	72	430 ± 30	340 ± 8	79

2.5 Carbon and nitrogen analysis

Carbon in coastal wetlands is present as a mixture of organic and inorganic forms. To determine organic carbon (C_{org}), inorganic carbonates were removed prior to analysis. Common approaches include acid fuming and direct acid treatments with subsequent washing with deionized water (P. Kennedy et al., 2005). Acid fumigation and direct acidification in the capsule were initially tested but did not completely remove carbonates. Therefore, acidification with HCl in an external container was applied to remove carbonates from the sediment. To do so, sediment samples were placed in centrifuge tubes and weighed. Acid (1 M HCl) was added to the sample and left to react overnight . After decantation, samples were rinsed with DI water and centrifuged several times, in order to remove as much acidity as possible to ensure the proper functioning of the elemental analyser. Sediments were then dried at approximately 65ºC and weighed again. The organic carbon fraction was estimated from the mass difference between untreated (bulk) and acidified samples, assuming that the loss of mass corresponds to the removal of inorganic carbonates (Eq. 2.3):

$$C_{org}(\%) = C_{EA}\ x\ \frac{m_{acidified}}{m_{bulk}} \qquad \text{(Eq. 2.3)}$$

Where C_{EA} is the C(%) result from the elemental analyzer, $m_{acidifed}$ is the mass of acidified sediment (g), while m_{bulk} is the mass of untreated sediment (g).

Regarding nitrogen, both its organic and inorganic forms are of interest in sedimentological analysis. We refer to this as total nitrogen (TN). Non-decarbonated sediments were employed and encapsulated in tin for analysis.

Both C_{org} and TN contents, as well as $\delta^{13}C$ and $\delta^{15}N$ isotopic compositions, were determined by running the encapsulated samples through an elemental analyzer (EA) connected to an isotope ratio mass spectrometer (IRMS). During this process, the EA combusts the samples to produce CO_2 and N_2 gases, whose isotopic ratios are subsequently measured by the IRMS. For details on the specific models, labs and used standards, refer to the method section in each chapter.

2.6 Stable isotope results and mixing models

$\delta^{13}C$ is the normalized ratio of the two most common carbon isotopes, ^{13}C and ^{12}C, expressed in parts per thousand (‰) relative to the Vienna Pee Dee Belemnite (VPDB) (Eq. 2.4). $\delta^{13}C$ is used as a tracer of organic matter sources because different primary producers and carbon pools have distinct isotopic signatures. Variations in $\delta^{13}C$ values therefore allow the identification of terrestrial and marine contributions to sedimentary organic matter, as well as changes in carbon sources through time.

$$\delta^{13}C = \left(\frac{\left(\frac{^{13}C_{sample}}{^{12}C_{sample}} \right)}{\left(\frac{^{13}C_{standard}}{^{12}C_{standard}} \right)} - 1 \right) x\ 1000 \qquad \text{(Eq. 2.4)}$$

$\delta^{15}N$ is the normalized ratio of the two most common nitrogen isotopes, ^{15}N and ^{14}N, expressed in parts per thousand(‰) relative to atmospheric N_2 as standard (Eq. 2.5). $\delta^{15}N$ is widely used as an indicator of nitrogen sources and biogeochemical processes, as different nitrogen inputs and transformations produce distinct isotopic signatures. Variations in sedimentary $\delta^{15}N$ values can therefore help identify contributions from anthropogenic nutrient sources (e.g. sewage, fertilizers) or trace changes in nitrogen cycling processes (e.g. denitrification).

$$\delta^{15}N = \left(\frac{\left(\frac{^{15}N_{sample}}{^{14}N_{sample}} \right)}{\left(\frac{^{15}N_{standard}}{^{14}N_{standard}} \right)} - 1 \right) x\ 1000 \qquad \text{(Eq. 2.5)}$$

Carbon isotope ratios were corrected for ^{17}O following standard IRMS procedures (Brand et al., 2010). Isotopic accuracy was monitored through routine analyses of in-house standards and calibrated against international standards.

Mixing models use stable isotope data, both $\delta^{13}C$ and $\delta^{15}N$ to estimate the proportion of sources contributing to a mixture. Historically, they have been widely employed in several fields of ecology, especially diet studies, but have also been widely applied to study soil and sediment composition (Catry et al., 2016; Cooray et al., 2026). Conventional approaches made several assumptions such as fixed source signatures that limited the application of these models. Recently, new models that provide probabilistic approaches to the mixing systems have been proposed, allowing uncertainty in the isotopic composition of sources and consumers to be incorporated (Parnell et al., 2013). One of the most important advances was accounting for concentration dependence, namely that concentration of carbon and nitrogen differs between sources (Phillips & Koch, 2002). The first Bayesian mixing model was MixSIR (Stock et al., 2018). MixSiAR is the most recently developed framework that develops a Bayesian model based on the input data, which is supported with an R package of the same name (Stock et al., 2018), and extends earlier models by allowing greater flexibility through the inclusion of covariates, hierarchical structures, and more complex error formulations. In this thesis, this R package has been used to apply concentration-dependent mixing models. Input data include $\delta^{13}C$, $\delta^{15}N$ for all models, together with C_{org} and TN data when applying concentration dependence, and temporal and spatial data as categorical fixed effects. Uninformative priors were applied, using broad prior distributions that assign equal probability to all potential sources, so that posterior estimates are primarily driven by the observed isotopic data. The equations for non-concentration dependent (Eq. 2.6) and concentration dependent models (Eq. 2.7) are shown below.

$$\delta_{mix} = \sum_{i=1}^{n} f_i \delta_i \qquad \text{(Eq. 2.6)}$$

$$\delta_{mix} = \frac{\sum_{i=1}^{n} f_i \, C_i \delta_i}{\sum_{i=1}^{n} f_i \, C_i} \qquad \text{(Eq. 2.7)}$$

Where δ_{mix} is isotopic value of the mixture, f_i the fraction of source i (sum = 1), δ_i the isotopic value of source i, and C_i the concentration of the element of interest (e.g., %C or %N in source i).

2.7 Estimation of stocks and accumulation rates

A stock represents the total amount of a substance stored in a given area or volume. In the case of sediments, stocks are expressed per unit area, and can be calculated based on a common depth, cumulative mass, or common age. In Chapter 3, metal stocks have been estimated from 1900 until 2020, while in Chapters 4 and 5, C_{org} stocks and TN stocks (g m^{-2} or Mg ha^{-1}) have been calculated at 30 and 22.5 cm and for Chapter 4, at the dating horizon established by ^{210}Pb dating. 30 cm was chosen because it is a commonly reported value in literature and allows for comparisons. When continuous C_{org} or TN measurements did not extend to 30 cm depth, concentrations were interpolated between measured intervals or extrapolated using linear relationships with DBD when these showed a good fit.

Elemental accumulation rates (g m^{-2} yr^{-1}) (Eq. 2.8), also referred to as burial rates, describe the rate at which a substance or element accumulates in the sediment matrix. Accumulation rates were calculated as the product of the sediment mass accumulation rate (MAR) and the concentration of the element in the sediment. These calculations have also been applied to C_{org}, TN, and metals:

$$AR_X = MAR \cdot C_x \quad \text{(Eq. 2.8)}$$

where AR_x is the accumulation rate for a specific compound, MAR the sediment mass accumulation rate, and C_x the fraction of constituent x in the dry sediment over the dated depth.

3. A Century of Sediment Metal Contamination of Mar Menor, Europe's Largest Saltwater Lagoon

This chapter is based on:

A century of sediment metal contamination of Mar Menor, Europe's largest saltwater lagoon (2025). Alorda-Montiel, I., Rodellas, V., Arias-Ortiz, A., Palanques, A., Bravo, A. G., Rodriguez-Puig, J., Alorda-Kleinglass, A., Green-Ruiz, C., Diego-Feliu, M., Masqué, P., Gilabert, J., & Garcia-Orellana, J. Marine Pollution Bulletin, 220, 118347. https://doi.org/10.1016/j.marpolbul.2025.118347

Tot s'extreu
de la mina.

Existir és excavar.

Anna Gual

3.1 Introduction

Coastal lagoons are vulnerable to anthropogenic impacts because they favor the accumulation of contaminants from the surrounding watersheds, especially in their sediments, which act as long-term sinks and potential secondary sources (Förstner & Wittmann, 1998). Metal contamination can be particularly relevant in lagoons hydraulically connected to current and former mining sites (Fernandez et al., 2006). This is the case of Mar Menor, located in the southeast of the Iberian Peninsula, the largest saltwater lagoon in Europe. This ecosystem is included in the Ramsar Convention for Wetlands and the European Natura 2000 network, in addition to containing several regionally protected landscapes. Its climatic conditions and natural resources have encouraged the development of economic activities that menace the ecosystem's equilibrium, namely coastal urban development and intensive agricultural practices, added to past mining exploitation (Conesa & Jiménez-Cárceles, 2007). These activities have affected important resources for local livelihoods like fisheries, and highly valued ecosystem services such as tourism and landscape (Perez-Ruzafa et al., 1991; A. M. Velasco et al., 2018).

Several studies have reported large metal contamination in sediments of the Mar Menor coastal lagoon (García & Muñoz-Vera, 2015; Marín-Guirao, Cesar, et al., 2005; Pacheco, 2010; Pérez-Ruzafa et al., 2023; Serrano et al., 2019), with concentrations as high as 5,700 $mg \cdot kg^{-1}$ for Pb, up to three times higher than in other areas greatly affected by metal pollution, such as the industrial site of Venice lagoon (Bellucci et al., 2002). The high concentrations reported in Mar Menor have been linked to the former mining activities in the district of Sierra Minera de Cartagena-La Unión, located a few kilometers to the southwest of the lagoon, which started in Carthaginians' time and reactivated at an industrial level in the 19th century (Vilar Ramírez & Egea Bruno, 1985), until ceasing in 1991. Other infrastructures that have been pointed as sources of metals to Mar Menor are nautical activities related to the eight yacht ports located on its shore due to the release of Cu contained in antifouling paints (B. Jones & Bolam, 2007; Pérez-Ruzafa et al., 2023).

Most of the previous studies on sediment metal contamination in the lagoon have solely focused on surface samples (Marín-Guirao, Cesar, et al., 2005; Pacheco, 2010; Serrano et al., 2019), while those that have used dated sediment cores lacked high

spatial resolution across the lagoon(García & Muñoz-Vera, 2015; Pérez-Ruzafa et al., 2023). To better understand the drivers of metal fluxes into the sediments and their temporal evolution, historical reconstructions of metal contamination inferred from multiple dated sediment cores can help identify the processes influencing metal accumulation in sediments, such as sedimentation dynamics, land use changes like urbanization (Garcia-Orellana et al., 2011), and policy changes like environmental regulation (Palanques et al., 2017), in addition to tracing contaminant sources and transport pathways (Heim & Schwarzbauer, 2013; Valette-Silver, 1993).

This study aims to examine the spatial distribution and decadal variability of sedimentary metal concentrations, fluxes, and sources over time in Mar Menor by using ^{210}Pb dated sediment cores evenly distributed across the lagoon. In this study, results will focus on Pb, Hg, As, Cu, Zn, and Ag due to their historical importance, different potential sources, and ecotoxicological and health impacts (Harada, 1978; Pérez-Ruzafa et al., 2023). This approach will help to comprehend one of the causes of the environmental stress this location has endured in the past century, how it relates to socioeconomic changes, and inform future management plans.

3.2 Methods

3.2.1 Study site

Mar Menor is a hypersaline coastal lagoon located on the Iberian Peninsula Mediterranean coast (Fig. 3.1). It spans over 135 km^2, with average and maximum depths of 4.5 and 6.5 meters, respectively (Baudron et al., 2015). It has only one surface watercourse that maintains a regular flow of fresh water, the Albujón, resulting from a water transfer that started in 1979 and a subsequent irrigation-induced phreatic rising (García-Pintado et al., 2007). The lagoon is connected to the Mediterranean Sea by three main channels within the 22 km-long sandy bar known as La Manga (Perez-Ruzafa et al., 1991). Water circulation in the lagoon is mainly wind-driven (Pérez-Ruzafa et al., 2005), with a primary circulation gyre in the center and two other circulation subsystems north of El Estacio channel and south of the Barón and Perdiguera Islands (Fig. 3.1). Most of the lagoon sediment is currently muddy and enriched in organic matter with percentages close to 25% in central

surface sediments (Belando et al., 2021), and anoxic conditions at depth, while sandy sediments can be found in the shallowest areas and close to Las Encañizadas inlet (Pérez-Ruzafa et al., 2023). Most sediments present basic pH and are anoxic from the most surface milimetres (Eh< 100 mV) except for some sandy areas with vegetation with values between 100 and 200 mV (Álvarez Rogel et al., 2021).

Based on circulation patterns and characteristics, the lagoon can be divided into three sections: the north (north of the main outlet to the sea, El Estacio channel), the center (main circulation gyre, anticlockwise), and the south (south of the islands, with downward currents from the Albujón and El Estacio circulating to the southernmost part of the lagoon) (Fig. 3.1). The northern sector receives little runoff from ephemeral streams, and it is influenced by the natural connection to the sea (Las Encañizadas). The central sector is mainly affected by the El Estacio channel and the discharge of the permanent watercourse, the Albujón. Finally, the southern sector of the lagoon has historically received mining tailings' debris through ephemeral streams that carry water only after significant rainfall events. In this work, the north-center-south division has been used to present and discuss our data.

The influence of human activities in the lagoon has lasted for more than three millennia (Perez-Ruzafa et al., 1991). The mines from the Sierra Minera de Cartagena-La Unión started being exploited 3,500 years ago by the Carthaginians and the Romans (Conesa & Jiménez-Cárceles, 2007; Oen et al., 1975; Robles-Arenas et al., 2006), mainly to obtain silver and lead from argentiferous galena (Manteca Martínez, 1992). The Pb-Zn-Fe ores of the area occur in a zone with paragenenses and in direct association with late-Tertiary subvolcanic rocks (Oen et al., 1975). Four ephemeral streams connect the mining area to the southern portion of Mar Menor, allowing mining debris to reach the lagoon (Cuevas et al., 2023). At the beginning of the 19th century, the mining industry resurfaced through smallholder exploitations (García & Muñoz-Vera, 2015). Close to 1840, a more intense activity started in the Sierra de Cartagena (Sánchez i Bassols, 2008), and by the end of the century, the mining district had already become a national force as a lead producer (Vilar Ramírez & Egea Bruno, 1985). Production was always centered on lead and silver, but zinc and iron were also extracted (Manteca Martínez, 1992) with remarkably high productivity until the mid-20th century (Cerdà i Domènech, 2020; Conesa &

Jiménez-Cárceles, 2007). Mining activities started to affect the local environment in the mid-19th century (Sánchez i Bassols et al., 2008).

As a consequence of a strong social mobilization (Pérez-Ruzafa et al., 1987), from 1955 onwards the authorities banned mining-derived spills in the lagoon, and ponds were constructed to store sludges (Vilar Ramírez et al., 1991). While these measures were implemented, open-pit mining started, majorly based on the exploitation of lead and zinc (García & Muñoz-Vera, 2015). This increased the number of processed materials (Conesa & Jiménez-Cárceles, 2007). In 1968, most of the subterranean mining activities ended (García & Muñoz-Vera, 2015), and in 1991 all mining ceased (Marín-Guirao et al., 2007). However, mining tailings continued to be eroded and metals reached the lagoon, particularly during typical Mediterranean torrential rains (María-Cervantes et al., 2009; Marín-Guirao, Atucha, et al., 2005). In 2022, dams were installed to stop the transport of these wastes to the lagoon (Ministerio de Transición Ecológica y Reto Demográfico, 2021, 2023).

Beyond mining activities, other important impacts in this ecosystem include intensive agriculture since the 1990s and a far-reaching urban expansion fueled by the tourism industry since the 1970s (Fig. 3.1), which have caused major ecological changes such as the introduction of allochthonous species and turning the ecosystem progressively more eutrophic, with biota mass mortality events happening recurrently since 2016 (García-Pintado et al., 2007; Instituto Español de Oceanografía, 2020). In 2022, after a strong social mobilization, a Popular Legislative Initiative (ILP) triggered the creation of Law 19/2022, which recognizes the lagoon's right to exist as an ecosystem and to evolve naturally, as well as its right to protection, conservation, maintenance, and restoration (M.-C. Fuchs, 2023), being the first European ecosystem to be acknowledged as such (Krämer, 2023). For further details on the impacts of agriculture and urban expansion, refer to Chapter 4.

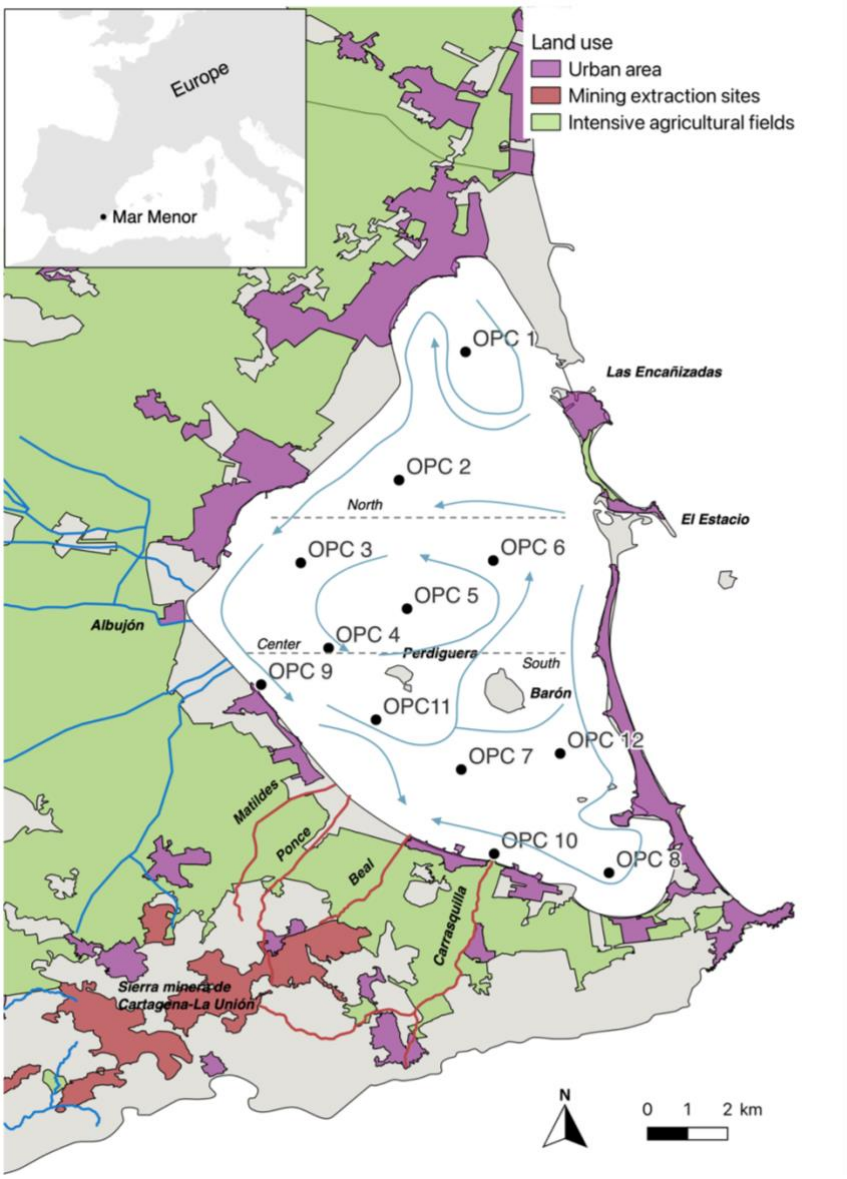


Figure 3.1 Location of the sampled sediment cores and surrounding land uses based on the CORINE land cover (2018) in the Mar Menor coastal lagoon, SE Iberian Peninsula. Red lines represent watercourses that run through former mining areas. The dashed grey line in the lagoon separates what is considered as north, center, and south in this article. The blue arrows show the present day lagoon circulation, based on Pérez-Ruzafa et al., (2023), and J. Gilabert (personal communication, June 20, 2024).

3.2.2 Sampling and sample processing

Twelve sediment cores were collected in December 2020 and June 2021 (Fig. 3.1). Sampling sites for cores OPC9 and OPC10 were accessed from the beach by foot, while the deeper cores were collected by divers. All cores were extracted by manual hammering using clear PVC tubes (120 cm long, 8.5 cm internal diameter). Cores have been grouped into three regions: north (OPC1 and OPC2), center (OPC3, OPC4, OPC5, OPC6 and OPC9) and south (OPC7, OPC8, OPC10, OPC11 and OPC12). Cores were sliced every 1 cm and processed following the procedures described in Chapter 2.

Dry bulk density ($g \cdot cm^{-3}$) of each slice was calculated by dividing dry weight per sample volume. In this study, we display sediment profiles using accumulated mass ($g \cdot cm^{-2}$) instead of depth (in cm), since the former is not affected by compaction processes (Gifford & Roderick, 2003; Wendt & Hauser, 2013).

3.2.3 Analytical and dating methods

Grain size fraction were determined following the procedures described in Chapter 2. Sediments were dated with two ^{210}Pb dating models: Constant Rate of Supply (CRS) (Appleby & Oldfield, 1978), and Constant Flux: Constant Supply (CF:CS) (Krishnaswamy et al., 1971). For each core, the most appropriate model was selected by comparing the results from both models and validating them (Arias-Ortiz, Masqué et al., 2018; Smith, 2001). Sediment mass accumulation rates (MAR) ($g \cdot cm^{-2} \cdot yr^{-1}$) for the datable period were obtained for each complete core based on the chosen model, using the excess ^{210}Pb horizon as a guide.

Bulk sediment metal concentrations ($mg \cdot kg^{-1}$) were determined by ICPM-MS after total microwave digestion following the procedures described in Chapter 2. Analyzed metals comprise Na, Al, Si, Ca, Ti, Cr, Fe, Ni, Cu, Zn, As, Sr, Ag, Cd, and Pb. Reported results are not corrected.

Total Hg in sediment samples was determined by a thermal decomposition step, followed by amalgamation and atomic absorption spectrophotometric detection according to the U.S. EPA method 7473 (US EPA, 2007), and using AMA-254

(Altec s.r.l., Czech Republic). The accuracy of measurements was repeatedly checked by analyzing lake sediment reference material MESS-3 (National Water Research Institute, Canada). The measured values were in the certified range for all analyses. Precision determined by replicate analysis was better than 5%.

3.2.4 Enrichment factors and sediment quality guidelines

Enrichment factors (EF; Eq. 3.1) were calculated to estimate the relative level of contamination shown by the metal concentrations in the sediment cores (Martinez et al., 2023). EFs are used to normalize concentrations of metals (Me) concerning a common element in the continental crust (Ti in this study). Ti has been used over Al and Fe due to the low recovery factors obtained for Al (Table 2.1), and because Fe is a product of the mining activities conducted in the region and therefore there are substantial contributions of this element in the area, rendering it unsuitable as a normalizing element (Boës et al., 2011; Sakan et al., 2015). EFs are calculated as follows:

$$EF = \frac{[\frac{Me}{Ti}]sample}{[\frac{Me}{Ti}]background} \quad (3.1)$$

where $[Me/Ti]_{sample}$ is the normalized concentration of a metal in a sample, and $[Me/Ti]_{background}$ is the normalized concentration of a metal in the background samples. The background samples' concentrations were considered as the metal concentrations for the deepest layers of each core, which date before the 19th century. The calculated results represent a conservative estimate since the maximum depth of the collected cores (75 cm) might still be affected by smallholder mining occurring at the time.

The measured metal concentrations were compared with sediment quality guidelines (SQG) to estimate their potential ecotoxicological effects. The chosen SQG are the Threshold Effect Level (TEL) and Probable Effects Level (PEL) (Long et al., 1995; Macdonald et al., 1996), which are, respectively, the sediment metal concentration below which adverse effects rarely occur in benthic organisms and the concentration at which adverse effects are frequently observed in benthic communities. These

values are indicated in Fig. 3.2 along with the metal concentrations in the sediment profile.

3.2.5 Interpolation and statistical analysis

Inverse Distance Weighting (IDW) was used to explore the spatial distribution of MARs, metal stocks, and metal concentrations within the study area (software QGIS, default power value of 2). Spearman correlation analysis was conducted to evaluate significant relationships between metal concentrations, dry bulk density, and grain size fractions. Normality for metal distribution in each lagoon core and region (north, center, south) was checked for with a Shapiro-Wilk test. Kruskal-Wallis's rank sum test was used to detect if metal differences by core or sector were significant. Dunn test with Bonferroni correction was performed for pairwise comparisons among cores and sectors and reported p-values were adjusted to this correction. The suitability of the data for factor analysis was checked with the Kaiser-Meyer-Olkin criterion (Kaiser, 1974). Major sources of metals were then identified by a Principal Component Analysis (PCA) that included metal concentrations, grain size, and dry bulk density variables. The R package *rshift* (Room et al., 2023) was used to detect significant temporal shifts in Pb, As, Hg, Cu, Zn, and Ag sediment concentrations with depth (i.e., time). STARS algorithm (Sequential T-test Analysis of Regime Shifts) (Rodionov, 2004) was used for cases with a normal distribution (significance level = 0.05, cut-off length = 3 cm, which can amount to 2 to 15 years). The resulting Regime Shift Index (RSI) quantifies the size of the shift (the more positive, the greater). Lanzante's non-parametric L-Method (Lanzante, 1996) was performed for non-normal distributions (significance level = 0.05). Its resulting p-values also express the size of the shift.

The data supporting the analyses presented in this chapter are publicly available through the dataset *Replication Data for: A Century of Sediment Metal Contamination of Mar Menor, Europe's Largest Saltwater Lagoon* (Alorda-Montiel et al., 2025; DOI: 10.34810/DATA1894).

3.3 Results

3.3.1 Sediment grain size and dry bulk densities

The dominant grain size fraction in most of the samples was silt, with an average value of 65% and a maximum content of 89% (Fig. 7.2), except for samples collected in shallow areas in front of the mouth of ephemeral streams (cores OPC9 and OPC10), which had a greater sand content. This was specifically the case for the first 20 cm of OPC9 (average sand proportion of 82%) and the entire OPC10 (average value of 96%). The second most significant fraction was either clay or sand. Clay was the second most prevalent fraction in the surface layers of OPC4 and OPC11, the middle sections of OPC5, and all sections of OPC6 and OPC7. Sand was the second most common fraction in some deep sections of OPC4 and OPC11, surface sections from OPC5, and all sections of OPC12. Cores in the north and center-west (OPC1, OPC2, and OPC3) exhibited an increase in sand content from mid-depths (~15 cm) downcore. The upper sections of these north-western cores presented a high silt content (from 44 to 85%).

Generally, dry bulk density (DBD) (Fig. 7.3) increased with depth across most sediment cores, from 0.19 $g \cdot cm^{-3}$ to 3.2 $g \cdot cm^{-3}$. Cores located nearshore close to stream mouths (OPC9 and OPC10) had greater DBD fluctuations along the sediment profile and generally presented higher values, on average (1.6, as opposed to 0.7 $g \cdot cm^{-3}$ for the rest).

3.3.2 Lead-210 dating

Lead-210 specific activities showed decreasing trends punctuated with deviations from the general pattern until reaching constant values at depths from 8 to 26 cm (approx. accumulated mass of 5 to 18 $g \cdot cm^{-2}$). Average ^{226}Ra specific activities were 24 ± 4 $Bq \cdot kg^{-1}$ (n=2), 29 ± 10 $Bq \cdot kg^{-1}$ (n=6), and 12 ± 5 $Bq \cdot kg^{-1}$ (n=7) in the northern, central, and southern sectors of the lagoon, respectively (Fig. 7.1). Some mixing was present along the entire cores OPC2 and OPC7, as inferred by the ^{210}Pb profiles. Cores located in front of ephemeral streams' mouths (OPC9 and OPC10) showed no excess ^{210}Pb specific activities, thus preventing the determination of age

models. Since these cores are sand-rich and ^{210}Pb is not scavenged by sand it cannot be discarded that there has been sand accumulation over time. The ^{210}Pb-specific activity profile for core OPC4, located close to the Albujón mouth (Fig. 7.1), showed depleted activities in the upper sediment sections, which were also characterized by higher dry bulk density values and higher sand content (Figs. 7.2 and 7.3).

Mean MARs derived from ^{210}Pb are depicted in Table 3.1. They averaged 0.059 ± 0.011, 0.060 ± 0.005, and 0.120 ± 0.017 g·cm^{-2}·yr^{-1} in the north, center, and south of the lagoon, respectively. The highest MAR values are in the south, except for OPC4.

Table 3.1 Sediment mass accumulation sediment rates (MAR in g·cm^{-2}·yr^{-1}) for the dated cores in the lagoon.

Region	Core	MAR (g·cm^{-2}·yr^{-1})		
North	OPC1	0.045	±	0.002
	OPC2	0.073	±	0.018
Center	OPC3	0.054	±	0.016
	OPC4	0.13	±	0.02
	OPC5	0.074	±	0.013
	OPC6	0.052	±	0.007
South	OPC7	0.15	±	0.03
	OPC8	0.09	±	0.04
	OPC11	0.120	±	0.007
	OPC12	0.106	±	0.008

3.3.3 Depth profiles of metal concentrations and accumulation rates

Concentration profiles of Pb, Hg, As, Cu, Zn, and Ag with depth (expressed as accumulated mass: $g \cdot cm^{-2}$) and time for representative cores of each sector are presented in Fig. 3.2. Profiles for the rest of the cores can be found in Supplementary Information for Chapter 3.

The highest sediment metal concentrations were found in the south, with levels decreasing spatially toward the north. Preindustrial metal concentrations were similar for all metals except Cu in the three sectors. Metal concentrations increased significantly in all the regions from the late 19th century until the 1950s (See Regime Shift Indices and p-values in Table 7.4). The highest concentrations for all metals except Cu were found in the southern sector during this industrial mining period. with values of 3400, 0.53, 100, 50, 3700, and 5.5 $mg \cdot kg^{-1}$ for Pb, Hg, As, Cu, Zn, and Ag.

After the 1950s, concentrations of most metals (except Cu) started to decrease significantly in the center and, particularly, the south of the lagoon. However, some metals followed different patterns. Mercury concentrations in the north of the lagoon rose again significantly in the mid-1970s. In the south, after Hg concentrations increased until the 1950s, they followed a significant decrease during the 1980s. From the 1980s to the 2000s, there were small Hg increases in the north and the center. Arsenic presented significant increases in the central sector during the 1960s and 2000s. For Cu, significant increments were observed in the 1970s in the north and the center. These concentrations stayed similar or increased, especially in the northern sector at the beginning of the 21st century. Ag concentrations increased in the southern sector during the 1980s and in the northern sector in the 2000s.

Metal accumulation rates (Fig. 3.3) consistently showed higher values in the southern region than in the rest of the lagoon after 1920. Accumulation rates peaked in that sector from the 1930s to the 1950s for Pb (3.0 ± 1.4 $g \cdot m^{-2} \cdot yr^{-1}$), Hg ($0.5 \pm 0.2$ $mg \cdot m^{-2} \cdot yr^{-1}$), As ($0.07 \pm 0.03$ $g \cdot m^{-2} \cdot yr^{-1}$), Zn ($3.3 \pm 1.5$ $g \cdot m^{-2} \cdot yr^{-1}$) and Ag ($5 \pm 2$

$mg \cdot m^{-2} \cdot yr^{-1}$). For Cu, the highest value occurred in the 2000s (0.04 ± 0.02 $g \cdot m^{-2} \cdot yr^{-1}$).

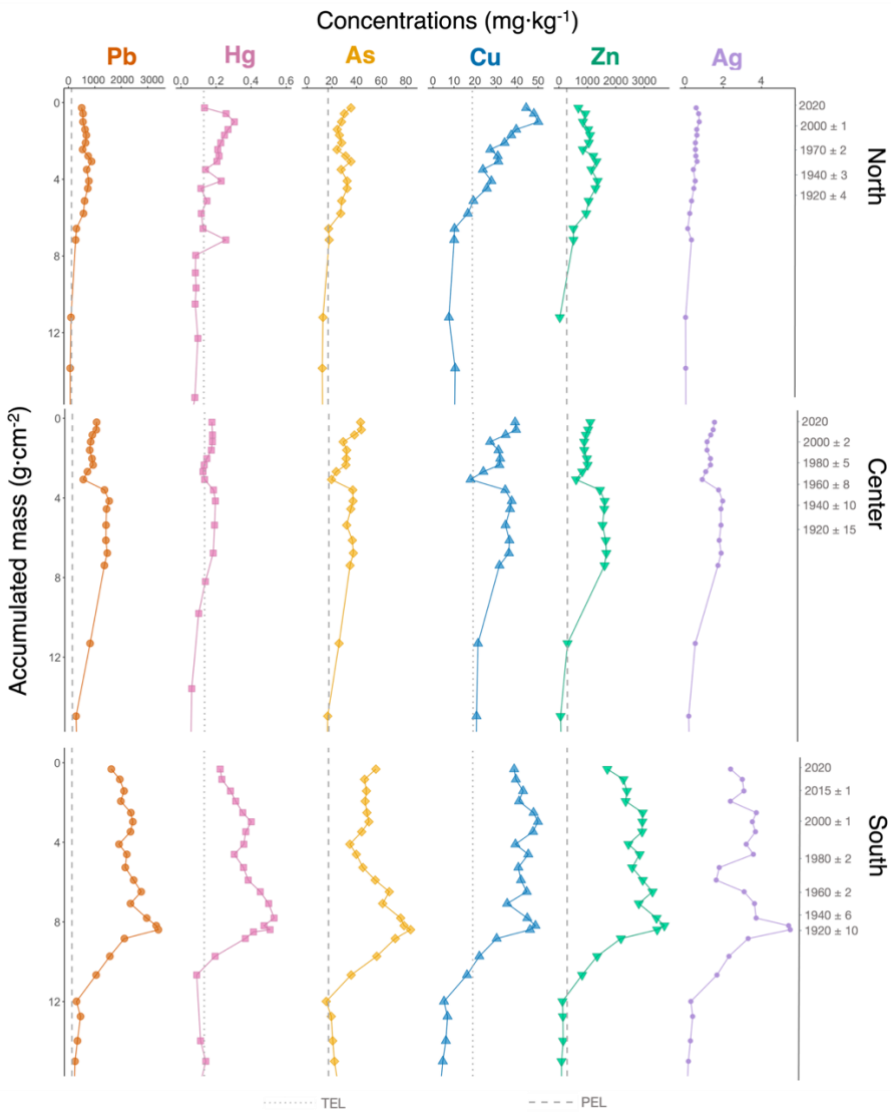


Figure 3.2 Concentration profiles of Pb, Hg, As, Cu, Zn, and Ag of selected cores representative of the different lagoon sectors (OPC1 in the north, OPC6 in the center, and OPC8 in the south). Profiles for all the other cores are in Section F of the Appendices. The dotted lines depict the Threshold Effects Levels (TEL) (Hg = 0.13 mg·kg^{-1} and Cu = 18.7 mg·kg^{-1}) and the dashed lines the Probable Effects Levels (PEL) (Pb = 112 mg·kg^{-1}, As = 17 mg·kg^{-1}, and Zn = 271 mg·kg^{-1}).

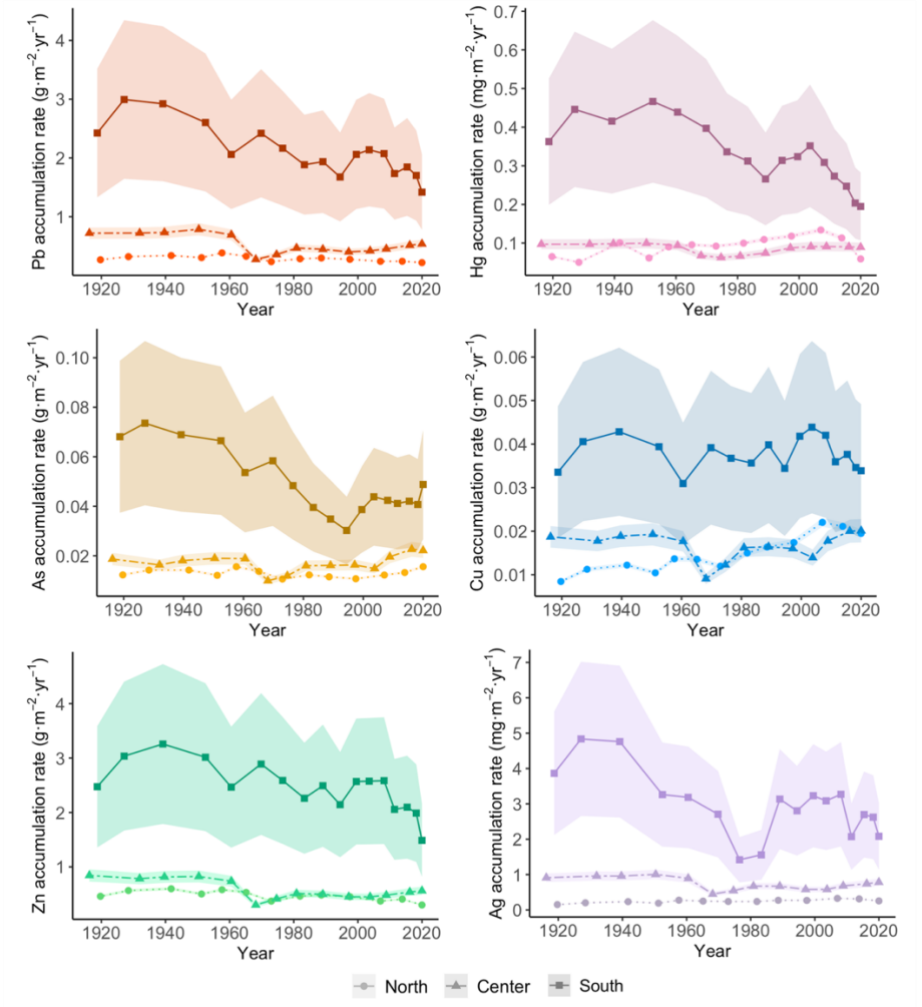


Figure 3.3 Pb, Hg, As, Cu, Zn, and Ag accumulation rates during the last century for cores OPC1 (north), OPC6 (center), and OPC8 (south). Note that units are g·m^{-2}·yr^{-1} for Pb, As, Cu, and Zn and mg·m^{-2}·yr^{-} for Hg and Ag. The shaded area represents the associated error, derived from the uncertainties from the dating models.

3.3.4 Spatial distribution of metals

Metal concentrations in sediments are summarized in Table 7.2. As already observed in the depth profiles, metals like Pb, Hg, As, Cu, Zn, and Ag showed the highest concentrations in the south. In contrast, the highest concentrations of Ca and Sr were found in the north, and the central part of the lagoon presented the highest concentrations of Ti, Al, Ni and Cr. Significant differences ($p < 0.01$) (Table 7.3) were observed among the lagoon sectors regarding Pb, Hg, As, Cu, Zn, and Ag concentrations, with higher values in the south.

Metal stocks accumulated since the start of the industrial mining period (~1900) were highest in the southern sector (Fig. 3.4), coincident with higher metal concentrations and greater sediment accumulation rates. The highest values for these stocks were 210 $g \cdot m^{-2}$ for Pb, 0.031 $g \cdot m^{-2}$ for Hg, 5.2 $g \cdot m^{-2}$ for As, 4.6 $g \cdot m^{-2}$ for Cu, 230 $g \cdot m^{-2}$ for Zn and 0.29 $g \cdot m^{-2}$ for Ag. Total stocks for the whole lagoon (135 km^2) accumulated during the last century were estimated to be 9,100, 1.6, 450, 270, 10,000, and 12 tons of Pb, Hg, As, Cu, Zn, and Ag, respectively.

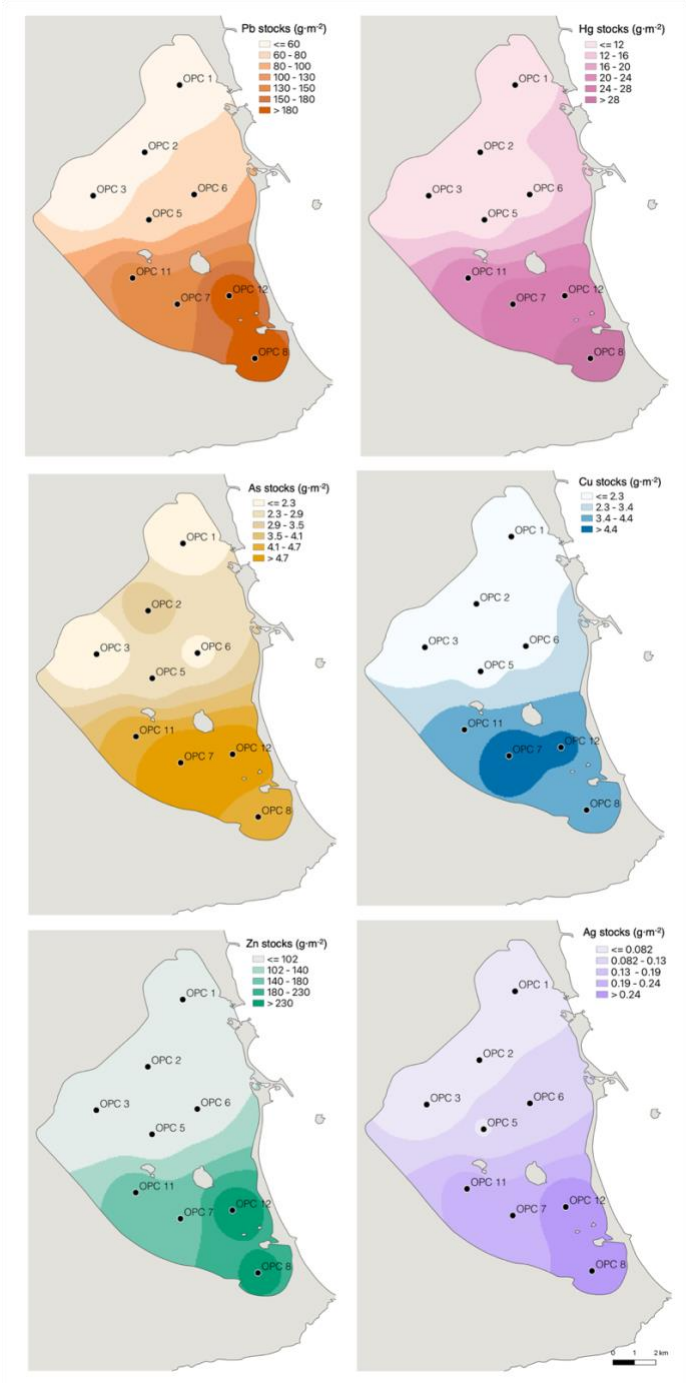


Figure 3.4 Spatially interpolated sediment metal stocks of Pb, As, Hg, Cu, Zn, and Ag accumulated from 1900 ± 20 until 2020.

3.3.5 Correlation and Principal Component Analysis (PCA)

The correlation analysis showed that the silt content was positively and significantly correlated with most metals, with higher correlations for Cr, Ti, and Ni ($r > 0.5$) and negatively and significantly correlated with Sr ($r < -0.5$) and Ca ($r > -0.5$) (Table 7.4). Sand fraction content positively correlated with Sr ($r > 0.5$), Ca ($r < 0.5$), and negatively correlated with Cr, Ni, and Ti ($r < -0.5$). Most metals correlated negatively and significantly with DBD since metal content was typically higher in surface sections, which tend to be less dense than their deeper counterparts.

A Principal Component Analysis (PCA) was computed with metal concentrations, dry bulk densities, and grain size data from sections dated from 1900 to 2020. The two principal components explained a cumulative variance of 60% (Fig. 3.5). Principal Component 1 (Dim1, horizontal axis), explaining 39% of the variability, was mainly influenced by Cu, Pb, Zn, Ag, Fe, As, Cd, and Hg with contributions between 6% and 11% for each metal. Principal Component 2 (Dim2, vertical axis), explaining 21% of the variance, was influenced by Sr, Ni, Cr, Ti, Si, sand, and silt (contributions between 6% and 11%).

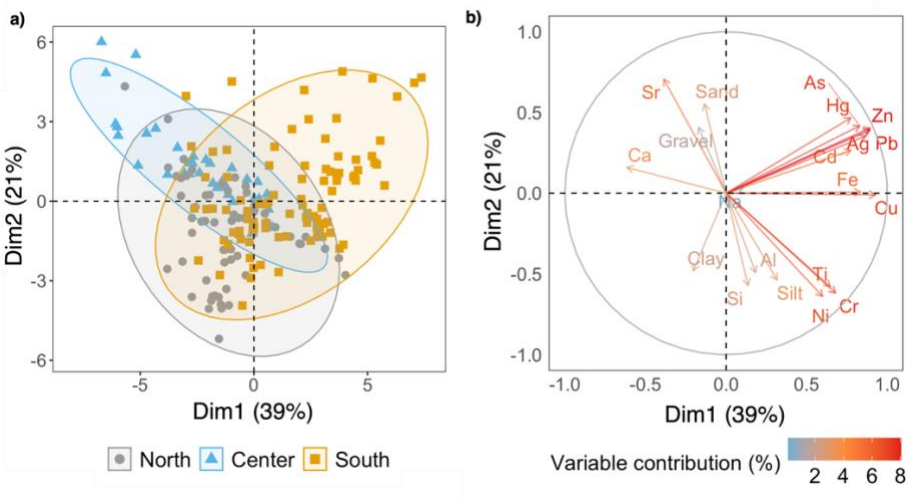


Figure 3.5 Principal Component Analysis biplots for a) individuals (core sections) and b) the sediment variables. Sections included dates from 1900 to 2020 (i.e., the sections within the excess ^{210}Pb horizon). Data used includes grain size and metal concentration results. Superimposed on the a) plot are the confidence ellipses (95%) for the lagoon sectors: north (grey circles), center (blue triangles), and south (orange squares). In the b) plot, the variable contributions (%) represent the percentage that each variable contributes to the cumulative (total) variance.

3.4 Discussion

3.4.1 Last century sedimentation patterns in Mar Menor are driven by inputs from streams and mining materials

Sedimentation processes in the Mar Menor coastal lagoon result from different sediment delivery mechanisms and redistribution processes. The higher MAR values in the southern sector indicate a combined influence of the proximity of inputs from streams and the secluded southern circulation that promotes sediment accumulation in the southeastern region (Fig. 3.1). Mining-derived sediments constitute a major fraction of the depositional materials in this region, as evidenced by its high metal concentrations and stocks. In the shoreline cores (OPC9 and OPC10), the absence of excess ^{210}Pb is produced by the negligible accumulation of fine sediment fractions locally (Figs. 7.1 and 7.2). For core OPC4, located near the shore and the Albujón

watercourse, the ^{210}Pb depleted sections might be the result of a recent deposition event (Burnett et al., 2023; Walsh & Nittrouer, 2004) from extreme storms (cut-off lows) which transported large amounts of sediments to the lagoon (Machado Toffolo et al., 2022). The event-corrected dating model indicated that the initial sediment layer beneath the rapid deposit sections dates to 2016, coinciding with the first cut-off low event that had relevant effects on the lagoon mass mortality episodes.

Sandy materials in the lagoon have been associated with marine influences, such as inputs from the sandy barrier that separates the lagoon from the Mediterranean Sea (García & Muñoz-Vera, 2015), and to shoreline sediments in front of watercourses. In contrast, finer sediments, such as clay and silt, have been linked to terrigenous inputs (Pérez-Ruzafa et al., 2023). Metals like Ti and Sr further highlight this terrestrial or marine origin, respectively. Sr and Ca, probably originated from calcareous organisms, presented their highest concentrations in the north (Table 7.2), suggesting a marine source through seawater inflow via sandbar channels rather than fluvial inputs. High concentrations of metals like Ti or Al but also Cr and Ni in the central sector were attributed to lithogenic sources and the runoff input from the Albujón watercourse (Cuevas et al., 2023). In the southern sector, significantly higher concentrations of Pb, As, Cu, and Ag were linked to the proximity to the mouths of the mining-affected ephemeral streams, which would preferentially deliver these metals, combined with the effect of lagoon circulation.

Natural and anthropogenic factors have influenced the sediment composition and changes in metal concentrations in the Mar Menor coastal lagoon over the past century. In the northwest of the lagoon, the sand-rich deeper sections of cores OPC2 and OPC3 suggested a higher influence of Las Encañizadas sandy materials in the past. The increase in silt content in recent (after 1910) core sections coincides with an increase in metal concentrations and with the developing period of industrial mining. Therefore, there might be a confluence of factors in the north that explain this increase in sedimentation of finer materials from the late 19th century onwards.

Cores from the north and central sectors showed lower sedimentation rates and thinner layers of mining contamination (upper 15 cm at most), with lower metal concentrations and less variability, as indicated in the PCA biplots (Fig. 3.5).

Southern cores, more affected by mining-derived materials, spanned over a larger biplot area (Fig. 3.5a) and therefore showed a more diverse influence of the different variables. Additionally, these cores exhibited higher differences in metal concentrations before and after industrial mining. For instance, core OPC8 showed concentrations of 120 $mg \cdot kg^{-1}$ for Pb before industrial mining, which increased to 3400 $mg \cdot kg^{-1}$ after industrial mining began. Conversely, core OPC1 (in the north) presented concentrations of 43 $mg \cdot kg^{-1}$ for Pb in undated (before ~1900), deep sediments, which increased to 870 $mg \cdot kg^{-1}$ after the onset of industrial mining.

The PCA generated two underlying variables that explained the variability of our data. Dim1 differentiated mining-derived materials (positive values) from other sedimentary sources (negative values). Dim2 differentiated between terrestrial and marine sediment inputs as it reflected grain size variations (a larger proportion of finer materials for negative values) that could be linked to differences in terrestrial as opposed to marine inputs. Ca, Sr, sand, and gravel were probably marine-sourced (Abu-Zied et al., 2021) –either autochthonously produced or by marine inputs through the channels of the sand bar.

This analysis indicated that Pb, Zn, Ag, Cd, Fe, and As, found in ores historically mined in the Sierra Minera de Cartagena-La Unión, were associated with finer, terrigenous materials and mining runoff. Other metals not directly exploited in the mining area, such as Hg, also shared this origin. Ni, Cr, Al, Si, and Ti, were mainly influenced by the deposition of finer sediments but were not clustered with mining-derived materials, indicating that they were primary lithogenic runoff components. Cu presented an intermediate situation between the group of mining metals and the lithogenic runoff components, suggesting multiple sources.

3.4.2 Metal contamination is caused by industrial mining and recent anthropogenic contributions

The metal concentrations in the Mar Menor coastal lagoon sediments reflected a complex interplay of historical and recent contamination sources, which included mining and other anthropogenic activities. Mining metal concentrations followed similar temporal trends across all sectors of the lagoon, closely tied to the history of mining in the Sierra Minera de Cartagena-La Unión. Their concentrations presented

significant increases linked to the onset of industrial mining before and at the start of the 20th century. This increase in metal concentrations around 1900 has been observed in similar coastal systems (Buckley et al., 1995) . Maxima occurring in the first half of the 20th century. The significant decrease in most metal concentrations around the 1950s and 1960s, particularly in the central and southern sectors, can be explained by the 1955 ban on premeditated mining spills into the lagoon. After the ban, torrential rain runoff from the mining area still delivered metals to the lagoon (María-Cervantes et al., 2009; Marín-Guirao, Atucha, et al., 2005). Similarly, to Pb and Zn, As concentrations increased due to the development of large-scale mining activities, but recent higher concentrations could be related to continuous inputs of this metal even after the ceasing of mining activities. Inputs of As could be linked to the sensitivity of this metal to redox conditions (Zitoun et al., 2024), facilitating As leaching from soils after acidification and subsequent delivery to the lagoon through stream discharge (Martínez-López et al., 2020).

While mining has been a major contributor to metal contamination, other anthropogenic activities have emerged as significant sources in recent decades. For Hg, mining was the main contributor to its enhanced concentrations in sediments throughout most of the 20th century. However, high concentrations in recent sediments could be linked to non-mining sources, especially in the northern sector. Its proximity to large population centers, such as San Pedro del Pinatar and San Javier, may contribute to Hg contamination due to broad anthropogenic sources. Furthermore, the presence of an airport and a water treatment plant in San Javier and a landfill in San Pedro —infrastructures related to Hg emissions (Fang et al., 2018) — could further increase the supply of Hg to lagoon sediments. Other potential sources for Hg include agricultural wastes (Ruiz-Fernández et al., 2009).

Urban expansion can explain the increase in Cu concentrations at the start of the 21st century. Antifouling paints are the most probable source of Cu (Costa et al., 2016; J. Readman, 2006), especially near the large ports of Lo Pagán and La Manga, and after the enlargement of El Estacio channel for sailing in 1973. Additional sources of metals to the central and southern sectors could include fertilizer application, which can trigger the remobilization of metals in soils due to acidification (Krahforst et al., 2022). Although Ag accumulation through time is mainly controlled by the mining industry activities, there were increases in the 1980s

to the 2000s in the northern and southern basins that could be indicative of sewage releases (García-Pintado et al., 2007) due to the use of Ag nanoparticles in antibacterial consumer goods (Gallon & Flegal, 2015; Ravizza & Bothner, 1996).

As a consequence of the temporal variability of metal inputs and accumulation rates, metal concentrations in surface sediments of the lagoon have changed during the last 120 years. The characterization of the temporal evolution of surface sediments is relevant as they are a good representation of the metal concentrations that were readily available for benthic and planktonic organisms and prone to be mobilized to the water column. This is particularly relevant for those metals presenting high concentrations, such as those derived from mining activities. As shown before, metal-enriched sediments have consistently deposited in all sectors of the lagoon, but more prominently in the south, closer to the mouths of the streams from the mining area, and where there is a circulation gyre that enhances sediment accumulation.

Focusing on mining-derived metals and using Pb as an example (Fig. 3.6), concentrations in surface sediments of the lagoon were relatively low and showed minor spatial variability before industrial mining. At this period, the area in front of the ephemeral streams draining the mining area (Sierra Minera de Cartagena-La Unión), where OPC7 is located, already presented higher concentrations than the rest of the lagoon. These higher concentrations are probably caused because these watercourses run through the Sierra, which contains volcanic materials rich in minerals that were historically exploited. The period with the highest metal concentrations, which also contributes more to the accumulation of metal stocks, occurred during the 1920s and 1940s (Fig. 7.10 and Table 7.5). After the establishment of industrial mining, the highest concentrations were always found at the southernmost edge, due to the circulation gyre and the proximity of mining-derived inputs. As observed in the distributions in the 1970s and 1990s, surface metal concentrations in the lagoon started decreasing, particularly in the south, as a consequence of the mining spilling ban in 1955. This decrease began to affect the rest of the lagoon, especially the area in front of the ephemeral streams affected by mining (OPC7 and OPC11) after the 1990s. Contamination has also preferentially spread along the eastern coast of the lagoon, as shown in the maps for 1920, 1940, and 2020 (Fig. 3.6). The current flowing to the northeast, which runs between the

two main islands, could drag these materials, subsequently depositing them along the southward current flowing along La Manga (Fig. 3.1). In contrast, the north-western region, where cores OPC2 and OPC3 are located, might have been more influenced by ephemeral streams and Mediterranean inputs that do not supply mining-related metals.

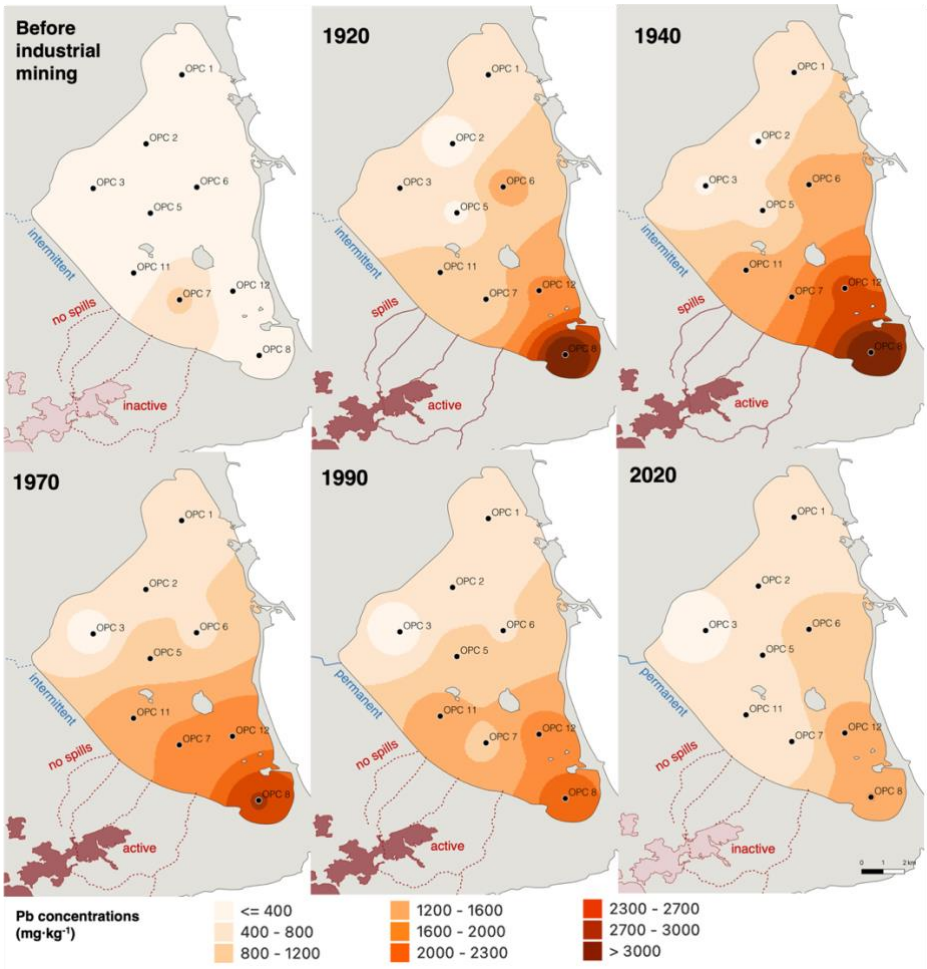


Figure 3.6 Pb surface concentrations (mg·kg^{-1}) at different periods. The dotted line in the ephemeral streams affected by mining indicates a minor influx of mining debris into the lagoon, either from preindustrial mining or due to the spilling ban. Similarly, the solid line in the Albujón watercourse signifies its permanency or intermittence. The clear and dark mining sites areas indicate the lack or presence of industrial exploitation.

3.4.3 Metal concentrations surpass sediment quality guidelines

Enrichment factors (EF) for Pb, As, Hg, Cu, Zn, and Ag before, during, and after mining industrial exploitation are shown in Fig. 3.7. Values were, on average, higher than 1.5 for the six metals during and after industrial mining, indicating accumulation of anthropogenic inputs (X. Gao & Li, 2012). The metal that showed the major enrichment was Zn, particularly during industrial mining times, followed by Ag. After the closure of all mining activities, average enrichment factors for Pb, Zn, and Ag decreased, with As being the closest to preindustrial values (EF close to 1). EF values for Pb, Zn, and Ag were significantly different when comparing every defined period ($p < 0.01$). For As, enrichment values did not show significant differences between periods ($p = 0.14$). This further demonstrates that factors other than the operational activity status of mining, such as recent leaching from mining watercourses, also play a role in the enrichment of this metal. Regarding Hg and Cu, the industrial mining and the post-mining periods were not significantly different, whereas the preindustrial mining values differed significantly when compared to mining and post-mining periods (both $p < 0.01$). This, again, underpins additional anthropogenic sources of Hg and Cu after mining cessation.

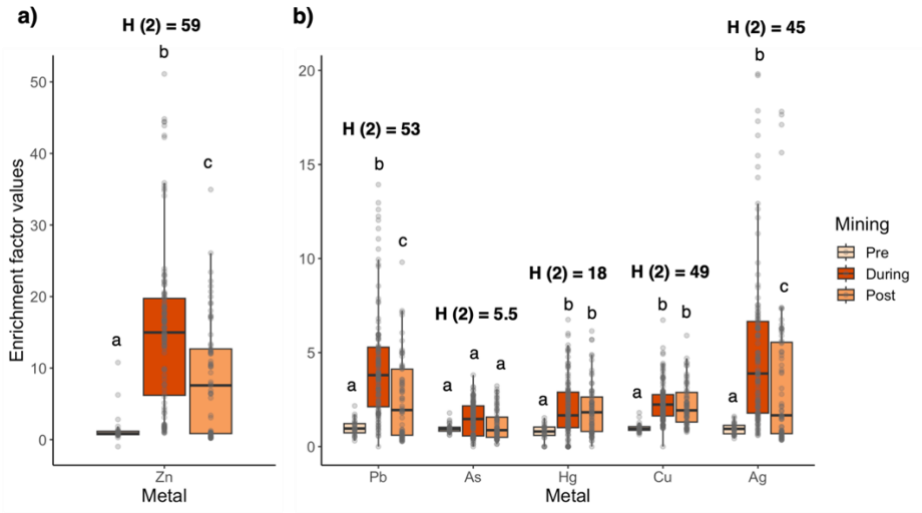


Figure 3.7 Enrichment factor values for a) Zn and b) Pb, As, Hg, Cu, and Ag in the periods previous (before the second half of the 19th century), during (from then to 1990), and after mining closure (post-1990), index H from Kruskal-Wallis analysis (for Pb, Hg, Cu, Zn and Ag $p < 0.01$; for As $p = 0.14$) and the results of Dunn's test (adjusted $p < 0.01$) for the pairwise differences. The columns with different letters (a, b, c) are significantly different from one another. Box comprises the data between the 25th and the 75th percentiles. Whisker size represents 1.5·SD.

Preindustrial mining concentrations of Pb, Hg, As, Cu, and Zn already exceeded TEL values, indicating pre-contemporary potentially toxic fluxes of these metals to the lagoon attributed to inputs from the watershed and in agreement with previous observations from Pérez-Ruzafa et al. (2023). Concentrations of Pb, As, and Zn during the preindustrial period even surpassed PEL values, although As concentrations only reached this level before the 20th century in the north and center regions. During the industrial mining era, these metal concentrations further increased, reaching up to 30, 6, and 14 times PEL values for Pb, As, and Zn, and 4 and 3 times TEL values for Hg and Cu, respectively. Current concentrations are still above PEL for Pb, As, and Zn and above TEL for Hg and Cu. For Hg, surface concentrations may soon show non-toxic values if the latest decreasing tendencies persist. Even though a general, relatively low bioconcentration factor has been found in most lagoon organisms, indicating effective metal retention by sediments (Pérez-Ruzafa et al., 2023), such high concentrations could have negative impacts on biota if their bioavailability changes.

3.4.4 Mar Menor sediments present some of the highest metal concentrations in coastal enclosed ecosystems

Metal sediment contamination in the Mar Menor coastal lagoon is notably high compared to other reported values in lagoons within the Mediterranean region and on a global scale (Table 3.2). Pb maximum concentrations in this study exceeded those reported in many similar ecosystems, including the industrial area of the Venice lagoon (Bellucci et al., 2002). This location was the only one that presented higher maximum As, Zn, and Hg values than Mar Menor. Cu maximum concentration in Mar Menor was of a similar magnitude to those reported in other lagoonal ecosystems like Berre (France) —affected by industry— and Naukaumi —affected by mining— (Japan) (Ahmed et al., 2010; Ontiveros-Cuadras et al., 2024), but notably lower than Nador and Al-Shuaiba lagoons, which are impacted by a combination of mining and urban pollution (Abu-Zied et al., 2021; Bloundi et al., 2009). For Pb, As, and Zn, Naukami presented lower sediment metal concentrations than Mar Menor (Ahmed et al., 2010). Ag maximum concentration was two times higher in the Mar Menor coastal lagoon than in the Vistula Baltic coastal lagoon, impacted by industry (Szefer et al., 1999). Lagoons affected by agricultural contamination also exhibit generally lower metal concentrations in their sediments than Mar Menor (Green-Ruiz & Páez-Osuna, 2001; Ontiveros-Cuadras et al., 2021), highlighting the polluting potential of industrial mining.

Table 3.2 Reported metal concentration ranges (mg·kg^{-1}) for coastal lagoons and bays.

Site	Sample type	Pb	Hg	As	Cu	Zn	Ag	References
Mar Menor - this study	**Sediment cores**	**10 – 3,400**	**0.01 - 0.53**	**4.6 - 100**	**1.1 - 50**	**2.6 – 3,700**	**0.020 - 2.3**	**This work**
Al-Shuaiba lagoon	Grab sampler	2 - 270	-	-	3 - 200	3 - 400	-	Abu-Zied et al. (2021)
Altata-Ensenada lagoon system	Grab sampler	46 – 290	-	-	5.6 – 64	19 – 170	1.6 – 7.0	Green-Ruiz & Páez-Osuna (2001)
Berre Lagoon, MedSea	Grab sampler	18 - 82	0.15 - 0.40	4 - 10	11 - 48	50 - 150	-	Accornero et al. (2008)
Laizhou Bay	Grab sampler	16 - 32	-	8.1 - 17	7.0 - 34	46 - 91	-	Dang et al. (2021)
Nakaumi lagoon	Grab sampler	12 - 35	-	4 - 19	8 - 51	42 - 210	-	Ahmed et al. (2010)
Nador lagoon, MedSea	Sediment cores	11 - 300	-	4 - 76	4 - 470	4 – 1,200	-	Bloundi et al. (2009)
Terminos lagoon	Sediment cores	6.9 - 19	-	0.9 - 11	13 - 23	40 - 66	-	Ontiveros-Cuadras et al. (2024)
Venice industrial site, MedSea	Sediment cores	41 - 930	1.2 - 48	7 - 130	-	100 – 8,300	-	Bellucci et al. (2002)
Vistula Baltic coast lagoon	Grab sampler	24 - 80	-	4 - 20	18 - 32	76 - 180	0.37 – 0.81	Szefer et al. (1999)
Xola-Paramán lagoon	Sediment cores	9 - 15	-	1.8 - 5.6	6.1 - 28	37 - 100	-	Ontiveros-Cuadras et al. (2021)

3.4.5 Enhanced resuspension could remobilize accumulated metals to the water column

Despite generally decreasing trends in metal concentrations in recent sediments, it is crucial to consider the substantial accumulation of metals in a vulnerable ecosystem such as the Mar Menor coastal lagoon. The mobility and potential ecological effects of these metals in sediments are influenced by various factors including grain size (Horowitz, 1985), pH (Bourg & Loch, 1995), dissolved oxygen (Abu-Zied et al., 2021), redox potential (Williams, 1992), iron-manganese oxides (González et al., 2007), organic matter content, salinity (Förstner et al., 1986), and the influence of living organisms (Souza et al., 2015).

Metals can become available for biological uptake when they detach from mineral oxides or clay coatings, a process enhanced by the oxidation of anaerobic sediments (Chapman et al., 2011). This phenomenon is particularly notable at the oxic-anoxic interface, which plays a dominant role in the fluxes of trace metals from sediments to the water column (Salomons, 1987). During resuspension episodes, metals can be exposed to oxygenated water layers and become more accessible for uptake (Caetano et al., 2003; Santos-Echeandía et al., 2023). Additional mechanisms such as diffusion, porewater exchange, and submarine groundwater discharge through sediments can also contribute to mobilizing metals from lagoon sediments to the water column (Alorda-Kleinglass et al., 2019; Martínez-Soto et al., 2016).

Albeit metal concentrations in Mar Menor's surface sediments exceed sediment quality guidelines for metals like Pb, Hg, As, Cu, and Zn, a general, relatively low bioconcentration factor is found in most lagoon organisms, indicating effective metal retention by sediments (Pérez-Ruzafa et al., 2023). The rise in organic matter fluxes to Mar Menor sediments due to agricultural activities and urban sewage discharge could have impacted the lagoon sediment's ability to absorb As and contribute to its release (Martínez-López et al., 2020) while retaining other metals in the sediments. This retention is presently preventing their bioavailability and mitigates potential ecotoxicological impacts (Zhang et al., 2017). However, there is evidence that in the event of strong winds, resuspension increases metal concentration in the water column for both the dissolved and particulate fraction (Santos-Echeandía et al., 2023).

Mediterranean coastal lagoons are particularly vulnerable habitats to future global change scenarios. The expected rise in extreme precipitation events (like the ones produced by cut-off lows in the region), more frequent in recent years in the western Mediterranean due to climate change (Benabdelouahab et al., 2020; Kyselý et al., 2012), could lead to more recurrent runoff-induced episodic discharges from contamination sources. Additionally, they could increase resuspension (Fong et al., 2020), especially in shallow environments like coastal lagoons (C. Tang et al., 2020). In Mar Menor's case, this could affect the most polluted sediments from the last decades (Palanques et al., 2020) and increase the availability of sediment-bound metals upon exposure to oxygen, as shown in Bancon-Montigny et al., (2019), potentially affecting the biota. Additionally, expected sea level rise from climate change could contribute to flooding the contaminated watershed soils and increase metal mobilization to the water column (Izaditame et al., 2022).

The 2016 and 2019 extreme precipitation events in the Mar Menor, could have contributed to delivering mining-polluted sediments by runoff and conveyed high organic matter and nutrient loads to the lagoon, which could contribute to metal retention but at the same time trigger new eutrophication peaks. Additional challenges, such as mass mortality episodes in benthic macrophyte meadows, could hamper their contribution to sediment-retaining processes and further increase resuspension events. Such delicate equilibrium in an already remarkably vulnerable ecosystem requires more detailed studies, especially focusing on resuspension risk and properly planned metal contamination monitoring programs.

4. Land-use change and hydrodynamic alteration reshape sediment carbon and nitrogen burial in a coastal lagoon

El meu voltant és verd com un xiclet de clorofil·la.

Maria Sevilla

4.1 Introduction

Nutrient burial in coastal sediments contributes not only to regulating nutrient availability and mitigating eutrophication, but also to the long-term sequestration of organic carbon, thereby linking nutrient cycling with the blue carbon function of coastal vegetated ecosystems. Seagrass meadows and rooted macroalgae promote sediment stabilization, enhance the retention of organic matter and nutrients, and reduce sediment resuspension, helping maintain water quality and ecosystem functioning (Bernardeau-Esteller et al., 2023; Brenner et al., 2006; Pérez-Ruzafa et al., 2002). However, this buffering capacity can be compromised under increasing anthropogenic pressure. Declines in seagrass meadows driven by eutrophication, reduced water quality, physical disturbance, and climate change may reduce nutrient retention and carbon burial, while shifts towards macroalgal dominance can alter the quality and fate of organic matter reaching the sediments (Arias-Ortiz et al., 2018; McGlathery et al., 2007; Orth et al., 2006; Serrano et al., 2016; Waycott et al., 2009). These feedbacks may accelerate ecosystem degradation by weakening the natural capacity of sediments to retain nutrients and organic carbon.

Despite the recognized importance of sediment nutrient burial as a crucial process in coastal ecosystem functioning, there is a limited understanding of how anthropogenic stressors, which are expected to continue or increase in the future (Canuel & Hardison, 2016), affect and drive ecosystem shifts in vulnerable habitats. A striking example of how anthropogenic stressors modify nutrient cycling is the Mar Menor coastal lagoon, the largest saltwater lagoon in Europe and the Western Mediterranean, which includes areas protected under the Ramsar convention (León & Bellido, 2016). After agriculture intensification and urban expansion in its watershed, this ecosystem has experienced several eutrophication and partial recovery cycles, with significant socioeconomic and ecological impacts, including widespread mortality of marine fauna, the loss of most extensions of native seagrass *Cymodocea nodosa,* the expansion of macroalgae *Caulerpa prolifera,* and a 43% reduction in housing investment returns (Lamas Rodríguez et al., 2023; Zamora-López et al., 2022).

Building on this context, this study investigates the evolution of sediment organic carbon (C_{org}) and total nitrogen (TN) dynamics in the Mar Menor coastal lagoon under increasing anthropogenic pressure in the 20th and 21st centuries. Specifically, we quantify burial rates of C_{org} and TN and evaluate changes in their sources to the sediments using stable isotope mixing models, distinguishing among terrestrial, Mediterranean, and macrophyte-derived inputs. Together, the results allow elucidate how human pressures have altered nutrient dynamics and ecosystem trajectories in the lagoon and provide information to support future management and policy strategies.

4.2 Methodology

4.2.1 Study site

Anthropogenic pressures on the Mar Menor lagoon have accumulated over millennia, progressively reshaping its physical, chemical, and ecological functioning. Early human impacts date back more than three thousand years ago, with mining being the first to leave a detectable imprint in the lagoon's sediments (Pérez-Ruzafa et al., 2023). These activities intensified with industrialization, reaching their peak during the 20th century and resulting in substantial accumulation of metals in lagoon sediments (Alorda-Montiel et al., 2025). For further details on the impacts of mining, refer to Chapter 3. From the 12th to the 19th centuries, land clearing and agricultural activities in the watershed, Campo de Cartagena, increased sediment delivery to the lagoon (Fig. 4.1). In the late 19th century, marine influence intensified when a series of storms breached the natural sand barrier separating the lagoon from the Mediterranean Sea, followed by the opening of two artificial channels—Marchamalo (Perez-Ruzafa et al., 1991) and Gola del Charco (García & Muñoz-Vera, 2015). The widening of the El Estacio channel in the early 1970s further enhanced water exchange with the Mediterranean (Perez-Ruzafa et al., 1991). This hydrodynamic change moderated temperature extremes (raising winter minima from ~7.5 ºC in 1970 to ~12 ºC by 1988) and reduced salinity from around 53-54.7 to 40-51 (Pérez-Ruzafa et al., 2012) in a system where evaporation typically exceeds freshwater inputs. In 2021, the average flushing time of lagoon waters was 130 days (Rodriguez-Puig et al., 2025), indicating that water remains in the lagoon for approximately four

months before being renewed. Increased connectivity facilitated the spread of the allochthonous macroalgae *Caulerpa prolifera*, which was first observed in the 1970s and scientifically documented in the 1980s (Pérez-Ruzafa et al., 1987) and jellyfish species such as *Cotylorhiza tuberculata* and *Rhizostoma pulmo* (Fernández-Alías et al., 2023). As a result, benthic habitats shifted from mainly sandy *Cymodocea nodosa* meadows to muddier substrates dominated by mixed stands of *C. prolifera* and *C. nodosa*, leading to higher organic matter and sulfide production in sediments, especially in central areas of the lagoon (Belando et al., 2021; Perez-Ruzafa et al., 1991). Parallel to these transformations, rapid urban expansion from the 1970s until the 2007 economic crisis, particularly along the sandbar, intensified pressures. The sharp seasonal rise in population during the summers –approximately 1.3 times higher than during the rest of the year– often led to direct wastewater discharges due to overloaded or damaged water treatment infrastructure (Guaita-García et al., 2022).

The commissioning of the Tajo-Segura transfer in 1979, a large-scale inter-basin diversion that rerouted water from the Tajo River in central Spain to the Segura basin for irrigation to the agricultural Mar Menor watershed, represented a major hydrological shift (Jiménez-Martínez et al., 2016). Although the Tajo-Segura transfer itself lies outside the study area shown in Figure 4.1, it supplies irrigation water to the Campo de Cartagena, which drains into the Mar Menor coastal lagoon. As a consequence, phreatic levels rose, and the Albujón stream became the only permanent watercourse in the basin (Velasco et al., 2006), initiating a chronic input of nutrient-rich runoff into the lagoon via both surface water inputs and groundwater discharge (Alcolea et al., 2019; Rodriguez-Puig et al., 2026). During the study period, its discharge ranged from 1.8×10^3 to 1.49×10^5 m^3 d^{-1} (data retrieved from the Mar Menor Environmental Monitoring System; Government of the Region of Murcia, accessed on 23 June 2026), with suspended particulate matter concentrations of approximately 0.3 g L^{-1}. These nutrient inflows, particularly nitrogen, contributed to the expansion of *C. prolifera* meadows (García & Muñoz-Vera, 2015). By the end of the 1990s, agricultural practices intensified, shifting from low-input dryland farming to high-input irrigated agriculture with substantial nitrogen fertilization, driving further nutrient loading to the lagoon (García-Ayllón & Miralles, 2014). Despite this, the lagoon exhibited remarkable resilience for two decades, with no clear signs of eutrophication based on water quality indicators (Salas et al., 2008). However, from the 2000s onward, intensive agriculture also expanded

into the southern watershed, increasing nutrient loading pressures. Despite these high nutrient inputs, eutrophication consequences were likely mitigated through two mechanisms: a strong top-down control of phytoplankton by jellyfish and sediment nutrient burial under benthic macrophytes (Fernández-Alías et al., 2022; Pérez-Ruzafa et al., 2002).

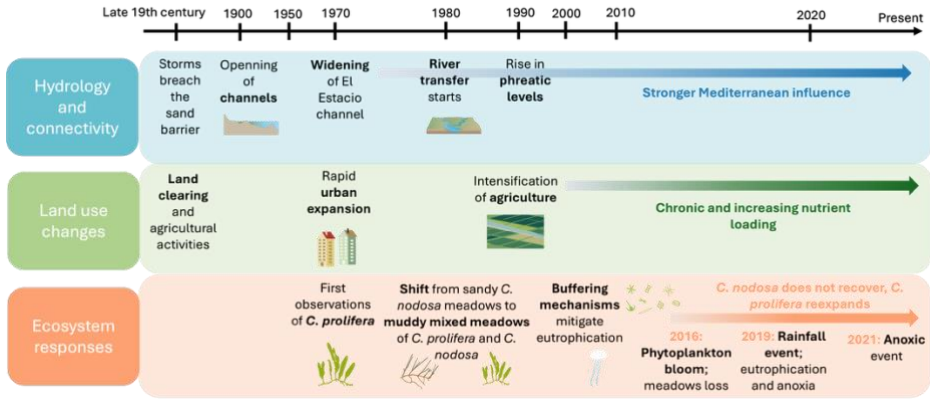


Figure 4.1. Schematic timeline summarizing the major anthropogenic and ecological changes in the Mar Menor lagoon from the late 19th century to the present.

In 2016, an exceptionally dry year, the combined effect of high nutrient loads and extreme summer heat triggered a long-lasting phytoplankton bloom that resulted in the loss of 85% of macrophyte meadows (Belando et al., 2017), and socio-economic disruption (Lamas Rodríguez et al., 2023). The lagoon partially recovered its physicochemical conditions in 2018 (Pérez-Ruzafa et al., 2019). In September of 2019, a severe flash flood produced by an extreme precipitation event in (172 mm, data from Sistema de Información Agraria de Murcia) transported large water and sediment loads to the lagoon, triggering a strong stratification in the lagoon's water column (Machado Toffolo et al., 2022; Pereira et al., 2026), ending in renewed eutrophication and anoxia, with the first fish mass mortality episode in the lagoon. In the summer of 2021, another anoxic event occurred, with widespread fauna mortality. Following these disturbances, *C. nodosa* meadows scarcely recovered, whereas *C. prolifera* mats re-expanded due to their higher tolerance to low-light conditions (GEAM IEO-CSIC, 2025). Fish assemblages and benthic polychaeta communities have been modified due to the eutrophication collapses as well (Sandonnini et al., 2022; Zamora-López et al., 2022). The impacts of the lagoon

collapse expanded beyond the ecosystem, triggering chronic stress and reduced shoot size on the nearby Mediterranean *Posidonia oceanica* meadows, the most extensive in south-eastern Spain (Jiménez-Casero et al., 2025). All of these major events resulted in mobilizations that eventually led to the Mar Menor being legally recognized as the first European ecosystem with a right to exist, to evolve naturally, and to be protected, preserved, and restored (M.-C. Fuchs, 2023; Krämer, 2023).

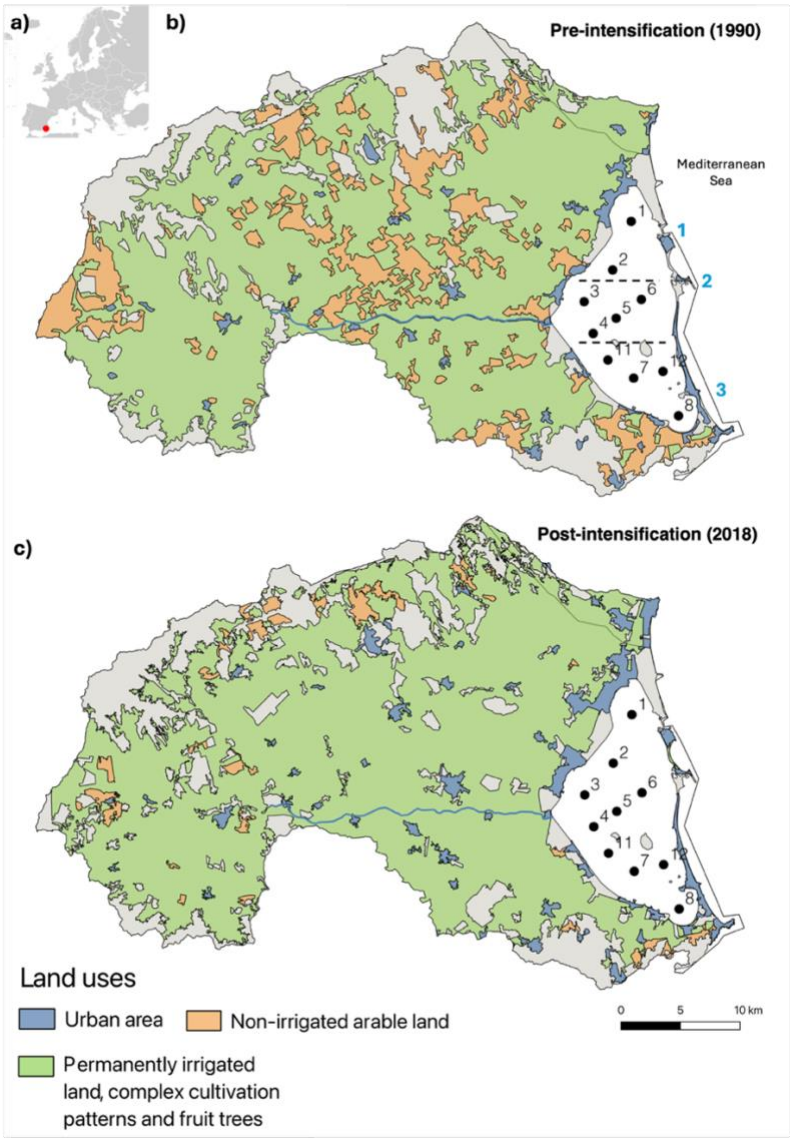


Figure 4.1 (a) Location of the Mar Menor coastal lagoon within Europe. (b-c) Land uses according to the CORINE land cover dataset for 1990 (b) and 2018 (c) from the Campo de Cartagena region and all the hydrological basins discharging to the Mar Menor lagoon, SE Spain, and location of the sampled sediment cores. The blue line represents the permanent Albujón river. In panel a, the dashed black lines separate North, Center, and South regions of the lagoon and blue numbers (1, 2 and 3) are, respectively, the channels Las Encañizadas (including Gola del Charco), El Estacio, and Marchamalo.

4.2.2 Sampling and sample processing

Details for core sampling, subsampling and ^{210}Pb dating can be seen in Chapters 2 and 3. Cores were considered to belong to North, Center, South C_{org}, TN, and carbon and nitrogen stable isotopic signatures ($\delta^{13}C$ and $\delta^{15}N$, respectively) were analyzed in sediment subsamples.

To constrain the main potential sources of nutrients to lagoon sediments, samples of vegetables, surface water algae, and benthic seagrass *C. nodosa,* and macroalgae *C. prolifera* were collected. Vegetables comprised citrus leaves, lettuce, celery, and almond tree leaves from the agricultural fields in Estación Experimental Agroalimentaria, Universidad Politécnica de Cartagena, which are some of the most common crops in the Campo de Cartagena basin (Centro Regional de Estadística de Murcia, 2026). *C. prolifera* specimens were collected close to cores 1, 4, 5 and 8, while *C. nodosa* specimens were sampled close to the sandbar, where there are some of its remaining monospecific meadows (Fig. 4.1). All these samples were frozen after collection, cleaned with deionized water, and seagrass and *C. prolifera* leaves were scraped to remove epiphytes. Then samples were dried at 65 ºC, ground with a ball mill , and weighed before C_{org} and TN analysis.

Additionally, we analyzed Suspended Particulate Organic Matter (SPOM) from the Albujón stream, the lagoon, and the Mediterranean Sea, which mainly consisted of *Posidonia oceanica* scrapes, as an additional source of nutrients to lagoon sediments. SPOM was sampled by filtering 2.5 to 11 L of lagoon, Albujón, and Mediterranean water through Whatman GF/F filters (diameter = 124 mm). These filters had been pre-combusted at 550 ºC during 24 h to remove all previous organic contamination, and right before filtering they were rinsed with deionized (DI) water to prevent breakage and avoid salt accumulation. After filtering, they were wrapped in aluminum foil and stored at -20ºC. Before analysis, samples were oven-dried at 65 ºC to constant weight, subsampled, and weighed for separate C_{org} and TN analyses. Albujón SPOM was considered a proxy for terrestrial inputs from the agricultural catchment, while Mediterranean *P. oceanica* was used as a proxy for Mediterranean influence.

4.2.3 Analytical methods

For C_{org} and $\delta^{13}C$ analyses, subsamples were decarbonated by adding HCl 1M and ensure only C_{org} was measured by an isotope ratio mass spectrometer (IRMS) (P. Kennedy et al., 2005). Sediments (0.1-0.3 g) were placed in 50 ml centrifuge tubes, acid was added to fill the volume of the tube, and samples were left to react overnight. After centrifugation and decantation, samples were rinsed with DI water and centrifuged again. This procedure was repeated four times to ensure the sample was at a neutral pH, after which they were oven-dried. Subsamples for TN and $\delta^{15}N$ were not pretreated and were analyzed directly. All samples were encapsulated in tin.

C_{org} and TN contents were determined with a Costech Elemental Analyser (ECS 4010) connected to a Thermo Scientific™ Delta V Advantage isotope ratio mass spectrometer at the Stable Isotope Biogeochemistry Laboratory (SIBL), at Durham University (United Kingdom). Isotopic accuracy was monitored through routine analyses of in-house standards, which were stringently calibrated against international standards (e.g., IAEA-600, IAEA-CH-3, IAEA-CH-6, IAEA-N-1, IAEA-N-2, NBS 19, USGS24, USGS40). International and in-house standards were run daily and provided a linear range for $\delta^{13}C$ between –46 ‰ and +3 ‰ and in $\delta^{15}N$ between –4.5 ‰ and +20.4 ‰. Analytical uncertainty in carbon and nitrogen isotope analysis was typically ±0.1 ‰ (2 sd) for replicate analyses of the international standards and <0.2 ‰ (2 sd) on replicate sample analysis. C_{org} and TN data were obtained as part of the isotopic analysis using the internal standard, glutamic acid (40.82 wt% C, 9.52 wt% N).

4.2.4 Mixing model setup for source contribution to nutrients

We applied the model MixSIAR to a mixture data consisting of $\delta^{13}C$ and $\delta^{15}N$ isotopic values (n = 285) collected from 10 sediment cores comprising surface to the ^{210}Pb dating horizon depth, which ranges from 15 to 30 cm of depth.

The model setup included core identity and age categories (Pre-1900, 1900–1950, 1950–1990, and 1990–2020) as categorical fixed effects, since these periods correspond to major phases of environmental change in the watershed, including a

period before the increased exchange with the Mediterranean Sea, the early urbanization process, and intensive agriculture and eutrophication dynamics. Uninformative priors were applied, assigning equal weight to all potential sources. Concentration dependence was integrated into the model to account for differences in composition among sources, ensuring that contributions were weighted according to their relative carbon and nitrogen content (Phillips & Koch, 2002), resulting in different C:N ratios in every source (i.e. *P.oceanica* C:N ratio = 42.9, *C.prolifera* C:N ratio= 14.2, Albujón SPOM C:N ratio= 12).

4.2.5 Spatial Interpolation and statistical analysis

Inverse Distance Weighting (IDW) was performed using a power parameter of p = 2 to explore the spatial distribution of carbon and nitrogen stocks and nutrient source contributions through the R package gstat (Pebesma, 2004). The obtained representations may exhibit local artifacts in the vicinity of sampling locations.

Since the distributions of C_{org}, TN, $\delta^{13}C$, and $\delta^{15}N$ deviated from normality, differences between regions were tested using the Kruskal-Wallis test followed by Dunn's post hoc test with Bonferroni correction. Depth intervals within cores were treated as individual observations; however, as these are not strictly independent, results should be interpreted as indicative of spatial patterns rather than formal statistical inference. The R package rshift (Room et al., 2023) was used to detect significant temporal shifts in C_{org}, TN, $\delta^{13}C$, and $\delta^{15}N$ sediment concentrations with depth (i.e., time). STARS algorithm (Sequential t-test Analysis of Regime Shifts) (Rodionov, 2004) was used for cases with a normal distribution (significance level = 0.05, cut-off length = 3 cm, which can amount to 2 to 15 years). The resulting Regime Shift Index (RSI) quantifies the magnitude of the shift (the more positive, the greater). Lanzante's non-parametric L-Method (Lanzante, 1996) was performed for non-normal distributions (significance level = 0.05), where the resulting p-values also express the significance and magnitude of the shift. Differences in carbon (CAR) and nitrogen (NAR) accumulation rates between time periods were evaluated using paired Wilcoxon signed-rank tests, with sediment cores treated as different samples from within each region.

4.3 Results

4.3.1 Depth profiles of C_{org} (%) and TN (%)

In all regions, the lowest C_{org} and TN concentrations occurred in the deepest sections, corresponding to pre-20th century sediments (Fig. 4.2), whereas maximum values were observed at the surface. Surface concentrations reached 9% and 1.1% in the north, 5.3% and 0.7% in the center, and 5.6% and 0.6% in the south for C_{org} and TN, respectively. Therefore, maximum surface values were almost twice as high in the northern region as in the rest of the lagoon.

The C_{org} and TN (%) profiles showed progressively increasing concentrations since the start of the 20th century, based on the temporal scale inferred from the ^{210}Pb-derived age model. In the north of the lagoon, both C_{org} and TN increased sharply around 1900 and continued to rise toward more recent sediments. In contrast, the central and southern cores showed a delayed increase, with concentrations rising significantly in the mid-20th century. Unlike the rest of the lagoon, the southern cores showed fluctuating values of both C_{org} and TN in the most recent surface layers, indicating a different pattern than in the rest of the lagoon.

No significant variability was observed in C_{org} and TN mass-weighted mean concentrations (%) among regions ($p > 0.05$) (Fig. 7.12). These values were, for C_{org} (%), 1.7 ± 0.3 in the northern region, 1.3 ± 0.7 in the central region, and 1.6 ± 1.3 in the southern region. Corresponding TN values were 0.2 ± 0.1, 0.2 ± 0.1, and 0.2 ± 0.2 %, respectively.

Alternatively, significant temporal differences were detected among periods ($p < 0.05$). Mass-weighted mean C_{org} concentrations increased from 0.6 ± 0.3 in pre-1900 sediments to 1.9 ± 0.9 (1900-1950), 3.2 ± 1.4 (1950-1990), and 3.9 ± 1.6 % (1990-2020). Post hoc comparisons indicated significantly lower values in the pre-1900 period relative to both 1950-1990 and 1990-2020 sediments. TN concentrations (%) showed a similar pattern, increasing from 0.08 ± 0.03 in pre-1900 sediments to 0.2 ± 0.1, 0.4 ± 0.2, and 0.5 ± 0.2 in the 1900-1950, 1950-1990, and 1990-2020 periods, respectively. Significant pairwise differences were detected between the pre-1900

and 1950-1990 and 1990-2020. Additionally, significant differences in C_{org} and TN contents were also observed between the periods of 1900-1950 and 1990-2020.

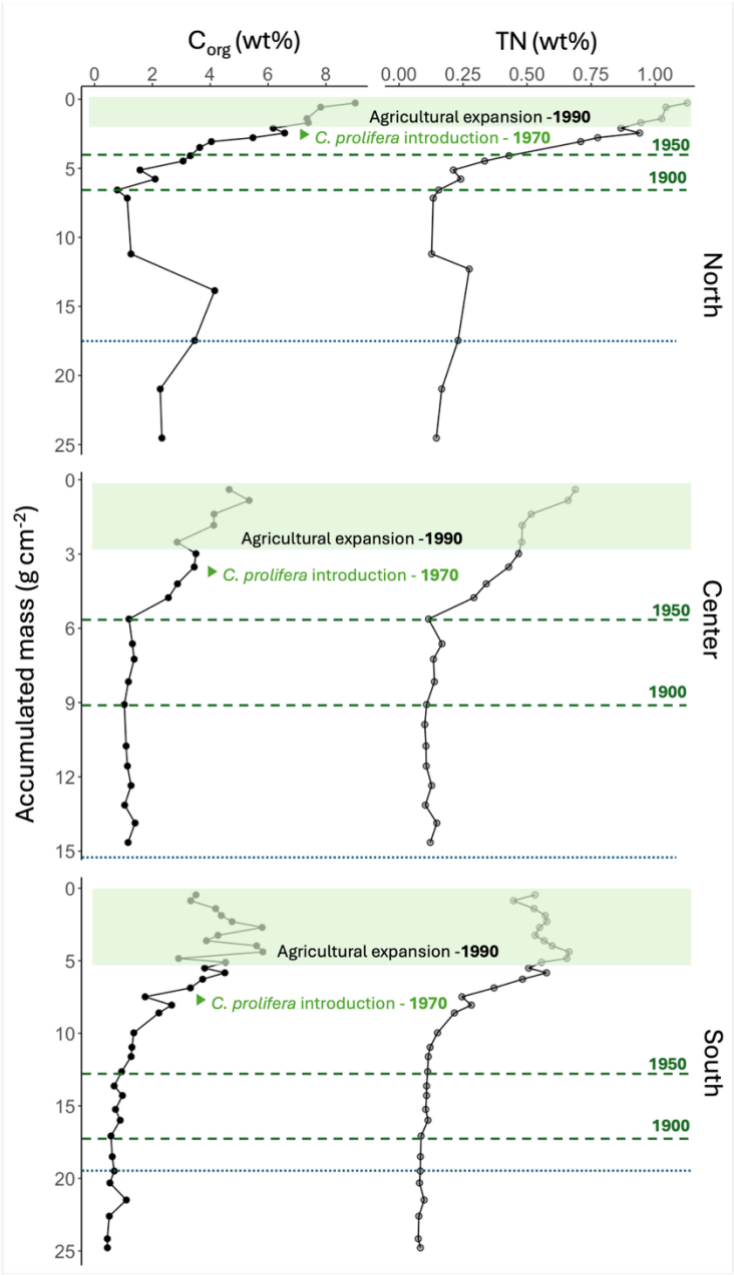


Figure 4.2 C_{org} and TN concentration profiles (%) of selected cores representative of the different lagoon sectors (OPC1 in the north, OPC5 in the center, and OPC7 in the south). Profiles for the rest of the cores are provided in the Supplementary Information for Chapter 4 (Figs. 7.13 and 7.14). Green shading indicates the period of agricultural expansion. The dotted line indicates 30 cm of depth.

4.3.2 Carbon and nitrogen stocks and accumulation rates

Carbon and nitrogen burial was evaluated using complementary metrics that capture different aspects of sediment nutrient dynamics, including stocks integrated over fixed depth (30 cm), stocks integrated over the last century and accumulation rates derived from ^{210}Pb dating. Spatial differences on C_{org} and TN stocks depended on whether they were calculated for the upper 30 cm of sediment or for the last century (Fig. 4.3). Stocks calculated over the standard upper 30 cm of sediment were highest in the northernmost (53 Mg C ha^{-1} and 6 Mg N ha^{-1}) and southwestern areas (~50–52 Mg C ha^{-1} and 6-7 Mg N ha^{-1}), whereas the southernmost and northwestern regions presented the lowest stocks (C ~24–28 Mg ha^{-1}, N ~4 Mg ha^{-1}).

In contrast, when stocks were integrated over the ^{210}Pb horizon (i.e. from ~1900 to present), they were highest in the southwestern region (ranging from 24 to 47 Mg C ha^{-1} and 4 to 6 Mg N ha^{-1}), while the lowest values occurred in the northwest (~20 Mg C ha^{-1}, ~3 Mg N ha^{-1}). This comparison highlights how stock estimates vary depending on the integration framework applied (a time-integrated ^{210}Pb horizon versus a fixed-depth, in this case 30 cm). Values for C_{org} and TN stocks at 30 cm were approximately 30% higher than values for the last 100 years. While the southwestern sector, with the highest sedimentation rates, consistently exhibited high values under both approaches, the northern region ranked among the highest when the fixed-depth was considered, reflecting differences between time-dependent and depth-dependent estimates.

Mean carbon and nitrogen accumulation rates (CAR and NAR, respectively), derived from ^{210}Pb dating, ranged from 12.6 to 51.8 g C m^{-2} yr^{-1} and from 1.7 to 5.9 g N m^{-2} yr^{-1}). CAR and NAR were greatest in the cores exhibiting the highest sediment mass accumulation rates (e.g., OPC7 and OPC8), in the south of the lagoon (Table 4.1). When divided by periods (1900-1950, 1950-1990, and 1990-2020), CAR and NAR showed a consistent temporal increase across most regions, with the highest values generally occurring during 1990-2020 and the lowest during 1900-1950 (Table 4.2). This pattern was particularly pronounced in the southern sector, where CAR increased from ~18–37 g C·m^{-2}·yr^{-1} in 1900-1950 to ~51–89 g C·m^{-2}·yr^{-1} in 1990-2020, and NAR from ~2–5 g N m^{-2} yr^{-1} to ~8–12 g N m^{-2} yr^{-1}. Increases were more moderate in the central and northern regions, but still evident (e.g., CAR from ~4–

15 to ~9–30 g C m^{-2} yr^{-1}), whereas the northern region exhibited lower rates overall. Despite these regional differences, the temporal trend of increasing accumulation toward the present was consistent across the lagoon.

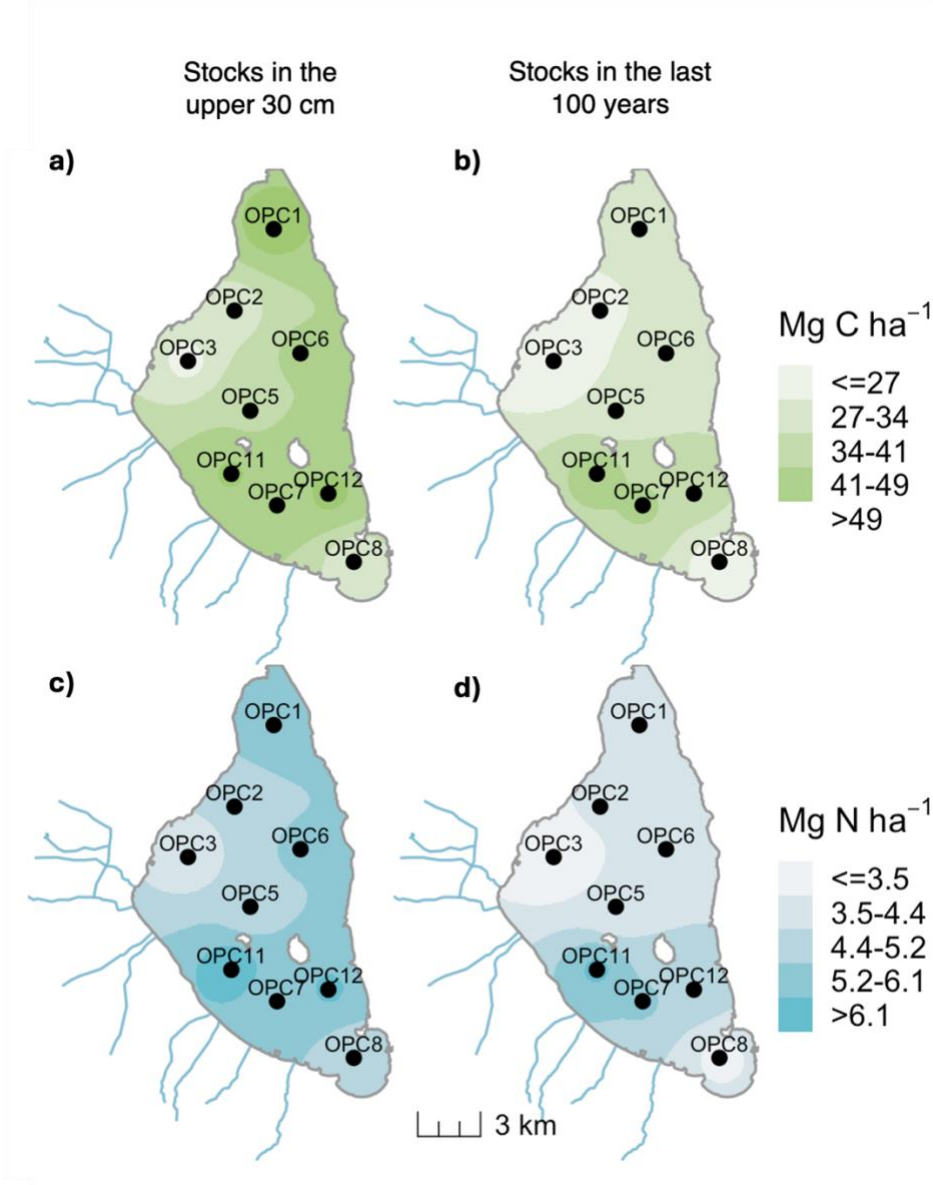


Figure 4.3 Spatial distribution of sediment C_{org} and TN stock maps (Mg · ha^{-1}) across the study area. (a, c) Stocks integrated over the upper 30 cm of sediment; (b, d) stocks accumulated over the last 100 years.

Table 4.1 Carbon (CAR) and nitrogen (NAR) accumulation rates (g $m^{-2} \cdot yr^{-1}$) since 1900 for dated cores in the lagoon.

Region	Core	MAR (g sed m^{-2} yr^{-1})	CAR (g C_{org} m^{-2} yr^{-1})	NAR (g TN m^{-2} yr^{-1})
North	OPC1	450 ± 40	17.5 ± 1.4	1.1 ± 0.2
	OPC2	730 ± 180	13.7 ± 3.4	1.9 ± 0.4
Center	OPC3	540 ± 160	12.6 ± 3.8	2.1 ± 0.6
	OPC4	1270 ± 250	25.9 ± 5.1	3.6 ± 0.5
	OPC5	740 ± 130	18.2 ± 3.3	2.8 ± 0.4
	OPC6	520 ± 70	24.0 ± 3.2	3.3 ± 0.4
South	OPC7	2000 ± 180	51.8 ± 4.4	6.8 ± 0.4
	OPC8	2000 ± 200	47.7 ± 5.0	8.0 ± 0.7
	OPC11	1200 ± 100	36.2 ± 2.1	5.1 ± 0.2
	OPC12	1100 ± 100	30.6 ± 2.3	4.1 ± 0.3

Table 4.2 Carbon (CAR) and nitrogen (NAR) accumulation rates (g $m^{-2} \cdot yr^{-1}$) for different historical periods in dated sediment cores from the Mar Menor lagoon.

Region	Core	Periods	CAR (g C_{org} m^{-2} yr^{-1})	NAR (g TN m^{-2} yr^{-1})
North	OPC1	1990-2020	34.7 ± 2.8	4.6 ± 0.4
		1950-1990	25.3 ± 2.0	3.0 ± 0.3
		1900-1950	7.7 ± 0.6	2.4 ± 0.1
	OPC2	1990-2020	24.6 ± 6.1	3.7 ± 0.9
		1950-1990	20.7 ± 5.1	2.8 ± 0.7
		1900-1950	7.5 ± 1.8	1.0 ± 0.3
Center	OPC3	1990-2020	8.6 ± 2.6	1.1 ± 0.3
		1950-1990	10.2 ± 3.1	1.4 ± 0.4
		1900-1950	5.8 ± 1.8	0.7 ± 0.2
	OPC4	1990-2020	36.6 ± 7.1	5.9 ± 1.1
		1950-1990	35.5 ± 11.1	6.2 ± 1.2
		1900-1950	-	-
	OPC5	1990-2020	30.2 ± 5.5	4.1 ± 0.7
		1950-1990	22.6 ± 4.1	2.8 ± 0.5
		1900-1950	3.9 ± 0.7	0.4 ± 0.1
	OPC6	1990-2020	34.3 ± 4.5	4.6 ± 0.6
		1950-1990	27.5 ± 3.6	3.7 ± 0.5
		1900-1950	14.8 ± 2.0	1.6 ± 0.2
South	OPC7	1990-2020	89.2 ± 7.6	11.5 ± 1.0
		1950-1990	48.2 ± 4.1	5.6 ± 0.5
		1900-1950	18.1 ± 1.6	2.2 ± 0.2
	OPC8	1990-2020	59.4 ± 6.2	8.7 ± 0.9
		1950-1990	38.3 ± 4.0	6.1 ± 0.6
		1900-1950	37.0 ± 3.9	4.9 ± 0.5
	OPC11	1990-2020	74.6 ± 4.3	10.7 ± 0.6
		1950-1990	38.8 ± 2.2	5.3 ± 0.4
		1900-1950	13.8 ± 0.8	1.7 ± 0.1
	OPC12	1990-2020	51.4 ± 3.9	7.5 ± 0.6
		1950-1990	29.8 ± 2.3	3.8 ± 0.3
		1900-1950	18.1 ± 1.4	2.2 ± 0.2

4.3.3 Depth profiles of $\delta^{13}C$ (‰) and $\delta^{15}N$ (‰)

Before 1900, $\delta^{13}C$ values showed pronounced spatial differences, with relatively enriched values in the northern region (~-14‰) and more depleted values in the central (~-22‰) and south regions (~-20‰) (Fig. 4.4). During the 20th century, $\delta^{13}C$ profiles displayed region-specific trajectories. In the northern region, $\delta^{13}C$ values increased progressively from the early 20th century, reaching maximum enrichment in the 1990s (-11‰), before declining toward present-day values (-14‰). In the central region, $\delta^{13}C$ values were strongly depleted in pre-1900 sediments, followed by a rapid enrichment during the first half of the 20th century that subsequently stabilized at less negative values in the upper layers. In the south region, $\delta^{13}C$ values were more variable before 1900, remained relatively stable until the mid-20th century, and then showed a marked enrichment followed by a subsequent decline toward recent values (-15‰). Across the lagoon, $\delta^{13}C$ values converged toward similar compositions in surface sediments from the different regions (~ -15‰), in contrast to the stronger differences observed in deeper layers.

$\delta^{15}N$ profiles exhibited pronounced temporal variability across the lagoon, revealing three distinct phases. Prior to the 20th century, $\delta^{15}N$ values were relatively low in the northern region (around 1‰), higher in the central region (approximately 5‰), and intermediate but variable in the south region (roughly 2.5–5‰), indicating spatial differentiation between the three regions. During the first half of the 20th century, $\delta^{15}N$ values declined in the northern and central regions, reaching minima in the mid-century (0.9‰), while the southern region maintained relatively elevated values (4‰). Around the 1970s, $\delta^{15}N$ increased sharply in the northern and central regions. In the south, $\delta^{15}N$ decreased progressively from 1960s until the 1990s, after which the isotopic signature began to increase sharply. All regions ultimately converged toward elevated $\delta^{15}N$ values in recent sediments (~ 4-5‰), though higher in the south, suggesting intensified and spatially homogenized nitrogen enrichment during the last decades.

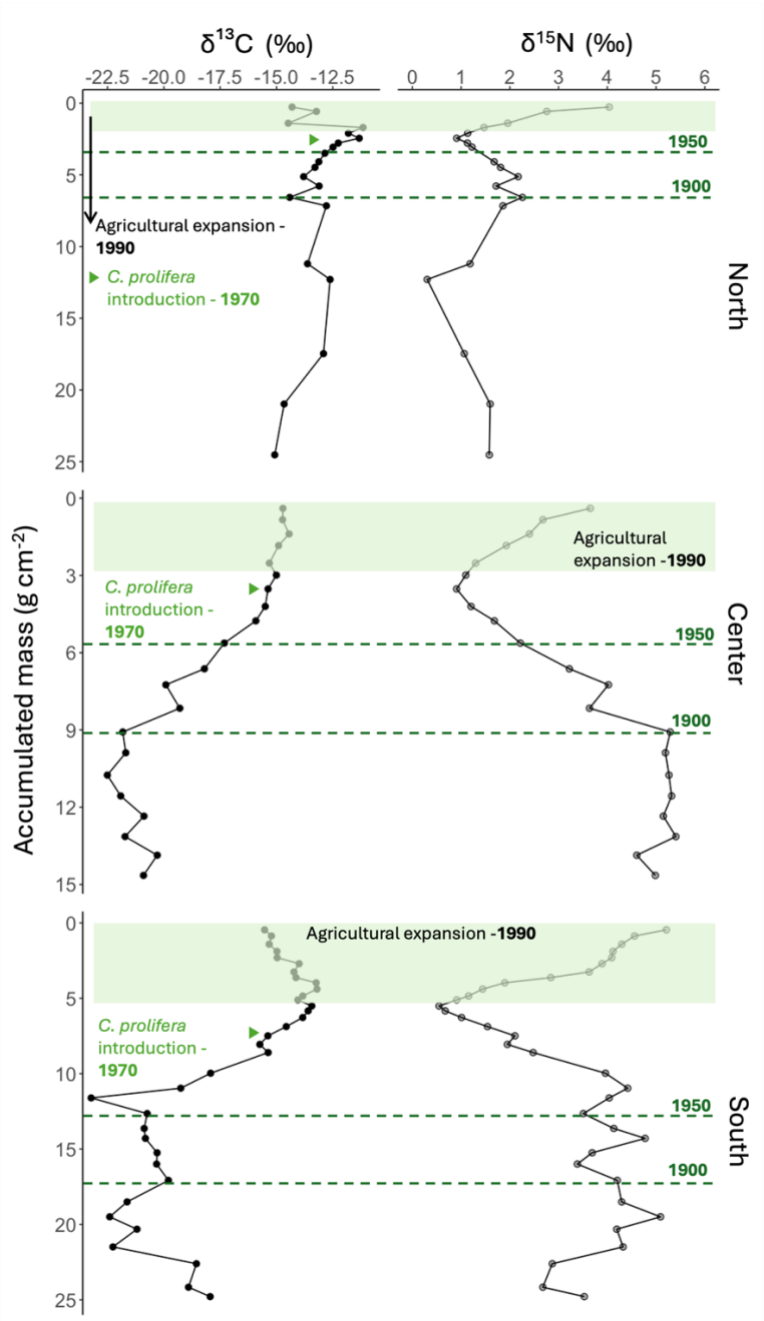


Figure 4.4 $\delta^{13}C$ profiles and $\delta^{15}N$ (‰) of selected cores representative of the different lagoon sectors (OPC1 in the north, OPC5 in the center, and OPC7 in the southwest). Profiles for the rest of the cores are provided in the Supplementary Information for Chapter 4 (Figs. 7.15 and 7.16).

4.3.4 Stable isotope mixing models

To characterize the sources of organic matter contributing to sediment nutrient burial, multiple mixing model configurations were tested. These combined potential endmembers representing the main organic matter inputs to the lagoon (i.e. sources): SPOM from the Albujón stream (terrestrial proxy), water surface algae, *C. prolifera* and *C. nodosa* in the lagoon, and *P. oceanica* in the Mediterranean Sea (Mediterranean proxy). Model configurations evaluated are detailed in the Supplementary Information for Chapter 4 and included configurations with and without concentration dependence, as well as five-sources and reduced three-source models (Albujón SPOM, *C. prolifera*, and *P. oceanica*). The final model with concentration dependence retained all five endmembers, as this configuration best constrained the isotopic space occupied by the sediment samples in the $\delta^{13}C$ and $\delta^{15}N$ crossplot (Fig. 4.5).

Sediment C_{org} and TN exhibited $\delta^{13}C$ and $\delta^{15}N$ values consistent with a mixture of sources mainly bounded by terrestrial organic matter (Albujón SPOM $\delta^{13}C$(‰) = -26.2; $\delta^{15}N$(‰) = 8.4) and Mediterranean-derived *P. oceanica* organic matter ($\delta^{13}C$(‰) = -12.8 ± 1.6; $\delta^{15}N$(‰) = 1.3 ± 0.3), with additional influence from other primary producers such as *C. prolifera* (Fig. 4.5). The relative position of sediment samples within this isotopic space varied with sediment age, indicating temporal changes in source contributions.

Sediment samples predating the 20th century showed a wide range in $\delta^{13}C$ and $\delta^{15}N$ (i.e., from -10 to -25‰ and from 0 to 6‰, respectively), which points to large variability in source contributions. Additionally, they were most closely associated with terrestrial isotopic signatures relative to later periods. Dated sediments from the late 20th and 21st century showed closer isotopic values to Mediterranean sources and *C. prolifera*. During the 1900-1950 period, $\delta^{13}C$ values became slightly less negative, while $\delta^{15}N$ values remained comparable to earlier ones. Between 1950 and 1990, $\delta^{15}N$ values decreased, and $\delta^{13}C$ values continued to become less negative. From 1990 to 2020, $\delta^{15}N$ values increased, whereas $\delta^{13}C$ values remained relatively stable. A few post-2016 samples that showed signatures similar to the Albujón endmember were from a core collected near the Albujón stream mouth and corresponded to a

rapid deposition event and show the highest $\delta^{15}N$ values (Alorda-Montiel et al., 2025).

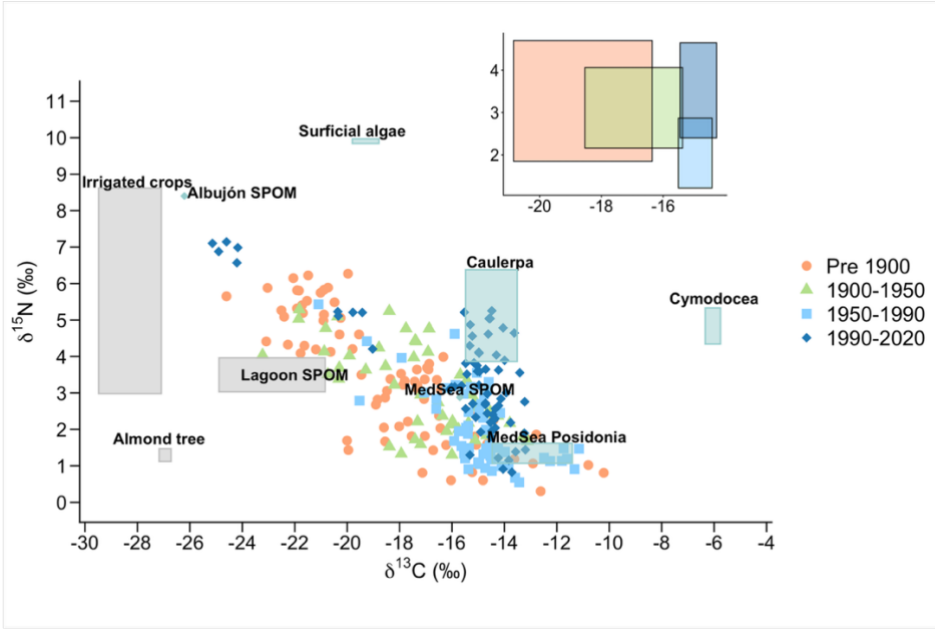


Figure 4.5 Crossplots of $\delta^{13}C$ and $\delta^{15}N$ values for sediment samples and sampled endmembers. Values for sediment samples are coloured by period Pre 1900, 1900-1950, 1950-1990, and 1990-2020. The subgroup of five 1990-2020 samples close to Albujón SPOM are the ones estimated to come from a rapid deposition event. All collected endmember ranges are displayed in boxes. Grey boxes represent the unused endmembers in the final model, while selected endmembers are shown in light teal color (Surficial algae, *C. prolifera*, MedSea Posidonia, and *C. nodosa*). The inset in the upper-right quadrant shows the central 50% of the values of each period distribution.

Different model configurations showed consistent large-scale patterns. Terrestrial contributions (represented by Albujón SPOM) and Mediterranean contributions (represented by MedSea Posidonia) constituted the main sources of organic matter to the sediments from all the represented endmembers (Fig. 4.6). Across the lagoon and through all periods, Mediterranean contributions to nutrients dominated sediment organic matter (68 to 77%), although its spatial distribution varied. General terrestrial contributions ranged from 13 to 21%.

Between 1900 and 1950, sediment organic matter derived from the Mediterranean was particularly dominant in the northern sector where contributions exceeded 80%. Lower Mediterranean influence (55-65%) and comparatively higher terrestrial contributions (25-30%) were observed in the southern and southwestern lagoon, indicating a marked north-south spatial gradient in source composition. Terrestrial-derived organic matter generally accounted for 15-25% of the sediment pool across the lagoon during this period.

From 1950 to 1990, Mediterranean contributions remained dominant throughout most of the lagoon (> 65–80%), particularly in the north and central-eastern sectors, while relatively greater terrestrial influence persisted near the western shore and southern region. During this period, contributions from the macroalgae *C. prolifera* first appeared in the sediment organic matter pool, although they remained relatively low (generally 1-6%) and spatially restricted to southern and southwestern areas.

During 1990-2020, Mediterranean-derived organic matter continued to dominate the lagoon sediment pool, especially in central and eastern sectors not directly influenced by fluvial inputs. However, terrestrial contributions increased again in areas affected by the Albujón stream and the southern lagoon, where values commonly reached 20-30%. At the same time, *C. prolifera* contributions became more widespread and increased in magnitude, particularly in southern and southwestern sectors where they reached up to 8-11%. Overall, the mixing model results indicate a long-term transition toward Mediterranean-dominated sediment organic matter, while retaining localized terrestrial enrichment associated with fluvial influence and the recent expansion of macroalgal inputs.

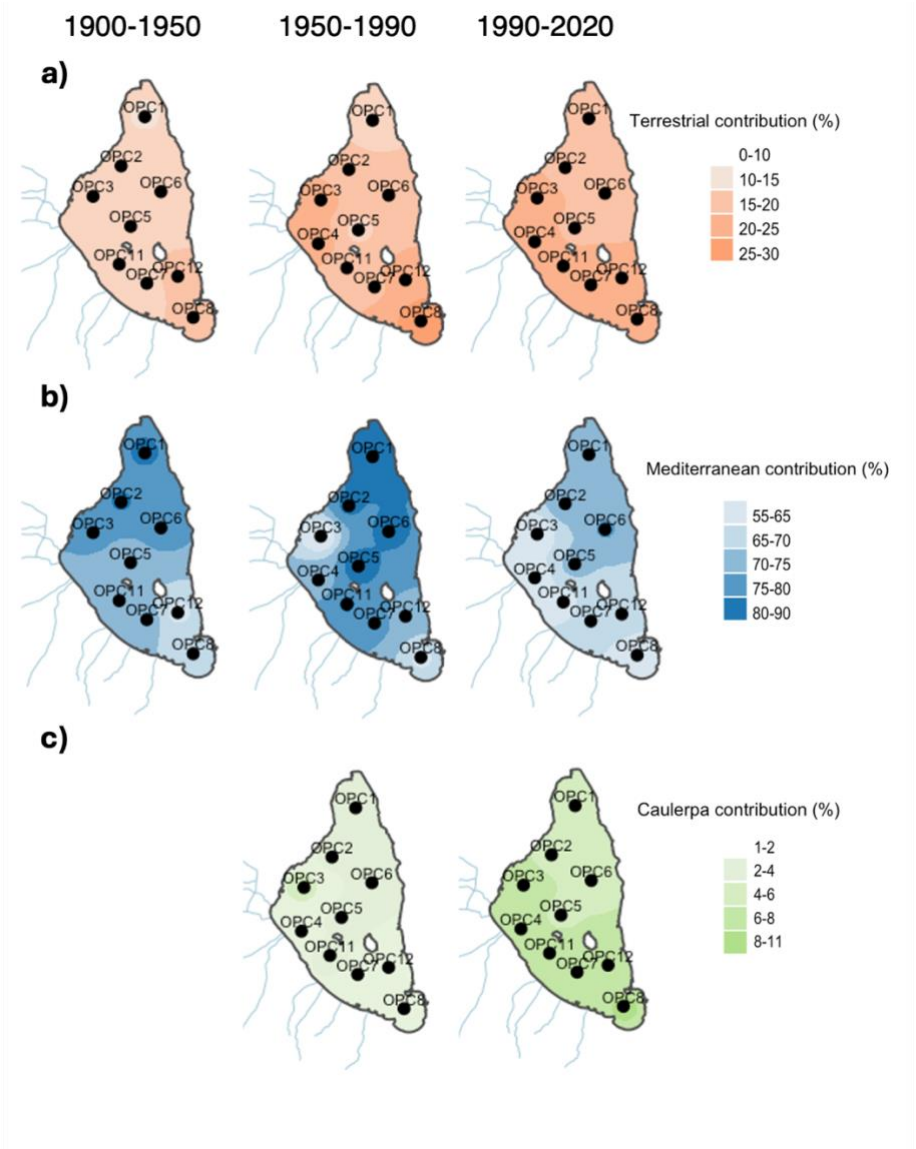


Figure 4.6 Spatially interpolated C_{org} and N source contributions to the sediments (%) of Albujón SPOM (Terrestrial contribution), *P.oceanica* (Mediterranean contribution) and *C. prolifera* sources for 1900-1950, 1950-1990, and 1990-2020 for the model with five endmembers and concentration dependence. Other model configuration results can be found in Supplementary Information. Contributions from *C. prolifera* are only shown for the 1950–1990 and 1990–2020 periods, consistent with its introduction to the lagoon in the 1970s.

4.4 Discussion

4.4.1 Human activities and derived stressors have reshaped nutrient sources and sediment organic matter composition

The $\delta^{13}C$ and $\delta^{15}N$ records illustrate how land use and hydrodynamic modifications since the start of the 20th century altered the composition and sources of organic carbon and nitrogen preserved in lagoon sediments. Before the 20th century, sediments exhibited marked spatial heterogeneity in both isotopic ratios (Fig. 4.4), suggesting stronger spatial separation of organic matter sources and nutrient dynamics across the lagoon prior to the major hydrodynamic and watershed transformations of the 20th century. Breaches of the sandbar in the late 19th century (Perez-Ruzafa et al., 1991) may have contributed to the progressive Mediterranean influence observed afterwards by enhancing lagoon-sea connectivity.

During much of the 20th century, $\delta^{15}N$ values decreased in the central and southern regions, while $\delta^{13}C$ values became progressively less negative. It is important to note that the stable isotope records and mixing model outputs primarily reflect the sources of organic matter ultimately preserved in lagoon sediments. Consequently, the estimated source contributions represent the fraction of nutrients that escaped remineralization and became buried, rather than the total nutrient load entering the lagoon or directly sustaining primary production in the water column. Therefore, the dominance of Mediterranean-derived organic matter in the sedimentary record during much of the 20th century should not be interpreted as evidence that marine sources dominated the overall nutrient inputs to the ecosystem. Contemporary eutrophication dynamics in the Mar Menor are instead strongly linked to terrestrial nutrient inputs, particularly dissolved inorganic nitrogen associated with agricultural runoff (Rodriguez-Puig et al., 2026).

In this context, these concurrent isotopic shifts indicate increasing Mediterranean influence and enhanced water exchange. This evidence supports a transition from a more hydrologically restricted lagoon toward a system increasingly influenced by Mediterranean-derived organic matter and enhanced lagoon-sea exchange. Hydrodynamic modifications further reinforced this shift. The widening of the

Estacio channel in 1973 for navigation purposes, driven by increasing urban development around the lagoon, altered circulation patterns (López-Castejón et al., 2026) and lowered salinities (Pérez-Ruzafa et al., 1987). These modifications enhanced water exchange with the Mediterranean Sea and reinforced the transition toward a more marine-influenced system already underway during the early 20th century. The isotopic evidence is also consistent with documented ecological changes in the lagoon such as the introduction of *C. prolifera* during the late twentieth century (Belando et al., 2021).

From the 1970s onward, $\delta^{15}N$ values increased consistently across the lagoon. This rise reflects the growing influence of isotopically enriched nitrogen sources, which could be *C. prolifera* (average $\delta^{15}N$ 5.3 ± 1.0‰), increasing terrestrial inputs from intensive agriculture, organic fertilizers delivered through the Albujón stream (average 17.4 ± 1.2‰; Choi et al., 2006), and sewage discharges (between 4 and 19 ‰, Xue et al., 2009). Similar enrichments in coastal lagoons have often been linked to raw household sewage discharges from expanding populations (Farias et al., 2024; Marín-Guirao et al., 2008). In the Mar Menor, this isotopic changed aligns with increasing anthropogenic nutrient loading due to agricultural activity and urban pressures, which changed the earlier Mediterranean-driven isotopic shift. Simultaneously, the introduction and expansion of *C. prolifera* after the 1970s modified the composition of the sedimentary nitrogen and organic carbon pool mostly in the south and southwest of the lagoon, coinciding with the areas showing the greatest macroalgal cover (Belando et al., 2021). Prior to this shift, the Mar Menor lagoon was extensively covered by submerged seagrass meadows, including *C. nodosa*, *Zostera marina*, *Zostera nana*, and *Ruppia maritima* (Lozano, 1954; Simonneau, 1973). The widespread occurrence of *C. nodosa* before the late twentieth century supports its use as a representative marine endmember for the pre-eutrophication period.

The southern sector displayed a different trajectory. There, the $\delta^{13}C$ signature remained relatively stable between 1900 and 1950 before shifting toward less negative values, suggesting that terrestrial inputs remained comparatively important for longer. Only after mid-century did $\delta^{13}C$ enrichment parallel that observed in the northern and central sectors, indicating delayed but eventual integration into the broader Mediterranean-influenced regime. This spatial heterogeneity highlights that

hydrodynamic connectivity and internal productivity did not evolve synchronously across the lagoon.

An additional and noteworthy outcome of these isotopic trends is the progressive convergence of $\delta^{13}C$ and $\delta^{15}N$ values toward similar compositions in surface sediments across the lagoon. Whereas pre-20th century sediments exhibited pronounced spatial heterogeneity, recent deposits show reduced isotopic differentiation among regions, suggesting increasing spatial homogenization of nutrient sources and processing pathways, likely driven by system-wide anthropogenic pressures.

This interpretation should, however, be considered in light of methodological and diagenetic constraints. Down-core increases in C_{org} and TN concentrations may partially reflect post-depositional alteration, as older sediments have been exposed to longer periods of remineralization, which can preferentially remove labile organic matter and reduce nitrogen contents through diagenetic processes. Furthermore, differential preservation among organic matter sources may alter their relative representation downcore, as more labile material is preferentially degraded while more recalcitrant fractions are retained. Consequently, reconstructed source contributions may partly reflect differences in preservation potential in addition to changes in organic matter inputs through time. In addition, mixing model outputs rely on the assumption of temporally constant source signatures, and the use of present-day endmembers may bias reconstructed contributions, particularly for older sediments. Although the isotopic composition of primary producers likely varied through time in response to changing environmental conditions, published $\delta^{13}C$ and $\delta^{15}N$ values, including relatively oligotrophic Mediterranean sites, are broadly comparable to those measured in this study (H. Kennedy et al., 2010; Mascaró et al., 2009). This suggests that the selected endmember falls within the range reported for the species. This limitation may be particularly relevant for fertilizer $\delta^{15}N$, as isotopic signatures can vary substantially depending on fertilizer type, production pathway, and the degree of transformation before reaching the lagoon. The mixing model also assumes conservative isotopic mixing, while potential post-depositional fractionation processes are not explicitly evaluated. For example, denitrification may preferentially remove ^{14}N and enrich the remaining sedimentary nitrogen pool in

^{15}N (F. Tang & Maggi, 2012), whereas methanogenesis under strongly reducing conditions may also modify isotopic compositions (Whiticar, 1999).

Despite these limitations, the consistency of temporal trends across multiple cores, together with known historical changes in land use and hydrodynamics, supports the robustness of the observed long-term patterns. Differences between mixing model configurations were most evident for the 1900–1950 interval, highlighting greater uncertainty in reconstructing early nutrient sources, whereas trends in recent decades were robust across models. The comparison also highlights the influence of concentration dependence on estimated source contributions, suggesting that its inclusion may improve the representation of organic matter mixtures in systems where sources differ in elemental composition. Therefore, the mixing model results are interpreted primarily as evidence of relative temporal changes in sedimentary organic matter sources rather than as precise quantitative reconstructions of historical source contributions.

4.4.2 Sediment nutrient stocks and accumulation rates reflect different facets of nutrient storage and burial efficiency

Sediment nutrient stocks and accumulation rates in the Mar Menor lagoon diverge spatially, revealing that areas of high C_{org} and TN storage do not necessarily coincide with areas of efficient burial (Fig. 4.3). These patterns indicate that long-term nutrient storage and contemporary burial efficiency represent complementary but distinct aspects of sediment functioning within the lagoon.

High C_{org} stocks in the upper 30 cm provide information on potential remobilization of nutrient-enriched surface sediments, which are particularly susceptible to wind-induced resuspension. In the Mar Menor lagoon, this potential vulnerability is particularly relevant in the northern lagoon and near the Albujón stream mouth, where large stocks may pose a higher risk under enhanced resuspension conditions, a process already identified as a major pathway for nutrient release (Morote-Sánchez et al., 2025).

Temporally, both CAR and NAR across the lagoon were significantly higher during 1990-2020 compared to earlier periods ($p < 0.05$), with the largest differences

observed between 1900-1950 and 1990-2020. This pattern indicates a clear intensification of nutrient burial during recent decades, consistent with increased sedimentation rates and enhanced external nutrient inputs. The southern sector exhibited the largest accumulation rates, driven by high sedimentation, produced by a combination of stream inputs and lagoon hydrodynamics (Alorda-Montiel et al., 2025). These areas, therefore, represent the most efficient C_{org} and TN burial zones within the lagoon, potentially reducing remineralization losses while contributing to nutrient removal from the water column and partially buffering the eutrophication processes experienced by many coastal lagoons under increasing nutrient loads.

Mean C_{org} burial rates (CAR) in the southern Mar Menor (30.6 ± 2.3 to 51.8 ± 4.4 g $C \cdot m^{-2} \cdot yr^{-1}$; median of 25 g C m^{-2} yr^{-1}) were comparable to global burial rates estimates reported for seagrass ecosystems (mean±SD: 44 ± 80 g $C \cdot m^{-2} \cdot yr^{-1}$; median of 25 g $C \cdot m^{-2} \cdot yr^{-1}$) (Arias-Ortiz et al., 2026). In the rest of the lagoon, CAR values were also comparable or lower, reflecting reduced MARs and less focused sedimentation. Mean nitrogen burial rates (NAR), ranging from 1.1 ± 0.2 to 8.0 ± 0.7 g $N \cdot m^{-2} \cdot yr^{-1}$, were also within the range reported for other vegetated coastal ecosystems. A recent global synthesis reported median accumulation rates of 7.52 g $N \cdot m^{-2} \cdot yr^{-1}$ (IQR of 4.12-13.61) in mangroves and 8.19 g $N \cdot m^{-2} \cdot$ yr-1 (IQR of 5.37 to 12.44) in salt marshes (Langley et al., 2025). Additionally, NAR values observed in the Mar Menor were comparable to those reported by de los Santos et al., (2022) for a sheltered bay affected by urbanization and aquaculture with *C. nodosa* and *C. prolifera* monospecific meadows. However, there is a significant lack of reported NAR values in the literature, particularly in macroalgae-dominated systems, limiting broader comparisons. and highlighting a critical gap in understanding long-term nitrogen burial in coastal vegetated habitats.

This distinction between nutrient stocks and burial rates is particularly relevant in blue carbon studies, which often focus on C_{org} stocks at fixed depths without accounting for accumulation rates, despite burial efficiency ultimately depending on sediment accumulation processes. Beyond the specific dynamics of the Mar Menor lagoon, these findings also contribute to the broader discussion regarding the role of macroalgae-dominated ecosystems in C_{org} and nitrogen cycling. Historically, macroalgae have been excluded from the blue carbon framework, which focuses on seagrasses, mangroves, and salt marshes due to their well-documented capacity for

long-term burial (Duarte et al., 2013). This exclusion is largely based on the assumption that macroalgae grow predominantly on hard substrates, which prevents them from developing C_{org} sedimentary deposits (Duarte et al., 2013). However, this assumption is likely not true for rhizophytic macroalgae like *C. prolifera* (Hendriks et al., 2010), and there is increasing evidence that macroalgae support significant C_{org} burial (Bellgrove, 2016; Hill et al., 2015; Krause-Jensen et al., 2018; Moreda et al., 2024), Particularly, in Mediterranean shallow bays, *C. prolifera* has been found to significantly contribute to C_{org} accumulation, because of its dense canopy and root systems (de los Santos et al., 2022; Moreda et al., 2024), and significant recalcitrant fraction of C_{org} (Yamuza-Magdaleno et al., 2024).

In the Mar Menor, where *C. prolifera* is presently the primary marine primary producer (Belando et al., 2021; Terrados & Ros, 1991), 30-cm C_{org} stocks under its mats (25 – 53 Mg C_{org} · ha^{-1}) overlap and in some cases exceed the interquartile range values reported for seagrass ecosystems over the same depth (12 - 45 Mg C_{org} · ha^{-1} Krause et al., 2025). However, mixing models indicate that only a fraction of the sedimentary nutrient pool (< 12%) is directly attributable to *C. prolifera* (Fig. 4.6), suggesting that these elevated stocks reflect the accumulation of organic matter from multiple sources rather than macroalgal production. Instead, *C. prolifera* likely contributes indirectly to the preservation of older C_{org} stocks by enhancing sediment retention.

4.4.3 Multiple stressors drive nutrient dynamics and ecosystem transitions

The Mar Menor coastal lagoon has already undergone two major ecosystem transitions during the 20th and early 21st centuries, reflected in the sediment records documented in this study. The first involved a gradual increase in the contribution of Mediterranean-derived organic matter preserved in lagoon sediments, reflecting enhanced lagoon-sea exchange, and was recorded in the sediment archive through the progressive $\delta^{13}C$ enrichment and $\delta^{15}N$ decline observed primarily in the northern and central regions during much of the 20th century. The second corresponded to increasing anthropogenic nutrient loading associated with agricultural intensification in the Campo de Cartagena watershed, reflected by renewed $\delta^{15}N$ enrichment after

the 1970s together with increasing terrestrially-derived contributions in the 1990-2020 mixing model outputs.

These transitions occurred at different temporal scales. The increase in marine influence developed progressively throughout the 20th century as hydrological connectivity with the Mediterranean Sea increased, whereas the shift from oligotrophic to eutrophic conditions occurred more rapidly. The late-20th century increases in $\delta^{15}N$ values across all regions, together with renewed terrestrial contributions in the 1990-2020 mixing model outputs, indicate an accelerated increase in anthropogenic nutrient loading preceding the 2016 collapse, mainly due to the intensification of agriculture.

Since the 1990s, elevated anthropogenic nutrient inputs promoted the expansion of *C. prolifera* meadows and enhanced phytoplankton activity (Instituto Español de Oceanografía, 2020; Lloret et al., 2005). Eventually, the lagoon's buffering mechanisms failed, and the ecosystem exhibited dynamics consistent with a tipping point (Scheffer et al., 2001) in 2016. During this collapse, water quality deteriorated sharply, and the lagoon entered a new eutrophic state that persisted until 2018, when conditions temporarily returned to pre-2016 levels. However, full recovery did not occur: *C. nodosa* monospecific meadows are now restricted to localized shallow areas, while *C. prolifera* has become the dominant macrophyte species across most lagoon bottoms (Instituto Español de Oceanografía, 2020)

This shift reflects well-documented mechanisms of ecosystem phase transitions from seagrass- to macroalgae-dominated states (Duarte, 1995), driven primarily by elevated nutrient concentrations, increased turbidity, and reduced light availability, all of which disproportionately affect seagrasses. Subsequent anoxic and eutrophic episodes in Mar Menor lagoon in 2019 and 2021 further reflect the system's instability. The current dominance of *C. prolifera*, with its ability to grow under low-light conditions and recover quickly, may enhance ecosystem resilience to eutrophication.

This study identifies the southwestern sector of the lagoon as a particularly vulnerable area. It exhibits the highest carbon and nitrogen accumulation rates, together with some of the largest sedimentary nutrient stocks, reflecting intense

depositional dynamics. Its proximity to the Albujón stream mouth and hydrodynamic conditions characterized by relatively long water residence times further increase its susceptibility to hypoxia, as nutrient-rich inputs and accumulated organic matter can enhance oxygen consumption during periods of stratification. These conditions exemplify potential feedback loops that could be triggered in the event of a new highly eutrophic event. Macrophyte loss could enhance the resuspension of organic-rich sediments, releasing large nutrient stocks and further intensifying eutrophication and oxygen depletion in the water column (Morote-Sánchez et al., 2025).

Potential additional consequences could include higher CO_2 and CH_4 emissions from the lagoon (Vallejo et al., 2021), the release of the toxic metal concentrations stored in Mar Menor sediments (maximum of 3400 mg kg^{-1} of Pb) into the water column (Alorda-Montiel et al., 2025; Santos-Echeandía et al., 2023), and an increased formation of more harmful contaminant species such as methylmercury (Lavergne et al., 2025). The convergence of these stressors could produce long-lasting impacts on the lagoonal ecosystem. These effects could be amplified during extreme events such as the 2019 extreme precipitation event, when nutrient and metal-enriched runoff (Cuevas et al., 2025) could act synergistically with resuspension. Consequently, reducing nutrient inputs to the lagoon, which has proven effective at recovering seagrass populations (Greening & Janicki, 2006), remains the most urgent and widely supported measure (Guaita-García et al., 2022) to prevent further degradation and aim for the recovery of the Mar Menor socioecological system.

5. Response of soil carbon, nitrogen, and greenhouse gas fluxes to tidal marsh restoration

Tenim a tocar l'aigua
i no ens sabem mullar.

Mireia Calafell

5.1 Introduction

The extent to which coastal wetland restoration reinstates biogeochemical functioning remains uncertain, as recovery trajectories can take decades and vary widely among sites (Kasak et al., 2026; Moreno-Mateos et al., 2012; Valach et al., 2021), depending on vegetation establishment, latitude, and changes in hydrology and disturbance. Restored coastal wetlands have been found to achieve 37-76% of soil carbon and 43-83% of soil nitrogen compared to natural wetlands within decades (H.-Y. Chen et al., 2025), yet full recovery of ecosystem functioning may require longer timescales (Brown & Norris, 2018), and active restoration strategies may be needed to accelerate successional trajectories (Allan et al., 2024).

These uncertainties highlight the need to understand better how soil processes respond to restoration and how they translate into ecosystem-scale carbon and nitrogen dynamics. Evaluating wetland restoration outcomes requires assessing how key ecosystem functions, such as nutrient burial and greenhouse gas exchange, respond over time (Billah et al., 2022). Soil-based measurements, including changes in carbon and nitrogen stocks or accumulation rates, are widely used to assess restoration effects, as they integrate long-term biogeochemical processes. Stock changes or burial integrate the net result of carbon and nitrogen gains (e.g. net ecosystem exchange, including allochthonous carbon and nitrogen deposition, and nitrogen fixation) and losses (e.g. respiration as CO_2 or CH_4, denitrification, and lateral exports of dissolved species of carbon and nitrogen) (Arias-Ortiz et al., 2021; Bai et al., 2020). However, soil-based approaches do not account for CH_4 emissions, are limited in spatial scale and sampling frequency and the signal/effect of restoration is often challenging to detect due to the slow nature of soil accretion (Ballantine & Schneider, 2009). In contrast, eddy covariance (EC) measurements (D. D. Baldocchi et al., 1988) provide continuous and spatially integrated observations of the net vertical exchange of gases between ecosystems and the atmosphere, capturing the variability of ecosystem responses before, during, and after restoration interventions such as tidal reconnection (D. D. Baldocchi, 2020). While EC is primarily used to quantify CO_2 and CH_4 fluxes, direct measurements of nitrogen gases are less common (for N_2O) or technically challenging (NH_3) (Kroon et al., 2010; Moravek et al., 2019). Additionally, EC cannot supply information on past conditions or lateral fluxes between wetlands and adjacent water bodies, an

important process in tidal contexts (Bogard et al., 2020; Y. Gao et al., 2018). Therefore the combination of these approaches, often applied independently, offers the potential for obtaining a more comprehensive picture of how restoration affects carbon and nitrogen cycling in coastal wetlands.

Here, we combine high-frequency eddy covariance measurements of land-atmosphere carbon fluxes with soil carbon and nitrogen stocks in an estuarine marsh before and after tidal reconnection to assess the post-restoration trajectory of wetland carbon and nitrogen cycling. Tidal reconnection is a widely implemented wetland restoration strategy, increasingly promoted within blue carbon frameworks for its potential to enhance carbon sequestration and reduce greenhouse gas emissions (e.g. BlueCAM Australia, Lovelock et al., 2023). However, despite its recognized climate mitigation potential, substantial uncertainties remain regarding the temporal trajectory of ecosystem recovery and its short and long-term biogeochemical implications. To address this, we characterize soil concentration profiles and stocks of organic carbon and total nitrogen (sampled before and after restoration in 2021 and 2024, respectively) and analyze temporal dynamics of CO_2 and CH_4 fluxes via EC measurements conducted from seven months before tidal reconnection to 4 years after. By combining soil and atmospheric data, we evaluate whether tidal reconnection promotes a rapid recovery of carbon and nitrogen sink function or if the ecosystem remains a net source. Additionally, we assess the extent to which soil carbon dynamics are coupled with atmospheric fluxes.

5.2 Methods

5.2.1 Study site

This study was conducted in a tidally reconnected wetland, the Hill Slough marsh (Lat: 38.2368, Long: -122.0212; AmeriFlux ID: US-Hsm), located in the Hill Slough Wildlife Area in Suisun Bay (California, USA), near the confluence of the Sacramento and San Joaquin rivers (Fig. 5.1). The wetland covers an area of approximately 2.6 km^2, with elevation ranging from 0.7 to 2.1 m (NAVD88) and is characterized by a Mediterranean climate with wet, cool winters and dry, hot summers (Knox et al., 2015). The area includes alluvial soils, inceptisols of minimal

horizon development —typical of young geomorphic surfaces— in the upper areas of the wetland, and histosols, rich in organic matter, at lower elevations (UC Davis map of soils, 2026).

At the regional scale, tidal wetlands across the upper San Francisco estuary have undergone extensive hydrological modification since the mid-19th century. In the Sacramento—San Joaquin Delta, extensive tidal freshwater marshes historically covered an area of ~2200 km^2 (Shlemon & Begg, 1975), much of which was drained and converted to agriculture, leaving only about 10% of the original extent remaining by 1950 (Callaway et al., 2011). In Suisun Bay, which is located downstream of the Delta, wetlands were also extensively diked and hydrologically modified but were more commonly managed as seasonal wetlands rather than fully converted to agriculture (Moyle et al., 2014). As a result, before restoration, Hill Slough marsh functioned as a managed seasonal wetland, experiencing ponding and waterlogging during the rainy season (November - March), and remaining mostly dry during the rest of the year, when it was primarily used for cattle and sheep grazing.



Figure 5.1 a) Location map of the Hill Slough wetland in the Sacramento-San Joaquin Delta system, California, USA. b) Sediment core sampling sites within the wetland (blue) and the location of the eddy covariance tower (US-Hsm) (red). White contour lines depict the tower footprint for the period 2021-2024. From smallest to largest, they correspond to the 50, 60, 70, 80, and 90% upwind area that contributes to the measured fluxes. The footprint was calculated following Hsieh et al., (2000).

Restoration was carried out on 5 October 2021 by Ducks Unlimited through levee breaching and lowering at five locations to reintroduce tidal exchange, promote vegetation growth, and improve habitat conditions for wildlife (Kasak et al., 2026). Following restoration, the site became influenced by a semidiurnal tidal regime, resulting in regular inundation of low-lying areas. The current mean tidal range at the site throughout the year is 0.70 ± 0.01 m. Low tides expose the soil surface, and high tides reach 1.27 m above ground level (Busquets-Rubiés et al., under preparation). The site is brackish, with salinity currently fluctuating from 0.5 in winter to 12 in summer.

At present, much of the wetland consists of unvegetated or sparsely vegetated mudflats covered by microbial biofilms that are inundated by tidal flooding. Vegetation remains limited, and most of the wetland is open water during high tide, although higher elevation zones outside of the average tower footprint are increasingly being colonized by emergent species such as tule (*Schoenoplectus spp.*), cattails (*Typha spp.*), alkali heath (*Frankenia salina*), curled dock (*Rumex crispus*), and

pickleweed (*Salicornia spp.*). Prior to restoration, vegetation was also sparse and primarily dominated by pickleweed and salt grass (*Distichlis spicata*).

5.2.2 Soil sampling and analyses

Soil cores were collected in July of 2021 (before restoration) and June of 2024 (after restoration) at the same locations (Fig. 5.1) by manually hammering cores up to 30 cm long into the sediment, with three to four replicates obtained at each site. Cores were transported to the laboratory, where they were stored at -20 °C until processing. Using an extruding mechanism, cores were sliced every 2.5 cm. Each section was weighed wet and then again after drying at 60 ºC until a constant weight was achieved. Vegetation remains were removed before sediment homogenization with a mortar and pestle. Dry bulk density (DBD; g cm^{-3}) was estimated as the sediment slice's dry mass divided by its volume in the core tube. Cumulative dry mass (g dry sediment cm^{-2}) was calculated for each core by dividing the dry mass of each section by the tube area sampled and cumulatively summing these values from the surface to the base of the core. Because this metric is independent of soil compaction, all depth profiles are expressed on a cumulative soil mass basis (g cm^2) rather than a depth (cm) basis.

Soil organic carbon (C_{org}), total nitrogen (TN), and their stable isotopes ($\delta^{13}C$ and $\delta^{15}N$) were measured in all samples at 2.5 cm resolution along one representative core per location. Prior to analysis, samples were acidified to remove inorganic carbonates. Pre-restoration samples (2021) were acidified with 6% H_2SO_3 applied directly in silver capsules followed by drying at 60 °C, with the procedure repeated twice to ensure complete carbonate removal. Post-restoration samples (2024) were treated with 1 M HCl. in centrifuge tubes, followed by rinsing with deionized water, driyng, and subsequent encapsulation. Although previous studies have reported potential effects of acidification methods on stable isotope measurements (P. Kennedy et al., 2005), no clear systematic differences in $\delta^{13}C$ and $\delta^{15}N$ values associated with the different treatments were observed in this study. All samples were analyzed using an elemental analyzer-isotope ratio mass spectrometry (EA-IRMS) at the University of California, Santa Cruz, and the University of California, Berkeley. Total nitrogen and $\delta^{15}N$ were additionally measured in non-acidified post-restoration samples. Analytical precision, assessed from replicate measurements,

showed standard deviations of 0.4% for C_{org}, 0.28% for TN, 0.11‰ for $\delta^{13}C$, and 0.22‰ for $\delta^{15}N$ in 2021 samples, and 8.9% for C_{org}, 16% for TN, 0.086‰ for $\delta^{13}C$ and 0.154‰ for $\delta^{15}N$ in 2024 samples. Isotopic accuracy, evaluated using certified reference materials, was better than ±0.2‰ for both $\delta^{13}C$ and $\delta^{15}N$.

Organic matter content was determined in all cores, including replicates using loss-on-ignition (LOI; 5h at 550°C), and C_{org} was subsequently estimated using the C_{org}:OM relationship derived from directly measured samples (Fig. 7.23). TN was estimated for replicates using the C_{org}: TN relationship (Fig. 7.24). Replicates for post-restoration samples are part of ongoing work. Organic carbon and nitrogen stocks (kg m^{-2}) were calculated for a common depth for most cores, 20 cm. When analytical data were missing (n= 2 cores), values were linearly interpolated.

5.2.3 Wetland-Atmosphere Carbon Exchange

We used the eddy covariance (EC) method to measure exchanges of CO_2 and CH_4 between the ecosystem and the atmosphere. An EC tower was installed on the eastern side of the Hill Slough marsh on March 11, 2021. Predominant winds from the southwest allowed for the tower footprint to fall within the wetland area (Fig. 5.1). Gas concentrations were measured using open-path infrared gas analyzers installed in the tower (LI-7500 for CO_2 and LI-7700 for CH_4; LI-COR Inc. Lincoln, NE, USA). A Sonic anemometer was used to measure three-dimensional wind vectors and speed of sound that together with gas concentrations were sampled at 20 Hz (WindMaster Pro 1352 or 1590, Gill Instruments Ltd., UK).

Fluxes were then calculated with the 30-min covariance between vertical wind speed and each scalar concentration, following correction procedures and quality control filters, which included high-frequency data despiking, 2-D coordinate rotations, sensor separation distance, density corrections, and site-specific friction velocity (u*) filtering (Knox et al., 2015; Leuning, 2007). Additional filtering of CO_2 fluxes for spurious night-time uptake using covariance between signal strength and vertical windspeed was applied, with values less than -0.01 m s^{-1} filtered out as water droplets are likely compromising the measurements.

Daily net ecosystem exchange (NEE) and CH_4 fluxes were computed from the 30-min data, and the net atmospheric carbon balance was estimated as the sum of NEE and the flux of CH_4 in g C-CO_2 d^{-1} and g C-CH_4 d^{-1}, respectively. Atmospheric carbon exchange was evaluated over two temporal scales each year: the growing season and the annual period. The growing season comprised day of year (DOY) 70-273, corresponding to the period between tower installation in March of 2021 and tidal restoration in October of 2021. This interval is also characterized by lower net CO_2 and higher CH_4 fluxes at the site (Fig. 7.26). Annual atmospheric C exchange was calculated using natural years, extending from October to September rather than calendar years, aligning with California´s water year and allowing conditions before and after tidal restoration to be separated without mixing both periods into a single annual estimate.

Because EC measurements began in March 2021, fluxes for the missing period from October 2020 to February 2021 were estimated by assuming that monthly fluxes were similar to those observed in March 2021, prior to tidal restoration. To evaluate the sensitivity of this assumption, annual atmospheric carbon balances for years with complete datasets (excluding 2021) were recalculated by replacing January-February and October-December daily fluxes with the average March flux. This approach altered annual atmospheric carbon balances by an average of 5% relative to estimates based on complete observations. Differences between the reference emissions before restoration (2021) and the annual emissions for the remaining years during 2022-2024 were considered the emissions generated by the restoration efforts. The selected period spans from 2022 to 2024, as these are the years in which pre-restoration cores and post-restoration cores were sampled.

5.3 Results

5.3.1 Depth profiles of sediment organic carbon and nitrogen

Prior to restoration, most sediment cores exhibited the highest surface C_{org} and TN concentrations, with C_{org} concentrations generally between ~10 and 25% and TN concentrations between ~1 and 2.5%. This was followed by a progressive decrease with increasing depth or cumulative dry mass (Fig. 5.2). Some cores showed minor increases in C_{org} and TN in deeper sections. Cores 8 and 9, located in the upland

ecotone, differed from the general trend. Core 8 showed low and constant C_{org} and TN concentrations in the upper 25 g cm^{-2}, and increasing C_{org} and TN below this depth. Core 9, showed relatively high (24%, 2.1%) surface concentrations, followed by a sharp decrease below the uppermost section.

After restoration, most cores showed lower surface C_{org} and TN concentrations relative to pre-restoration conditions, followed by subsurface peaks between 0.9 and 4 g cm^{-2}, and a subsequent decrease with depth. This pattern was observed across most cores, except cores 7 and 9. Core 7 exhibited low and relatively homogeneous concentrations in the upper 5 g $cm^{-2,}$ followed by increasing values toward the base of the core (~7 g cm^{-2}) instead of a subsurface peak. However, this pattern may reflect the restored core capturing a shallower mass-equivalent depth. Upland core 9 presented the same pattern before and after restoration.

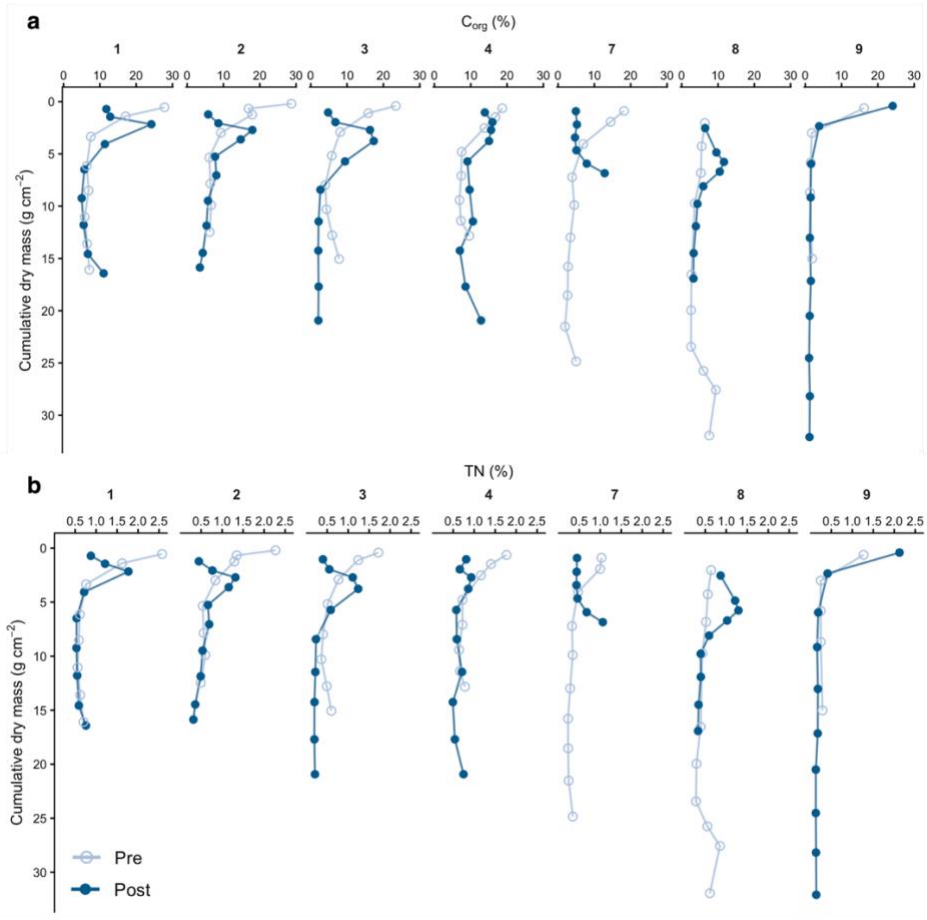


Figure 5.2 a) Sediment organic carbon content (C_{org}, %) and (b) total nitrogen content (TN, %) as a function of cumulative dry mass (g cm^{-2}) in cores collected before (open light-blue circles) and after (filled dark-blue circles) restoration across sites.

Prior to restoration, minimum sediment DBD values were generally observed in the most superficial samples, with values increasing progressively with cumulative dry mass. This vertical pattern shifted downward following restoration and rewetting, when minimum DBD values (0.2-0.7 g cm^{-3}) were instead found in some shallow surface layers and values again increased with cumulative dry mass to levels similar to those observed prior to restoration (Fig. 5.3). This pattern was consistent across most sites, although the cumulative dry mass at which minimum and maximum values occurred varied among cores. Exceptions were observed at sites 7 and 9. The

upland site 9 exhibited higher downcore DBD values after restoration, whereas site 7 showed lower downcore DBD values relative to pre-restoration conditions.

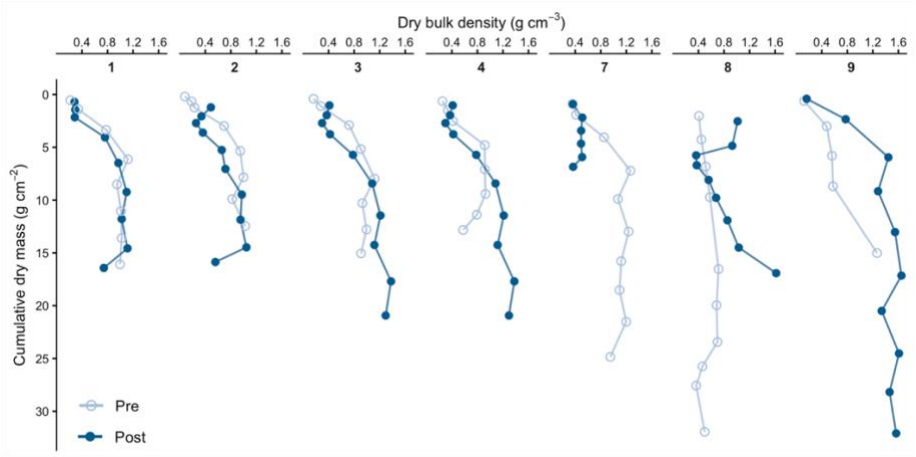


Figure 5.3 Profiles of sediment dry bulk density (g cm^{-3}) as a function of cumulative dry mass (g cm^{-2}) in cores collected before (open light-blue circles) and after (filled dark-blue circles) restoration across sites 1, 2, 3, 4, 7, 8, and 9.

5.3.2 Organic carbon and total nitrogen stocks

Organic carbon and total nitrogen stocks standardized to a depth of 20 cm presented limited variability before and after restoration. Across sites, C_{org} stocks (Fig. 4a) generally decreased after restoration, with an average reduction of 12%, except at site 4, where an increase of 27% was observed. Total nitrogen (TN) stocks (Fig. 4b) showed a similar pattern, with an average decrease of 20% between pre- and post-restoration conditions, although increases were recorded at site 8 (0.4%). Mean C_{org} stock changes between 2021 and 2024 (pre- and 3 years post-restoration) were -78 g C m^{-2}. As a first-order estimate, this corresponds to an annualized decrease of 27 g C m^{-2} yr^{-1}. Median TN stocks decreased by 0.034 g N m^{-2}, corresponding to an annualized decline of 0.011 g N m^{-2} yr^{-1}.

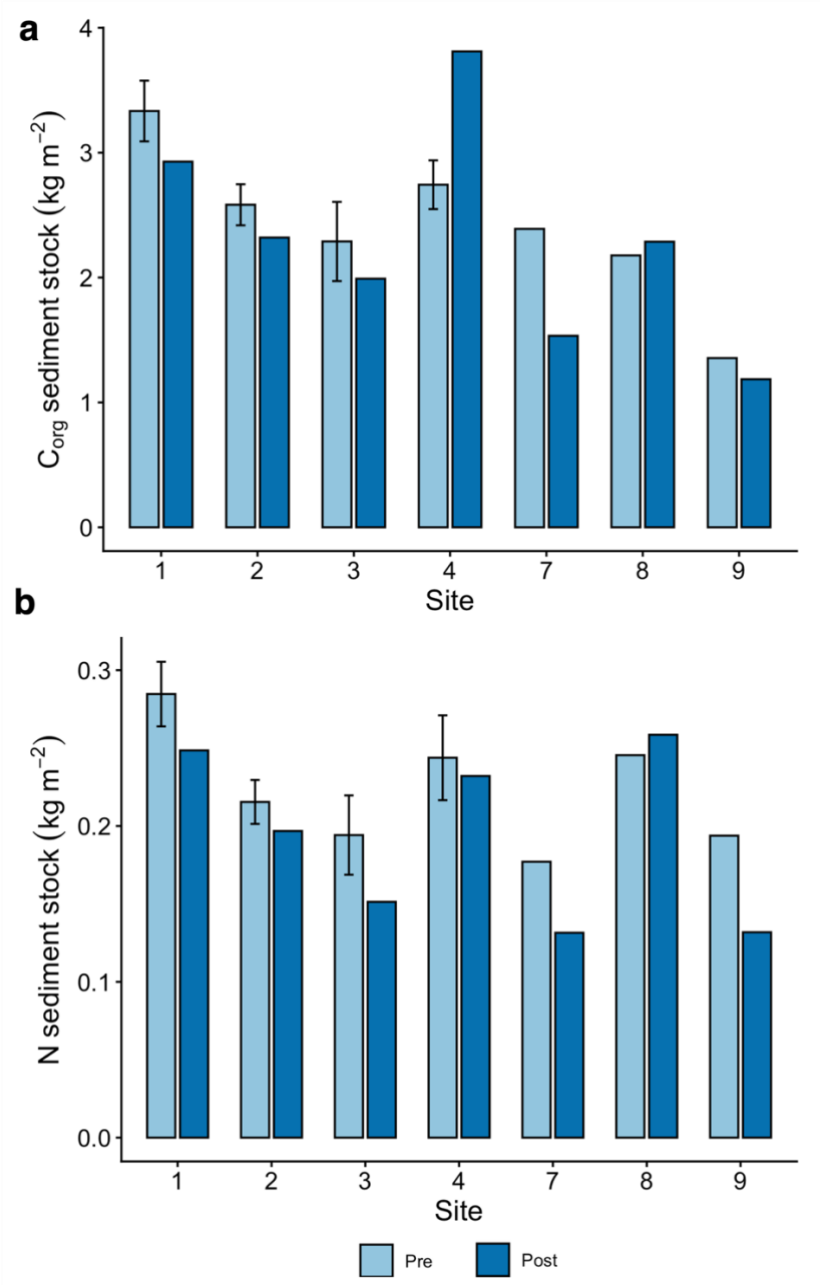


Figure 5.4 Sediment a) C_{org} and b) N stocks (kg m^{-2}) down to 20 cm depth in cores before (light blue) and after (dark blue) restoration. Error bars represent the standard deviation of replicate sediment cores collected at four sites (n=3).

5.3.3 $\delta^{13}C$ and $\delta^{15}N$ endmembers and Principal Component Analysis

The $\delta^{13}C$–$\delta^{15}N$ signatures of sediments differed between pre- and post-restoration conditions, with greater variability and a broader distribution of values after restoration. The $\delta^{13}C$–$\delta^{15}N$ signatures of sediments are compared to potential endmembers of the system (i.e., primary producers of the area), as detailed in Cloern et al., (2002). Marsh vegetation endmembers (e.g., tules, cattails, marsh gum, and pickleweed) occupied a relatively narrow range of $\delta^{13}C$ values but displayed substantial variability in $\delta^{15}N$. In contrast, estuarine-marine phytoplankton and benthic diatom endmembers showed a broader spread in $\delta^{13}C$ and comparatively more constrained $\delta^{15}N$ values. During the pre-restoration period, sediment samples were predominantly clustered between −28 and −24‰ for $\delta^{13}C$ and 2 and 6‰ for $\delta^{15}N$, overlapping in a greater extent with marsh emergent vegetation. In contrast, post-restoration samples displayed a broader distribution, spanning over a wider range of $\delta^{13}C$ (approximately −29 to −22‰) and generally higher $\delta^{15}N$ (0 to ~10‰) values (Fig. 5.5). This expansion showed greater overlap of the post-restoration sediments with estuarine-marine phytoplankton and sources with higher $\delta^{15}N$.

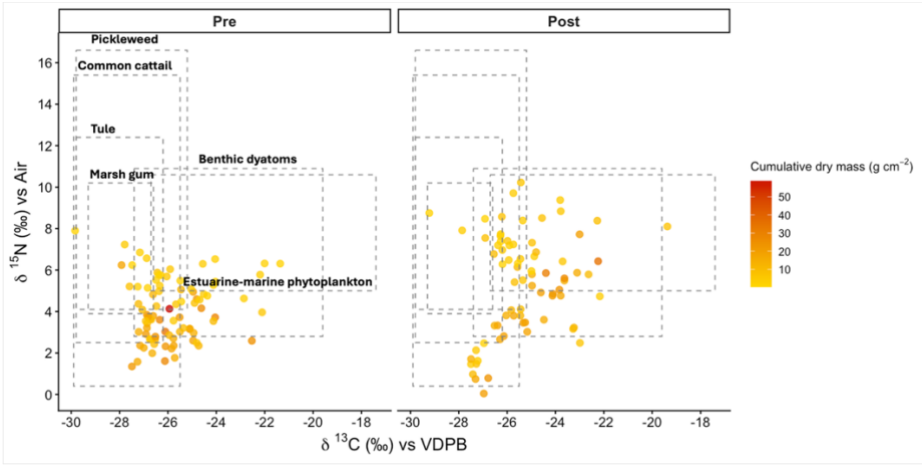


Figure 5.5 $\delta^{13}C$ and $\delta^{15}N$ biplot with all sediment samples as dots. Squares show the main primary producers in the San Francisco Bay estuarine system, as detailed in Cloern et al., (2002). The color gradient indicates core depth in cumulative dry mass (g cm^{-2}) units.

Principal Component Analysis (PCA) results showed that PC 1 (PC1; 41.7%) and PC 2 (PC2; 26.2%) explained identical proportions of variability in both pre and post restoration periods (Fig. 5.6). Cumulatively, that accounted for 67.9% of the total variance. Principal Component 1 (horizontal axis) was mainly influenced by C_{org} (%), TN (%), and Cumulative dry mass (g cm^{-2}), with contributions between 15 and 30% for before and after restoration. Principal Component 2 (vertical axis) was mainly influenced by surface elevation, $\delta^{15}N$ and C:N ratio before restoration (contributions between 15 and 40%) and by $\delta^{15}N$ and C:N ratio after (contributions between 20 and 50%). Although samples were broadly dispersed across the PCA under both conditions, the distribution of samples post-restoration showed an inverse association between $\delta^{13}C$ and C:N ratio (Fig. 7.25), indicating change in organic matter sources following restoration. Additionally, $\delta^{15}N$ gaining relevancy in the PCA results post-restoration also indicates possible source change. The wider dispersion of samples in the post-restoration period reflects increased heterogeneity.

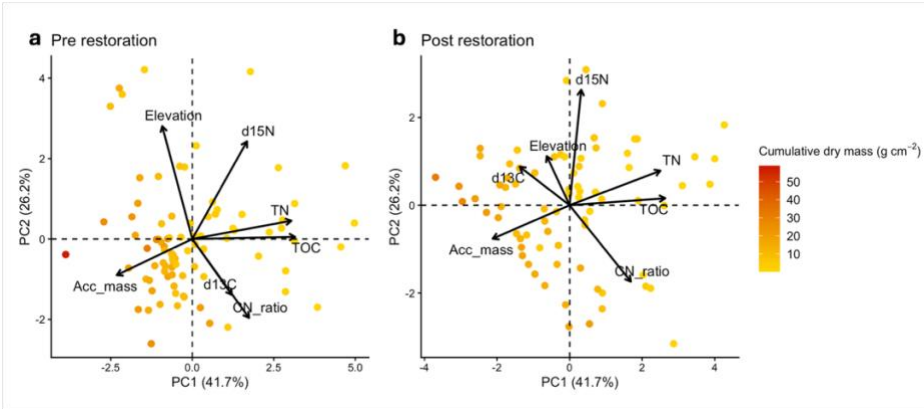


Figure 5.6 Principal Component Analysis biplots for a) pre restoration cores and b) post restoration cores. Variables used include C_{org} (%), TN (%), $\delta^{13}C$, $\delta^{15}N$, C:N ratio, cumulative dry mass (g cm^{-2}), here expressed as Acc_mass, and surface elevation (m NAVD88).

5.3.4 Greenhouse gas flux evolution and annual budgets

Carbon fluxes measured through eddy covariance showed interannual variability for both CO_2 (NEE) and CH_4 (Fig. 5.7). The wetland was a net CO_2 source throughout the study period except during the peak of the growing season in 2025, 4 years after tidal restoration, showing net uptake for a short period of time. NEE (Fig. 5.7 and Fig. 7.27) followed a seasonal pattern across the year, with the lowest, albeit generally positive, values (-0.2 to 1.2 g C-CO_2 m^{-2} d^{-1}) from April to August (DOY 100 to 240), and highest values (0.3-2.1 g C-CO_2 m^{-2} d^{-1}) from August to March. Immediately after tidal reconnection in 2021, a pronounced spike in CO_2 emissions was observed, lasting for several months before progressively stabilizing and transitioning into a more regular seasonal pattern. The first full year after restoration (2022) showed the weakest seasonal variability in NEE, whereas the amplitude of seasonal fluctuations increased progressively in subsequent years.

A similar increase in seasonal amplitude was observed for CH_4 fluxes, although with an opposite seasonal dynamic to CO_2. Methane (CH_4) emissions (Fig. 5.7 and Fig. 7.27) were minimal before flooding. Following tidal reconnection, an initial increase in emissions was observed. Afterward, CH_4 fluxes increased progressively over the

following years, with a marked amplification of the seasonal cycle, which was practically absent before restoration. The years following restoration, emissions remained consistently low during winter and early spring, increased around DOY 120 to 150, and peaked during mid to late summer. Compared to NEE, CH_4 fluxes showed greater relative interannual variability in the magnitude of peak emissions. Notably, years with higher CH_4 emissions (2023 and 2024) exhibited more pronounced and sustained peaks, whereas other years maintained lower and more stable fluxes throughout the growing season (2021, 2022, and 2025).

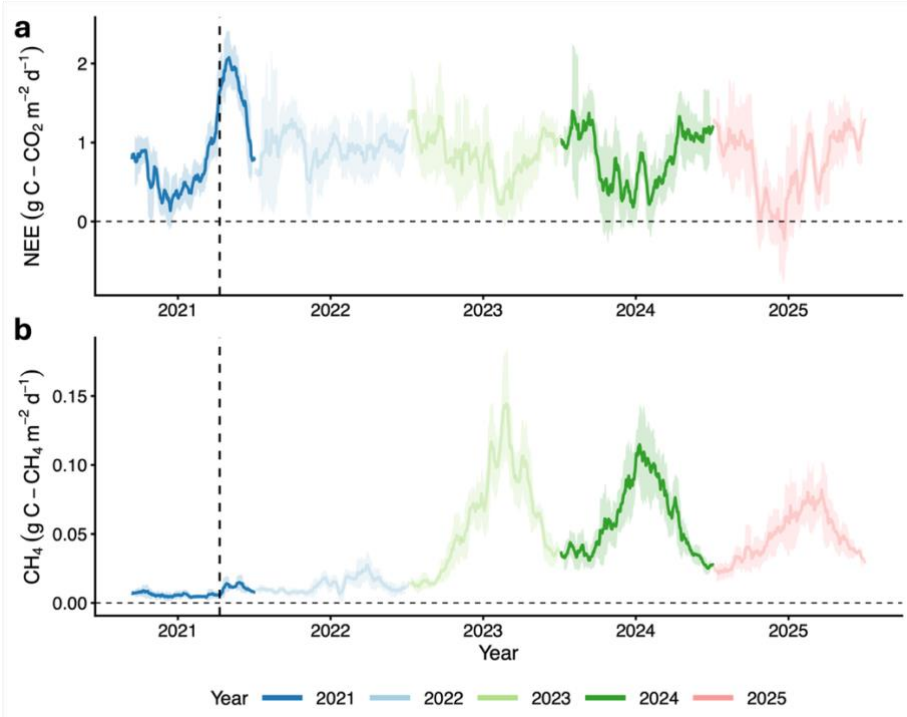


Figure 5.7 Daily sums of net ecosystem exchange a) (NEE; g C-CO_2 m^{-2} d^{-1}) and methane fluxes b) (CH_4; g C–CH_4 m^{-2} d^{-1}) across the period 2021-2025, smoothed using a 15-day centered rolling means to account for spring–neap tidal variability. Shaded areas indicate ±1 standard deviation around the smoothed values. The years when core sampling was conducted (2021 and 2024) are depicted with darker colors. The dashed vertical line represents the date of tidal restoration and flooding in October 2021. The dashed horizontal line represents the threshold where NEE and CH_4=0, with positive values indicating net carbon release to the atmosphere, whereas negative values indicate net carbon uptake.

The growing season (GS) atmospheric carbon balance varied more markedly across years than the annual balance (Fig. 5.8a and 7.27). The initial post-restoration increase in atmospheric carbon emissions was primarily driven by higher net ecosystem exchange (NEE), while CH_4 represented a smaller but consistently positive contribution to the overall balance. Following this initial peak, GS atmospheric carbon emissions declined in subsequent years (Fig. 5.8b). By the final year of the study, 2025, the atmospheric carbon balance

had shifted towards a net carbon sink relative to pre-restoration baseline. Despite this progressive decline in total atmospheric carbon emissions, the temporal dynamics of CO_2 and CH_4 differed markedly. CO_2 emissions progressively declined throughout the study period, indicating a gradual increase in ecosystem carbon uptake over time, although the net ecosystem exchange was still dominated by respiration. In contrast, CH_4 emissions increased substantially after restoration relative to pre-restoration conditions. This increase was initially moderate, but emissions later reached a maximum during 2023 and 2024 before declining slightly in 2025, while remaining well above pre-restoration levels.

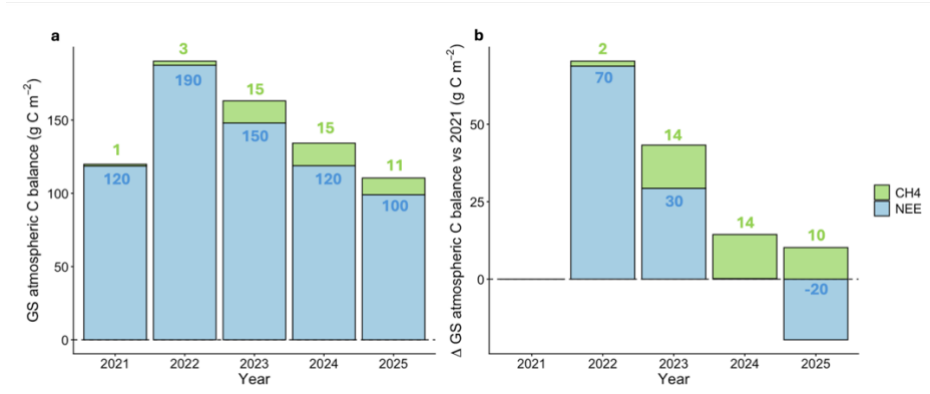


Figure 5.8 a) Atmospheric C balance (g C m^{-2}) for the growing season (GS) of all studied years. b) Increment of the growing season atmospheric C balance with respect to 2021 values (g C m^{-2}).

The annual atmospheric carbon balance remained positive throughout the study period, indicating that the wetland acted as a net carbon source before (320 g C m^{-2}) and after restoration (290 – 350 g C m^{-2}) (Fig. 7.27). Similar to the growing season dynamics, annual atmospheric carbon emissions peaked during the first full year following restoration (2022) and progressively declined afterwards. This decline was primarily driven by progressively lower CO_2 emissions through time, whereas CH_4 emissions remained consistently elevated relative to pre-restoration conditions. Comparisons relative to the 2021 baseline further showed that reductions in annual

CO_2 emissions became progressively larger through time, while the post-restoration increase in CH_4 emissions stabilized after 2023 (Fig. 7.27). By 2025, decreases in annual CO_2 emissions more than compensated for the sustained increase in CH_4 emissions, resulting in annual atmospheric carbon emissions slightly below pre-restoration levels. Relative to pre-restoration conditions, the net C balance became negative only four years after restoration, indicating that the wetland had transitioned into a net C sink relative to the baseline. However, CH_4 has a much higher radiative efficiency than CO_2 and is therefore a particularly powerful greenhouse gas, with a warming potential approximately 30 times greater than the same mass of CO_2. Accordingly, when applying the sustained-flux global warming potential framework of Neubauer & Megonigal (2015) over a 100 year horizon, radiative forcing of the restoration action remains positive of about 3.1 kg CO_2-eq m^{-2}. The contribution of CH_4 to the net restoration-induced SGWP exceeded 100%, reflecting the fact that the CO_2 component was negative relative to the pre-restoration baseline and therefore partially compensated for the positive CH_4 forcing.

5.4 Discussion

5.4.1 Sediment carbon and nitrogen dynamics reflect early-stage biogeochemical changes after restoration

Tidal restoration led to a reorganization of sedimentation dynamics, reflected in changes to the vertical distribution of C_{org} and TN. Prior to restoration, most cores exhibited surface-enriched profiles with concentrations decreasing with depth. In contrast, post-restoration profiles showed lower surface values and the development of a subsurface peak. This may indicate a shift in the balance between organic matter production, accumulation, decomposition, and transport. Isotopic data further support this shift, as post-restoration samples occupied a wider $\delta^{13}C$–$\delta^{15}N$ space, indicating a greater diversity and variability of organic matter sources, including benthic and pelagic primary producers as well as marsh-derived material, following tidal reconnection. Similar patterns have been reported in other restored wetlands, including brackish tidal marshes restored by dyke removal, where changes in hydrology, vegetation, and connectivity promote the coexistence of multiple production pathways and organic matter sources (Drexler et al., 2020).

In parallel to the changes observed for C_{org} and TN, dry bulk density (DBD) profiles showed a change in patterns before and after restoration. Prior to restoration, DBD increased monotonically with depth, whereas post-restoration sediments showed a decrease in the upper layers followed by an increase below the subsurface minimum. Rewetting of previously drained organic-rich sediments can trigger substantial chemical transformations, including organic matter loss, which may contribute to altered carbon and nitrogen storage trajectories after restoration (Anthony & Silver, 2020).

The absence of significant increases in surface TN and C_{org} contents, together with change in DBD three years after restoration, suggests that Hill Slough has not yet developed the surface sediment characteristics typically associated with mature tidal wetlands, with higher sediment carbon and nitrogen content (Kasak et al., 2026). These results indicate that such changes may require longer timescales to emerge and that the system likely remains in an early stage of post-restoration adjustment, during which geomorphological and biogeochemical processes are still reorganizing following tidal reconnection. Unlike active restoration approaches which often involve the prior construction of channel networks and revegetation, restoration at Hill Slough relied on a more passive strategy, allowing natural tidal hydrodynamics to progressively reshape the site (Ducks Unlimited, 2016). Hydrodynamic modelling conducted prior to restoration predicted substantial increases in flow velocities within the wetland, particularly near breach zones, where erosion and sediment redistribution were expected to occur. Such active sediment reworking may delay the accumulation of organic-rich, low-density surface sediments during the first years after restoration.

The observed reduction in surface TN could also reflect enhanced nitrogen losses through denitrification exceeding nitrogen accumulation in newly deposited sediments, or the incomplete recovery of plant-microbe interactions in recently restored systems (i.e., mutualistic symbionts such as nitrogen-fixing bacteria and mycorrhizal fungi), which can remain absent for decades following restoration (Moreno-Mateos et al., 2012). Reduced nitrogen availability may, in turn, constrain primary productivity, as nitrogen limitation can slow plant growth and delay carbon accumulation in restored wetlands (van Groenigen et al., 2006). However, chronosequence studies in restored wetlands suggest that these properties may

recover progressively over longer timescales. For example, older restored freshwater marshes in the Florida Everglades generally exhibited higher nitrogen contents than younger wetlands (Q. Wang et al., 2015), while a recent global meta-analysis of restored wetlands estimated that sediment nitrogen contents in restored wetlands reached only a fraction of values observed in natural wetlands after several decades (H.-Y. Chen et al., 2025). Given the strong coupling between nitrogen availability and carbon accumulation (L. Yu et al., 2017), these findings suggest that carbon sequestration capacity at Hill Slough may increase as the system continues to mature, a process linked to the NEE evolution and that would be enhanced if CO_2 uptake becomes a more important process, a dynamic already starting in 2025. This interpretation is consistent with previous studies showing that tidal reconnection can enhance long-term carbon accumulation compared to other restoration approaches (H.-Y. Chen et al., 2025), even when short-term recovery of surface sediment properties remains limited.

Despite these changes, the main environmental drivers of sediment composition appear to remain similar, as indicated by multivariate analysis. The proportion of variance explained by PC1 and PC2 remained similar before and after restoration, suggesting the same environmental gradients continue to structure the sediment composition. This is consistent with an early-stage reorganization of sediment dynamics without a full transition to a newer system, a pattern typical of transitional or rehabilitated systems (Hemes et al., 2018). In these systems, hydrological reconnection rapidly increases spatial heterogeneity and diversifies organic matter sources and pathways, but does not immediately restore pre-disturbance biogeochemical functioning of the wetland (Drexler et al., 2020). Similar transitional trajectories have been described in restored or rehabilitated wetlands, where physical and compositional responses can occur rapidly, whereas the recovery of microbial communities, vegetation structure, sediment processes, and carbon and nitrogen stocks may require decades (Berkowitz & White, 2013; Emsens et al., 2020; Kreyling et al., 2021; Yu et al., 2017).

Tidal and riverine wetlands, linked to larger hydrological regimes, have been shown to recover biogeochemical functions and biological structure within approximately 20 and 30 years, respectively, whereas non-tidal depressional wetlands fed by precipitation or groundwater have not reached reference conditions even after 50

years of restoration (Moreno-Mateos et al., 2012). More recently, a global synthesis of restored tidal marshes reported that most ecosystem service indicators approached or exceeded reference conditions within five years of restoration, although soil carbon stocks generally remained below reference values even after 30 years, despite increasing significantly with restoration age (Rowland et al., 2024).

This interpretation is also consistent with observations from restored tidal marshes where passive hydrological reconnection does not immediately lead to the development of organic-rich, low-density marsh soils. For example, in a restored salt marsh in the Nisqually River Delta (Washington, USA), a formerly diked marsh restored by levee removal remained largely unvegetated six years after restoration and accumulated predominantly inorganic sediments with higher bulk density and lower organic carbon contents than nearby reference marshes (Drexler et al., 2019). Such patterns suggest that passive tidal restoration, particularly in subsided or strongly reworked systems, may initially promote sediment redistribution and vertical accretion before vegetation-driven organic matter accumulation becomes dominant.

5.4.2 Greenhouse gas fluxes indicate a system functioning as a carbon source the first years after restoration

The atmospheric carbon balance remained positive throughout the study period, indicating that the wetland functioned as a net source of carbon to the atmosphere in all years considered. Total emissions consistently exceeded 300 g C m^{-2} yr^{-1}, with respiration as CO_2 representing the dominant contribution. When evaluated relative to the 2021 baseline, 2022 showed the largest increase in atmospheric carbon emissions, driven by elevated CO_2 and CH_4 fluxes. In subsequent years (2023–2025), total emissions progressively decreased relative to the 2022 peak, primarily due to lower CO_2 emissions. However, atmospheric carbon emissions remained above 2021 levels until 2025 (Fig. 5.8), when the wetland becomes a C sink compared to the baseline emissions. Despite this decline, respiration still dominated over CO_2 uptake over the annual scale.

This contrasts with other restored tidal wetlands in the Delta and San Francisco Bay Estuary, including sites restored using both passive and active approaches (Kasak et al., 2026), in which their net ecosystem carbon balance is strongly negative and

dominated by CO_2 uptake even shortly after restoration. This is the case for Dutch Slough (AmeriFlux ID: US-Dmg), a restored brackish tidal marsh, which ranks among the most productive wetland ecosystems globally, with maximum annual CO_2 uptake exceeding -800 g C m^{-2} yr^{-1} (Arias Ortiz & Baldocchi, 2026; D. Baldocchi et al., 2018). However, restoration design differed substantially between sites. At Dutch Slough, restored included earthmoving to achieve elevations for a gradually sloping marsh plain, the construction of a complex network of tidal channels, and site revegetation prior to levee breaching. The site was then maintained as a non-tidal wetland for two growing seasons prior to levee breaching, allowing vegetation and carbon uptake capacity to become established before tidal reconnection. Similar rapid transitions to carbon sink conditions have also been observed in restored non-tidal wetlands within the Delta, where vegetation recovery can occur within one or two growing seasons (Hemes et al., 2019). In contrast, restoration at Hill Slough relied on a more passive approach, with no active revegetation or tidal channel construction. Following hydrological reconnection, vegetation establishment and tidal channel formation were left to develop naturally through tidal processes and ecosystem reorganization. The reduction in CO_2 emissions may reflect reduced net respiration or increased carbon uptake during the growing season. Similar patterns have been observed in non-tidal restored wetlands, where the first year after flooding was characterized by elevated respiration and neutral or positive NEE, driven by incomplete vegetation establishment and enhanced decomposition of previously accumulated organic matter (Hemes et al., 2019; Kasak et al., 2026; Knox et al., 2015).

Methane emissions increased after restoration, particularly during the growing season, indicating enhanced methanogenic activity under more reducing conditions and consistent with the temperature sensitivity of this process (R. Conrad, 2023). Prior to restoration, Hill Slough remained largely dry during summer months, and therefore CH_4 emissions were likely negligible under pre-restoration conditions (Kasak et al., 2026). The post-restoration increase in CH_4 emissions likely reflects the establishment of prolonged inundation and anaerobic conditions following tidal reconnection. However, annual CH_4 fluxes remained relatively low (2-14 g C m^{-2} yr^{-1}) compared to many freshwater restored wetlands and were at the lower end of the range reported by the FLUXNET-CH4 network. This is consistent with observations from other tidal wetlands, where saline conditions suppress

methanogenesis through sulfate reduction and other competitive microbial pathways (Arias-Ortiz et al., 2024; Poffenbarger et al., 2011). Methane emissions in other restored wetlands of the Delta, including both tidal and non-tidal ecosystems, also show strong seasonal dynamics linked to plant productivity and hydrological conditions, and are substantially higher than those observed under other land uses (Knox et al., 2015). Similar post-restoration trajectory have been reported in restored freshwater wetlands, where methane emissions increase sharply following flooding and decline over subsequent years as ecosystem structure and function develop (Bartolucci et al., 2021; Bortolotti et al., 2016; Delwiche et al., 2025). In these systems, the control on methane production and transport can also shift through time as vegetation, hydrology, and microbial communities progressively reorganize after restoration (Delwiche et al., 2025).

At Hill Slough, we observed a divergence in NEE and CH_4 flux trends during 2022-2023, with an initial increase in both CO_2 and CH_4 emissions in the first year following restoration, followed by increasing CH_4 emissions and lower net CO_2 emissions. These different responses between NEE and CH_4 fluxes are commonly observed in rewetted wetlands, where anaerobic decomposition and methane production are promoted (Bridgham et al., 2013; Knox et al., 2015), while CO_2 uptake has been reported to become dominant once restored wetlands reach approximately 55% vegetation cover, based on a synthesis of 21 restored freshwater and brackish wetlands (Valach et al., 2021). The revegetation process increases the production of labile organic matter and root exudates, which can promote CH_4 production (Waldo et al., 2019).

The interannual variability in NEE and CH_4 fluxes is characteristic of restored wetlands during the first years after restoration, when ecosystem processes are still adjusting to new hydrological conditions. This highlights the importance of multi-year measurements, as short-term observations may capture only transient post-restoration conditions rather than the long-term trajectory of ecosystem recovery (Delwiche et al., 2025). At Hill Slough restored marsh, greenhouse gas flux monitoring indicate that the ecosystem-scale carbon exchange remains in a transitional state following restoration, with carbon dynamics still dominated by emissions before longer-term recovery of sink function.

Although CH_4 represented a smaller fraction of the total carbon mass emitted, its climatic importance increased substantially when emissions were expressed as CO_2-equivalents using the 100-year sustained-flux global warming potential ($SGWP_{100}$) (Neubauer & Megonigal, 2015). However, because the ecosystem is still in transition, current emissions are unlikely to represent long-term conditions and represent an early stage of ecosystem recovery, and the time required for the system to shift from a net GHG source to a sink may decrease as vegetation and biogeochemical functions develop (Delwiche et al., 2025), which will be observable as monitoring continues.

Efforts to enhance carbon sequestration in wetland restoration projects may therefore be accompanied by increased greenhouse gas emissions during the first years following restoration, potentially delaying the realization of net climate benefits (Arias-Ortiz et al., 2021; Hemes et al., 2019).

5.4.3 Sediment and atmospheric carbon dynamics are partially aligned across spatial scales

Both sediment carbon and nitrogen profiles and atmospheric fluxes reflect the existence of a transitional phase following restoration, during which the ecosystem remains in the early stages of adjustment. Throughout the monitoring period, atmospheric fluxes and soil stocks changed in the same direction, with restoration initially increasing net carbon losses relative to the pre-restoration baseline through increased carbon emissions to the atmosphere and a reduction in soil stocks.

The median reduction in C_{org} stocks was of 180 g C m^{-2}. Over the same period, the cumulative difference in atmospheric carbon balance relative to the pre-restoration baseline was 220 g C m^{-2}. Assuming that stock reduction is linear during sampling years, the median annual difference in C_{org} stocks would be of 62 g C m^{-2} yr^{-1}, comparable in magnitude to the median annual increase in atmospheric carbon fluxes estimated from eddy covariance (71 g C m^{-2} yr^{-1}). Although this comparison is approximate, both approaches therefore indicate a net carbon loss following restoration.

The comparison between changes in atmospheric carbon fluxes and sediment carbon stocks should, however, be interpreted with caution, as it relies on several

assumptions. Each method captures different pathways and scales of carbon cycling. Sediment inventories integrate changes in sediment stored carbon at discrete sampling locations, while eddy covariance integrates ecosystem-atmosphere exchange over a larger and spatially heterogeneous footprint, which may include not only emissions from the wetland sediments and vegetation, but also respiration from the water column and carbon exchanges associated with hydrological transport of adjacent estuarine waters. The spatial heterogeneity of the marsh may further contribute to these differences, as the eddy covariance footprint is dominated by lower-elevation areas (0.6 – 1.0 m), including frequently inundated mudflats and sparsely vegetated zones, whereas sediment cores were collected at a broader set of elevations (0.6 – 2 m). The observed changes in surface carbon stocks were spatially heterogeneous across cores, with most locations showing decreases averaging ~12%, while one location exhibited an increase of ~27%. The coefficient of variation (CV) of surface carbon stocks was 24% before restoration and 36% after restoration, indicating substantial spatial variability across the wetland. Given that the magnitude of the observed stock reductions was of similar order to the spatial variability represented by the CV, part of the detected differences may reflect natural heterogeneity in sediment properties and deposition patterns in addition to restoration-driven changes. Increasing the number of replicate cores would improve characterization of spatial variability and allow a clearer separation between natural variability and real changes in sediment carbon stocks following restoration.

One important process that we have not accounted for is the contribution of lateral carbon export and imports, which would entail additional hydrological and biogeochemical measurements. In addition to vertical burial and mineralization, carbon can be exchanged as dissolved or particulate organic carbon, a process widely documented in wetlands influenced by hydrological connectivity and tidal exchange (Bogard et al., 2020; Z. A. Wang et al., 2016). Tidal restoration likely altered not only vertical sediment processes but also the pathways through which carbon is redistributed within and beyond the system.

Together, these findings suggest that hydrological restoration does not necessarily lead to an immediate recovery of carbon sink function but instead initiates a transitional phase. However, the absence of net carbon sequestration in the first years after restoration does not imply that the restoration process is not delivering

benefits in other ecological functions. Habitat provision, and increased biodiversity are all relevant services that the restored wetland is already providing (Mitsch et al., 2015).

Finally, these results highlight the importance of combining sediment and atmospheric approaches to assess post-restoration carbon dynamics. The reduction in surface sediment C_{org} stocks observed after tidal reconnection could be interpreted as evidence of enhanced CO_2 emissions, but it may also reflect the redistribution of organic matter within the wetland or lateral carbon losses through tidal export. In this study, atmospheric measurements showed a consistent initial increase in carbon emissions following restoration, supporting the interpretation that the observed sediment carbon losses were at least partially associated with enhanced ecosystem respiration during the early restoration phase. However, continuous eddy covariance measurements also reveal that the system has only recently begun to show signs of recovering carbon sink capacity during parts of the growing season, a signal not yet detectable in the sediment stocks. Together, these findings illustrate the different temporal and process-based perspectives captured by soils and atmospheric measurements and demonstrate that combining both approaches provides a more complete understanding of restoration trajectories and carbon dynamics in restored wetlands. A combined approach is therefore necessary to fully resolve carbon budgets in restored wetland systems and provides a more complete assessment of restoration consequences. Tracking vegetation development, porewater chemistry, and sediment geochemistry could improve interpretation of restored wetland carbon and nitrogen dynamics (Anthony & Silver, 2020; Delwiche et al., 2025).

This is an ongoing work and ^{210}Pb dating, organic matter replicates and core sampling representativeness using randomized accumulation curves will be added to it.

6. Conclusions and future perspectives

We can still explore the overgrown verges of our blasted landscapes.

Anna Tsing

6.1 Conclusions

The aim of this thesis was to reconstruct how anthropogenic pressures have altered sediment, nutrient, and metal fluxes to coastal wetlands through the study of sedimentary archives, and to evaluate how these impacts have shaped ecosystem functioning. Specifically, the research goals included 1) reconstructing the evolution of sedimentary metal concentrations, fluxes, and sources into the sediments of a coastal lagoon, and linking them to the development of the mining industry and other anthropogenic activities; 2) evaluating how anthropogenic nutrient inputs derived from agriculture and urban expansion altered carbon and nitrogen cycling in the sediments of a coastal lagoon; and 3) assessing the effects of tidal wetland restoration on carbon and nitrogen dynamics in sediments and greenhouse gas fluxes in a tidal marsh. Each one of these objectives is addressed in a different thesis chapter. The main conclusions derived from these chapters are summarized below.

In **Chapter 3**, the fluxes of metals over the last century to the sediments of Mar Menor, Europe's largest saltwater lagoon were reconstructed to evaluate how the development of the mining industry in the Sierra Minera de Cartagena-La Unión shaped metal accumulation and contamination patterns in the lagoon. As a consequence, lagoon sediments are enriched in Pb, As, Zn, Hg, Cu, and Ag in concentrations that surpass sediment toxicity thresholds and are generally higher than values reported in other marine coastal enclosed ecosystems affected by metal contamination. The southern sector of the lagoon, closest to the mining mountain range, has accumulated the highest metal stocks. The mining industry is responsible for the increase in metal concentrations everywhere in the lagoon from the start of the 20th century until the 1950s. Since then, the general decline in metal concentrations can be largely attributed to the 1955 ban on mining spills and the cessation of mining activities in 1991. After mining activities ceased, leaching from the watershed soils continued to supply metals to the sediments. Additional anthropogenic sources, such as antifouling paints and sewage discharges, also delivered Hg, Cu, and Ag to the lagoon. Nowadays, surface metal concentrations still exceed sediment quality guidelines, and although sediments appear to be effectively retaining these metals, changes in the lagoon conditions could alter this situation and promote their mobility. Extreme precipitation events driven by climate change and eutrophication episodes might increase the resuspension risk of

historically accumulated contaminated sediments, favoring their bioavailability, and endangering biota. Marine ecosystems affected by historical metal contamination and vulnerable to resuspension risks, could experience renewed effects of this legacy pollution. Therefore, studies focused on metal contamination from the source and remobilization perspectives are crucial for developing future management plans for marine coastal ecosystems.

In **Chapter 4**, sedimentary carbon and nitrogen records were used to reconstruct how agricultural intensification, hydrodynamic modifications, urban development, and the expansion of the non-indigenous macroalgae *Caulerpa prolifera* reshaped nutrient dynamics and sediment organic matter composition in the Mar Menor coastal lagoon throughout the 20th and early 21st centuries. Sedimentary $\delta^{13}C$ and $\delta^{15}N$ records documented a progressive shift from a hydrologically restricted system toward one increasingly influenced by Mediterranean-derived organic matter and terrestrially derived nitrogen inputs. This shift was mainly derived from i) the widening of the lagoon-sea connection (Estacio channel) in 1973 and, ii) the growing anthropogenic inputs from sewage discharge and intensive agriculture from the 1970s onward. Prior to the 1970s, the lagoon exhibited a stronger spatial heterogeneity in sedimentary nutrient concentrations and accumulation patterns, whereas the increase in anthropogenic nutrient inputs progressively homogenized nutrient sources across the lagoon, promoted *C. prolifera* expansion, increased phytoplankton productivity, and eventually contributed to the 2016 ecosystem collapse and transition toward a eutrophic, macroalgae-dominated state. Carbon and nitrogen burial rates increased significantly after 1990, reflecting intensified nutrient loading. The highest accumulation rates occurred in the southern sector, where values were comparable to global seagrass estimates, while nutrient-rich surface sediments in the northern lagoon and southwestern sector contain high nutrient stocks vulnerable to resuspension and subsequent remineralization. Although only a small fraction of sedimentary organic matter derives directly from *C. prolifera*, the species likely contributes indirectly to carbon preservation by enhancing sediment retention. Sediment remobilization of the areas with larger stocks under future eutrophic or extreme climatic conditions could intensify oxygen depletion and eutrophication feedbacks.

In **Chapter 5**, the responses of a tidal wetland to hydrological restoration were studied, both analyzing sedimentary changes as in Chapters 3 and 4, and adding the evolution of greenhouse gases between the ecosystem and the atmosphere. Tidal restoration at Hill Slough marsh initiated an early-stage reorganization of sediment biogeochemistry and ecosystem carbon dynamics following hydrological reconnection. Post-restoration sediments showed lower surface C_{org} and TN contents, and changes in DBD profiles, indicating shifts in sediment accumulation. Stable isotope data also reflected an increased diversity of organic matter sources after restoration, associated with enhanced hydrological connectivity and the coexistence of benthic, pelagic, and marsh-derived inputs. However, three years after restoration, the wetland had not yet started to accrue sediment C_{org} and TN stocks above the pre-restoration baseline, suggesting that geomorphological and biogeochemical adjustment is still ongoing. Passive tidal reconnection may have promoted sediment redistribution from localized erosion and deposition, while the vegetation cover is not sufficiently developed for CO_2 uptake to dominate ecosystem carbon exchange. These results are consistent with chronosequence or space-for-time studies and meta-analyses showing that the recovery of carbon and nitrogen stocks often requires decades after restoration. Greenhouse gas fluxes measured through eddy covariance further indicate that Hill Slough remained in a transitional state Emissions increased immediately after restoration, particularly during 2022, before progressively declining in subsequent years as vegetation and ecosystem functioning developed. Methane emissions also increased after tidal reconnection due to wetter and more reducing conditions, although fluxes remained relatively low under saline conditions. By 2025, however, the system showed carbon sink conditions relative to the pre-restoration baseline. Both sediment inventories and eddy covariance measurements captured signals of net carbon loss following restoration, although each method reflected different components and spatiotemporal scales of ecosystem carbon cycling influenced by vegetation, inundation patterns, respiration, and hydrological transport. Sediment stocks integrate localized changes in long-term carbon storage, whereas atmospheric flux monitoring capture ecosystem-scale exchanges at annual and subannual scales, thus expanding the available tools to study ecosystem impacts. Together, these findings show that hydrological restoration does not necessarily produce an immediate recovery of carbon sink function, but instead initiates a transitional phase characterized by complex and evolving carbon pathways.

Overall, this thesis demonstrates that sediment archives are powerful tools to reconstruct past changes in metals, and nutrient fluxes in coastal wetlands and to identify the anthropogenic drivers controlling their evolution through time. By integrating sediment dating with geochemical proxies and greenhouse gas flux measurements, this work shows how human activities operating at the watershed scale, including mining, agriculture, urbanization, hydrological modification and wetland restoration, strongly influence sedimentary accumulation processes and biogeochemical cycle. These results also reveal that ecosystem responses to environmental change operate over different timescales, with some impacts persisting for decades despite management actions, while other biogeochemical responses can occur rapidly following environmental change. Coastal wetland recovery should therefore be understood as a long-term trajectory shaped by watershed-wide effects, internal feedbacks, buffering mechanisms, and indirect anthropogenic pressures. These insights are particularly relevant in the context of growing environmental pressure, where understanding how multiple stressors interact will be critical for designing effective management, conservation, and restoration strategies.

6.2 Future perspectives

Despite substantial progress in recent decades, major uncertainties remain regarding the role of coastal wetlands in global biogeochemical cycles and their response to increasing anthropogenic pressure. As multiple stressors intensify and co-occur, advancing our understanding of these systems will require more integrative and interdisciplinary approaches.

A key priority is the development of **multiproxy and high-resolution reconstructions** to better constrain the timing and drivers of ecosystem change through sedimentary processes. Combining geochronological techniques and geochemical proxies with emerging tracers, such as environmental DNA (eDNA) (Thomsen & Willerslev, 2015), would allow linking sedimentary records to specific biological communities and ecosystem shifts. Expanding sediment analyses to include other nutrients such as phosphorus and silicon, would also provide a more complete picture of the evolution of eutrophication dynamics and nutrient cycling,

particularly on systems where algal blooms are dominated by diatoms, such as the Mar Menor coastal lagoon.

Resuspension processes in coastal wetland sediments have been identified as key mechanisms controlling the transfer of nutrients, metals, and other contaminants from sediments to the water column (Liu et al., 2024). However, the tracers and methodological approaches required to quantify these processes remain underdeveloped. Future research should therefore focus on improving the identification, characterization, and quantification of sediment resuspension dynamics and their implications for the mobilization and bioavailability of contaminants and nutrients.

Further attention should be given to **nutrient burial** processes, particularly nitrogen, which remains poorly quantified at the global scale despite its importance as a buffering mechanism against eutrophication (Langley et al., 2025). While sediments can act as effective nutrient sinks, nitrogen-rich sediments may also become sources of this nutrient to the water column under changing environmental conditions, such as enhanced remineralization or resuspension. Generating broader datasets of nitrogen burial rates across different coastal wetland types would substantially improve global assessments of their role in nutrient retention and ecosystem resilience.

In the context of **blue carbon**, improving the quantification of carbon sequestration requires distinguishing between labile and recalcitrant organic matter fractions, as well as accounting for their biological degradation susceptibility, which differ from thermal degradation, and refining estimates of long-term burial, especially under future climate change scenarios (Sun et al., 2023). In addition, the potential role of macroalgal systems, such as *Caulerpa*-dominated habitats, as blue carbon ecosystems remain largely unexplored and deserves further investigation.

Future research should further explore the application of **concentration-dependent stable isotope mixing models** in sedimentary organic matter source determination studies. Stable isotope mixing models are usually used without employing concentration-dependent approaches, even though potential sources of organic matter to sediments often include a highly diverse array of materials, such as

dissolved and particulate organic matter from terrestrial and marine origin, macrophyte biomass (i.e., seagrasses, macroalgae, and saltmarsh vegetation), phytoplanktonic contributions, and microbial contributions. Because these sources usually present different proportions of C_{org} and TN contents (Lamb et al., 2006), approaches that do not account for concentration dependence may bias estimated source contributions. Integrating the widespread use of concentration-dependent models may therefore be the most suitable approach to more accurately determine the origin of the organic matter being deposited in sediments, particularly in complex coastal systems characterized by heterogeneous and shifting organic matter sources over time. Additionally, future studies should aim to bridge the gap between source determination and flux quantification by developing models for each nutrient. Such approaches could provide quantitative estimates of the contributions of specific organic matter sources to long-term C_{org} and TN burial fluxes.

A major gap persists in the integration of **sediment processes with greenhouse gas fluxes and their future trajectories**. Quantifying carbon burial alongside CO_2, CH_4, and N_2O emissions is essential to determine whether coastal wetlands function as net carbon sinks or sources, particularly in degraded or restored systems. However, beyond present-day quantifications, a critical challenge lies in **forecasting how these fluxes will respond to ongoing environmental change**. Predicting the future greenhouse gas balance of coastal wetlands requires a detailed understanding of the interactions between carbon accumulation, nutrient cycling, and environmental drivers such as temperature, salinity, hydrodynamics, and sea-level rise.

Finally, the increasing **co-occurrence of multiple stressors on coastal wetlands** (Newton et al., 2020) additionally demands a more holistic research and management framework. Future studies should explicitly address interactions between contaminants, nutrient enrichment, hydrodynamics, and climate change, while also accounting for the human activities that drive these pressures. In this context, integrating local and ecological knowledge with scientific research can improve both the interpretation of environmental changes and the effectiveness of management strategies (Albuquerque et al., 2021). Moving beyond one-size-fits-all conservation approaches toward adaptive, context-specific solutions that involve local communities in decision-making processes will be essential (Macreadie et al., 2026)

to ensure that conservation and restoration efforts deliver both ecological and societal benefits.

7. Appendices

7.1 Supplementary Information for Chapter 3

7.1.1 Coordinates for sampled cores

Table 7.1 Geographic coordinates of sediment cores collected in the Mar Menor lagoon reported in decimal degrees (WGS84).

Core	Latitude (°N)	Longitude (°E)
OPC1	37.79362	0.78102
OPC2	37.7588	0.80345
OPC3	37.73748	0.82937
OPC4	37.7062	0.8325
OPC5	37.71538	0.79613
OPC6	37.73971	0.76807
OPC7	37.68908	0.81547
OPC8	37.64905	0.74179
OPC9	37.6983	0.83944
OPC10	37.65036	0.77346
OPC11	37.68834	0.80692
OPC12	37.67878	0.75476

7.1.2 Specific activity profiles of ^{210}Pb

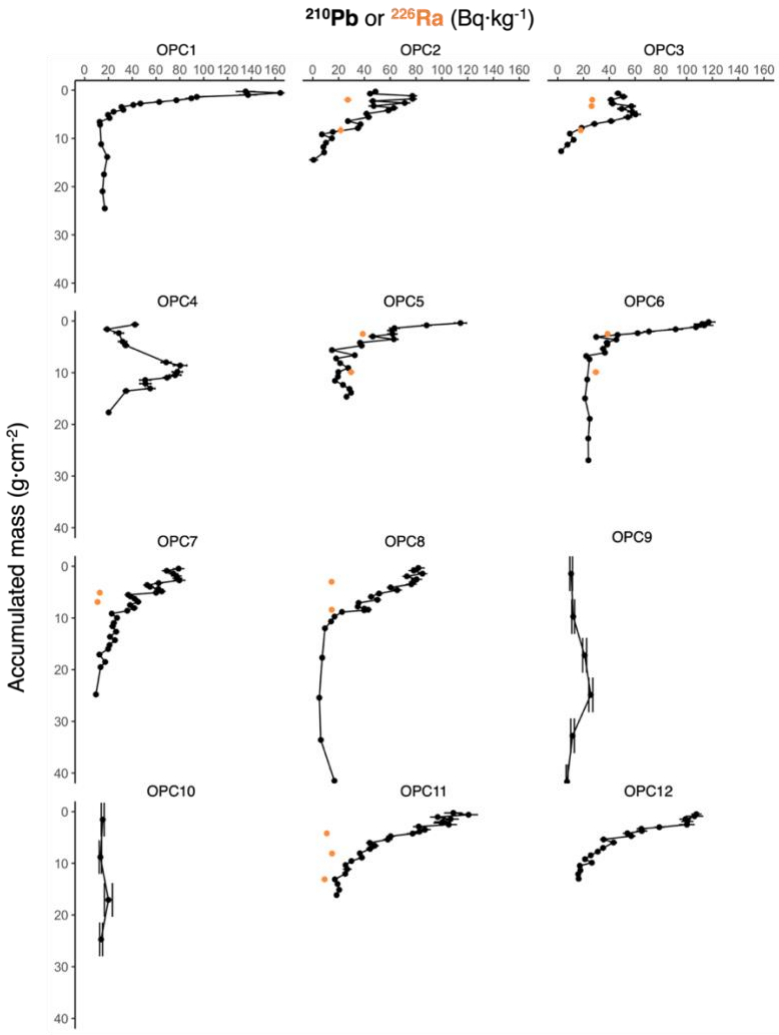


Figure 7.1 Total ^{210}Pb (in black) and ^{226}Ra (in orange) specific activity profiles for all cores.

7.1.3 Grain size and dry bulk density

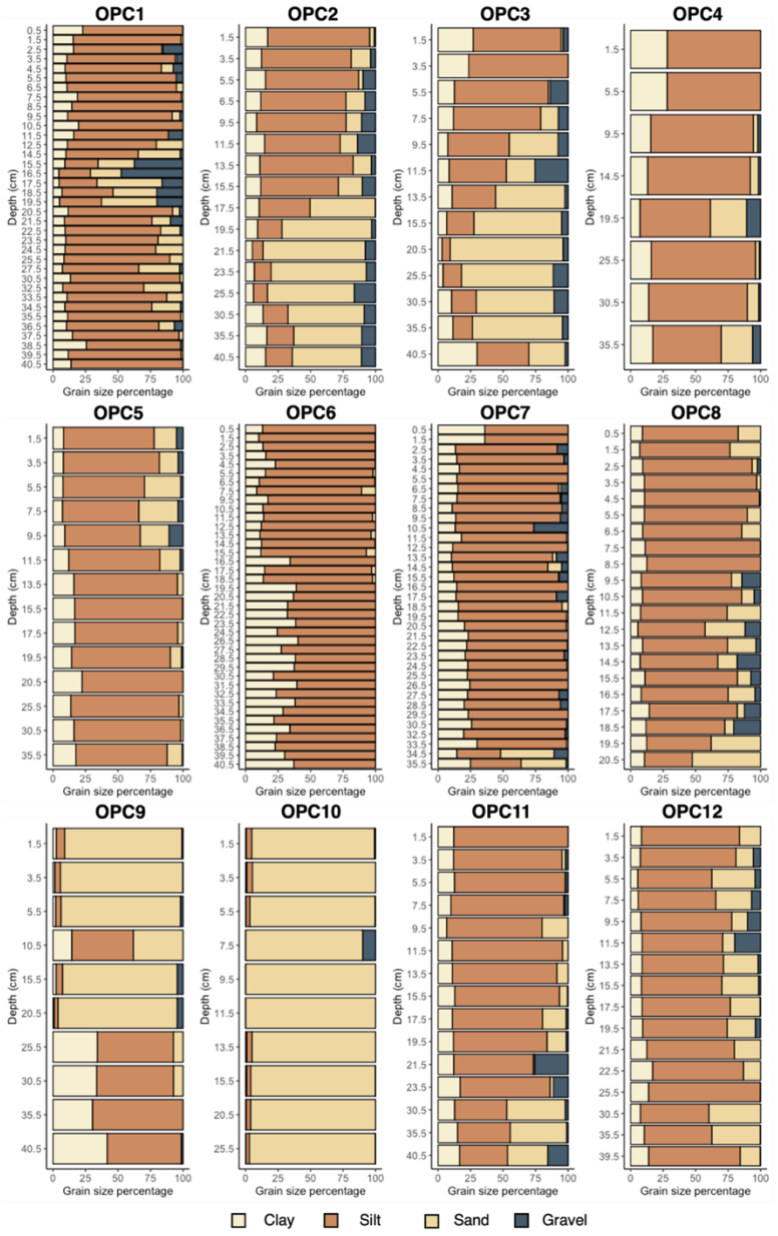


Figure 7.2 Grain size percentage distribution by depth for all sampled cores. Note that Gravel includes shells and biogenic remains.

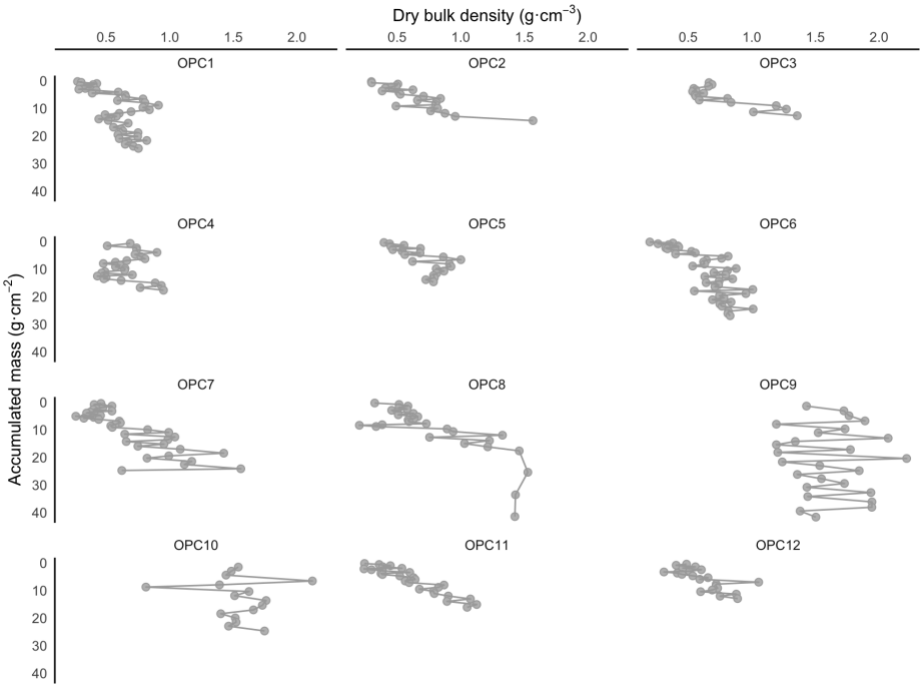


Figure 7.3 Dry bulk density (g·cm^{-3}) profiles.

7.1.4 Summary of metal concentrations

Lowest and highest metal concentration value for each circulation sector.

Metal ($mg \cdot kg^{-1}$ or $g \cdot kg^{-1}$*)	Lowest values			Highest values		
	North	Center	South	North	Center	South
Al*	8.0	18	11	18	48	31
Ag	0.13	0.21	0.18	0.82	1.9	5.5
As	18	14	19	35	43	100
Ca*	170	100	140	310	170	200
Cd	0.13	0.35	0.10	9.6	9.5	14
Cr	18	36	25	36	67	53
Cu	6.1	13	7.7	57	39	50
Fe*	6.7	14	8.4	12	25	60
Hg	0.041	0.050	0.053	0.31	0.19	0.53
Na*	8.5	8.7	10	130	29	36
Ni	11	21	12	25	35	37
Pb	76	180	200	870	1,500	3,400
Si*	35	81	60	93	140	210
Sr	1,900	910	1,600	3,400	2,300	3,500
Ti	770	1,300	870	1,400	2,060	2,020
Zn	26	85	130	1,400	1,600	3,700

7.1.5 Results for statistical tests

Table 7.3 H values and Z values ($p < 0.01$) for Kruskal-Wallis and Dunn tests for differences between lagoon regions.

	Pb	Hg	As	Cu	Zn	Ag
H values	66	63	67	50	66	83
Z for North-Center	-	-2.9	-	-	-	-
Z for North-South	-5.1	-3.2	-4.4	-4.2	-3.8	-6.5
Z for Center-South	-7.7	-7.9	-8	-6.8	-8.1	-8.2

7.1.6 Metal concentration profiles for all cores

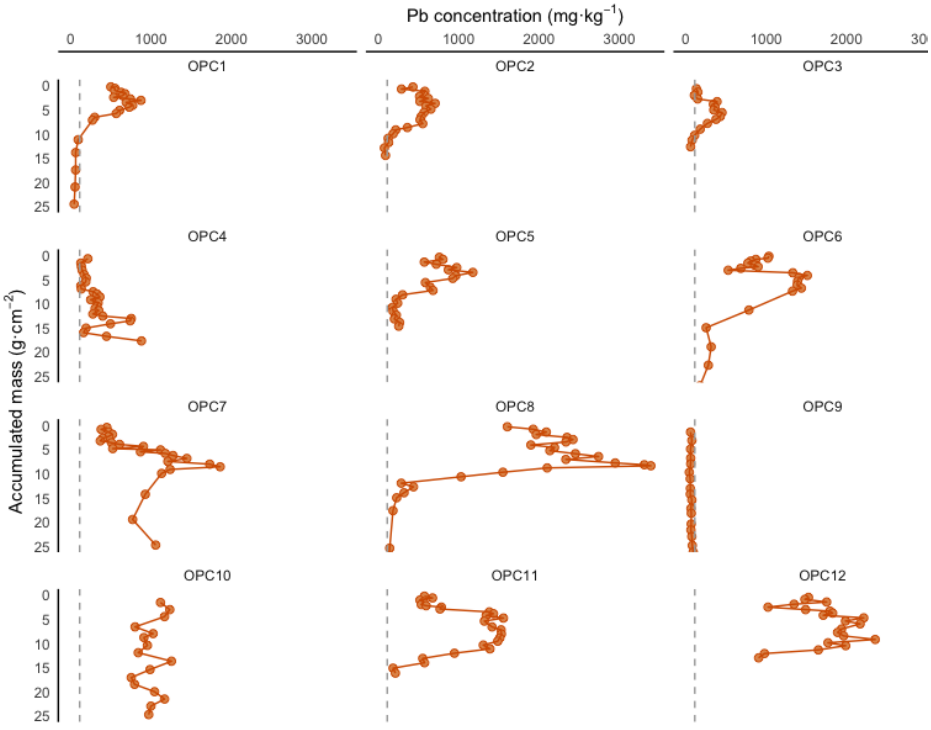


Figure 7.4 Pb concentration (mg·kg^{-1}) profiles for cores. The dashed line represents the Probable Effects Level (PEL) concentration, 112 mg·kg^{-1}.

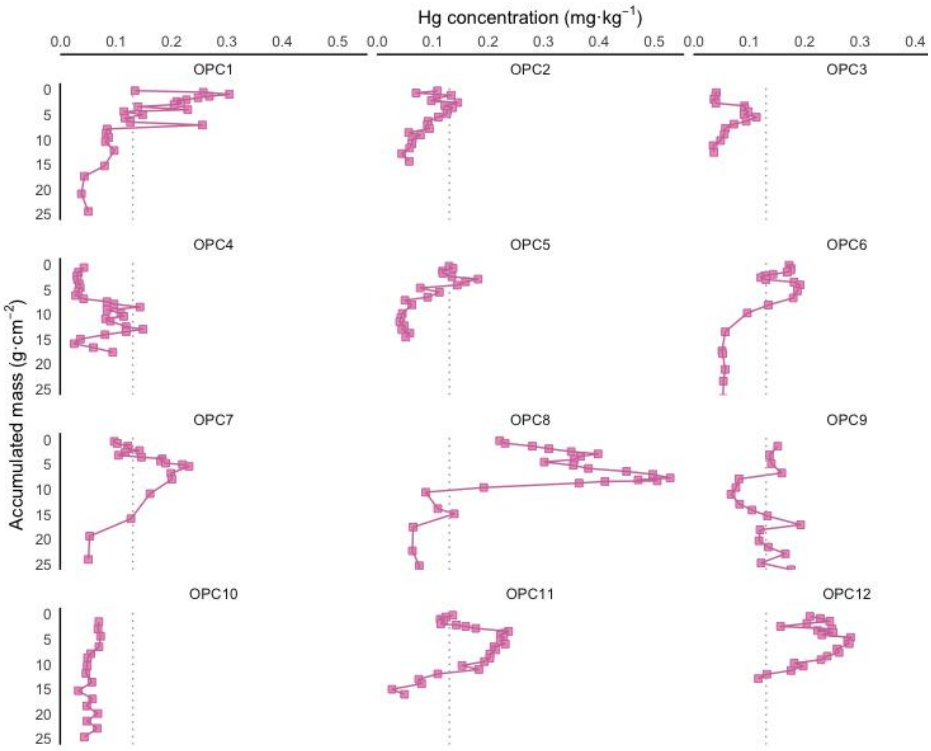


Figure 7.5 Hg concentration (mg·kg^{-1}) profiles for cores. The dotted line represents the Threshold Effects Level (TEL) concentration, 0.13 mg·kg^{-1}.

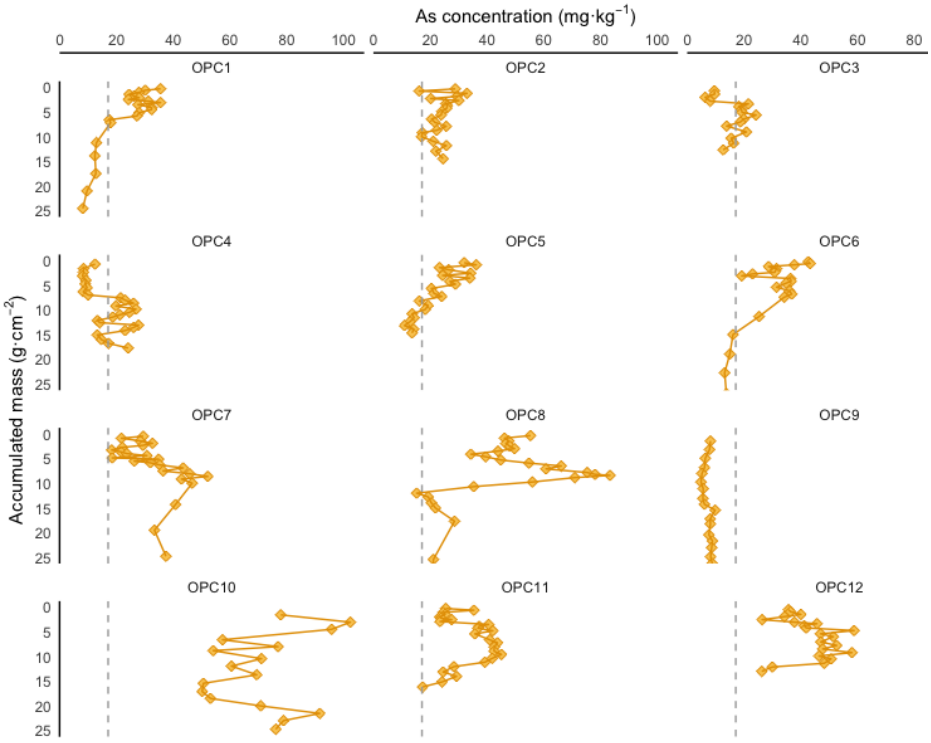


Figure 7.6 Arsenic concentration (mg·kg^{-1}) profiles for cores. The dashed line represents the Probable Effects Level (PEL) concentration, 17 mg·kg^{-1}.

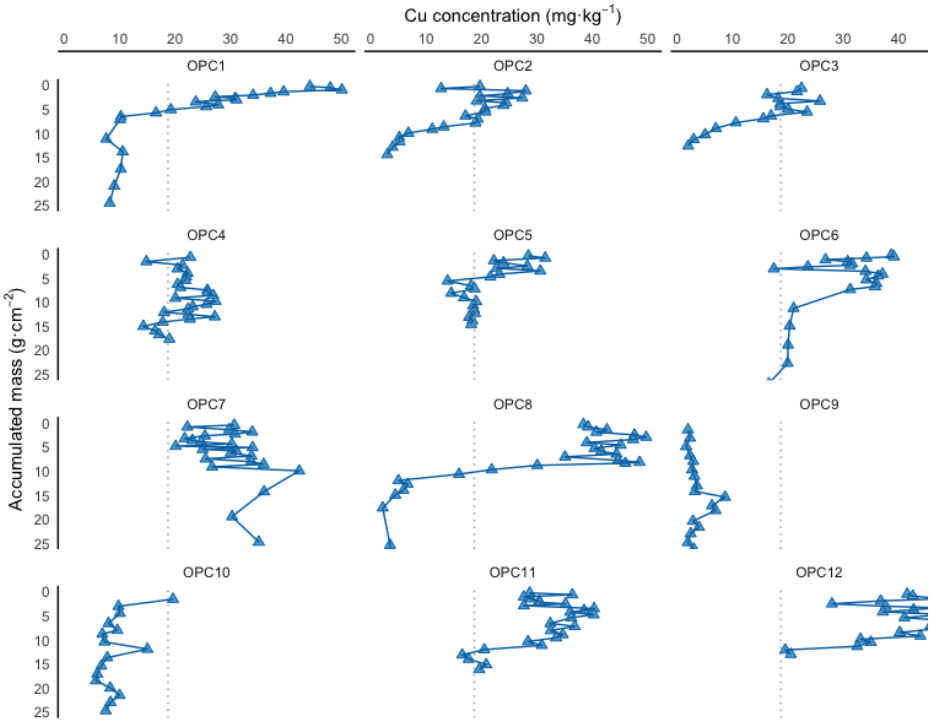


Figure 7.7 Cu concentration (mg·kg^{-1}) profiles for cores. The dotted line represents the Threshold Effects Level (TEL) concentration, 18.7 mg·kg^{-1}.

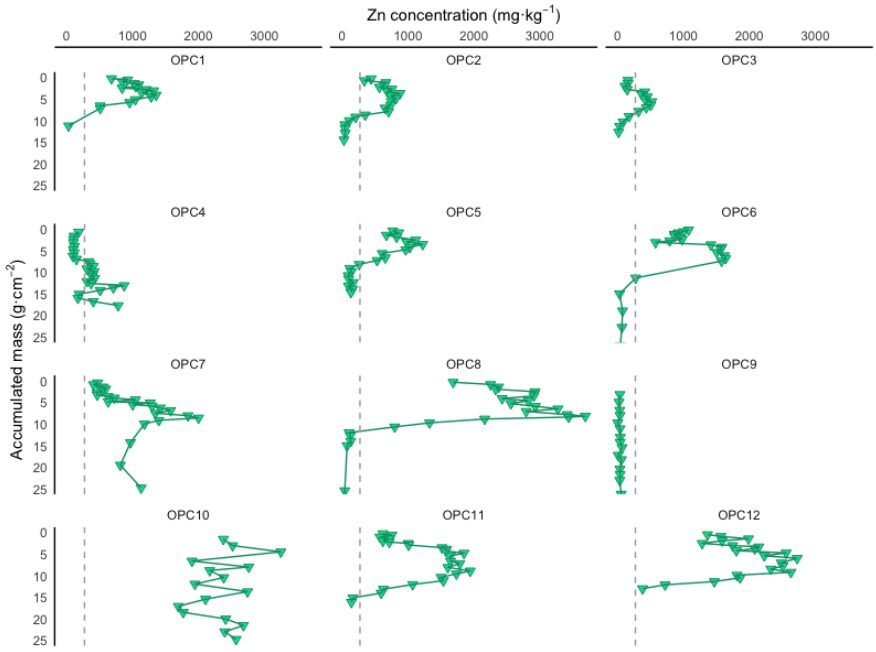


Figure 7.8 Zn concentration (mg·kg^{-1}) profiles for cores. The dashed line represents the Probable Effects Level (PEL) concentration, 271 mg·kg^{-1}.

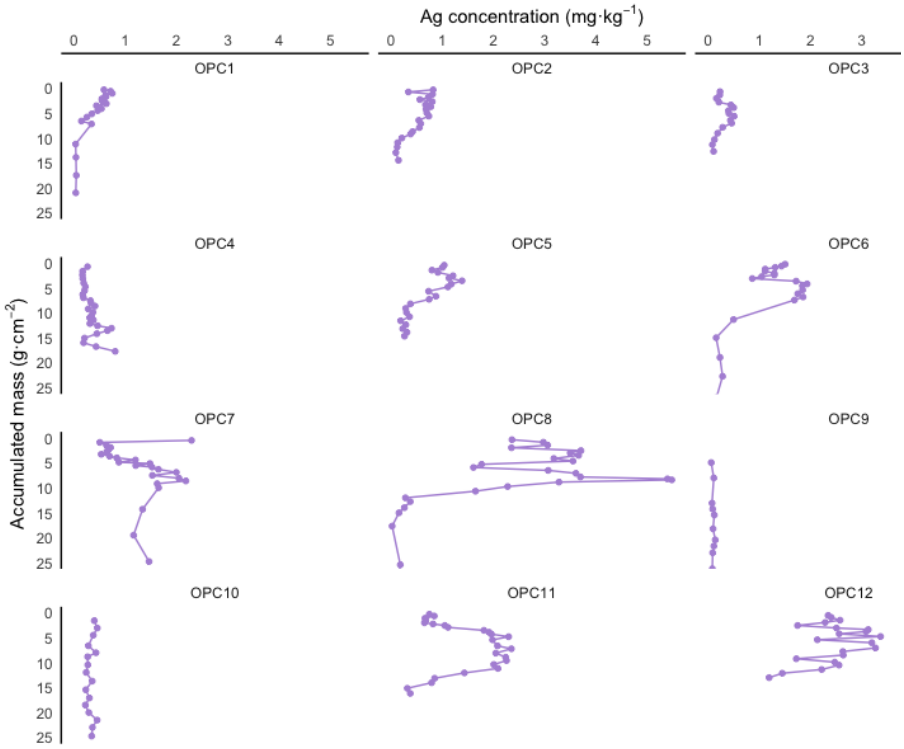


Figure 7.9 Ag concentration (mg·kg^{-1}) profiles for cores.

7.1.7 Sequential T-test Analysis of Regime Shifts (STARS) results

Table 7.4 RSI and p-values. for cores OPC1 (North), OPC6 (Center) and OPC8 (South).

	Metal	Year	RSI or p-vals*
North	Pb	Before 20th century	2.2
		1900s	1.7
	Hg	Before 20th century	1
		1980s	1.1
	As	Before 20th century	1.5
		1900s	1.5
	Cu	1900s	1.7
		1920s	0.041
		1970s	1.4
		2000s	1.4
	Zn	1900s	3.3
	Ag	Before 20th century	1.1
		1920s	1.5
		2000s	0.2
Center	Pb	Before 20th century	2.7
		1960s	1.4
	Hg	Before 20th century	2.9
		1900s - 1920s	1
		1960s	1.6
		1990s	0.73
	As	Before 20th century	2.2
		1960s	0.52
		2000s	1.4
	Cu	Before 20th century	1.7
		1960s	0.99
		1970s	0.05
	Zn	Before 20th century	3.9
		1960s	1.2
	Ag	Before 20th century	3.7

		1960s	0.95
South	Pb	Before 20th century	2.7
		1900s - 1910s	2.8
		1960s	0.15
	Hg	Before 20th century	3.8
		1910s - 1920s	1.2
		1980s	1.3
	As	Before 20th century	3
		1900s – 1910s	1.6
		1960s	0.8
		1980s	1.3
	Cu	Before 20th century	2.6
		1900s - 1910s	2.7
	Zn	1900s - 1910s	0.037*
	Ag	Before 20th century	1.8
		1920s - 1930s	1.9
		1980s	0.0024
		1990s	0.3

7.1.8 Metal correlations with dry bulk density and grain size

Table 7.5 R correlation coefficient (Spearman) between dry bulk density, grain size, and metal concentrations in sediments.

	Dry bulk density ($g \cdot cm^{-3}$)	Clay (%)	Silt (%)	Sand (%)	Gravel (%)
Ag	-0.59**	-0.17*	0.34**	-0.19*	-0.053
Al	-0.30**	0.26**	0.26**	-0.30**	-0.090
As	-0.31**	-0.32**	0.10	0.056	-0.028
Ca	0.37**	0.043	-0.40**	0.30**	0.30**
Cd	-0.55**	0.19*	0.33**	-0.14	0.024
Cr	-0.43**	0.37**	0.57**	-0.55**	-0.33**
Cu	-0.75	0.033	0.58**	-0.44**	-0.13
Fe	-0.23**	-0.13	0.21**	-0.12	-0.27**
Na	-0.87	0.05	0.54**	-0.46**	0.12
Ni	-0.47	0.34**	0.59**	-0.55**	-0.31**
Pb	-0.48**	-0.29**	0.25**	-0.067	-0.051
Si	0.16*	-0.13	-0.038	0.072	-0.13
Sr	0.38**	-0.42**	-0.55**	0.61**	0.39**
Ti	-0.50**	0.32**	0.63**	-0.54**	-0.35**
Zn	-0.42**	-0.39**	0.21**	-0.013	-0.09

*Correlation is significant at the 0.05 level.

**Correlation is significant at the 0.01 level.

7.1.9 Accumulated Pb stocks

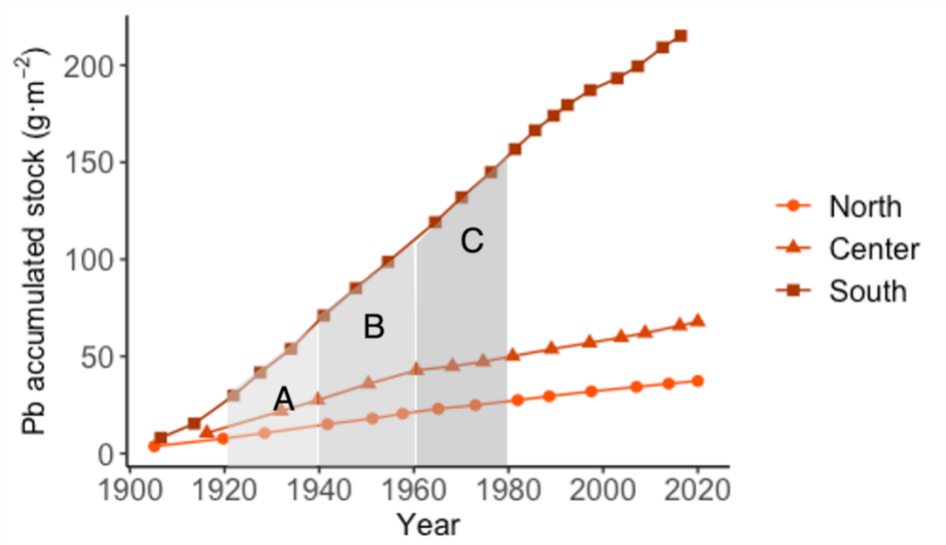


Figure 7.10 Pb accumulated stock for cores OPC1 (North), OPC6 (Center), OPC8 (South). A period corresponds to 1920-1940, when industrial mining was expanding, B to 1940-1960, when the exploitation reached its peak, and C to 1960-1980, following the implementation of spilling bans to Mar Menor.

Table 7.6 Accumulated Pb by periods and core for each area.

Accumulated Pb (g·m^{-2})	North	Center	South
A: 1920-1940	7.4	17	41
B: 1940-1960	7.9	15	48
C: 1960-1980	4.5	7.3	38

7.2 Supplementary Information for Chapter 4

Source	n	TOC (%)	TN (%)	C:N	$\delta^{13}C$ (‰)	$\delta^{15}N$ (‰)
Lemon tree leaves	4	40.73 ± 1.69	1.84 ± 0.23	26.0 ± 2.2	-28.35 ± 0.84	6.33 ± 0.67
Lettuce	1	43.32	3.83	13.2	-28.19	8.62
Celery	3	42.03 ± 2.06	4.74 ± 0.33	10.4 ± 1.2	-29.34 ± 0.23	4.75 ± 2.99
Almond tree leaves	2	43.26 ± 0.16	2.09 ± 0.11	24.3 ± 1.3	-26.95 ± 0.32	1.30 ± 0.25
Floating algae	3	29.94 ± 2.21	3.34 ± 0.09	10.5 ± 0.5	-19.13 ± 0.58	9.48 ± 0.47
Caulerpa prolifera	15	44.64 ± 1.97	3.82 ± 0.72	14.2 ± 3.5	-14.68 ± 0.68	5.05 ± 1.00
Cymodocea nodosa	3	41.19 ± 0.33	2.87 ± 0.02	16.7 ± 0.2	-6.14 ± 0.33	4.75 ± 0.52
Posidonia oceanica (Mediterranean)	3	27.63 ± 2.19	0.75 ± 0.04	42.9 ± 5.1	-12.78 ± 1.54	1.30 ± 0.29
Albujón SPOM	2	0.64 ± 0.02	0.053*	12.0*	-16.41 ± 0.43	8.40*
Coastal lagoon SPOM	4	0.21 ± 0.03	0.010 ± 0.003	22.0 ± 5.7	-22.86 ± 2.11	3.45 ± 0.46
Mediterranean SPOM	1	0.51	0.013	38	-15.7	2.9

7.2.1 Spatial patterns of C_{org}, TN, $\delta^{13}C$ and $\delta^{15}N$ for all sediment data by region

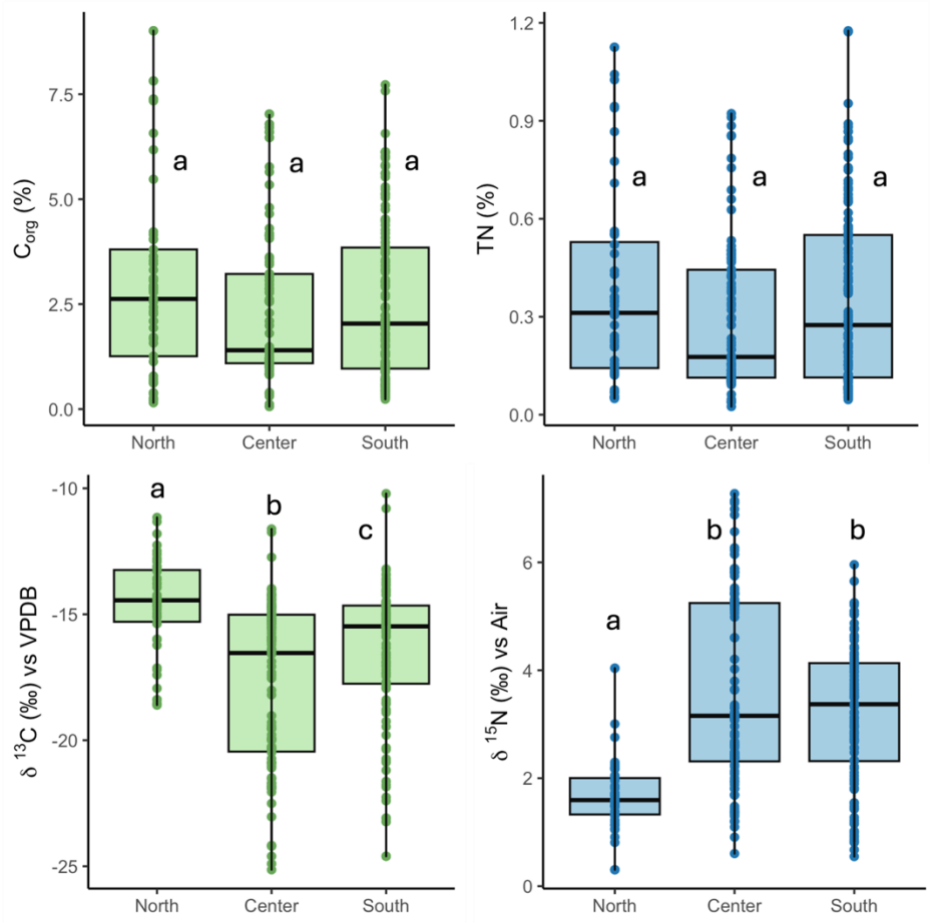


Figure 7.11 Boxplots for C_{org}, TN, $\delta^{13}C$ and $\delta^{15}N$ grouped by lagoon sector (North, Center, South). Points represent individual sediment samples, boxes represent the interquartile range (IQR), horizontal lines indicate medians, and whiskers extend to 1.5 x IQR. Letters denote statistically significant differences among sectors (Dunn's post hoc test, $p < 0.05$).

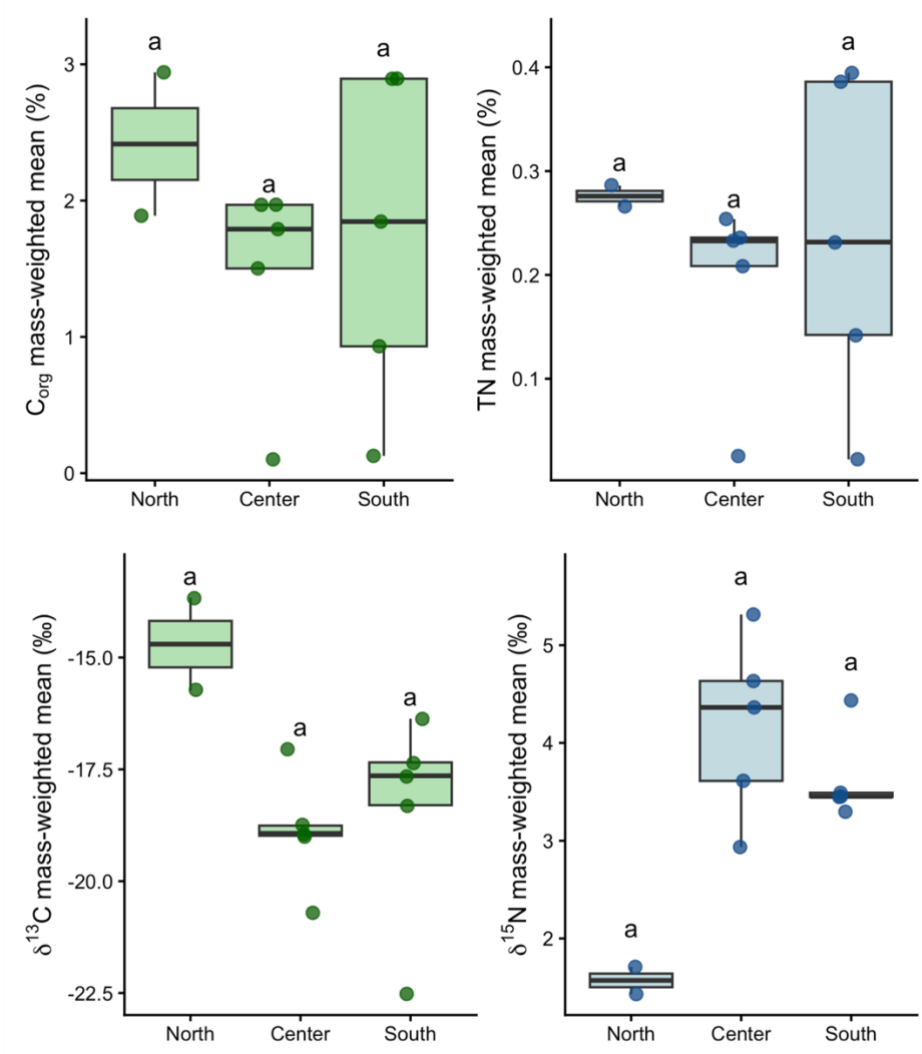


Figure 7.12 Mass-weighted mean boxplots for C_{org}, TN, $\delta^{13}C$ and $\delta^{15}N$ grouped by lagoon sector (North, Center, South). Points represent individual sediment samples, boxes represent the interquartile range (IQR), horizontal lines indicate medians, and whiskers extend to 1.5 x IQR. Letters denote statistically significant differences among sectors (Dunn's post hoc test, $p < 0.05$).

7.2.2 C_{org} (%), TN (%), $\delta^{13}C$ (‰) and $\delta^{15}N$ (‰) depth profiles

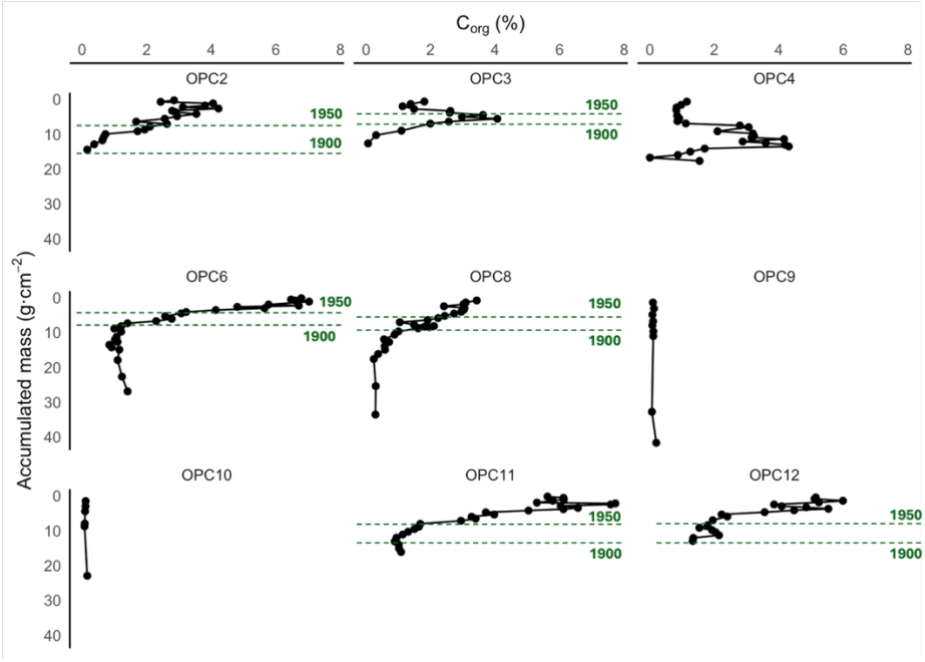


Figure 7.13 C_{org} concentration profiles (%) of the cores not shown in the main text. Cores are grouped by region: north (OPC2), center (OPC3, OPC4, OPC6), and south (OPC8, OPC9, OPC10, OPC11, OPC12).

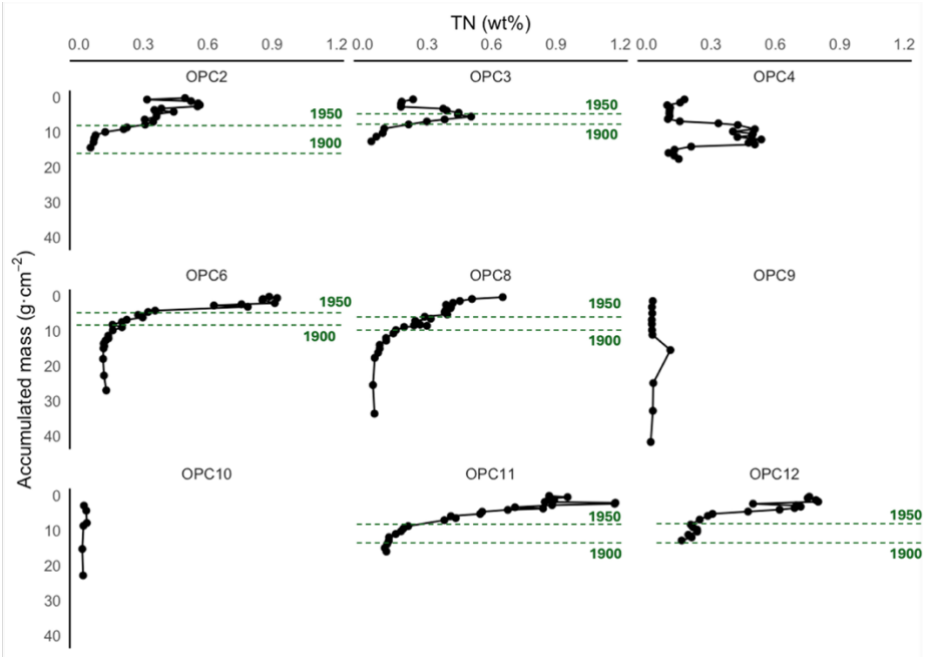


Figure 7.14 TN concentration profiles (%) of the cores not shown in the main text. Cores are grouped by region: north (OPC2), center (OPC3, OPC4, OPC6), and south (OPC8, OPC9, OPC10, OPC11, OPC12).

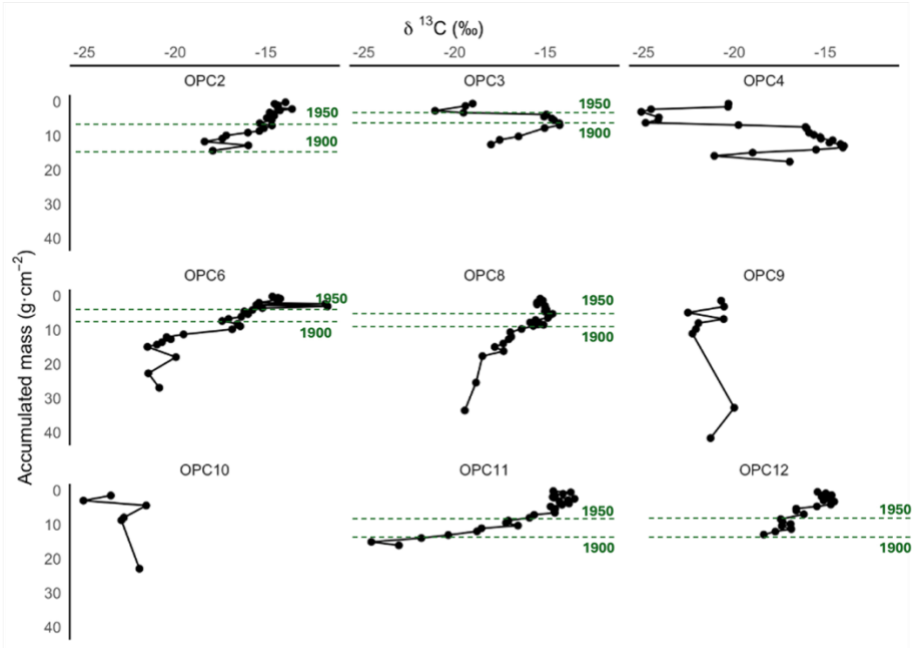


Figure 7.15 $\delta^{13}C$ profiles (‰) of the cores not shown in the main text. Cores are grouped by region: north (OPC2), center (OPC3, OPC4, OPC6), and south (OPC8, OPC9, OPC10, OPC11, OPC12).

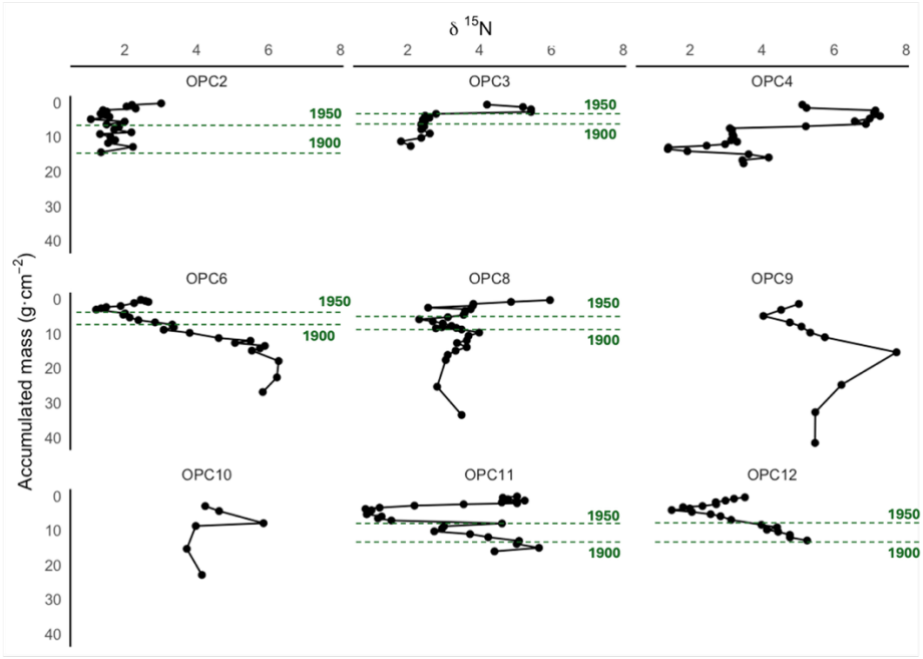


Figure 7.16 $\delta^{15}N$ profiles (‰) of the cores not shown in the main text. Cores are grouped by region: north (OPC2), center (OPC3, OPC4, OPC6), and south (OPC8, OPC9, OPC10, OPC11, OPC12).

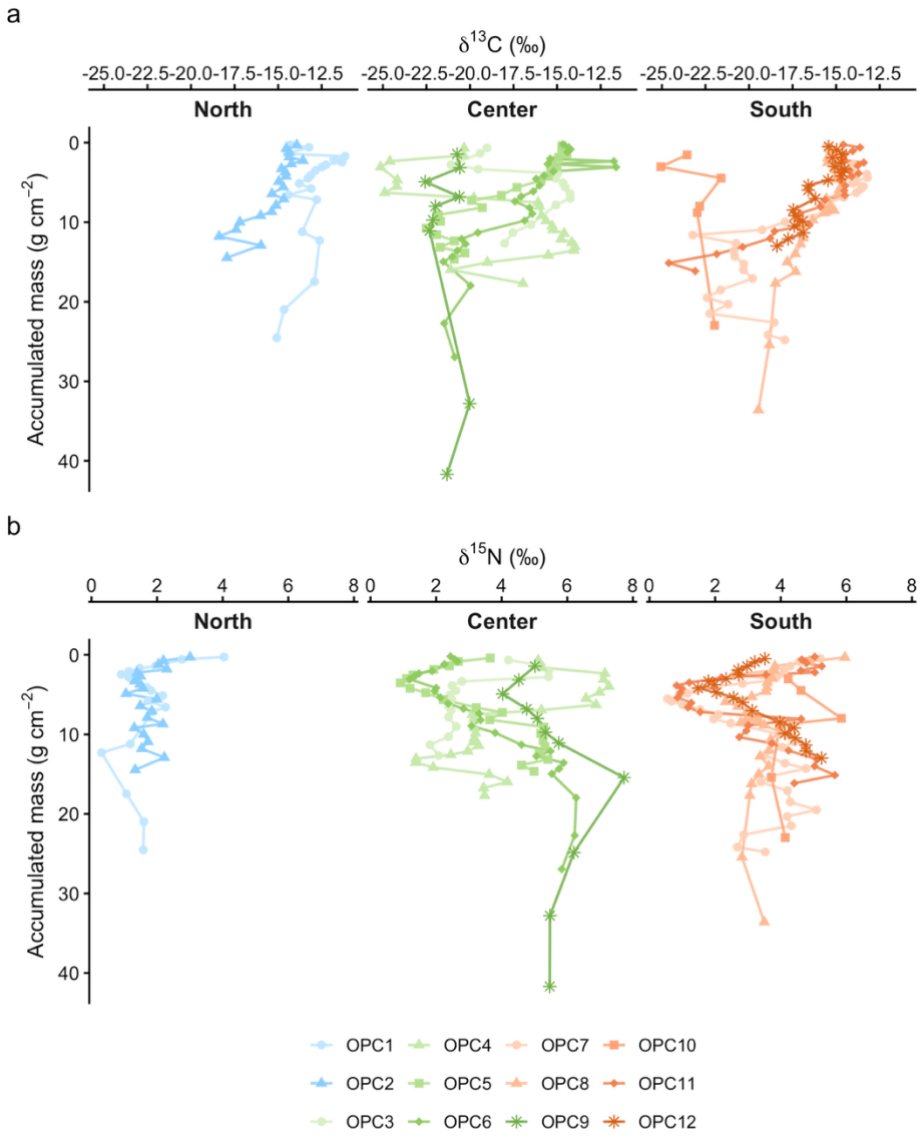


Figure 7.16 $\delta^{13}C$ and $\delta^{15}N$ profiles (‰) of all cores.

7.2.3 C:N ratios depth profiles

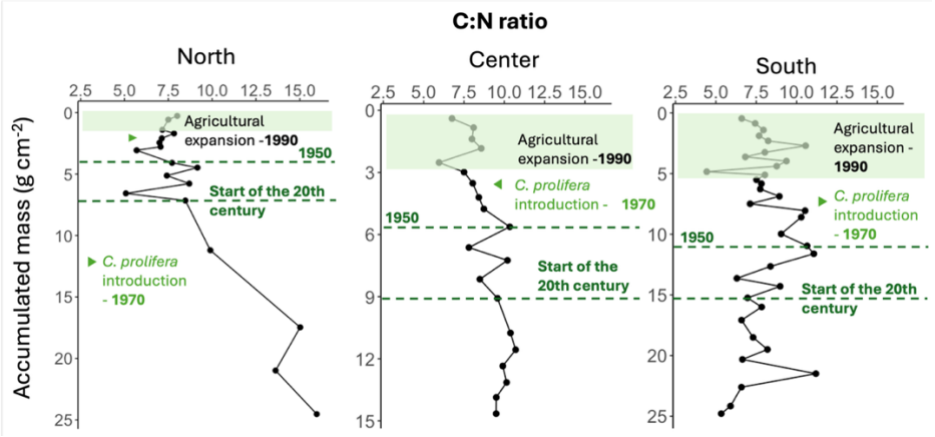


Figure 7.17 C:N ratio profiles of selected cores representative of the different lagoon sectors (OPC1 in the north, OPC5 in the center, and OPC7 in the southwest).

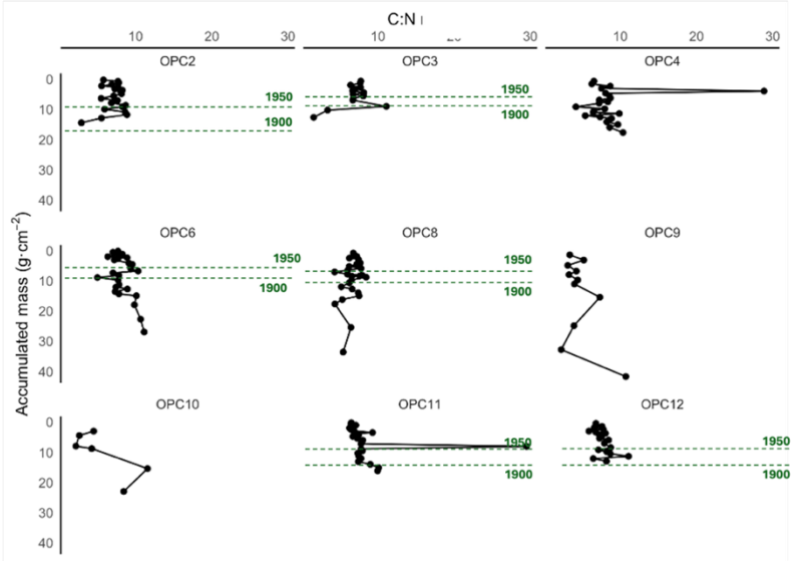


Figure 7.18 C:N ratio profiles of the cores not shown in the main text. Cores are grouped by region: north (OPC2), center (OPC3, OPC4, OPC6), and south (OPC8, OPC9, OPC10, OPC11, OPC12).

7.2.4 Mixing model without concentration dependence and 5 endmembers

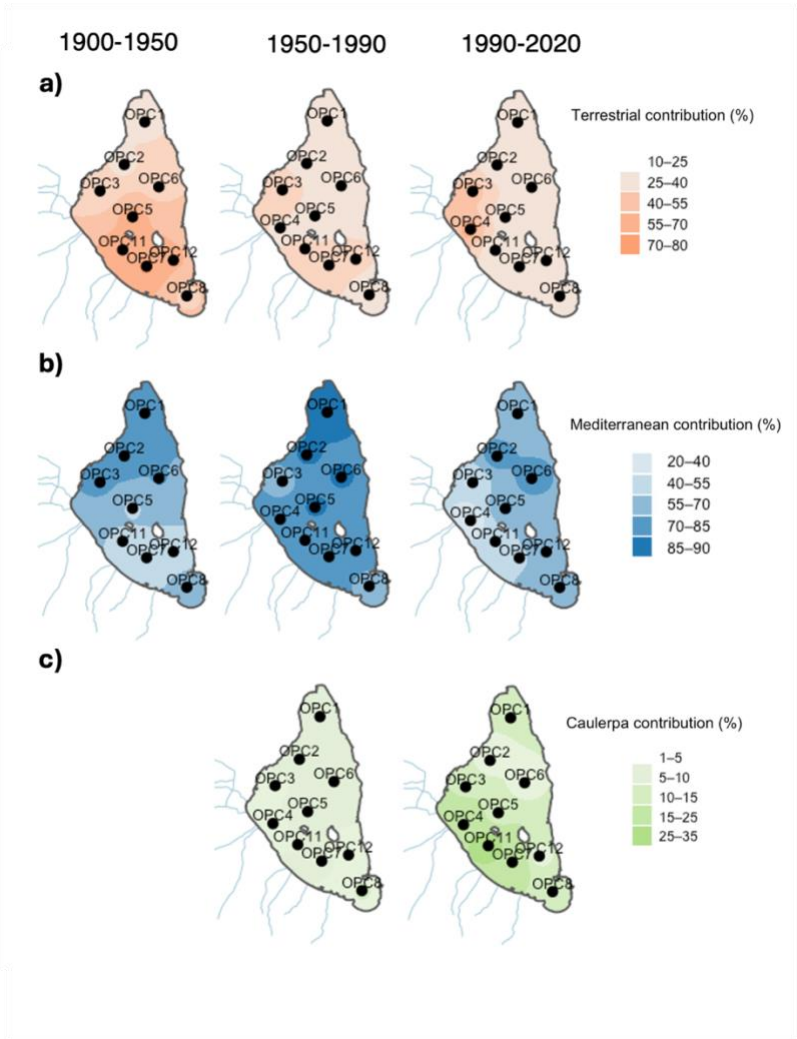


Figure 7.19 Spatially interpolated nutrient contributions (%) of Terrestrial, Mediterranean, and *Caulerpa prolifera* sources for 1900-1950, 1950-1990, and 1990-2020 for model configuration without concentration dependence and 5 endmembers: the aforementioned ones, *C. nodosa* and surficial algae. For representation purposes, categories are different from the figure in the main text.

7.2.5 Mixing model with concentration dependence and 3 endmembers

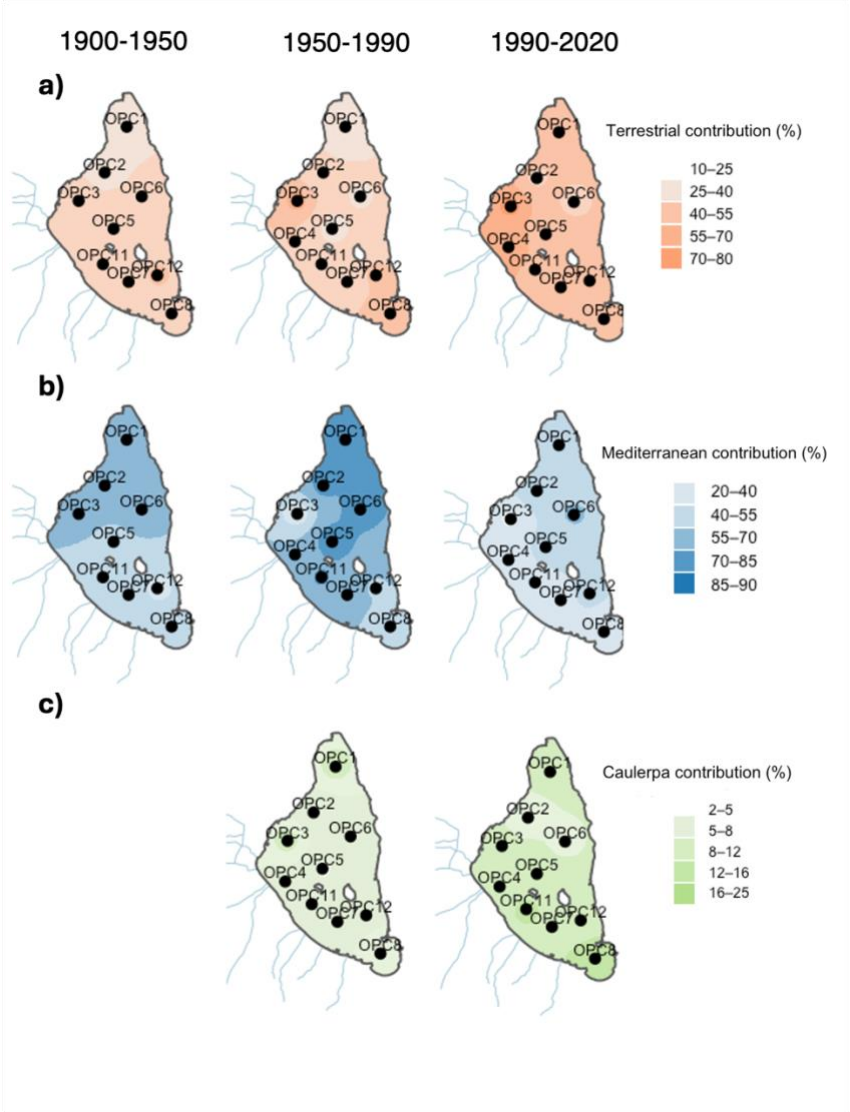


Figure 7.20 Spatially interpolated nutrient contributions (%) of Terrestrial, Mediterranean, and *Caulerpa prolifera* sources for 1900-1950, 1950-1990, and 1990-2020 for model configuration with concentration dependence and these three endmembers. For representation purposes, categories are different from the figure in the main text.

7.3 Supplementary Information for Chapter 5

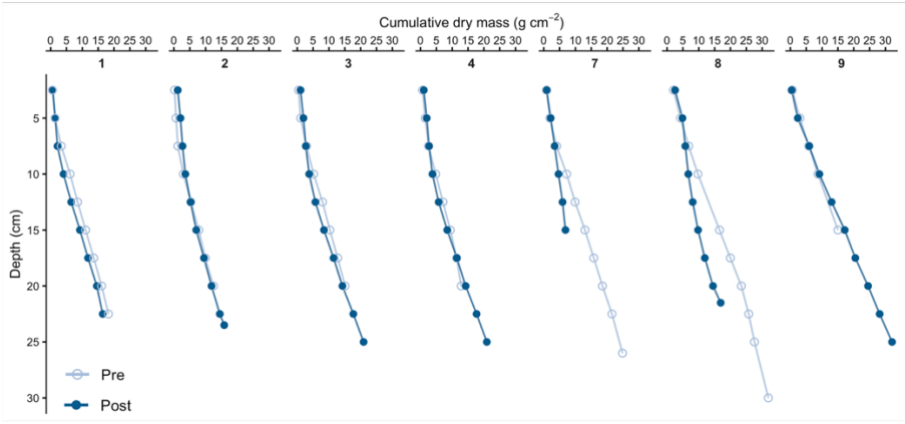


Figure 7.21 Cumulative dry mass (g cm^{-2}) profiles by depth for collected cores before (open light-blue circles) and after (filled dark-blue circles) restoration.

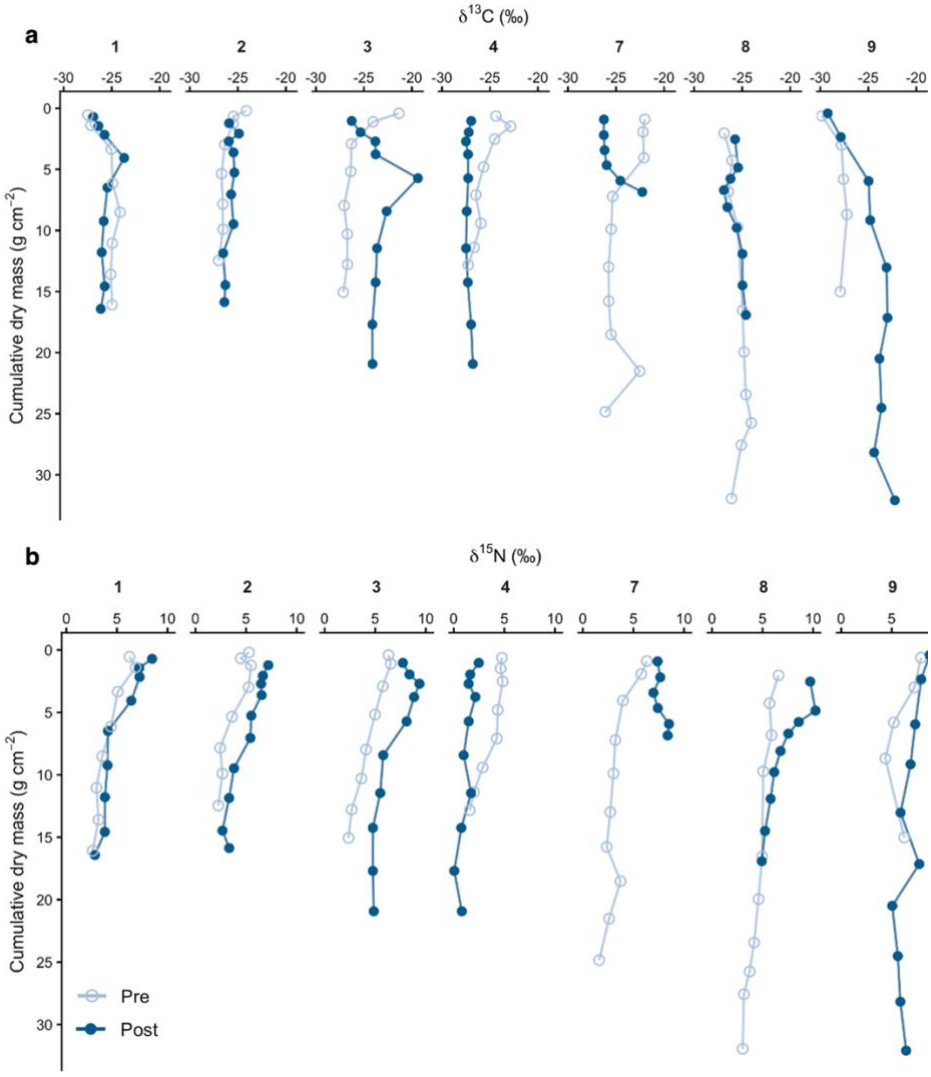


Figure 7.22 a) $\delta^{13}C$ (‰) and (b) $\delta^{15}N$ (‰) as a function of cumulative dry mass (g cm^{-2}) in cores collected before (open light-blue circles) and after (filled dark-blue circles) restoration across sites.

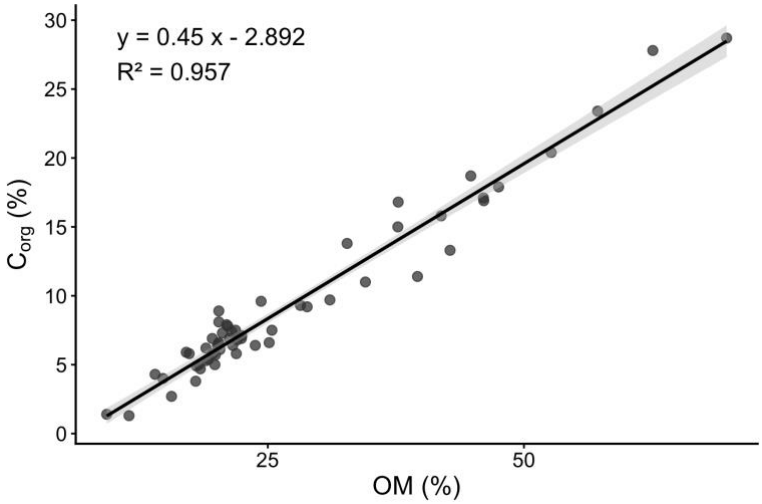


Figure 7.23 Relationship between organic matter (OM, %) and organic carbon content (Corg, %) in Hill Slough sediment samples from before restoration. Points represent individual samples collected across all cores and sampling periods. The solid line represents the linear regression fit, and the shaded area the 95% confidence interval.

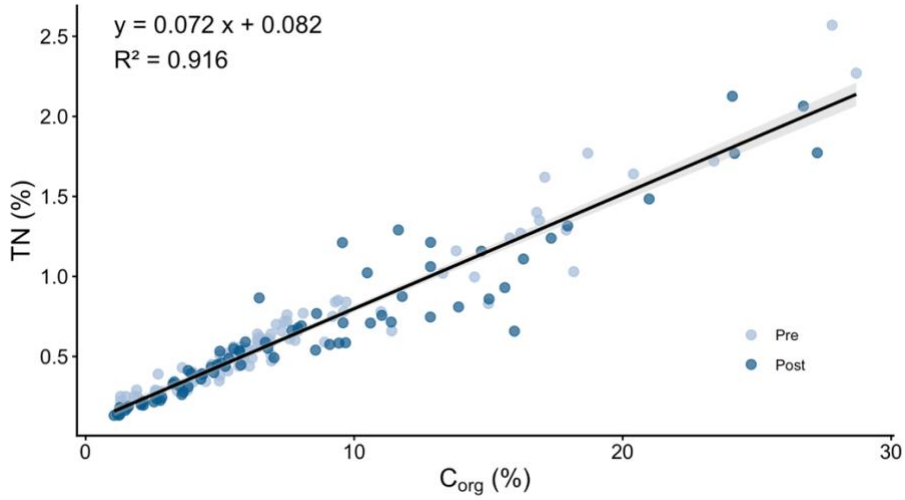


Figure 7.24 Relationship between sediment organic carbon (Corg, %) and total nitrogen (TN, %) concentrations in sediment samples. The solid black line represents the linear regression fit, while the shaded area indicates the 95% confidence interval.

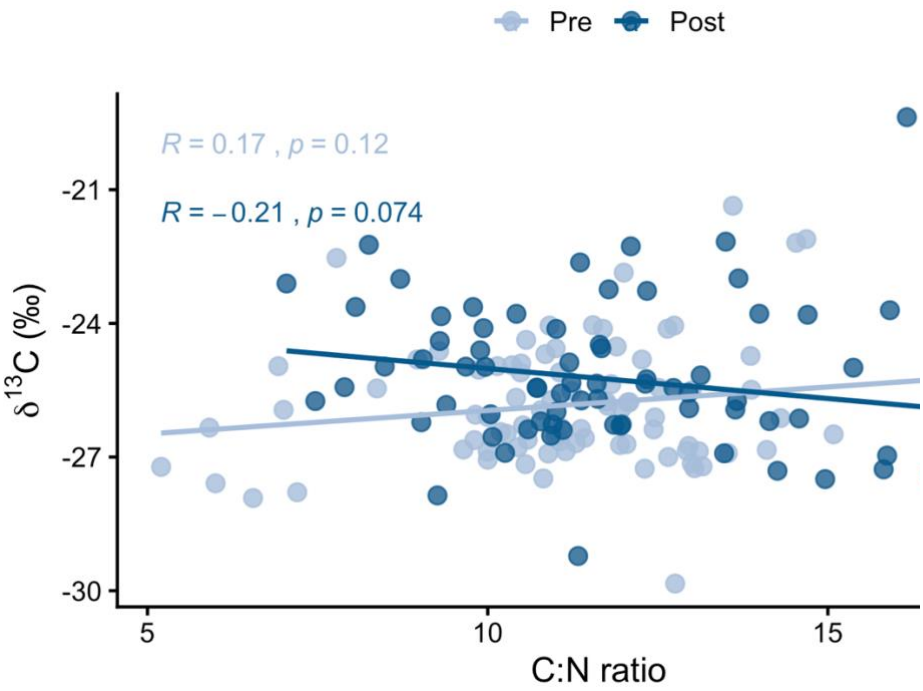


Figure 7.25 Relationship between sediment C:N ratio and $\delta^{13}C$ values before (Pre) and after (Post) tidal restoration at Hill Slough. Solid lines represent linear regressions for each period. No significant relationship between C:N ratio and $\delta^{13}C$ was found. A sample with C:N ratio over 20 was considered an outlier for the post-restoration samples and is not displayed in this graph nor accounted in the linear regression.

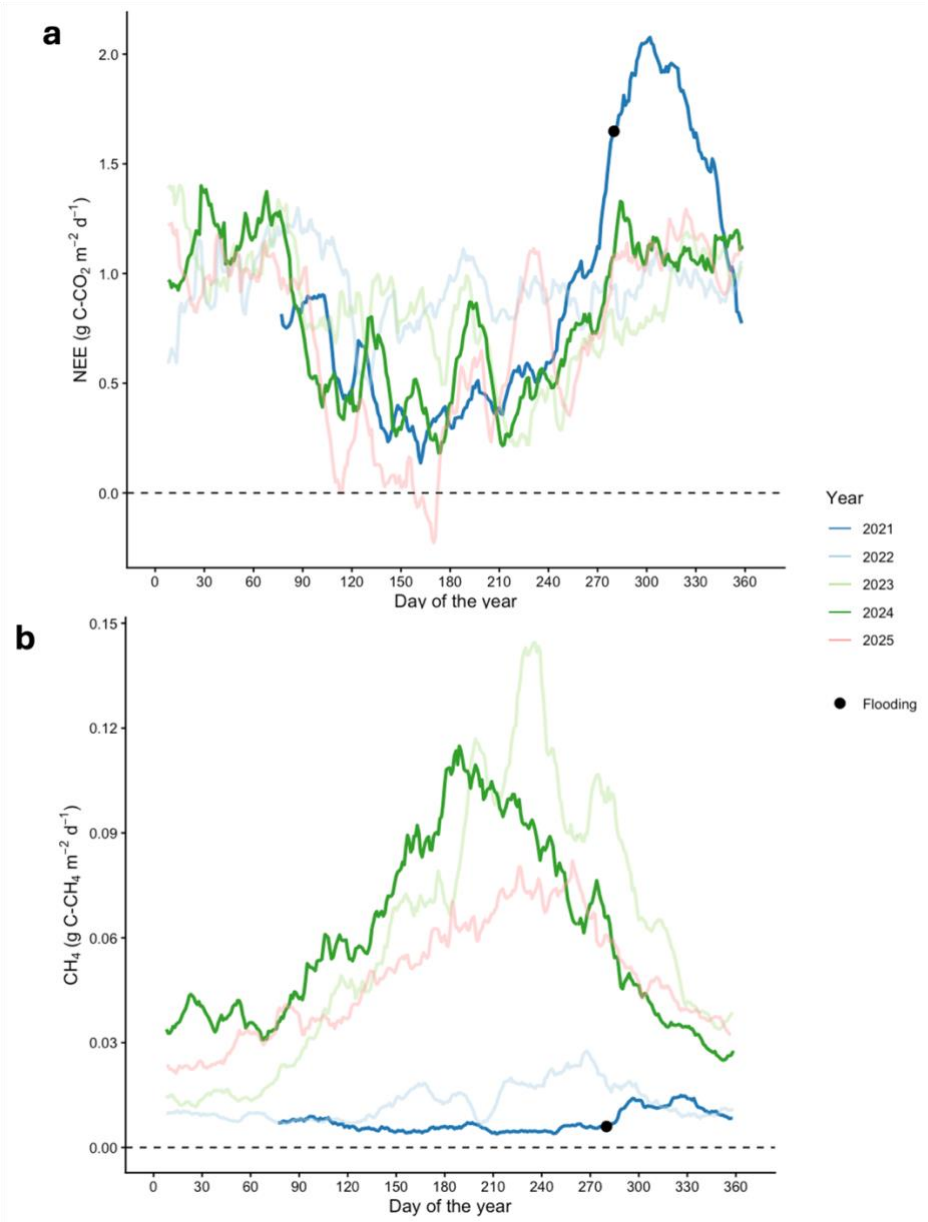


Figure 7.26 a) Net ecosystem exchange (g C-CO_2 m^{-2} d^{-1}) and b) CH_4 (g C-CH_4 m^{-2} d^{-1}) flux evolution over the period 2021-2025. The black dot indicates the flooding moment in 2021. Dark blue and dark green lines apply to the soil sampling years (2021, 2024).

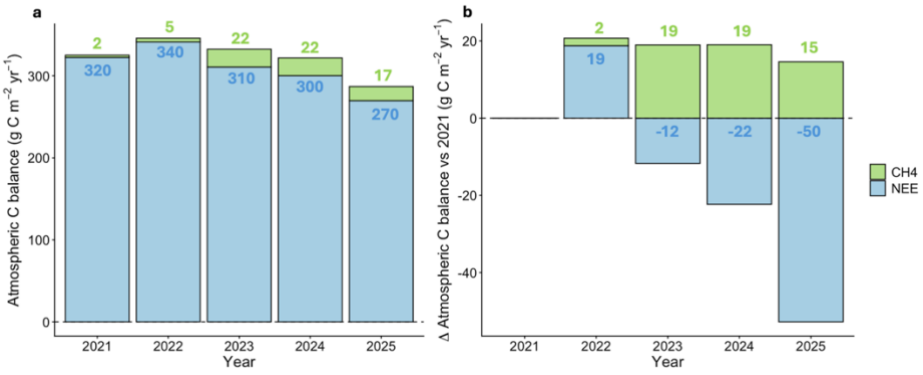


Figure 7.27 a) Annual atmospheric C balance (g C m^{-2} yr^{-1}) for years 2021-2025. b) Increment of the annual atmospheric C balance with respect to 2021 (g C m^{-2} yr^{-1}).

8. References

Abu-Zied, R. H., Al-Mur, B. A., Orif, M. I., Al Otaibi, A., & Ghandourah, M. A. (2021). Concentration distribution, enrichment and controlling factors of metals in Al-Shuaiba Lagoon sediments, Eastern Red Sea, Saudi Arabia. *Environmental Earth Sciences*, *80*(10), 385. https://doi.org/10.1007/s12665-021-09676-6

Ahmed, F., Bibi, M. H., Seto, K., Ishiga, H., Fukushima, T., & Roser, B. P. (2010). Abundances, distribution, and sources of trace metals in Nakaumi–Honjo coastal lagoon sediments, Japan. *Environ Monit Assess*, 19.

Aiello, I. W., Endris, C., Cunningham, S., Fountain, M., Grand, M. M., Heim, W., Kahn, A. S., & Wasson, K. (2025). Coastal wetland deposition of cathode metals from the world's largest lithium-ion battery fire. *Scientific Reports*, *15*(1), 42113. https://doi.org/10.1038/s41598-025-25972-8

Albuquerque, U. P., Ludwig, D., Feitosa, I. S., de Moura, J. M. B., Gonçalves, P. H. S., da Silva, R. H., da Silva, T. C., Gonçalves-Souza, T., & Ferreira Júnior, W. S. (2021). Integrating traditional ecological knowledge into academic research at local and global scales. *Regional Environmental Change*, *21*(2), 45. https://doi.org/10.1007/s10113-021-01774-2

Alcolea, A., Contreras, S., Hunink, J. E., García-Aróstegui, J. L., & Jiménez-Martínez, J. (2019). Hydrogeological modelling for the watershed management of the Mar Menor coastal lagoon (Spain). *Science of The Total Environment*, *663*, 901–914. https://doi.org/10.1016/j.scitotenv.2019.01.375

Alexandre, A., & Santos, R. (2020). High Nitrogen and Phosphorous Acquisition by Belowground Parts of Caulerpa prolifera (Chlorophyta) Contribute to the Species' Rapid Spread in Ria Formosa Lagoon, Southern Portugal. *Journal of Phycology—Wiley Online Library*. https://onlinelibrary.wiley.com/doi/10.1111/jpy.12988

Algeo, T. J., & Liu, J. (2020). A re-assessment of elemental proxies for paleoredox analysis. *Chemical Geology*, *540*, 119549. https://doi.org/10.1016/j.chemgeo.2020.119549

Allan, J. M., Guêné-Nanchen, M., Rochefort, L., Douglas, D. J. T., & Axmacher, J. C. (2024). Meta-analysis reveals that enhanced practices accelerate

vegetation recovery during peatland restoration. *Restoration Ecology*, *32*(3), e14015. https://doi.org/10.1111/rec.14015

Alongi, D. M. (2020a). Global Significance of Mangrove Blue Carbon in Climate Change Mitigation. *Sci*, *2*(3), 67. https://doi.org/10.3390/sci2030067

Alongi, D. M. (2020b). Nitrogen Cycling and Mass Balance in the World's Mangrove Forests. *Nitrogen*, *1*(2), 167–189. https://doi.org/10.3390/nitrogen1020014

Alongi, D. M. (2025). Global Meta-Analysis of Mangrove Primary Production: Implications for Carbon Cycling in Mangrove and Other Coastal Ecosystems. *Forests*, *16*(5), 747. https://doi.org/10.3390/f16050747

Alorda-Kleinglass, A., Garcia-Orellana, J., Rodellas, V., Cerdà-Domènech, M., Tovar-Sánchez, A., Diego-Feliu, M., Trezzi, G., Sánchez-Quilez, D., Sanchez-Vidal, A., & Canals, M. (2019). Remobilization of dissolved metals from a coastal mine tailing deposit driven by groundwater discharge and porewater exchange. *Science of The Total Environment*, *688*, 1359–1372. https://doi.org/10.1016/j.scitotenv.2019.06.224

Alorda-Montiel, I., Rodellas, V., Arias-Ortiz, A., Palanques, A., Bravo, A. G., Rodriguez-Puig, J., Alorda-Kleinglass, A., Green-Ruiz, C., Diego-Feliu, M., Masqué, P., Gilabert, J., & Garcia-Orellana, J. (2025). A century of sediment metal contamination of Mar Menor, Europe's largest saltwater lagoon. *Marine Pollution Bulletin*, *220*, 118347. https://doi.org/10.1016/j.marpolbul.2025.118347

Álvarez Rogel, J., Otero Pérez, X. L., Tercero Gómez, M. del C., Conesa Alcaraz, H. M., Bernardeau-Esteller, J., Belando, M. D., García-Muñoz, R., & Ruíz Martínez, J. M. (2021). *Morphological characteristics and Eh/pH conditions in sediments from the bottom of the Mar Menor: Relationships with the uses of the territory*. IX Simposio Nacional sobre Control de la Degradación y Recuperación de Suelos. https://doi.org/10.5555/20210437819

Amaral, V., Santos-Echeandía, J., Ortega, T., Álvarez-Salgado, X. A., & Forja, J. (2023). Dissolved organic matter distribution in the water column and sediment pore water in a highly anthropized coastal lagoon (Mar Menor, Spain): Characteristics, sources, and benthic fluxes. *Science of The Total Environment*, *896*, 165264. https://doi.org/10.1016/j.scitotenv.2023.165264

Anthony, T. L., & Silver, W. L. (2020). Mineralogical associations with soil carbon in managed wetland soils. *Global Change Biology*, *26*(11), 6555–6567. https://doi.org/10.1111/gcb.15309

Apostolaki, E. T., Lavery, P. S., Litsi-Mizan, V., Serrano, E., Inostroza, K., Gerakaris, V., Dailianis, T., Glampedakis, J., Holitzki, T., Johnson, E., Mateo, M. A., & Serrano, O. (2024). Patterns of Carbon and Nitrogen Accumulation in Seagrass (Posidonia oceanica) Meadows of the Eastern Mediterranean Sea. *Journal of Geophysical Research: Biogeosciences*, *129*(12), e2024JG008163. https://doi.org/10.1029/2024JG008163

Appleby, P. G., & Oldfield, F. (1978). The calculation of lead-210 dates assuming a constant rate of supply of unsupported 210Pb to the sediment. *CATENA*, *5*(1), 1–8. https://doi.org/10.1016/S0341-8162(78)80002-2

Aquino-López, M. A., Blaauw, M., Christen, J. A., & Sanderson, N. K. (2018). Bayesian Analysis of ^{210}Pb Dating. *Journal of Agricultural, Biological and Environmental Statistics*, *23*(3), 317–333. https://doi.org/10.1007/s13253-018-0328-7

Aquino-López, M. A., Ruiz-Fernández, A. C., Blaauw, M., & Sanchez-Cabeza, J.-A. (2020). Comparing classical and Bayesian 210Pb dating models in human-impacted aquatic environments. *Quaternary Geochronology*, *60*, 101106. https://doi.org/10.1016/j.quageo.2020.101106

Arias-Ortiz, A., Lafratta, A., Colarusso, P., Fourqurean, J., Fu, C., Kennedy, H., Krause, J., Lavery, P., Leiva-Dueñas, C., Marba, N., Mateo, M., Mazarrasa, I., Poursanidis, D., Salinas, C., Serrano, O., Stankovic, M., Piñeiro, N., Werner, A., Wesselmann, M., … Masque, P. (2026). *Seagrass sediment organic carbon burial rates are globally significant*. In Review. https://doi.org/10.21203/rs.3.rs-8462059/v1

Arias-Ortiz, A., & Baldocchi, D. (2026). *DOI Listing for US-Dmg*. Ameriflux. AmeriFlux. https://ameriflux.lbl.gov/doi/AmeriFlux/US-Dmg/

Arias Ortiz, A., Wolfe, J., Bridgham, S., Knox, S., Mcnicol, G., Needelman, B. a, Shahan, J., Stuart-haëntjens, E. j, Windham-myers, L., Oikawa, P., Baldocchi, D., Caplan, J., Capooci, M., Czapla, K. M., Derby, R. kyle, Diefenderfer, H. L., Forbrich, I., Groseclose, G., Keller, J. K., … Holmquist, J. R. (2024). Methane fluxes in tidal marshes of the

conterminous United States. *Global Change Biology*, *30*. https://doi.org/10.1111/gcb.17462

Arias-Ortiz, A., Oikawa, P. Y., Carlin, J., Masqué, P., Shahan, J., Kanneg, S., Paytan, A., & Baldocchi, D. D. (2021). Tidal and Nontidal Marsh Restoration: A Trade-Off Between Carbon Sequestration, Methane Emissions, and Soil Accretion. *Journal of Geophysical Research: Biogeosciences*, *126*(12), e2021JG006573. https://doi.org/10.1029/2021JG006573

Arias-Ortiz, A., Serrano, O., Masqué, P., Lavery, P. S., Mueller, U., Kendrick, G. A., Rozaimi, M., Esteban, A., Fourqurean, J. W., Marbà, N., Mateo, M. A., Murray, K., Rule, M. J., & Duarte, C. M. (2018). A marine heatwave drives massive losses from the world's largest seagrass carbon stocks. *Nature Climate Change*, *8*(4), Article 4. https://doi.org/10.1038/s41558-018-0096-y

Arias-Ortiz, A., Masqué, P., Garcia-Orellana, J., Serrano, O., Mazarrasa, I., Marbà, N., Lovelock, C. E., Lavery, P. S., & Duarte, C. M. (2018). Reviews and syntheses: 210Pb-derived sediment and carbon accumulation rates in vegetated coastal ecosystems – setting the record straight. *Biogeosciences*, *15*(22), 6791–6818. https://doi.org/10.5194/bg-15-6791-2018

Aswathanarayana, U. (2003). *Mineral Resources Management and the Environment*. CRC Press. https://doi.org/10.1201/9780203971222

Bai, J., Yu, L., Du, S., Wei, Z., Liu, Y., Zhang, L., Zhang, G., & Wang, X. (2020). Effects of flooding frequencies on soil carbon and nitrogen stocks in river marginal wetlands in a ten-year period. *Journal of Environmental Management*, *267*, 110618. https://doi.org/10.1016/j.jenvman.2020.110618

Baldocchi, D., Chu, H., & Reichstein, M. (2018). Inter-annual variability of net and gross ecosystem carbon fluxes: A review. *Agricultural and Forest Meteorology*, *249*, 520–533. https://doi.org/10.1016/j.agrformet.2017.05.015

Baldocchi, D. D. (2020). How eddy covariance flux measurements have contributed to our understanding of Global Change Biology. *Global Change Biology*, *26*(1), 242–260. https://doi.org/10.1111/gcb.14807

Baldocchi, D. D., Hincks, B. B., & Meyers, T. P. (1988). Measuring Biosphere-Atmosphere Exchanges of Biologically Related Gases with Micrometeorological Methods. *Ecology*, *69*(5), 1331–1340. https://doi.org/10.2307/1941631

Ballantine, K., & Schneider, R. (2009). *Fifty-five years of soil development in restored freshwater depressional wetlands*. https://doi.org/10.1890/07-0588.1

Ballut-Dajud, G. A., Sandoval Herazo, L. C., Fernández-Lambert, G., Marín-Muñiz, J. L., López Méndez, M. C., & Betanzo-Torres, E. A. (2022). Factors Affecting Wetland Loss: A Review. *Land*, *11*(3), 434. https://doi.org/10.3390/land11030434

Bancon-Montigny, C., Gonzalez, C., Delpoux, S., Avenzac, M., Spinelli, S., Mhadhbi, T., Mejri, K., Hlaili, A. S., & Pringault, O. (2019). Seasonal changes of chemical contamination in coastal waters during sediment resuspension. *Chemosphere*, *235*, 651–661. https://doi.org/10.1016/j.chemosphere.2019.06.213

Bartolucci, N. N., Anderson, T. R., & Ballantine, K. A. (2021). Restoration of retired agricultural land to wetland mitigates greenhouse gas emissions. *Restoration Ecology*, *29*(3), e13314. https://doi.org/10.1111/rec.13314

Baskaran, M. (2011). Po-210 and Pb-210 as atmospheric tracers and global atmospheric Pb-210 fallout: A Review. *Journal of Environmental Radioactivity, International Topical Meeting on Polonium and Radioactive Lead Isotopes*, *102*(5), 500–513. https://doi.org/10.1016/j.jenvrad.2010.10.007

Baskaran, M., & Santschi, P. H. (1993). The role of particles and colloids in the transport of radionuclides in coastal environments of Texas. *Marine Chemistry, Second International Symposium on the Biogeochemistry of Model Estuaries: Estuarine Processes in Global Change*, *43*(1), 95–114. https://doi.org/10.1016/0304-4203(93)90218-D

Baudron, P., Cockenpot, S., Lopez-Castejon, F., Radakovitch, O., Gilabert, J., Mayer, A., Garcia-Arostegui, J. L., Martinez-Vicente, D., Leduc, C., & Claude, C. (2015). Combining radon, short-lived radium isotopes and hydrodynamic modeling to assess submarine groundwater discharge from an anthropized semiarid watershed to a Mediterranean lagoon (Mar Menor, SE Spain). *Journal of Hydrology*, *525*, 55–71. https://doi.org/10.1016/j.jhydrol.2015.03.015

Bayen, S. (2012). Occurrence, bioavailability and toxic effects of trace metals and organic contaminants in mangrove ecosystems: A review. *Environment International*, *48*, 84–101. https://doi.org/10.1016/j.envint.2012.07.008

Belando, M. D., Bernardeau-Esteller, J., García-Muñoz, R., Ramos-Segura, A., Santos-Echeandía, J., García-Moreno, P., Carreño, F., & Ruiz, J. M. (2017). *Evaluación del estado de conservación de las praderas de Cymodocea nodosa en la*

laguna costera del Mar Menor (p. 157) [Informe del Instituto Español de Oceanografía y la Asociación de Naturalistas del Sureste. Murcia.].

Belando, M. D., Bernardeau-Esteller, J., Paradinas, I., Ramos-Segura, A., García-Muñoz, R., García-Moreno, P., Marín-Guirao, L., & Ruiz, J. M. (2021). Long-term coexistence between the macroalga Caulerpa prolifera and the seagrass Cymodocea nodosa in a Mediterranean lagoon. *Aquatic Botany*, *173*, 103415. https://doi.org/10.1016/j.aquabot.2021.103415

Bellgrove, A. (2016). *Comparison of marine macrophytes for their contributions to blue carbon sequestration*. https://doi.org/10.6084/m9.figshare.c.3308118.v1

Bellucci, L. G., Frignani, M., Paolucci, D., & Ravanelli, M. (2002). Distribution of heavy metals in sediments of the Venice Lagoon: The role of the industrial area. *Science of The Total Environment*, *295*(1), 35–49. https://doi.org/10.1016/S0048-9697(02)00040-2

Benabdelouahab, T., Gadouali, F., Boudhar, A., Lebrini, Y., Hadria, R., & Salhi, A. (2020). Analysis and trends of rainfall amounts and extreme events in the Western Mediterranean region. *Theoretical and Applied Climatology*, *141*(1), 309–320. https://doi.org/10.1007/s00704-020-03205-4

Bentley, S. J., Sheremet, A., & Jaeger, J. M. (2006). Event sedimentation, bioturbation, and preserved sedimentary fabric: Field and model comparisons in three contrasting marine settings. *Continental Shelf Research, Special Issue in Honor of Richard W. Sternberg's Contributions to Marine Sedimentology*, *26*(17), 2108–2124. https://doi.org/10.1016/j.csr.2006.07.003

Berkowitz, J. F., & White, J. R. (2013). Linking Wetland Functional Rapid Assessment Models with Quantitative Hydrological and Biogeochemical Measurements across a Restoration Chronosequence. *Soil Science Society of America Journal*, *77*(4), 1442–1451. https://doi.org/10.2136/sssaj2013.01.0044

Bernardeau-Esteller, J., Sandoval-Gil, J. M., Belando, M. D., Ramos-Segura, A., García-Muñoz, R., Marín-Guirao, L., & Ruiz, J. M. (2023). The Role of Cymodocea nodosa and Caulerpa prolifera Meadows as Nitrogen Sinks in Temperate Coastal Lagoons. *Diversity*, *15*(2), Article 2. https://doi.org/10.3390/d15020172

Billah, M. M., Bhuiyan, M. K. A., Islam, M. A., Das, J., & Hoque, A. R. (2022). Salt marsh restoration: An overview of techniques and success indicators.

Environmental Science and Pollution Research, *29*(11), 15347–15363. https://doi.org/10.1007/s11356-021-18305-5

Biró, M., Molnár, Z., Babai, D., Dénes, A., Fehér, A., Barta, S., Sáfián, L., Szabados, K., Kiš, A., Demeter, L., & Öllerer, K. (2019). Reviewing historical traditional knowledge for innovative conservation management: A re-evaluation of wetland grazing. *Science of The Total Environment*, *666*, 1114–1125. https://doi.org/10.1016/j.scitotenv.2019.02.292

Bloundi, M. K., Duplay, J., & Quaranta, G. (2009). Heavy metal contamination of coastal lagoon sediments by anthropogenic activities: The case of Nador (East Morocco). *Environmental Geology*, *56*(5), 833–843. https://doi.org/10.1007/s00254-007-1184-x

Boës, X., Rydberg, J., Martinez-Cortizas, A., Bindler, R., & Renberg, I. (2011). Evaluation of conservative lithogenic elements (Ti, Zr, Al, and Rb) to study anthropogenic element enrichments in lake sediments. *Journal of Paleolimnology*, *46*(1), 75–87. https://doi.org/10.1007/s10933-011-9515-z

Bogard, M. J., Bergamaschi, B. A., Butman, D. E., Anderson, F., Knox, S. H., & Windham-Myers, L. (2020). Hydrologic Export Is a Major Component of Coastal Wetland Carbon Budgets. *Global Biogeochemical Cycles*, *34*(8), e2019GB006430. https://doi.org/10.1029/2019GB006430

Bortolotti, L. E., St. Louis, V. L., Vinebrooke, R. D., & Wolfe, A. P. (2016). Net Ecosystem Production and Carbon Greenhouse Gas Fluxes in Three Prairie Wetlands. *Ecosystems*, *19*(3), 411–425. https://doi.org/10.1007/s10021-015-9942-1

Bossio, D. A., Cook-Patton, S. C., Ellis, P. W., Fargione, J., Sanderman, J., Smith, P., Wood, S., Zomer, R. J., von Unger, M., Emmer, I. M., & Griscom, B. W. (2020). The role of soil carbon in natural climate solutions. *Nature Sustainability*, *3*(5), 391–398. https://doi.org/10.1038/s41893-020-0491-z

Bourg, A. C. M., & Loch, J. P. G. (1995). Mobilization of Heavy Metals as Affected by pH and Redox Conditions. In W. Salomons & W. M. Stigliani (Eds.), *Biogeodynamics of Pollutants in Soils and Sediments: Risk Assessment of Delayed and Non-Linear Responses* (pp. 87–102). Springer. https://doi.org/10.1007/978-3-642-79418-6_4

Brand, W. A., Assonov, S. S., & Coplen, T. B. (2010). Correction for the 17O interference in δ(13C) measurements when analyzing CO2 with stable

isotope mass spectrometry (IUPAC Technical Report). *Pure and Applied Chemistry*, *82*(8), 1719–1733. https://doi.org/10.1351/PAC-REP-09-01-05

Breithaupt, J. L., & Steinmuller, H. E. (2022). Refining the Global Estimate of Mangrove Carbon Burial Rates Using Sedimentary and Geomorphic Settings. *Geophysical Research Letters*, *49*(18), e2022GL100177. https://doi.org/10.1029/2022GL100177

Brewton, R. A., & Lapointe, B. E. (2023). The green macroalga *Caulerpa prolifera* replaces seagrass in a nitrogen enriched, phosphorus limited, urbanized estuary. *Ecological Indicators*, *156*, 111035. https://doi.org/10.1016/j.ecolind.2023.111035

Bridgham, S. D., Cadillo-Quiroz, H., Keller, J. K., & Zhuang, Q. (2013). Methane emissions from wetlands: Biogeochemical, microbial, and modeling perspectives from local to global scales. *Global Change Biology*, *19*(5), 1325–1346. https://doi.org/10.1111/gcb.12131

Brown, J., & Norris, M. D. (2018). Detecting soil and plant community changes in restored wetlands using a chronosequence approach. *Wetlands Ecology and Management*, *26*(3), 299–314. https://doi.org/10.1007/s11273-017-9574-7

Buckley, D. E., Smith, J. N., & Winters, G. V. (1995). Accumulation of contaminant metals in marine sediments of Halifax Harbour, Nova Scotia: Environmental factors and historical trends. *Applied Geochemistry*, *10*(2), 175–195. https://doi.org/10.1016/0883-2927(94)00053-9

Bunting, P., Rosenqvist, A., Hilarides, L., Lucas, R. M., Thomas, N., Tadono, T., Worthington, T. A., Spalding, M., Murray, N. J., & Rebelo, L.-M. (2022). Global Mangrove Extent Change 1996–2020: Global Mangrove Watch Version 3.0. *Remote Sensing*, *14*(15), 3657. https://doi.org/10.3390/rs14153657

Burnett, W. C., Bidorn, B., & Wang, Y. (2023). Can 210Pb be used as a paleo-storm proxy? *Quaternary Science Reviews*, *315*, 108242. https://doi.org/10.1016/j.quascirev.2023.108242

Cacabelos, E., Faria, J., Martins, G. M., Mir, C., Parente, M. I., Gabriel, D., Sánchez, R., Altamirano, M., Costa, A. C., Reine, W. P. van, & Neto, A. I. (2019). First record of Caulerpa prolifera in the Azores (NE Atlantic). *Botanica Marina*, *62*(2), 155–160. https://doi.org/10.1515/bot-2018-0075

Cadier, C., Bayraktarov, E., Piccolo, R., & Adame, M. F. (2020). Indicators of Coastal Wetlands Restoration Success: A Systematic Review. *Frontiers in Marine Science*, *7*. https://doi.org/10.3389/fmars.2020.600220

Caetano, M., Madureira, M.-J., & Vale, C. (2003). Metal Remobilisation during Resuspension of Anoxic Contaminated Sediment: Short-Term Laboratory Study. *Water, Air, and Soil Pollution*, *143*(1), 23–40. https://doi.org/10.1023/A:1022877120813

Cahoon, D. R. (2006). A review of major storm impacts on coastal wetland elevations. *Estuaries and Coasts*, *29*(6), 889–898. https://doi.org/10.1007/BF02798648

Callaway, J. C., Parker, V. T., Vasey, M. C., Schile, L. M., & Herbert, E. R. (2011). Tidal Wetland Restoration in San Francisco Bay: History and Current Issues. *San Francisco Estuary and Watershed Science*, *9*(3). https://doi.org/10.15447/sfews.2011v9iss3art2

Campbell, A. D., Fatoyinbo, L., Goldberg, L., & Lagomasino, D. (2022). Global hotspots of salt marsh change and carbon emissions. *Nature*, *612*(7941), 701–706. https://doi.org/10.1038/s41586-022-05355-z

Canuel, E. A., Brush, G. S., Cronin, T. M., Lockwood, R., & Zimmerman, A. R. (2017). Paleoecology Studies in Chesapeake Bay: A Model System for Understanding Interactions Between Climate, Anthropogenic Activities and the Environment. In K. Weckström, K. M. Saunders, P. A. Gell, & C. G. Skilbeck (Eds.), *Applications of Paleoenvironmental Techniques in Estuarine Studies* (pp. 495–527). Springer Netherlands. https://doi.org/10.1007/978-94-024-0990-1_20

Canuel, E. A., & Hardison, A. K. (2016). Sources, Ages, and Alteration of Organic Matter in Estuaries. *Annual Review of Marine Science*, *8*(1), 409–434. https://doi.org/10.1146/annurev-marine-122414-034058

Catry, T., Lourenço, P. M., Lopes, R. J., Carneiro, C., Alves, J. A., Costa, J., Rguibi-Idrissi, H., Bearhop, S., Piersma, T., & Granadeiro, J. P. (2016). Structure and functioning of intertidal food webs along an avian flyway: A comparative approach using stable isotopes. *Functional Ecology*, *30*(3), 468–478. https://doi.org/10.1111/1365-2435.12506

Cerdà i Domènech, M. (2020). Fluxos d'aigua subterrània i concentració de metalls en dipòsits marins costaners contaminats: Aproximació metodològica i casos d'estudi a la costa mediterrània de la Península Ibèrica = Submarine

groundwater discharge and metal concentration in polluted coastal marine deposits: methodological approach and case studies on the Mediterranean coast of the Iberian Peninsula [Ph.D. Thesis, Universitat de Barcelona]. In *TDX (Tesis Doctorals en Xarxa)*. https://www.tdx.cat/handle/10803/672444

Chapin, F. S., Woodwell, G. M., Randerson, J. T., Rastetter, E. B., Lovett, G. M., Baldocchi, D. D., Clark, D. A., Harmon, M. E., Schimel, D. S., Valentini, R., Wirth, C., Aber, J. D., Cole, J. J., Goulden, M. L., Harden, J. W., Heimann, M., Howarth, R. W., Matson, P. A., McGuire, A. D., … Schulze, E.-D. (2006). Reconciling Carbon-cycle Concepts, Terminology, and Methods. *Ecosystems*, *9*(7), 1041–1050. https://doi.org/10.1007/s10021-005-0105-7

Chapman, P., Wang, F., Janssen, C., Persoone, G., & Allen, H. (2011). Ecotoxicology of Metals in Aquatic Sediments: Binding and Release, Bioavailability, Risk Assessment, and Remediation. *Canadian Journal of Fisheries and Aquatic Sciences*, *55*, 2221–2243. https://doi.org/10.1139/cjfas-55-10-2221

Chen, H.-Y., Ge, Z.-M., Zhu, K.-H., Zhao, W., Chen, X.-C., Li, X.-Z., Xin, P., Zhou, Z., Chen, S., & Bellerby, R. (2025). Ecosystem carbon and nitrogen recovery in restored coastal wetlands. *Communications Earth & Environment*, *7*(1), 8. https://doi.org/10.1038/s43247-025-03036-z

Chen, X., Wang, Q., Cui, B., Chen, G., Xie, T., & Yang, W. (2023). Ecological time lags in biodiversity response to habitat changes. *Journal of Environmental Management*, *346*, 118965. https://doi.org/10.1016/j.jenvman.2023.118965

Chen, Z. L., & Lee, S. Y. (2022). Tidal Flats as a Significant Carbon Reservoir in Global Coastal Ecosystems. *Frontiers in Marine Science*, *9*. https://doi.org/10.3389/fmars.2022.900896

Cheng, F. Y., Van Meter, K. J., Byrnes, D. K., & Basu, N. B. (2020). Maximizing US nitrate removal through wetland protection and restoration. *Nature*, *588*(7839), 625–630. https://doi.org/10.1038/s41586-020-03042-5

Choi, W. J., Arshad, M. A., Chang, S. X., & Kim, T. H. (2006). Grain 15N of crops applied with organic and chemical fertilizers in a four-year rotation. *Plant and Soil*, *284*(1), 165–174. https://doi.org/10.1007/s11104-006-0038-8

Clark, J. R., Lewis, M. A., & Pait, A. S. (1993). Pesticide inputs and risks in coastal wetlands. *Environmental Toxicology and Chemistry*, *12*(12), 2225–2233. https://doi.org/10.1002/etc.5620121206

Clarke, A., Juggins, S., & Conley, D. (2003). A 150-year reconstruction of the history of coastal eutrophication in Roskilde Fjord, Denmark. *Marine Pollution Bulletin*, *46*(12), 1615–1618. https://doi.org/10.1016/S0025-326X(03)00375-8

Cloern, J. E., Canuel, E. A., & Harris, D. (2002). Stable carbon and nitrogen isotope composition of aquatic and terrestrial plants of the San Francisco Bay estuarine system. *Limnology and Oceanography*, *47*(3), 713–729. https://doi.org/10.4319/lo.2002.47.3.0713

Conesa, H. M., & Jiménez-Cárceles, F. J. (2007). The Mar Menor lagoon (SE Spain): A singular natural ecosystem threatened by human activities. *Marine Pollution Bulletin*, *54*(7), 839–849. https://doi.org/10.1016/j.marpolbul.2007.05.007

Conesa, H. M., & Schulin, R. (2010). The Cartagena–La Unión mining district (SE spain): A review of environmental problems and emerging phytoremediation solutions after fifteen years research. *Journal of Environmental Monitoring*, *12*(6), 1225–1233. https://doi.org/10.1039/C000346H

Conrad, R. (2023). Complexity of temperature dependence in methanogenic microbial environments. *Frontiers in Microbiology*, *14*. https://doi.org/10.3389/fmicb.2023.1232946

Conrad, S. R., Santos, I. R., White, S., & Sanders, C. J. (2019). Nutrient and Trace Metal Fluxes into Estuarine Sediments Linked to Historical and Expanding Agricultural Activity (Hearnes Lake, Australia). *Estuaries and Coasts*, *42*(4), 944–957. https://doi.org/10.1007/s12237-019-00541-1

Cooray, I. G., Chalmers, G., & Chittleborough, D. (2026). Degraded coastal agricultural lands hold significant soil carbon stocks and are potential candidates for blue carbon restoration. *Environmental Research*, *293*, 123742. https://doi.org/10.1016/j.envres.2026.123742

Costa, L. D. F., Mirlean, N., Wasserman, J. C., & Wallner-Kersanach, M. (2016). Variability of labile metals in estuarine sediments in areas under the influence of antifouling paints, southern Brazil. *Environmental Earth Sciences*, *75*(7), 580. https://doi.org/10.1007/s12665-016-5355-5

Cox, J. R., Huismans, Y., Knaake, S. M., Leuven, J. R. F. W., Vellinga, N. E., van der Vegt, M., Hoitink, A. J. F., & Kleinhans, M. G. (2021). Anthropogenic Effects on the Contemporary Sediment Budget of the Lower Rhine-Meuse Delta Channel Network. *Earth's Future*, *9*(7), e2020EF001869. https://doi.org/10.1029/2020EF001869

CREM - Datos Municipales Cartagena—3. Evolución de la superficie dedicada a cada grupo de cultivo. (n.d.). Retrieved October 16, 2023, from https://econet.carm.es/inicio/-/crem/sicrem/PU_CartagenaCifrasNEW/P8004/sec4.html

Cuevas, J. G., Faz, Á., Martínez-Martínez, S., Beltrá, J. C., & Acosta, J. A. (2025). Influence of rainfall on physicochemical characteristics of runoff water and sediments in riverbeds affected by mining and agricultural activities. *Science of the Total Environment*, *958*. Scopus. https://doi.org/10.1016/j.scitotenv.2024.177889

Cuevas, J. G., Faz, A., Martínez-Martínez, S., Gabarrón, M., Beltrá, J. C., Martínez, J., & Acosta, J. A. (2023). Spatial distribution and pollution evaluation in dry riverbeds affected by mine tailings. *Environmental Geochemistry and Health*. https://doi.org/10.1007/s10653-022-01469-5

Dang, P., Gu, X., Lin, C., Xin, M., Zhang, H., Ouyang, W., Liu, X., He, M., & Wang, B. (2021). Distribution, sources, and ecological risks of potentially toxic elements in the Laizhou Bay, Bohai Sea: Under the long-term impact of the Yellow River input. *Journal of Hazardous Materials*, *413*, 125429. https://doi.org/10.1016/j.jhazmat.2021.125429

Davidson, E. A., & Seitzinger, S. (2006). The Enigma of Progress in Denitrification Research. *Ecological Applications*, *16*(6), 2057–2063. https://doi.org/10.1890/1051-0761(2006)016%5B2057:TEOPID%5D2.0.CO;2

Davidson, E. A., & Verchot, L. V. (2000). Testing the Hole-in-the-Pipe Model of nitric and nitrous oxide emissions from soils using the TRAGNET Database. *Global Biogeochemical Cycles*, *14*(4), 1035–1043. https://doi.org/10.1029/1999GB001223

Davidson, I. C., Cott, G. M., Devaney, J. L., & Simkanin, C. (2018). Differential effects of biological invasions on coastal blue carbon: A global review and meta-analysis. *Global Change Biology*, *24*(11), 5218–5230. https://doi.org/10.1111/gcb.14426

Davidson, N. C., & Finlayson, C. M. (2019). Updating global coastal wetland areas presented in Davidson and Finlayson (2018). *Marine & Freshwater Research*, *70*(8), 1195–1200. https://doi.org/10.1071/MF19010

de los Santos, C. B., Egea, L. G., Martins, M., Santos, R., Masqué, P., Peralta, G., Brun, F. G., & Jiménez-Ramos, R. (2022). Sedimentary Organic Carbon and Nitrogen Sequestration Across a Vertical Gradient on a Temperate Wetland Seascape Including Salt Marshes, Seagrass Meadows and Rhizophytic Macroalgae Beds. *Ecosystems*. https://doi.org/10.1007/s10021-022-00801-5

Delwiche, K., Matthes, J. H., Arias-Ortiz, A., Knox, S. H., Oikawa, P., Sturtevant, C., Verfaillie, J., Szutu, D., Keenan, T. F., & Baldocchi, D. (2025). Dynamic methane emissions in a restored wetland: Decadal insights into uncertain climate outcomes and critical science needs. *Agricultural and Forest Meteorology*, *373*, 110735. https://doi.org/10.1016/j.agrformet.2025.110735

Dieter, C. D. (1990). The Importance of Emergent Vegetation in Reducing Sediment Resuspension in Wetlands. *Journal of Freshwater Ecology*, *5*(4), 467–473. https://doi.org/10.1080/02705060.1990.9665263

Doody, J. P. (2004). 'Coastal squeeze'—An historical perspective. *Journal of Coastal Conservation*, *10*(1), 129–138. https://doi.org/10.1652/1400-0350(2004)010%5B0129:CSAHP%5D2.0.CO;2

Drexler, J. Z., Davis, M. J., Woo, I., & De La Cruz, S. (2020). Carbon Sources in the Sediments of a Restoring vs. Historically Unaltered Salt Marsh. *Estuaries and Coasts*, *43*(6), 1345–1360. https://doi.org/10.1007/s12237-020-00748-7

Drexler, J. Z., de Fontaine, C. S., & Deverel, S. J. (2009). The legacy of wetland drainage on the remaining peat in the Sacramento—San Joaquin Delta, California, USA. *Wetlands*, *29*(1), 372–386. https://doi.org/10.1672/08-97.1

Drexler, J. Z., Woo, I., Fuller, C. C., & Nakai, G. (2019). *Carbon accumulation and vertical accretion in a restored versus historic salt marsh in southern Puget Sound, Washington, United States*. https://doi.org/10.1111/rec.12941

Duarte, C. M. (1995). Submerged aquatic vegetation in relation to different nutrient regimes. *Ophelia*, *41*(1), 87–112. https://doi.org/10.1080/00785236.1995.10422039

Duarte, C. M., Losada, I. J., Hendriks, I. E., Mazarrasa, I., & Marbà, N. (2013). The role of coastal plant communities for climate change mitigation and adaptation. *Nature Climate Change*, *3*(11), 961–968. https://doi.org/10.1038/nclimate1970

Duarte, C. M., Gattuso, J.-P., Hancke, K., Gundersen, H., Filbee-Dexter, K., Pedersen, M. F., Middelburg, J. J., Burrows, M. T., Krumhansl, K. A., Wernberg, T., Moore, P., Pessarrodona, A., Ørberg, S. B., Pinto, I. S., Assis, J., Queirós, A. M., Smale, D. A., Bekkby, T., Serrão, E. A., & Krause-Jensen, D. (2022). Global estimates of the extent and production of macroalgal forests. *Global Ecology and Biogeography*, *31*(7), 1422–1439. https://doi.org/10.1111/geb.13515

Ducks Unlimited. (2016). *Modeling of Local and Regional Impacts of the Proposed Hill Slough Tidal Marsh Restoration, Suisun Marsh, California Technical Memorandum March 2016*. Ducks Unlimited.

Edwards, R. J. (2007). *Low Energy Coasts Sedimentary Indicators*.

Ellegaard, M., Clokie, M. R. J., Czypionka, T., Frisch, D., Godhe, A., Kremp, A., Letarov, A., McGenity, T. J., Ribeiro, S., & John Anderson, N. (2020). Dead or alive: Sediment DNA archives as tools for tracking aquatic evolution and adaptation. *Communications Biology*, *3*(1), 169. https://doi.org/10.1038/s42003-020-0899-z

Emsens, W.-J., van Diggelen, R., Aggenbach, C. J. S., Cajthaml, T., Frouz, J., Klimkowska, A., Kotowski, W., Kozub, L., Liczner, Y., Seeber, E., Silvennoinen, H., Tanneberger, F., Vicena, J., Wilk, M., & Verbruggen, E. (2020). Recovery of fen peatland microbiomes and predicted functional profiles after rewetting. *The ISME Journal*, *14*(7), 1701–1712. https://doi.org/10.1038/s41396-020-0639-x

Enwright, N. M., Griffith, K. T., & Osland, M. J. (2016). Barriers to and opportunities for landward migration of coastal wetlands with sea-level rise. *Frontiers in Ecology and the Environment*, *14*(6), 307–316.

Estes, L., Elsen, P. R., Treuer, T., Ahmed, L., Caylor, K., Chang, J., Choi, J. J., & Ellis, E. C. (2018). The spatial and temporal domains of modern ecology. *Nature Ecology & Evolution*, *2*(5), 819–826. https://doi.org/10.1038/s41559-018-0524-4

Fang, G.-C., Tsai, K.-H., Huang, C.-Y., Yang, K.-P. O., Xiao, Y.-F., Huang, W.-C., & Zhuang, Y.-J. (2018). Seasonal variations of ambient air mercury species nearby an airport. *Atmospheric Research*, *202*, 96–104. https://doi.org/10.1016/j.atmosres.2017.11.008

Farias, R. N. de, Arueira, T. D., Bauer, A. de B., Rezende, C. E. de, Almeida, M. G. de, Carvalho, C. R. A., Vidal, M., Barreto, G. S., Novaes, J. A. A., Barros, M. P. F. de, Molisani, M. M., & Esteves, F. de A. (2024). Effects of recent urbanization on carbon and nitrogen burial rates of sedimentary records in a tropical coastal lagoon (Brazil). *Environmental Research*, *263*, 120161. https://doi.org/10.1016/j.envres.2024.120161

Fennessy, S. M., & Lei, G. (2018). *Wetland restoration for climate change resilience* (Convention on Wetlands, Ed.; First Edition). Convention on Wetlands. https://doi.org/10.69556/strp.bn10.18.eng

Fernandez, J.-M., Ouillon, S., Chevillon, C., Douillet, P., Fichez, R., & Gendre, R. L. (2006). A combined modelling and geochemical study of the fate of terrigenous inputs from mixed natural and mining sources in a coral reef lagoon (New Caledonia). *Marine Pollution Bulletin*, *52*(3), 320–331. https://doi.org/10.1016/j.marpolbul.2005.09.010

Fernández-Alías, A., Molinero, J. C., Quispe-Becerra, J. I., Bonnet, D., Marcos, C., & Pérez-Ruzafa, A. (2023). Phenology of scyphozoan jellyfish species in a eutrophication and climate change context. *Marine Pollution Bulletin*, *194*, 115286. https://doi.org/10.1016/j.marpolbul.2023.115286

Fernández-Alías, A., Montaño-Barroso, T., Conde-Caño, M.-R., Manchado-Pérez, S., López-Galindo, C., Quispe-Becerra, J.-I., Marcos, C., & Pérez-Ruzafa, A. (2022). Nutrient overload promotes the transition from top-down to bottom-up control and triggers dystrophic crises in a Mediterranean coastal lagoon. *Science of The Total Environment*, *846*, 157388. https://doi.org/10.1016/j.scitotenv.2022.157388

Fitzgerald, D. M., Fenster, M. S., Argow, B. A., & Buynevich, I. V. (2008). Coastal Impacts Due to Sea-Level Rise. *Annual Review of Earth and Planetary Sciences*, *36*, 601–647. https://doi.org/10.1146/annurev.earth.35.031306.140139

Fluet-Chouinard, E., Stocker, B. D., Zhang, Z., Malhotra, A., Melton, J. R., Poulter, B., Kaplan, J. O., Goldewijk, K. K., Siebert, S., Minayeva, T., Hugelius, G., Joosten, H., Barthelmes, A., Prigent, C., Aires, F., Hoyt, A. M., Davidson, N., Finlayson, C. M., Lehner, B., … McIntyre, P. B. (2023).

Extensive global wetland loss over the past three centuries. *Nature*, *614*(7947), 281–286. https://doi.org/10.1038/s41586-022-05572-6

Fong, C. R., Gaynus, C. J., & Carpenter, R. C. (2020). Extreme rainfall events pulse substantial nutrients and sediments from terrestrial to nearshore coastal communities: A case study from French Polynesia. *Scientific Reports*, *10*(1), Article 1. https://doi.org/10.1038/s41598-020-59807-5

Forbes, D. L. (2019). Arctic Deltas and Estuaries: A Canadian Perspective. In *Coasts and Estuaries* (pp. 123–147). Elsevier. https://doi.org/10.1016/B978-0-12-814003-1.00008-3

Förstner, U., & Wittmann, G. T. W. (1981). *Metal pollution in the aquatic environment* (2nd rev. ed.). Springer-Verlag. https://doi.org/10.1007/978-3-642-69385-4

Förstner, U., Ahlf, W., Calmano, W., Kersten, M., & Salomons, W. (1986). Mobility of Heavy Metals in Dredged Harbor Sediments. In P. G. Sly (Ed.), *Sediments and Water Interactions* (pp. 371–380). Springer. https://doi.org/10.1007/978-1-4612-4932-0_31

Foucher, A., Chaboche, P.-A., Sabatier, P., & Evrard, O. (2021). A worldwide meta-analysis (1977–2020) of sediment core dating using fallout radionuclides including ^{137}Cs and $^{210}Pb_{xs}$. *Earth System Science Data*, *13*(10), 4951–4966. https://doi.org/10.5194/essd-13-4951-2021

Friess, D. A., Yando, E. S., I, J. B. A., Wong, L.-W., Soto, S. D., & Bhatia, N. (2020). Ecosystem services and disservices of mangrove forests and salt marshes. In *Oceanography and Marine Biology*. CRC Press.

Fuchs, A., Davidson, I. C., Megonigal, J. P., Devaney, J. L., Simkanin, C., Noyce, G. L., Lu, M., & Cott, G. M. (2025). Stronger increase of methane emissions from coastal wetlands by non-native Spartina alterniflora than non-native Phragmites australis. *PLANTS, PEOPLE, PLANET*, *7*(1), 62–79. https://doi.org/10.1002/ppp3.10578

Fuchs, M.-C. (2023). Rights of Nature Reach Europe: The Mar Menor Case in Spain in the Light of Latin American Precedents. *Verfassungsblog*. https://doi.org/10.17176/20230224-185211-0

Gacia, E., Duarte, C. M., & Middelburg, J. J. (2002). Carbon and nutrient deposition in a Mediterranean seagrass (Posidonia oceanica) meadow. *Limnology and Oceanography*, *47*(1), 23–32. https://doi.org/10.4319/lo.2002.47.1.0023

Gallon, C., & Flegal, A. R. (2015). Sources, Fluxes, and Biogeochemical Cycling of Silver in the Oceans. In D. M. Whitacre (Ed.), *Reviews of Environmental Contamination and Toxicology Volume 235* (pp. 27–48). Springer International Publishing. https://doi.org/10.1007/978-3-319-10861-2_2

Galloway, J. N., Aber, J. D., Erisman, J. W., Seitzinger, S. P., Howarth, R. W., Cowling, E. B., & Cosby, B. J. (2003). The Nitrogen Cascade. *BioScience*, *53*(4), 341–356. https://doi.org/10.1641/0006-3568(2003)053%5B0341:TNC%5D2.0.CO;2

Gao, X., & Li, P. (2012). Concentration and fractionation of trace metals in surface sediments of intertidal Bohai Bay, China. *Marine Pollution Bulletin*, *64*(8), 1529–1536. https://doi.org/10.1016/j.marpolbul.2012.04.026

Gao, Y., Ouyang, Z., Shao, C., Chu, H., Su, Y.-J., Guo, H., Chen, J., & Zhao, B. (2018). Field Observation of Lateral Detritus Carbon Flux in a Coastal Wetland. *Wetlands*, *38*(3), 613–625. https://doi.org/10.1007/s13157-018-1005-x

García, G., & Muñoz-Vera, A. (2015). Characterization and evolution of the sediments of a Mediterranean coastal lagoon located next to a former mining area. *Marine Pollution Bulletin*, *100*(1), 249–263. https://doi.org/10.1016/j.marpolbul.2015.08.042

García-Ayllón, S., & Miralles, J. L. (2014). The environmental impacts of land transformation in the coastal perimeter of the mar menor lagoon (spain). *International Journal of Design & Nature and Ecodynamics*, *9*(2), 109–128. https://doi.org/10.2495/DNE-V9-N2-109-128

Garcia-Orellana, J., Cañas, L., Masqué, P., Obrador, B., Olid, C., & Pretus, J. (2011). Chronological reconstruction of metal contamination in the Port of Maó (Minorca, Spain). *Marine Pollution Bulletin*, *62*(8), 1632–1640. https://doi.org/10.1016/j.marpolbul.2011.06.013

García-Pintado, J., Martínez-Mena, M., Barberá, G. G., Albaladejo, J., & Castillo, V. M. (2007). Anthropogenic nutrient sources and loads from a Mediterranean catchment into a coastal lagoon: Mar Menor, Spain. *Science of The Total Environment*, *373*(1), 220–239. https://doi.org/10.1016/j.scitotenv.2006.10.046

Gattuso, J.-P., Frankignoulle, M., & Wollast, R. (1998). CARBON AND CARBONATE METABOLISM IN COASTAL AQUATIC ECOSYSTEMS. *Annual Review of Ecology, Evolution, and Systematics*,

29(Volume 29, 1998), 405–434. https://doi.org/10.1146/annurev.ecolsys.29.1.405

GEAM IEO-CSIC. (2025). *Cartografía de las praderas marinas del Mar Menor 2024*. Proyecto BELICH: Monitorización, Estudio y Modelización del Mar Menor (MAPMM-MITECO). IEO-CSIC. https://belich-ieo-csic-es.eu1.proxy.openathens.net/

Ghosh, S., Anju, P., Pattanayak, R., & Sahu, N. C. (2024). Fisheries and Aquaculture in Wetland Ecosystems: A Review of Benefits, Risks, and Future Prospects in India. *Journal of Coastal Research*, *40*(3), 598–612. https://doi.org/10.2112/JCOASTRES-D-23-00045.1

Gifford, R. M., & Roderick, M. L. (2003). Soil carbon stocks and bulk density: Spatial or cumulative mass coordinates as a basis of expression? *Global Change Biology*, *9*(11), 1507–1514. https://doi.org/10.1046/j.1365-2486.2003.00677.x

Girones, L., Oliva, A. L., Negrin, V. L., Marcovecchio, J. E., & Arias, A. H. (2021). Persistent organic pollutants (POPs) in coastal wetlands: A review of their occurrences, toxic effects, and biogeochemical cycling. *Marine Pollution Bulletin*, *172*, 112864. https://doi.org/10.1016/j.marpolbul.2021.112864

Gomis, E., Strydom, S., Foster, N. R., Montemayor, D., Mateo, M. A., Serrano, E., Inostroza, K., McCallum, R., Lafratta, A., Webster, C. L., O'Dea, C. M., Said, N. E., Dunham, N., Bernasconi, R., Werner, A., Vitelli, F., Puigcorbé, V., D'Cruz, A., Salinas, C., … Serrano, O. (2025). Global estimates of seagrass blue carbon stocks in biomass and net primary production. *Nature Communications*, *16*(1), 9530. https://doi.org/10.1038/s41467-025-64667-6

González, I., Águila, E., & Galán, E. (2007). Partitioning, bioavailability and origin of heavy metals from the Nador Lagoon sediments (Morocco) as a basis for their management. *Environmental Geology*, *52*(8), 1581–1593. https://doi.org/10.1007/s00254-006-0602-9

Greening, H., & Janicki, A. (2006). Toward reversal of eutrophic conditions in a subtropical estuary: Water quality and seagrass response to nitrogen loading reductions in Tampa Bay, Florida, USA. *Environmental Management*, *38*(2), 163–178. https://doi.org/10.1007/s00267-005-0079-4

Green-Ruiz, C., & Páez-Osuna, F. (2001). Heavy metal anomalies in lagoon sediments related to Intensive agriculture in Altata-Ensenada del Pabellon coastal system (SE Gulf of California). *ENVIRONMENT INTERNATIONAL*, *26*(4), 265–273. https://doi.org/10.1016/S0160-4120(00)00116-1

Guaita-García, N., Martínez-Fernández, J., Barrera-Causil, C. J., & Fitz, H. C. (2022). Stakeholder analysis and prioritization of management measures for a sustainable development in the social-ecological system of the Mar Menor (SE, Spain). *Environmental Development*, *42*, 100701. https://doi.org/10.1016/j.envdev.2022.100701

Hadas, O., Altabet, M. A., & Agnihotri, R. (2009). Seasonally varying nitrogen isotope biogeochemistry of particulate organic matter in Lake Kinneret, Israel. *Limnology and Oceanography*, *54*(1), 75–85. https://doi.org/10.4319/lo.2009.54.1.0075

Hajdas, I., Ascough, P., Garnett, M. H., Fallon, S. J., Pearson, C. L., Quarta, G., Spalding, K. L., Yamaguchi, H., & Yoneda, M. (2021). Radiocarbon dating. *Nature Reviews Methods Primers*, *1*(1), 62. https://doi.org/10.1038/s43586-021-00058-7

Hamza, F., Abdi, A. M., Chokri, M.-A., Yacoubi, L., Dlensi, H., Hammouda, N., Ghlis, A., Jemaa, B., Elghoul, M., Hedhili, A., & Hanane, S. (2024). Landscape context and wetland attributes influence wintering waterbirds in important bird and biodiversity areas: Implications for conservation and management. *Landscape Ecology*, *39*(8), 151. https://doi.org/10.1007/s10980-024-01942-9

Harada, M. (1978). Congenital Minamata disease: Intrauterine methylmercury poisoning. *Teratology*, *18*(2), 285–288. https://doi.org/10.1002/tera.1420180216

Heim, S., & Schwarzbauer, J. (2013). Pollution history revealed by sedimentary records: A review. *Environmental Chemistry Letters*, *11*. https://doi.org/10.1007/s10311-013-0409-3

Hemes, K. S., Chamberlain, S. D., Eichelmann, E., Anthony, T., Valach, A., Kasak, K., Szutu, D., Verfaillie, J., Silver, W. L., & Baldocchi, D. D. (2019). Assessing the carbon and climate benefit of restoring degraded agricultural peat soils to managed wetlands. *Agricultural and Forest Meteorology*, *268*, 202–214. https://doi.org/10.1016/j.agrformet.2019.01.017

Hemes, K. S., Chamberlain, S. D., Eichelmann, E., Knox, S. H., & Baldocchi, D. D. (2018). A Biogeochemical Compromise: The High Methane Cost of Sequestering Carbon in Restored Wetlands. *Geophysical Research Letters*, *45*(12), 6081–6091. https://doi.org/10.1029/2018GL077747

Hendriks, I. E., Bouma, T. J., Morris, E. P., & Duarte, C. M. (2010). Effects of seagrasses and algae of the Caulerpa family on hydrodynamics and particle-trapping rates. *Marine Biology*, *157*(3), 473–481. https://doi.org/10.1007/s00227-009-1333-8

Hill, R., Bellgrove, A., Macreadie, P. I., Petrou, K., Beardall, J., Steven, A., & Ralph, P. J. (2015). Can macroalgae contribute to blue carbon? An Australian perspective. *Limnology and Oceanography*, *60*(5), 1689–1706. https://doi.org/10.1002/lno.10128

Hobbs, R. J., & Cramer, V. A. (2008). Restoration Ecology: Interventionist Approaches for Restoring and Maintaining Ecosystem Function in the Face of Rapid Environmental Change. *Annual Review of Environment and Resources*, *33*(1), 39–61. https://doi.org/10.1146/annurev.environ.33.020107.113631

Horowitz, A. J. (1985). *A Primer on Trace Metal Sediment Chemistry*.

Howard, J. L. (2018). *PATTERNS OF CARBON METABOLISM, STORAGE, AND REMINERALIZATION IN SEAGRASS ECOSYSTEMS* [Doctor of Philosophy Biomedical Sciences, Florida International University]. https://doi.org/10.25148/etd.FIDC004080

Hsieh, C.-I., Katul, G., & Chi, T. (2000). An approximate analytical model for footprint estimation of scalar fluxes in thermally stratified atmospheric flows. *Advances in Water Resources*, *23*(7), 765–772. https://doi.org/10.1016/S0309-1708(99)00042-1

Hulthe, G., Hulth, S., & Hall, P. O. J. (1998). Effect of oxygen on degradation rate of refractory and labile organic matter in continental margin sediments. *Geochimica et Cosmochimica Acta*, *62*(8), 1319–1328. https://doi.org/10.1016/S0016-7037(98)00044-1

Ignar, S., & Grygoruk, M. (2015). Wetlands and Water Framework Directive: Protection, Management and Climate Change. In S. Ignar & M. Grygoruk (Eds.), *Wetlands and Water Framework Directive: Protection, Management and Climate Change* (pp. 1–7). Springer International Publishing. https://doi.org/10.1007/978-3-319-13764-3_1

Instituto Español de Oceanografía. (2020). *INFORME DE EVOLUCIÓN Y ESTADO ACTUAL DEL MAR MENOR EN RELACIÓN AL PROCESO DE EUTROFIZACIÓN Y SUS CAUSAS*.

Izaditame, F., Siebecker, M. G., & Sparks, D. L. (2022). Sea-level-rise-induced flooding drives arsenic release from coastal sediments. *Journal of Hazardous Materials*, *423*, 127161. https://doi.org/10.1016/j.jhazmat.2021.127161

Jatobá-Junior, A. A., Masque, P., de Rezende, C. E., & Hatje, V. (2026). Stocks and fluxes of carbon and nitrogen in northeastern Brazil coastal seascapes. *Scientific Reports*, *16*(1), 3588. https://doi.org/10.1038/s41598-025-33546-x

Jia, M., Wang, Z., Mao, D., Ren, C., Song, K., Zhao, C., Wang, C., Xiao, X., & Wang, Y. (2023). Mapping global distribution of mangrove forests at 10-m resolution. *Science Bulletin*, *68*(12), 1306–1316. https://doi.org/10.1016/j.scib.2023.05.004

Jiménez-Casero, J., Ruiz, J. M., Bernardeau-Esteller, J., García-Muñoz, R., Sánchez-Lizaso, J. L., Marín-Guirao, L., & Belando, M. D. (2025). Cascading ecological impacts: From eutrophic coastal lagoon collapse to decline of *Posidonia oceanica* meadows in the Mediterranean. *Marine Pollution Bulletin*, *221*, 118536. https://doi.org/10.1016/j.marpolbul.2025.118536

Jiménez-Martínez, J., García-Aróstegui, J. L., Hunink, J. E., Contreras, S., Baudron, P., & Candela, L. (2016). The role of groundwater in highly human-modified hydrosystems: A review of impacts and mitigation options in the Campo de Cartagena-Mar Menor coastal plain (SE Spain). *Environmental Reviews*, *24*(4), 377–392. https://doi.org/10.1139/er-2015-0089

Jiménez-Ramos, R., Egea, L. G., D'Agostino, V. C., Degrati, M., & Loizaga, R. (2025). Carbon and nitrogen stocks in sediment at Península Valdés Biosphere Reserve: Novel insights into the potential contribution of large marine vertebrates to carbon sequestration. *Frontiers in Marine Science*, *12*. https://doi.org/10.3389/fmars.2025.1500594

Jin, Y., Yang, W., Sun, T., Yang, Z., & Li, M. (2016). Effects of seashore reclamation activities on the health of wetland ecosystems: A case study in the Yellow River Delta, China. *Ocean & Coastal Management*, *123*, 44–52. https://doi.org/10.1016/j.ocecoaman.2016.01.013

Jones, B., & Bolam, T. (2007). Copper speciation survey from UK marinas, harbours and estuaries. *Marine Pollution Bulletin*, *54*(8), 1127–1138. https://doi.org/10.1016/j.marpolbul.2007.04.021

Jones, H. P., Jones, P. C., Barbier, E. B., Blackburn, R. C., Rey Benayas, J. M., Holl, K. D., McCrackin, M., Meli, P., Montoya, D., & Mateos, D. M. (2018). Restoration and repair of Earth's damaged ecosystems. *Proceedings of the Royal Society B: Biological Sciences*, *285*(1873), 20172577. https://doi.org/10.1098/rspb.2017.2577

Jones, S. F., Arias-Ortiz, A., Baldocchi, D., Eagle, M., Friess, D. A., Gore, C., Noe, G., Nolte, S., Oikawa, P., Paytan, A., Raw, J. L., Roberts, B. J., Rogers, K., Schutte, C., Stagg, C. L., Thorne, K. M., Ward, E. J., Windham-Myers, L., & Yando, E. S. (2024). When and where can coastal wetland restoration increase carbon sequestration as a natural climate solution? *Cambridge Prisms: Coastal Futures*, *2*, e13. https://doi.org/10.1017/cft.2024.14

Jordi, A., Basterretxea, G., Tovar-Sánchez, A., Alastuey, A., & Querol, X. (2012). Copper aerosols inhibit phytoplankton growth in the Mediterranean Sea. *Proceedings of the National Academy of Sciences*, *109*(52), 21246–21249. https://doi.org/10.1073/pnas.1207567110

Junk, W. J., An, S., Finlayson, C. M., Gopal, B., Květ, J., Mitchell, S. A., Mitsch, W. J., & Robarts, R. D. (2013). Current state of knowledge regarding the world's wetlands and their future under global climate change: A synthesis. *Aquatic Sciences*, *75*(1), 151–167. https://doi.org/10.1007/s00027-012-0278-z

Kaiser, H. F. (1974). An index of factorial simplicity. *Psychometrika*, *39*(1), 31–36. https://doi.org/10.1007/BF02291575

Kasak, K., Ahmadi, A., Dronova, I., Arias-Ortiz, A., Wang, T., Valach, A. C., Szutu, D., Verfaillie, J., & Baldocchi, D. D. (2026). Interannual Variability in Greenhouse Gas Emissions Challenges Post-Restoration Net Sink Predictions in California Delta Wetlands. *Global Change Biology*, *32*(1), e70700. https://doi.org/10.1111/gcb.70700

Kennedy, H., Beggins, J., Duarte, C. M., Fourqurean, J. W., Holmer, M., Marbà, N., & Middelburg, J. J. (2010). Seagrass sediments as a global carbon sink: Isotopic constraints. *Global Biogeochemical Cycles*, *24*(4). https://doi.org/10.1029/2010GB003848

Kennedy, P., Kennedy, H., & Papadimitriou, S. (2005). The effect of acidification on the determination of organic carbon, total nitrogen and their stable isotopic composition in algae and marine sediment. *Rapid Communications in Mass Spectrometry*, *19*(8), 1063–1068. https://doi.org/10.1002/rcm.1889

Kirwan, M. L., & Megonigal, J. P. (2013). Tidal wetland stability in the face of human impacts and sea-level rise. *Nature*, *504*(7478), 53–60. https://doi.org/10.1038/nature12856

Knox, S. H., Sturtevant, C., Matthes, J. H., Koteen, L., Verfaillie, J., & Baldocchi, D. (2015). Agricultural peatland restoration: Effects of land-use change on greenhouse gas (CO2 and CH4) fluxes in the Sacramento-San Joaquin Delta. *Global Change Biology*, *21*(2), 750–765. https://doi.org/10.1111/gcb.12745

Kohn, M. J. (2010). Carbon isotope compositions of terrestrial C3 plants as indicators of (paleo)ecology and (paleo)climate. *Proceedings of the National Academy of Sciences*, *107*(46), 19691–19695. https://doi.org/10.1073/pnas.1004933107

Komada, T., Bravo, A., Brinkmann, M.-T., Lu, K., Wong, L., & Shields, G. (2022). "Slow" and "fast" in blue carbon: Differential turnover of allochthonous and autochthonous organic matter in minerogenic salt marsh sediments. *Limnology and Oceanography*, *67*(S2), S133–S147. https://doi.org/10.1002/lno.12090

Komatsu, T., Meinesz, A., & Buckles, D. (1997). Temperature and light responses of alga Caulerpa taxifolia introduced into the Mediterranean Sea. *Marine Ecology Progress Series*, *146*, 145–153. https://doi.org/10.3354/meps146145

Krahforst, C., Sherman, L. A., & Kehm, K. (2022). Trace metal enrichment in a tidally influenced, rural tributary of the upper Chesapeake Bay. *Marine Pollution Bulletin*, *175*, 113377. https://doi.org/10.1016/j.marpolbul.2022.113377

Krämer, L. (2023). Rights of Nature in Europe: The Spanish Lagoon Mar Menor Becomes a Legal Person. *Journal for European Environmental & Planning Law*, *20*(1), 5–23. https://doi.org/10.1163/18760104-20010003

Krause, J., Cameron, C., Arias-Ortiz, A., Cifuentes, M., Crooks, S., Dahl, M., Friess, D., Kennedy, H., Lim, K., Lovelock, C., Marba, N., McGlathery, K., Oreska, M., Pidgeon, E., Serrano, O., Vanderklift, M., Wong, L.-W., Yaakub, S., & Fourqurean, J. (2025). Global seagrass carbon stock variability and emissions from seagrass loss. *Nature Communications*, *16*. https://doi.org/10.1038/s41467-025-59204-4

Krause-Jensen, D., Lavery, P., Serrano, O., Marbà, N., Masque, P., & Duarte, C. M. (2018). Sequestration of macroalgal carbon: The elephant in the Blue

Carbon room. *Biology Letters*, *14*(6), 20180236. https://doi.org/10.1098/rsbl.2018.0236

Kreyling, J., Tanneberger, F., Jansen, F., van der Linden, S., Aggenbach, C., Blüml, V., Couwenberg, J., Emsens, W.-J., Joosten, H., Klimkowska, A., Kotowski, W., Kozub, L., Lennartz, B., Liczner, Y., Liu, H., Michaelis, D., Oehmke, C., Parakenings, K., Pleyl, E., … Jurasinski, G. (2021). Rewetting does not return drained fen peatlands to their old selves. *Nature Communications*, *12*(1), 5693. https://doi.org/10.1038/s41467-021-25619-y

Krishnaswamy, S., Lal, D., Martin, J. M., & Meybeck, M. (1971). Geochronology of lake sediments. *Earth and Planetary Science Letters*, *11*(1), 407–414. https://doi.org/10.1016/0012-821X(71)90202-0

Kroon, P. S., Hensen, A., Jonker, H. J. J., Ouwersloot, H. G., Vermeulen, A. T., & Bosveld, F. C. (2010). Uncertainties in eddy covariance flux measurements assessed from CH4 and N2O observations. *Agricultural and Forest Meteorology, Special Issue on Eddy Covariance (EC)Flux Measurements of Ch4 and N2O*, *150*(6), 806–816. https://doi.org/10.1016/j.agrformet.2009.08.008

Kyselý, J., Beguería, S., Beranová, R., Gaál, L., & López-Moreno, J. I. (2012). Different patterns of climate change scenarios for short-term and multi-day precipitation extremes in the Mediterranean. *Global and Planetary Change*, *98–99*, 63–72. https://doi.org/10.1016/j.gloplacha.2012.06.010

Lamas Rodríguez, M., Garcia Lorenzo, M. L., Medina Magro, M., & Perez Quiros, G. (2023). Impact of climate risk materialization and ecological deterioration on house prices in Mar Menor, Spain. *Scientific Reports*, *13*(1), 11772. https://doi.org/10.1038/s41598-023-39022-8

Lamb, A. L., Wilson, G. P., & Leng, M. J. (2006). A review of coastal palaeoclimate and relative sea-level reconstructions using δ13C and C/N ratios in organic material. *Earth-Science Reviews*, *75*(1–4), 29–57. https://doi.org/10.1016/j.earscirev.2005.10.003

Langley, A., Chapman, S., Wang, L., Maxwell, T., Rivera, P., Adame, F., Arias-Ortiz, A., Asanopoulos, C., Blanco-Libreros, J., Breithaupt, J., Canty, S., Chambers, L., Cornwell, J., Craft, C., Cross, S., Feller, I., Friess, D., Guntenspergen, G., Holmquist, J., … Weston, N. (2025). *Blue nitrogen follows the fate of tidal wetlands*. Research Square. https://doi.org/10.21203/rs.3.rs-5522814/v1

Langston, W. J. (1990). Toxic Effects of Metals and the Incidence of Metal Pollution in Marine Ecosystems. In *Heavy Metals in the Marine Environment*. CRC Press.

Lanzante, J. R. (1996). Resistant, Robust and Non-Parametric Techniques for the Analysis of Climate Data: Theory and Examples, Including Applications to Historical Radiosonde Station Data. *International Journal of Climatology*, *16*(11), 1197–1226. https://doi.org/10.1002/(SICI)1097-0088(199611)16:11%3C1197::AID-JOC89%3E3.0.CO;2-L

Larsen, M. M., Blusztajn, J. S., Andersen, O., & Dahllöf, I. (2012). Lead isotopes in marine surface sediments reveal historical use of leaded fuel. *Journal of Environmental Monitoring*, *14*(11), 2893–2901. https://doi.org/10.1039/C2EM30579H

Larson, R. A., Brooks, G. R., Schwing, P. T., Holmes, C. W., Carter, S. R., & Hollander, D. J. (2018). High-resolution investigation of event driven sedimentation: Northeastern Gulf of Mexico. *Anthropocene*, *24*, 40–50. https://doi.org/10.1016/j.ancene.2018.11.002

Lavergne, C., Rodriguez-Puig, J., Ruiz-González, C., Montero-Curiel, M., Casas, G., Romano-Gude, D., Alorda-Montiel, I., Dordal-Soriano, J., Alorda-Kleinglass, A., Diego-Feliu, M., Gilabert, J., Campillo-de La Maza, A., Romera-Castillo, C., Torres-Rodriguez, N., Heimbürger-Boavida, L.-E., García-Orellana, J., Rodellas, V., & G. Bravo, A. (2025). Unveiling Hidden Mercury and Methylmercury Sources: The Role of Submarine Groundwater Discharge in Coastal Lagoons. *Environmental Science & Technology*. https://doi.org/10.1021/acs.est.5c07191

León, V. M., & Bellido, J. M. (2016). *Mar Menor: Una laguna singular y sensible. Evlauación científica de su estado.* M. de E. y C. Instituto Español de Ocenografía. https://upcommons.upc.edu/server/api/core/bitstreams/5c932fb8-82fb-4a24-af79-0fc172868b1c/content

Leuning, R. (2007). The correct form of the Webb, Pearman and Leuning equation for eddy fluxes of trace gases in steady and non-steady state, horizontally homogeneous flows. *Boundary-Layer Meteorology*, *123*(2), 263–267. https://doi.org/10.1007/s10546-006-9138-5

Li, C., Wang, H., Liao, X., Xiao, R., Liu, K., Bai, J., Li, B., & He, Q. (2022). Heavy metal pollution in coastal wetlands: A systematic review of studies globally

over the past three decades. *Journal of Hazardous Materials*, *424*, 127312. https://doi.org/10.1016/j.jhazmat.2021.127312

Li, X., Bellerby, R., Craft, C., & Widney, S. E. (2018). Coastal wetland loss, consequences, and challenges for restoration. *Anthropocene Coasts*, *1*(1), 1–15. https://doi.org/10.1139/anc-2017-0001

Liang, Y., Ma, R., Prommer, H., Fu, Q.-L., Jiang, X., Gan, Y., & Wang, Y. (2024). Unravelling Coupled Hydrological and Geochemical Controls on Long-Term Nitrogen Enrichment in a Large River Basin. *Environmental Science & Technology*, *58*(48), 21315–21326. https://doi.org/10.1021/acs.est.4c05015

Lima, N. G. B. de, & Galvani, E. (2013). Mangrove Microclimate: A Case Study from Southeastern Brazil. *Earth Interactions*, *17*(2), 1–16. https://doi.org/10.1175/2012EI000464.1

Lin, W.-J., Wu, J., & Lin, H.-J. (2020). Contribution of unvegetated tidal flats to coastal carbon flux. *Global Change Biology*, *26*(6), 3443–3454. https://doi.org/10.1111/gcb.15107

Liu, X., Lan, C., Zhu, L., Yan, C., Wang, N., Chen, H., Zheng, G., Che, Y., Yang, Z., & Bao, R. (2024). Sediment resuspension as a driving force for organic carbon transference and rebalance in marginal seas. *Water Research*, *257*, 121672. https://doi.org/10.1016/j.watres.2024.121672

Lloret, J., Marin, A., Marin-Guirao, L., & Velasco, J. (2005). Changes in macrophytes distribution in a hypersaline coastal lagoon associated with the development of intensively irrigated agriculture. *Ocean & Coastal Management*, *48*(9–10), 828–842. https://doi.org/10.1016/j.ocecoaman.2005.07.002

Long, E. R., MacDonald, D. D., Smith, S. L., & Calder, F. D. (1995). Incidence of adverse biological effects within ranges of chemical concentrations in marine and estuarine sediments. *Environmental Management, 19*(1), 81–97. https://doi.org/10.1007/BF02472006

López-Castejón, F., Pereira, F., & Gilabert, J. (2026). Hydrodynamics of Mar Menor through field observations and numerical modeling: A wind-forced coastal lagoon. *Journal of Sea Research*, *211*, 102689. https://doi.org/10.1016/j.seares.2026.102689

Lovelock, C. E., Adame, M. F., Bradley, J., Dittmann, S., Hagger, V., Hickey, S. M., Hutley, L. B., Jones, A., Kelleway, J. J., Lavery, P. S., Macreadie, P. I., Maher, D. T., McGinley, S., McGlashan, A., Perry, S., Mosley, L., Rogers,

K., & Sippo, J. Z. (2023). An Australian blue carbon method to estimate climate change mitigation benefits of coastal wetland restoration. *Restoration Ecology*, *31*(7), e13739. https://doi.org/10.1111/rec.13739

Lovelock, C. E., Atwood, T., Baldock, J., Duarte, C. M., Hickey, S., Lavery, P. S., Masque, P., Macreadie, P. I., Ricart, A. M., Serrano, O., & Steven, A. (2017). Assessing the risk of carbon dioxide emissions from blue carbon ecosystems. *Frontiers in Ecology and the Environment*, *15*(5), 257–265. https://doi.org/10.1002/fee.1491

Lozano, F. (1954). *Una campaña de prospección pesquera en Mar Menor (Murcia). Boletín del Instituto Español de Oceanografía, 66*, 1–34.

Macdonald, D. D., Carr, R. S., Calder, F. D., Long, E. R., & Ingersoll, C. G. (1996). Development and evaluation of sediment quality guidelines for Florida coastal waters. *Ecotoxicology*, *5*(4), 253–278. https://doi.org/10.1007/BF00118995

Machado Toffolo, M., Grilli, F., Prandi, C., Goffredo, S., & Marini, M. (2022). Extreme Flooding Events in Coastal Lagoons: Seawater Parameters and Rainfall over A Six-Year Period in the Mar Menor (SE Spain). *Journal of Marine Science and Engineering*, *10*(10), Article 10. https://doi.org/10.3390/jmse10101521

Macreadie, P. I., Biddulph, G. E., Masque, P., Kennedy, H., Samper-Villarreal, J., Patrick Megonigal, J., Morrissette, H. K., Romero-Gonzalez, T. E., Hatje, V., Friedrich, J., Sasmito, S. D., Watanabe, K., Mazarrasa, I., Krause-Jensen, D., Adams, J. B., Cifuentes-Jara, M., Arias-Ortiz, A., Rovai, A. S., Stankovic, M., … Austin, W. E. N. (2026). Priority questions for the next decade of blue carbon science. *Nature Ecology & Evolution*, *10*(4), 751–764. https://doi.org/10.1038/s41559-026-03020-6

Magozzi, S., Yool, A., Vander Zanden, H. B., Wunder, M. B., & Trueman, C. N. (2017). Using ocean models to predict spatial and temporal variation in marine carbon isotopes. *Ecosphere*, *8*(5), e01763. https://doi.org/10.1002/ecs2.1763

Malone, T. C., & Newton, A. (2020). The Globalization of Cultural Eutrophication in the Coastal Ocean: Causes and Consequences. *Frontiers in Marine Science*, *7*. https://doi.org/10.3389/fmars.2020.00670

Maltby, J., Steinle, L., Löscher, C. R., Bange, H. W., Fischer, M. A., Schmidt, M., & Treude, T. (2018). Microbial methanogenesis in the sulfate-reducing zone

of sediments in the Eckernförde Bay, SW Baltic Sea. *Biogeosciences*, *15*(1), 137–157. https://doi.org/10.5194/bg-15-137-2018

Mancuso, M., Santucci, L., & Carol, E. (2020). Effects of intensive aquifers exploitation on groundwater salinity in coastal wetlands. *Hydrological Processes*, *34*(11), 2313–2323. https://doi.org/10.1002/hyp.13727

Manteca Martínez, J. I. (1992). *Los yacimientos Zn, Pb, Ag-Fe del distrito minero de la La Unión-Cartagena, Bética Oriental.* CSIC. https://repositorio.upct.es/handle/10317/443

Marbà, N., Arias-Ortiz, A., Masqué, P., Kendrick, G. A., Mazarrasa, I., Bastyan, G. R., Garcia-Orellana, J., & Duarte, C. M. (2015). Impact of seagrass loss and subsequent revegetation on carbon sequestration and stocks. *Journal of Ecology*, *103*(2), 296–302. https://doi.org/10.1111/1365-2745.12370

María-Cervantes, A., Jiménez-Cárceles, F. J., & Álvarez-Rogel, J. (2009). As, Cd, Cu, Mn, Pb, and Zn Contents in Sediments and Mollusks (Hexaplex trunculus and Tapes decussatus) from Coastal Zones of a Mediterranean Lagoon (Mar Menor, SE Spain) Affected by Mining Wastes. *Water, Air, and Soil Pollution*, *200*(1–4), 289–304. https://doi.org/10.1007/s11270-008-9913-7

Marín-Guirao, L., Atucha, A. M., Barba, J. L., López, E. M., & Fernández, A. J. G. (2005). Effects of mining wastes on a seagrass ecosystem: Metal accumulation and bioavailability, seagrass dynamics and associated community structure. *Marine Environmental Research*, *60*(3), 317–337. https://doi.org/10.1016/j.marenvres.2004.11.002

Marín-Guirao, L., Cesar, A., Marín, A., & Vita, R. (2005). Assessment of sediment metal contamination in the Mar Menor coastal lagoon (SE Spain): Metal distribution, toxicity, bioaccumulation and benthic community structure. *Ciencias Marinas*, *31*(2), 413–428. https://doi.org/10.7773/cm.v31i2.53

Marín-Guirao, L., Lloret, J., & Marin, A. (2008). Carbon and nitrogen stable isotopes and metal concentration in food webs from a mining-impacted coastal lagoon. *Science of The Total Environment*, *393*(1), 118–130. https://doi.org/10.1016/j.scitotenv.2007.12.023

Marín-Guirao, L., Lloret, J., Marín, A., García, G., & García Fernández, A. J. (2007). Pulse-discharges of mining wastes into a coastal lagoon: Water chemistry and toxicity. *Chemistry and Ecology*, *23*(3), 217–231. https://doi.org/10.1080/02757540701339422

Maron, M., Brownlie, S., Bull, J. W., Evans, M. C., Von Hase, A., Quétier, F., Watson, J. E. M., & Gordon, A. (2018). The many meanings of no net loss in environmental policy. *Nature Sustainability*, *1*(1), 19–27. https://doi.org/10.1038/s41893-017-0007-7

Martinetto, P., Alberti, J., Becherucci, M. E., Cebrian, J., Iribarne, O., Marbà, N., Montemayor, D., Sparks, E., & Ward, R. (2023). The blue carbon of southern southwest Atlantic salt marshes and their biotic and abiotic drivers. *Nature Communications*, *14*(1), 8500. https://doi.org/10.1038/s41467-023-44196-w

Martinez, A. E. J., Galoski, C. E., Lopes Figueira, R. C., De Lima Ferreira, P. A., & Froehner, S. (2023). 136 Years of variation of sediment-associated metals in a subtropical reservoir in southern Brazil: Implications for the environmental change. *CATENA*, *231*, 107315. https://doi.org/10.1016/j.catena.2023.107315

Martínez-Espinosa, C., Sauvage, S., Al Bitar, A., Green, P. A., Vörösmarty, C. J., & Sánchez-Pérez, J. M. (2021). Denitrification in wetlands: A review towards a quantification at global scale. *Science of The Total Environment*, *754*, 142398. https://doi.org/10.1016/j.scitotenv.2020.142398

Martínez-López, S., Martínez-Sánchez, M. J., Gómez-Martínez, M. del C., & Pérez-Sirvent, C. (2020). Assessment of the risk associated with mining-derived arsenic inputs in a lagoon system. *Environmental Geochemistry and Health*, *42*(8), Article 8. https://doi.org/10.1007/s10653-019-00385-5

Martínez-Soto, M. C., Tovar-Sánchez, A., Sánchez-Quiles, D., Rodellas, V., Garcia-Orellana, J., & Basterretxea, G. (2016). Seasonal variation and sources of dissolved trace metals in Maó Harbour, Minorca Island. *Science of The Total Environment*, *565*, 191–199. https://doi.org/10.1016/j.scitotenv.2016.03.244

Martini, I. P., Guy Morrison, R. I., F. Abraham, K., Sergienko, L. A., & Jefferies, R. L. (2019). Northern Polar Coastal Wetlands: Development, Structure, and Land Use. In *Coastal Wetlands* (pp. 153–186). Elsevier. https://doi.org/10.1016/B978-0-444-63893-9.00004-6

Martins, M., de los Santos, C. B., Masqué, P., Carrasco, A. R., Veiga-Pires, C., & Santos, R. (2022). Carbon and Nitrogen Stocks and Burial Rates in Intertidal Vegetated Habitats of a Mesotidal Coastal Lagoon. *Ecosystems*, *25*(2), 372–386. https://doi.org/10.1007/s10021-021-00660-6

Martinsen, K. T., Kragh, T., & Sand-Jensen, K. (2019). Carbon dioxide fluxes of air-exposed sediments and desiccating ponds. *Biogeochemistry*, *144*(2), 165–180. https://doi.org/10.1007/s10533-019-00579-0

Mascaró, O., Oliva, S., Pérez, M., & Romero, J. (2009). Spatial variability in ecological attributes of the seagrass Cymodocea nodosa. *Botanica Marina*, *52*, 429–438. https://doi.org/10.1515/BOT.2009.055

Mateo, M. A., Romero, J., Pérez, M., Littler, M. M., & Littler, D. S. (1997). Dynamics of Millenary Organic Deposits Resulting from the Growth of the Mediterranean SeagrassPosidonia oceanica. *Estuarine, Coastal and Shelf Science*, *44*(1), 103–110. https://doi.org/10.1006/ecss.1996.0116

Maxwell, T. L., Spalding, M. D., Friess, D. A., Murray, N. J., Rogers, K., Rovai, A. S., Smart, L. S., Weilguny, L., Adame, M. F., Adams, J. B., Austin, W. E. N., Copertino, M. S., Cott, G. M., Duarte de Paula Costa, M., Holmquist, J. R., Ladd, C. J. T., Lovelock, C. E., Ludwig, M., Moritsch, M. M., … Worthington, T. A. (2024). Soil carbon in the world's tidal marshes. *Nature Communications*, *15*(1), 10265. https://doi.org/10.1038/s41467-024-54572-9

Mays, P. A., & Edwards, G. S. (2001). Comparison of heavy metal accumulation in a natural wetland and constructed wetlands receiving acid mine drainage. *Ecological Engineering*, *16*(4), 487–500. https://doi.org/10.1016/S0925-8574(00)00112-9

McKee, K. L., Cahoon, D. R., & Feller, I. C. (2007). Caribbean mangroves adjust to rising sea level through biotic controls on change in soil elevation. *Global Ecology and Biogeography*, *16*(5), 545–556. https://doi.org/10.1111/j.1466-8238.2007.00317.x

McKenzie, L. J., Nordlund, L. M., Jones, B. L., Cullen-Unsworth, L. C., Roelfsema, C., & Unsworth, R. K. F. (2020). The global distribution of seagrass meadows. *Environmental Research Letters*, *15*(7), 074041. https://doi.org/10.1088/1748-9326/ab7d06

McKergow, L. A., Rutherford, J. C., & Timpany, G. C. (2012). *Livestock-Generated Nitrogen Exports from a Pastoral Wetland*. https://doi.org/10.2134/jeq2010.0435

Mcleod, E., Chmura, G. L., Bouillon, S., Salm, R., Björk, M., Duarte, C. M., Lovelock, C. E., Schlesinger, W. H., & Silliman, B. R. (2011). A blueprint

for blue carbon: Toward an improved understanding of the role of vegetated coastal habitats in sequestering CO2. *Frontiers in Ecology and the Environment*, *9*(10), 552–560. https://doi.org/10.1890/110004

Mengel, M., Levermann, A., Frieler, K., Robinson, A., Marzeion, B., & Winkelmann, R. (2016). Future sea level rise constrained by observations and long-term commitment. *Proceedings of the National Academy of Sciences*, *113*(10), 2597–2602. https://doi.org/10.1073/pnas.1500515113

Michener, W. K., Blood, E. R., Bildstein, K. L., Brinson, M. M., & Gardner, L. R. (1997). Climate Change, Hurricanes and Tropical Storms, and Rising Sea Level in Coastal Wetlands. *Ecological Applications*, *7*(3), 770–801. https://doi.org/10.1890/1051-0761(1997)007%5B0770:CCHATS%5D2.0.CO;2

Mielck, F., Michaelis, R., Hass, H. C., Hertel, S., Ganal, C., & Armonies, W. (2020). *Persistent effects of sand extraction on habitats and associated benthic communities in the German Bight*. Biodiversity and Ecosystem Function: Marine. https://doi.org/10.5194/bg-2020-17

Millennium Ecosystem Assessment (Program) (Ed.). (2005). *Ecosystems and human well-being: Wetlands and water synthesis: a report of the Millennium Ecosystem Assessment*. World Resources Institute.

Ministerio de Transición Ecológica y Reto Demográfico. (2021). *Informe de situación de las actuaciones para la recuperación del Mar Menor*. https://www.miteco.gob.es/content/dam/miteco/es/prensa/210716informeactualizacionmarmenor_limpio_tcm30-529327.pdf

Ministerio de Transición Ecológica y Reto Demográfico. (2023). *Ejecución presupuestaria del Marco de Actuaciones Prioritarias para Recuperar el Mar Menor*. https://www.lamoncloa.gob.es/serviciosdeprensa/notasprensa/ecologica/Documents/2019/291119-Mar%20Menor%20Actuaciones%20en%20marcha%20MITECO.pdf

Miranda, L. S., Ayoko, G. A., Egodawatta, P., & Goonetilleke, A. (2022). Adsorption-desorption behavior of heavy metals in aquatic environments: Influence of sediment, water and metal ionic properties. *Journal of Hazardous Materials*, *421*, 126743. https://doi.org/10.1016/j.jhazmat.2021.126743

Mishra, S., Di, H. J., Cameron, K. C., Monaghan, R., & Carran, A. (2005). Gross nitrogen mineralisation rates in pastural soils and their relationships with

organic nitrogen fractions, microbial biomass and protease activity under glasshouse conditions. *Biology and Fertility of Soils*, *42*(1), 45–53. https://doi.org/10.1007/s00374-005-0863-6

Mitsch, W. J., Bernal, B., & Hernandez, M. E. (2015). Ecosystem services of wetlands. *International Journal of Biodiversity Science, Ecosystem Services & Management*, *11*(1), 1–4. https://doi.org/10.1080/21513732.2015.1006250

Modis, K., Adam, K., Panagopoulos, K., & Kontopoulos, A. (1998). *Development and validation of a geostatistical model for prediction of acid mine drainage in underground sulphide mines*. https://dspace.lib.ntua.gr/xmlui/handle/123456789/25262

Möller, I., Kudella, M., Rupprecht, F., Spencer, T., Paul, M., van Wesenbeeck, B. K., Wolters, G., Jensen, K., Bouma, T. J., Miranda-Lange, M., & Schimmels, S. (2014). Wave attenuation over coastal salt marshes under storm surge conditions. *Nature Geoscience*, *7*(10), 727–731. https://doi.org/10.1038/ngeo2251

Moravek, A., Singh, S., Pattey, E., Pelletier, L., & Murphy, J. G. (2019). Measurements and quality control of ammonia eddy covariance fluxes: A new strategy for high-frequency attenuation correction. *Atmospheric Measurement Techniques*, *12*(11), 6059–6078. https://doi.org/10.5194/amt-12-6059-2019

Moreda, U., Mazarrasa, I., Cebrian, E., Kaal, J., Ricart, A. M., Serrano, E., & Serrano, O. (2024). Role of macroalgal forests within Mediterranean shallow bays in blue carbon storage. *Science of The Total Environment*, *934*, 173219. https://doi.org/10.1016/j.scitotenv.2024.173219

Moreno-González, R., Rodriguez-Mozaz, S., Gros, M., Barceló, D., & León, V. M. (2015). Seasonal distribution of pharmaceuticals in marine water and sediment from a mediterranean coastal lagoon (SE Spain). *Environmental Research*, *138*, 326–344. https://doi.org/10.1016/j.envres.2015.02.016

Moreno-Mateos, D., Power, M. E., Comín, F. A., & Yockteng, R. (2012). Structural and Functional Loss in Restored Wetland Ecosystems. *PLOS Biology*, *10*(1), e1001247. https://doi.org/10.1371/journal.pbio.1001247

Morote-Sánchez, B., Colomer, J., Soler, M., Gilabert, J., Rodellas, V., Garcia-Orellana, J., & Serra, T. (2025). Aquatic deoxygenation associated with resuspension of anthropogenic organic matter. *Water Research*, *278*, 123327. https://doi.org/10.1016/j.watres.2025.123327

Mount, J., & Twiss, R. (2005). Subsidence, Sea Level Rise, and Seismicity in the Sacramento–San Joaquin Delta. *San Francisco Estuary and Watershed Science*, *3*(1). https://doi.org/10.15447/sfews.2005v3iss1art7

Moyle, P., Manfree, A., & Fiedler, P. (2014). *Suisun Marsh: Ecological history and possible futures*. 1–239.

Mudd, S. M., D'Alpaos, A., & Morris, J. T. (2010). How does vegetation affect sedimentation on tidal marshes? Investigating particle capture and hydrodynamic controls on biologically mediated sedimentation. *Journal of Geophysical Research: Earth Surface*, *115*(F3). https://doi.org/10.1029/2009JF001566

Murphy, S. (2021, October 18). *Healing California's Delta—River Partners*. https://riverpartners.org/news/healing-californias-delta/

Murray, N. J., Phinn, S. R., DeWitt, M., Ferrari, R., Johnston, R., Lyons, M. B., Clinton, N., Thau, D., & Fuller, R. A. (2019). The global distribution and trajectory of tidal flats. *Nature*, *565*(7738), 222–225. https://doi.org/10.1038/s41586-018-0805-8

Myhre, G., Alterskjær, K., Stjern, C. W., Hodnebrog, Ø., Marelle, L., Samset, B. H., Sillmann, J., Schaller, N., Fischer, E., Schulz, M., & Stohl, A. (2019). Frequency of extreme precipitation increases extensively with event rareness under global warming. *Scientific Reports*, *9*(1), 16063. https://doi.org/10.1038/s41598-019-52277-4

Nakamura, F., Sudo, T., Kameyama, S., & Jitsu, M. (1997). Influences of channelization on discharge of suspended sediment and wetland vegetation in Kushiro Marsh, northern Japan. *Geomorphology*, *18*(3), 279–289. https://doi.org/10.1016/S0169-555X(96)00031-1

Neubauer, S. C., & Megonigal, J. P. (2015). Moving Beyond Global Warming Potentials to Quantify the Climatic Role of Ecosystems. *Ecosystems*, *18*(6), 1000–1013. https://doi.org/10.1007/s10021-015-9879-4

Newton, A., Icely, J., Cristina, S., Perillo, G. M. E., Turner, R. E., Ashan, D., Cragg, S., Luo, Y., Tu, C., Li, Y., Zhang, H., Ramesh, R., Forbes, D. L., Solidoro, C., Béjaoui, B., Gao, S., Pastres, R., Kelsey, H., Taillie, D., … Kuenzer, C. (2020). Anthropogenic, Direct Pressures on Coastal Wetlands. *Frontiers in Ecology and Evolution*, *8*. https://www.frontiersin.org/articles/10.3389/fevo.2020.00144

Ning, Z., Chen, C., Xie, T., Zhu, Z., Wang, Q., Cui, B., & Bai, J. (2021). Can the native faunal communities be restored from removal of invasive plants in coastal ecosystems? A global meta-analysis. *Global Change Biology*, *27*(19), 4644–4656. https://doi.org/10.1111/gcb.15765

Nixon, S. W. (1995). Coastal marine eutrophication: A definition, social causes, and future concerns. *Ophelia*, *41*(1), 199–219. https://doi.org/10.1080/00785236.1995.10422044

Oen, I. S., Fernandez, J. C., & Manteca, J. I. (1975). The lead-zinc and associated ores of La Union, Sierra de Cartagena, Spain. *Economic Geology*, *70*(7), 1259–1278. https://doi.org/10.2113/gsecongeo.70.7.1259

Ontiveros-Cuadras, J. F., Ruiz-Fernández, A. C., Cardoso-Mohedano, J. G., Pérez-Bernal, L. H., Santiago-Pérez, S., Velázquez-Reyes, D. A., Cisneros-Ramos, Z. J., Crisanto-Ruiz, A. S., Gómez-Ponce, M. A., Flores-Trujillo, J. G., & Sanchez-Cabeza, J.-A. (2024). Potentially toxic elements fluxes in 210Pb-dated sediment cores from a large coastal lagoon (southern Gulf of Mexico) under environmental stress. *Marine Pollution Bulletin*, *201*, 116226. https://doi.org/10.1016/j.marpolbul.2024.116226

Ontiveros-Cuadras, J. F., Ruiz-Fernández, A. C., Pérez-Bernal, L. H., Raygoza-Viera, J. R., & Sanchez-Cabeza, J.-A. (2021). Historical reconstruction of trace element concentrations and fluxes in a tropical coastal lagoon (Mexican Pacific) derived from 210Pb radiochronology. *Continental Shelf Research*, *213*, 104315. https://doi.org/10.1016/j.csr.2020.104315

Osland, M. J., Chivoiu, B., Grace, J. B., Enwright, N. M., Guntenspergen, G. R., Buffington, K. J., Thorne, K. M., Carr, J. A., Sweet, W. V., & Couvillion, B. R. (2024). Rising seas could cross thresholds for initiating coastal wetland drowning within decades across much of the United States. *Communications Earth & Environment*, *5*(1), 372. https://doi.org/10.1038/s43247-024-01537-x

Ouyang, X., Duarte, C. M., Cheung, S.-G., Tam, N. F.-Y., Cannicci, S., Martin, C., Lo, H. S., & Lee, S. Y. (2022). Fate and Effects of Macro- and Microplastics in Coastal Wetlands. *Environmental Science & Technology*, *56*(4), 2386–2397. https://doi.org/10.1021/acs.est.1c06732

Pacheco, R. L. R. (2010). *Integral analysis of pollution by Pb, Cd, Zn, Cu, Fe and Mn in hypersaline coastal lagoon (Mar Menor) in the Mediterranean Sea*. https://doi.org/10.13140/RG.2.1.2392.5204

Palanques, A., López, L., Guillén, J., & Puig, P. (2020). Trace metal variability controlled by hydrodynamic processes in a polluted inner shelf environment (Besòs prodelta, NW Mediterranean). *Science of The Total Environment*, *735*, 139482. https://doi.org/10.1016/j.scitotenv.2020.139482

Palanques, A., Lopez, L., Guillén, J., Puig, P., & Masqué, P. (2017). Decline of trace metal pollution in the bottom sediments of the Barcelona City continental shelf (NW Mediterranean). *Science of The Total Environment*, *579*, 755–767. https://doi.org/10.1016/j.scitotenv.2016.11.031

Parnell, A. C., Phillips, D. L., Bearhop, S., Semmens, B. X., Ward, E. J., Moore, J. W., Jackson, A. L., Grey, J., Kelly, D. J., & Inger, R. (2013). Bayesian stable isotope mixing models. *Environmetrics*, *24*(6), 387–399. https://doi.org/10.1002/env.2221

Paul, K. M., van Helmond, N. A. G. M., Slomp, C. P., & Jilbert, T. (2024). Trace metals in coastal marine sediments: Natural and anthropogenic sources, correlation matrices, and proxy potentials. *Science of The Total Environment*, *951*, 175789. https://doi.org/10.1016/j.scitotenv.2024.175789

Pebesma, E. J. (2004). Multivariable geostatistics in S: The gstat package. *Computers & Geosciences*, *30*(7), 683–691. https://doi.org/10.1016/j.cageo.2004.03.012

Pendleton, L., Donato, D. C., Murray, B. C., Crooks, S., Jenkins, W. A., Sifleet, S., Craft, C., Fourqurean, J. W., Kauffman, J. B., Marbà, N., Megonigal, P., Pidgeon, E., Herr, D., Gordon, D., & Baldera, A. (2012). Estimating Global "Blue Carbon" Emissions from Conversion and Degradation of Vegetated Coastal Ecosystems. *PLOS ONE*, *7*(9), e43542. https://doi.org/10.1371/journal.pone.0043542

Pereira, F., López-Castejón, F., Francés, F., Alcolea, A., Jiménez-Martínez, J., Dias, J. M., & Gilabert, J. (2026). Linking ROMS with watershed models for simulating hydrodynamics and thermohaline dynamics in a coastal lagoon affected by extreme weather events. *Ocean Modelling*, *200*, 102673. https://doi.org/10.1016/j.ocemod.2025.102673

Pérez-Ruzafa, A., Campillo, S., Fernández-Palacios, J. M., García-Lacunza, A., García-Oliva, M., Ibañez, H., Navarro-Martínez, P. C., Pérez-Marcos, M., Pérez-Ruzafa, I. M., Quispe-Becerra, J. I., Sala-Mirete, A., Sánchez, O., & Marcos, C. (2019). Long-Term Dynamic in Nutrients, Chlorophyll a, and

Water Quality Parameters in a Coastal Lagoon During a Process of Eutrophication for Decades, a Sudden Break and a Relatively Rapid Recovery. *Frontiers in Marine Science*, *6*, 26. https://doi.org/10.3389/fmars.2019.00026

Pérez-Ruzafa, A., Dezileau, L., Martínez-Sánchez, M. J., Pérez-Sirvent, C., Pérez-Marcos, M., von Grafenstein, U., & Marcos, C. (2023). Long-term sediment records reveal over three thousand years of heavy metal inputs in the Mar Menor coastal lagoon (SE Spain). *Science of The Total Environment*, 166417. https://doi.org/10.1016/j.scitotenv.2023.166417

Pérez-Ruzafa, A., Fernández, A. I., Marcos, C., Gilabert, J., Quispe, J. I., & García-Charton, J. A. (2005). Spatial and temporal variations of hydrological conditions, nutrients and chlorophyll a in a Mediterranean coastal lagoon (Mar Menor, Spain). *Hydrobiologia*, *550*(1), 11–27. https://doi.org/10.1007/s10750-005-4356-2

Pérez-Ruzafa, A., Gilabert, J., Gutiérrez, J. M., Fernández, A. I., Marcos, C., & Sabah, S. (2002). Evidence of a planktonic food web response to changes in nutrient input dynamics in the Mar Menor coastal lagoon, Spain. *Hydrobiologia*, *475–476*, 359–369. https://doi.org/10.1023/A:1020343510060

Pérez-Ruzafa, A., Marcos, C., Bernal, C. M., Quintino, V., Freitas, R., Rodrigues, A. M., García-Sánchez, M., & Pérez-Ruzafa, I. M. (2012). Cymodocea nodosa vs. Caulerpa prolifera: Causes and consequences of a long term history of interaction in macrophyte meadows in the Mar Menor coastal lagoon (Spain, southwestern Mediterranean). *Estuarine, Coastal and Shelf Science*, *110*, 101–115. https://doi.org/10.1016/j.ecss.2012.04.004

Pérez-Ruzafa, A., Marcos, C., Pérez-Ruzafa, I. M., & Ros, J. (1987). EVOLUCIÓN DE LAS CARACTERÍSTICAS AMBIENTALES y DE LOS POBLAMIENTOS DEL MAR MENOR (MURCIA, SE DE ESPAÑA). *Anales de Biología*, (12), Article 12.

Perez-Ruzafa, A., Marcos-Diego, C., & Ros, J. D. (1991). Environmental and biological changes related to recent human activities in the Mar Menor (SE of Spain). *Marine Pollution Bulletin*, *23*, 747–751. https://doi.org/10.1016/0025-326X(91)90774-M

Petrişor, A.-I., Hamma, W., Nguyen, H. D., Randazzo, G., Muzirafuti, A., Stan, M.-I., Tran, V. T., Aştefănoaiei, R., Bui, Q.-T., Vintilă, D.-F., Truong, Q. H.,

Lixăndroiu, C., Ţenea, D.-D., Sîrodoev, I., & Ianoş, I. (2020). Degradation of Coastlines under the Pressure of Urbanization and Tourism: Evidence on the Change of Land Systems from Europe, Asia and Africa. *Land*, *9*(8), 275. https://doi.org/10.3390/land9080275

Phillips, D. L., & Koch, P. L. (2002). Incorporating concentration dependence in stable isotope mixing models. *Oecologia*, *130*(1), 114–125. https://doi.org/10.1007/s004420100786

Pinto, M. I., Burrows, H. D., Sontag, G., Vale, C., & Noronha, J. P. (2016). Priority pesticides in sediments of European coastal lagoons: A review. *Marine Pollution Bulletin*, *112*(1–2), 6–16. https://doi.org/10.1016/j.marpolbul.2016.06.101

Poffenbarger, H., Needelman, B., & Megonigal, P. (2011). Salinity Influence on Methane Emissions from Tidal Marshes. *Wetlands*, *31*, 831–842. https://doi.org/10.1007/s13157-011-0197-0

Pollution history revealed by sedimentary records: A review | Environmental Chemistry Letters | Springer Nature Link. (n.d.). Retrieved March 27, 2026, from https://link.springer.com/article/10.1007/s10311-013-0409-3

Purvaja, R., Ramesh, R., Ray, A. K., & Rixen, T. (2008). Nitrogen cycling: A review of the processes, transformations and fluxes in coastal ecosystems. *Current Science*, *94*(11), 1419–1438.

Ratmaya, W., Laverman, A. M., Rabouille, C., Akbarzadeh, Z., Andrieux-Loyer, F., Barillé, L., Barillé, A.-L., Le Merrer, Y., & Souchu, P. (2022). Temporal and spatial variations in benthic nitrogen cycling in a temperate macro-tidal coastal ecosystem: Observation and modeling. *Continental Shelf Research*, *235*, 104649. https://doi.org/10.1016/j.csr.2022.104649

Ravizza, G. E., & Bothner, M. H. (1996). Osmium isotopes and silver as tracers of anthropogenic metals in sediments from Massachusetts and Cape Cod bays. *Geochimica et Cosmochimica Acta*, *60*(15), 2753–2763. https://doi.org/10.1016/0016-7037(96)00108-1

Readman, J. (2006). The world's waters: A chemical contaminant perspective. *In: An Introduction to Pollution Science. Ed.: R.M. Harrison. Royal Society of Chemistry publications. 77-121.* (pp. 77–121).

Readman, J. W. (2006). Development, Occurrence and Regulationof Antifouling Paint Biocides: Historical Review and Future Trends. In I. K.

Konstantinou (Ed.), *Antifouling Paint Biocides* (pp. 1–15). Springer. https://doi.org/10.1007/698_5_047

Reddy, K. R., & DeLaune, R. D. (2008). *Biogeochemistry of Wetlands: Science and Applications*. CRC Press. https://doi.org/10.1201/9780203491454

Reimann, L., Vafeidis, A. T., & Honsel, L. E. (2023). Population development as a driver of coastal risk: Current trends and future pathways. *Cambridge Prisms: Coastal Futures*, *1*, e14. https://doi.org/10.1017/cft.2023.3

Reimers, C. E., Alleau, Y., Bauer, J. E., Delaney, J., Girguis, P. R., Schrader, P. S., & Stecher, H. A. (2013). Redox effects on the microbial degradation of refractory organic matter in marine sediments. *Geochimica et Cosmochimica Acta*, *121*, 582–598. https://doi.org/10.1016/j.gca.2013.08.004

Riedel, B., Zuschin, M., & Stachowitsch, M. (2012). Tolerance of benthic macrofauna to hypoxia and anoxia in shallow coastal seas: A realistic scenario. *Marine Ecology Progress Series*, *458*, 39–52. https://doi.org/10.3354/meps09724

Robertson, B. P., & Savage, C. (2021). Thresholds in catchment nitrogen load for shifts from seagrass to nuisance macroalgae in shallow intertidal estuaries. *Limnology and Oceanography*, *66*(4), 1353–1366. https://doi.org/10.1002/lno.11689

Robles-Arenas, V. M., Rodríguez, R., García, C., Manteca, J. I., & Candela, L. (2006). Sulphide-mining impacts in the physical environment: Sierra de Cartagena–La Unión (SE Spain) case study. *Environmental Geology*, *51*(1), 47–64. https://doi.org/10.1007/s00254-006-0303-4

Rodionov, S. N. (2004). A sequential algorithm for testing climate regime shifts. *Geophysical Research Letters*, *31*(9). https://doi.org/10.1029/2004GL019448

Rodriguez-Puig, J., Ruiz-González, C., Diego-Feliu, M., Alorda-Montiel, I., Alorda-Kleinglass, A., Romano-Gude, D., Bravo, A. G., Dordal-Soriano, J., Gilabert, J., Bergeler, S., Lavergne, C., Casas, G., Manzano, M., Garcia-Orellana, J., & Rodellas, V. (2026). Recirculated submarine groundwater discharge dominates nutrient inputs and enhances eutrophication risk in a coastal lagoon. *Limnology and Oceanography*, *71*(4), e70371. https://doi.org/10.1002/lno.70371

Rodriguez-Puig, J., Rodellas, V., Diego-Feliu, M., Alcolea, A., Jiménez-Martínez, J., Alorda-Montiel, I., Alorda-Kleinglass, A., Pereira, F., Manzano, M., Gilabert, J., & Garcia-Orellana, J. (2025). Seasonality of submarine

groundwater discharge pathways in a coastal lagoon revealed by radium isotopes: The importance of porewater exchange in summer. *Journal of Hydrology*, *661*, 133616. https://doi.org/10.1016/j.jhydrol.2025.133616

Room, A. H., Franco-Gaviria, F., & Urrego, D. H. (n.d.). *rshift STARS manual—Regime shift analysis for paleoecological data v2.2*.

Rothwell, R. G., & Croudace, I. w. (2015). Twenty Years of XRF Core Scanning Marine Sediments: What Do Geochemical Proxies Tell Us? In I. W. Croudace & R. G. Rothwell (Eds.), *Micro-XRF Studies of Sediment Cores: Applications of a non-destructive tool for the environmental sciences* (pp. 25–102). Springer Netherlands. https://doi.org/10.1007/978-94-017-9849-5_2

Rouff, A. A., Eaton, T. T., & Lanzirotti, A. (2013). Heavy metal distribution in an urban wetland impacted by combined sewer overflow. *Chemosphere*, *93*(9), 2159–2164. https://doi.org/10.1016/j.chemosphere.2013.07.077

Rowland, P. I., Wartman, M., Bursic, J., & Carnell, P. (2024). Restored and created tidal marshes recover ecosystem services over time. *Environmental and Sustainability Indicators*, *24*, 100539. https://doi.org/10.1016/j.indic.2024.100539

Ruiz-Fernández, A. C., Frignani, M., Hillaire-Marcel, C., Ghaleb, B., Arvizu, M. D., Raygoza-Viera, J. R., & Páez-Osuna, F. (2009). Trace Metals (Cd, Cu, Hg, and Pb) Accumulation Recorded in the Intertidal Mudflat Sediments of Three Coastal Lagoons in the Gulf of California, Mexico. *Estuaries and Coasts*, *32*(3), 551–564. https://doi.org/10.1007/s12237-009-9150-3

Rumolo, P., Barra, M., Gherardi, S., Marsella, E., & Sprovieri, M. (2011). *Stable isotopes and C/N ratios in marine sediments as a tool for discriminating anthropogenic impact*. 10.

Sakan, S. M., Dević, G. J., Relić, D. J., Anđelković, I. B., Sakan, N. M., & Đorđević, D. S. (2015). Environmental Assessment of Heavy Metal Pollution in Freshwater Sediment, Serbia. *CLEAN – Soil, Air, Water*, *43*(6), 838–845. https://doi.org/10.1002/clen.201400275

Salas, F., Teixeira, H., Marcos, C., Marques, J. C., & Pérez-Ruzafa, A. (2008). Applicability of the trophic index TRIX in two transitional ecosystems: The Mar Menor lagoon (Spain) and the Mondego estuary (Portugal). *ICES Journal of Marine Science*, *65*(8), 1442–1448. https://doi.org/10.1093/icesjms/fsn123

Salomons, W. (1987). *Sediments as a source for contaminants?*

Sanchez-Cabeza, J. A., Masqué, P., & Ani-Ragolta, I. (1998). 210Pb and210Po analysis in sediments and soils by microwave acid digestion. *Journal of Radioanalytical and Nuclear Chemistry*, *227*(1), 19–22. https://doi.org/10.1007/BF02386425

Sandonnini, J., Del Pilar-Ruso, Y., Valverde-Urrea, M., & Giménez-Casalduero, F. (2024). Infauna evolution of the invertebrate community after a severe eutrophic crisis in the coastal lagoon of the Mar Menor (W Mediterranean). *Regional Studies in Marine Science*, *79*, 103824. https://doi.org/10.1016/j.rsma.2024.103824

Santos-Echeandía, J., Bernárdez, P., & Sánchez-Marín, P. (2023). Trace metal level variation under strong wind conditions and sediment resuspension in the waters of a coastal lagoon highly impacted by mining activities. *Science of The Total Environment*, *905*, 167806. https://doi.org/10.1016/j.scitotenv.2023.167806

Saunois, M., Stavert, A. R., Poulter, B., Bousquet, P., Canadell, J. G., Jackson, R. B., Raymond, P. A., Dlugokencky, E. J., Houweling, S., Patra, P. K., Ciais, P., Arora, V. K., Bastviken, D., Bergamaschi, P., Blake, D. R., Brailsford, G., Bruhwiler, L., Carlson, K. M., Carrol, M., … Zhuang, Q. (2020). The Global Methane Budget 2000–2017. *Earth System Science Data*, *12*(3), 1561–1623. https://doi.org/10.5194/essd-12-1561-2020

Savage, C. (2005). Tracing the Influence of Sewage Nitrogen in a Coastal Ecosystem Using Stable Nitrogen Isotopes. *AMBIO: A Journal of the Human Environment*, *34*(2), 145–150. https://doi.org/10.1579/0044-7447-34.2.145

Scheffer, M., Carpenter, S., Foley, J. A., Folke, C., & Walker, B. (2001). Catastrophic shifts in ecosystems. *Nature*, *413*(6856), 591–596. https://doi.org/10.1038/35098000

Schulten, H.-R., & Schnitzer, M. (1997). The chemistry of soil organic nitrogen: A review. *Biology and Fertility of Soils*, *26*(1), 1–15. https://doi.org/10.1007/s003740050335

Seitzinger, S. P., & Kroeze, C. (1998). Global distribution of nitrous oxide production and N inputs in freshwater and coastal marine ecosystems. *Global Biogeochemical Cycles*, *12*(1), 93–113. https://doi.org/10.1029/97GB03657

Serrano, O., Arias-Ortiz, A., Duarte, C. M., Kendrick, G. A., & Lavery, P. S. (2021). Impact of Marine Heatwaves on Seagrass Ecosystems. In J. G. Canadell & R. B. Jackson (Eds.), *Ecosystem Collapse and Climate Change* (pp. 345–364). Springer International Publishing. https://doi.org/10.1007/978-3-030-71330-0_13

Serrano, O., Davis, G., Lavery, P. S., Duarte, C. M., Martinez-Cortizas, A., Mateo, M. A., Masqué, P., Arias-Ortiz, A., Rozaimi, M., & Kendrick, G. A. (2016). Reconstruction of centennial-scale fluxes of chemical elements in the Australian coastal environment using seagrass archives. *Science of The Total Environment*, *541*, 883–894. https://doi.org/10.1016/j.scitotenv.2015.09.017

Serrano, R., Gras, L., Giménez-Casalduero, F., del-Pilar-Ruso, Y., Grindlay, G., & Mora, J. (2019). The role of Cymodocea nodosa on the dynamics of trace elements in different marine environmental compartments at the Mar Menor Lagoon (Spain). *Marine Pollution Bulletin*, *141*, 52–60. https://doi.org/10.1016/j.marpolbul.2019.02.019

Sharifuzzaman, S. M., Rahman, H., Ashekuzzaman, S. M., Islam, M. M., Chowdhury, S. R., & Hossain, M. S. (2016). Heavy Metals Accumulation in Coastal Sediments. In H. Hasegawa, I. Md. M. Rahman, & M. A. Rahman (Eds.), *Environmental Remediation Technologies for Metal-Contaminated Soils* (pp. 21–42). Springer Japan. https://doi.org/10.1007/978-4-431-55759-3_2

Sheoran, A. S., & Sheoran, V. (2006). Heavy metal removal mechanism of acid mine drainage in wetlands: A critical review. *Minerals Engineering*, *19*(2), 105–116. https://doi.org/10.1016/j.mineng.2005.08.006

Shlemon, R., J., & Begg, E., L. (1975). *Late Quaternary evolution of the Sacramento-San Joaquin Delta, California.* https://www.google.com/search?q=Late+Quaternary+evolution+of+the+Sacramento-San+Joaquin+Delta%2C+California.&rlz=1C5CHFA_enES999ES999&oq=Late+Quaternary+evolution+of+the+Sacramento-San+Joaquin+Delta%2C+California.&gs_lcrp=EgZjaHJvbWUyBggAEEUYOdIBBzEyNmowajSoAgCwAgE&sourceid=chrome&ie=UTF-8

Silva-Sánchez, N., & Armada, X.-L. (2023). Environmental Impact of Roman Mining and Metallurgy and Its Correlation with the Archaeological

Evidence: A European Perspective. *Environmental Archaeology*, *0*(0), 1–25. https://doi.org/10.1080/14614103.2023.2181295

Simonneau, J. (1973). *Mar Menor: Évolution sédimentologique et géochimique récente en remplissage* (Doctoral dissertation).

Smith, J. N. (2001). Why should we believe 210Pb sediment geochronologies? *Journal of Environmental Radioactivity*, *55*(2), 121–123. https://doi.org/10.1016/S0265-931X(00)00152-1

Sánchez i Bassols, M., Hidalgo Muñoz, M., Universitat de Girona, & Departament de Química. (2008). *Estudi de la mobilitat i biodisponibilitat de pol·luents en la zona minera del camp de Cartagena*. Universitat de Girona. http://www.tdx.cat/TDX-0312109-162749

Society for Ecological Restoration International. (2004). *The SER International Primer on Ecological Restoration*. https://www.academia.edu/102124411/The_SER_International_Primer_o_n_Ecological_Restoration

Soriano, Y., Doñate, E., Asins, S., Andreu, V., & Picó, Y. (2024). Fingerprinting of emerging contaminants in L'Albufera natural park (Valencia, Spain): Implications for wetland ecosystem health. *Chemosphere*, *364*, 143199. https://doi.org/10.1016/j.chemosphere.2024.143199

Souza, I. da C., Rocha, L. D., Morozesk, M., Bonomo, M. M., Arrivabene, H. P., Duarte, I. D., Furlan, L. M., Monferrán, M. V., Mazik, K., Elliott, M., Matsumoto, S. T., Milanez, C. R. D., Wunderlin, D. A., & Fernandes, M. N. (2015). Changes in bioaccumulation and translocation patterns between root and leafs of Avicennia schaueriana as adaptive response to different levels of metals in mangrove system. *Marine Pollution Bulletin*, *94*(1–2), 176–184. https://doi.org/10.1016/j.marpolbul.2015.02.032

Ståhl, N., & Weimann, L. (2022). Identifying wetland areas in historical maps using deep convolutional neural networks. *Ecological Informatics*, *68*, 101557. https://doi.org/10.1016/j.ecoinf.2022.101557

Sternberg, R. (2006). Damming the river: A changing perspective on altering nature. *Renewable and Sustainable Energy Reviews*, *10*(3), 165–197. https://doi.org/10.1016/j.rser.2004.07.004

Stock, B. C., Jackson, A. L., Ward, E. J., Parnell, A. C., Phillips, D. L., & Semmens, B. X. (2018). Analyzing mixing systems using a new generation of Bayesian tracer mixing models. *PeerJ*, *6*, e5096. https://doi.org/10.7717/peerj.5096

Sun, R., Sun, B., Li, X., Wei, S., Zhao, M., Chu, X., Song, W., Yuan, J., & Han, G. (2023). Seven-year experimental warming decreases labile but not recalcitrant soil organic carbon fractions in a coastal wetland. *Journal of Soils and Sediments*, *23*(8), 3071–3081. https://doi.org/10.1007/s11368-023-03536-5

Syvitski, J. P. M., Vörösmarty, C. J., Kettner, A. J., & Green, P. (2005). Impact of Humans on the Flux of Terrestrial Sediment to the Global Coastal Ocean. *Science*, *308*(5720), 376–380. https://doi.org/10.1126/science.1109454

Szefer, P., Glasby, G. P., Stüben, D., Kusak, A., Geldon, J., Berner, Z., Neumann, T., & Warzocha, J. (1999). Distribution of selected heavy metals and rare earth elements in surficial sediments from the polish sector of the Vistula Lagoon. *Chemosphere*, *39*(15), 2785–2798. https://doi.org/10.1016/S0045-6535(99)00208-8

Tan, L., Ge, Z., Ji, Y., Lai, D. Y. F., Temmerman, S., Li, S., Li, X., & Tang, J. (2022). Land use and land cover changes in coastal and inland wetlands cause soil carbon and nitrogen loss. *Global Ecology and Biogeography*, *31*(12), 2541–2563. https://doi.org/10.1111/geb.13597

Tang, C., Li, Y., He, C., & Acharya, K. (2020). Dynamic behavior of sediment resuspension and nutrients release in the shallow and wind-exposed Meiliang Bay of Lake Taihu. *Science of The Total Environment*, *708*, 135131. https://doi.org/10.1016/j.scitotenv.2019.135131

Tang, F., & Maggi, F. (2012). The effect of 15N to 14N ratio on nitrification, denitrification and dissimilatory nitrate reduction. *Rapid Communications in Mass Spectrometry : RCM*, *26*, 430–442. https://doi.org/10.1002/rcm.6119

Temmerman, S., Horstman, E. M., Krauss, K. W., Mullarney, J. C., Pelckmans, I., & Schoutens, K. (2023). Marshes and Mangroves as Nature-Based Coastal Storm Buffers. *Annual Review of Marine Science*, *15*(Volume 15, 2023), 95–118. https://doi.org/10.1146/annurev-marine-040422-092951

Terrados, J., & Ros, J. (1991). Production dynamics in a macrophyte-dominated ecosystem: The Mar Menor coastal lagoon (SE Spain). *Oecologia Aquatica*, *10*, 255–270.

Thienpont, J. R., Kokelj, S. V., Korosi, J. B., Cheng, E. S., Desjardins, C., Kimpe, L. E., Blais, J. M., Pisaric, M. F., & Smol, J. P. (2013). Exploratory Hydrocarbon Drilling Impacts to Arctic Lake Ecosystems. *PLOS ONE*, *8*(11), e78875. https://doi.org/10.1371/journal.pone.0078875

Thomsen, P. F., & Willerslev, E. (2015). Environmental DNA – An emerging tool in conservation for monitoring past and present biodiversity. *Biological Conservation, Special Issue: Environmental DNA: A Powerful New Tool for Biological Conservation*, *183*, 4–18. https://doi.org/10.1016/j.biocon.2014.11.019

Törnqvist, T. E., Cahoon, D. R., Morris, J. T., & Day, J. W. (2021). Coastal Wetland Resilience, Accelerated Sea-Level Rise, and the Importance of Timescale. *AGU Advances*, *2*(1), e2020AV000334. https://doi.org/10.1029/2020AV000334

Torres, I. C., Inglett, P. W., Brenner, M., Kenney, W. F., & Reddy, K. R. (2012). Stable isotope (d13C and d15N) values of sediment organic matter in subtropical lakes of different trophic status. *J Paleolimnol*, 14.

Tuya, F., Png-Gonzalez, L., Riera, R., Haroun, R., & Espino, F. (2014). Ecological structure and function differs between habitats dominated by seagrasses and green seaweeds. *Marine Environmental Research*, *98*, 1–13. https://doi.org/10.1016/j.marenvres.2014.03.015

Tweel, A. W., & Turner, R. E. (2014). Contribution of tropical cyclones to the sediment budget for coastal wetlands in Louisiana, USA. *Landscape Ecology*, *29*(6), 1083–1094. https://doi.org/10.1007/s10980-014-0047-6

Ukabi, S., Dubinsky, Z., Steinberger, Y., & Israel, A. (2013). Temperature and irradiance effects on growth and photosynthesis of *Caulerpa* (Chlorophyta) species from the eastern Mediterranean. *Aquatic Botany*, *104*, 106–110. https://doi.org/10.1016/j.aquabot.2012.08.007

UNESCO. (1971). *Ramsar Convention*.

Valach, A. C., Kasak, K., Hemes, K. S., Anthony, T. L., Dronova, I., Taddeo, S., Silver, W. L., Szutu, D., Verfaillie, J., & Baldocchi, D. D. (2021). Productive wetlands restored for carbon sequestration quickly become net CO2 sinks with site-level factors driving uptake variability. *PLOS ONE*, *16*(3), e0248398. https://doi.org/10.1371/journal.pone.0248398

Valette-Silver, N. J. (1993). The Use of Sediment Cores to Reconstruct Historical Trends in Contamination of Estuarine and Coastal Sediments. *Estuaries*, *16*(3), 577–588. https://doi.org/10.2307/1352796

Vallejo, B., Ponce, R., Ortega, T., Gómez-Parra, A., & Forja, J. (2021). "Greenhouse gas dynamics in a coastal lagoon during the recovery of the macrophyte meadow (Mar Menor, SE Spain)." *Science of The Total*

Environment, *779*, 146314. https://doi.org/10.1016/j.scitotenv.2021.146314

van Groenigen, K.-J., Six, J., Hungate, B. A., de Graaff, M.-A., van Breemen, N., & van Kessel, C. (2006). Element interactions limit soil carbon storage. *Proceedings of the National Academy of Sciences*, *103*(17), 6571–6574. https://doi.org/10.1073/pnas.0509038103

Velandia-Aquino, L. B., Botello, A. V., Ponce-Vélez, G., Armstrong-Altrin, J. S., Ruiz-Fernández, A. C., Prado, B., & Villanueva-Fragoso, S. (2023). 210Pb geochronology and metal concentrations in sediment cores recovered in the Alvarado Lagoon system, Veracruz, Mexico. *Chemosphere*, *330*, 138709. https://doi.org/10.1016/j.chemosphere.2023.138709

Velasco, A. M., Pérez-Ruzafa, A., Martínez-Paz, J. M., & Marcos, C. (2018). Ecosystem services and main environmental risks in a coastal lagoon (Mar Menor, Murcia, SE Spain): The public perception. *Journal for Nature Conservation*, *43*, 180–189. https://doi.org/10.1016/j.jnc.2017.11.002

Velasco, J., Lloret, J., Millan, A., Marin, A., Barahona, J., Abellan, P., & Sanchez-Fernandez, D. (2006). *NUTRIENT AND PARTICULATE INPUTS INTO THE MAR MENOR LAGOON (SE SPAIN) FROM AN INTENSIVE AGRICULTURAL WATERSHED*. 20.

Vilar Ramírez, J. B., & Egea Bruno, P. M. (1985). *La minería murciana contemporánea (1840-1930)*. https://dialnet.unirioja.es/servlet/libro?codigo=208346

Vilar Ramírez, J. B., Egea Bruno, P. M., & Fernández Gutiérrez, J. C. (1991). *La minería murciana contemporánea (1930-1985)*. https://dialnet.unirioja.es/servlet/libro?codigo=246531

Villèle, X. de, & Verlaque, M. (1995). *Changes and Degradation in a Posidonia oceanica Bed Invaded by the Introduced Tropical Alga Caulerpa taxifolia in the North Western Mediterranean*. *38*(1–6), 79–88. https://doi.org/10.1515/botm.1995.38.1-6.79

Vizza, C., West, W. E., Jones, S. E., Hart, J. A., & Lamberti, G. A. (2017). Regulators of coastal wetland methane production and responses to simulated global change. *Biogeosciences*, *14*(2), 431–446. https://doi.org/10.5194/bg-14-431-2017

Vizzini, S., Savona, B., Chi, T. D., & Mazzola, A. (2005). Spatial variability of stable carbon and nitrogen isotope ratios in a Mediterranean coastal lagoon. *Hydrobiologia*, *550*(1), 73–82. https://doi.org/10.1007/s10750-005-4364-2

Waldo, N. B., Hunt, B. K., Fadely, E. C., Moran, J. J., & Neumann, R. B. (2019). Plant root exudates increase methane emissions through direct and indirect pathways. *Biogeochemistry*, *145*(1), 213–234. https://doi.org/10.1007/s10533-019-00600-6

Walsh, J. P., & Nittrouer, C. (2004). Mangrove-bank sedimentation in a mesotidal environment with large sediment supply, Gulf of Papua. *Marine Geology - MAR GEOLOGY*, *208*, 225–248. https://doi.org/10.1016/j.margeo.2004.04.010

Wang, Q., Li, Y., & Zhang, M. (2015). Soil recovery across a chronosequence of restored wetlands in the Florida Everglades. *Scientific Reports*, *5*(1), 17630. https://doi.org/10.1038/srep17630

Wang, Z. A., Kroeger, K. D., Ganju, N. K., Gonneea, M. E., & Chu, S. N. (2016). Intertidal salt marshes as an important source of inorganic carbon to the coastal ocean. *Limnology and Oceanography*, *61*(5), 1916–1931. https://doi.org/10.1002/lno.10347

Ward, M., Kindinger, T. L., Hirsh, H. K., Hill, T. M., Jellison, B. M., Lummis, S., Rivest, E. B., Waldbusser, G. G., Gaylord, B., & Kroeker, K. J. (2022). Reviews and syntheses: Spatial and temporal patterns in seagrass metabolic fluxes. *Biogeosciences*, *19*(3), 689–699. https://doi.org/10.5194/bg-19-689-2022

Watanabe, K., & Kuwae, T. (2015). How organic carbon derived from multiple sources contributes to carbon sequestration processes in a shallow coastal system? *Global Change Biology*, *21*(7), 2612–2623.
https://doi.org/10.1111/gcb.12924

Waycott, M., Duarte, C. M., Carruthers, T. J. B., Orth, R. J., Dennison, W. C., Olyarnik, S., Calladine, A., Fourqurean, J. W., Heck, K. L., Hughes, A. R., Kendrick, G. A., Kenworthy, W. J., Short, F. T., & Williams, S. L. (2009). Accelerating loss of seagrasses across the globe threatens coastal ecosystems. *Proceedings of the National Academy of Sciences*, *106*(30), 12377–12381. https://doi.org/10.1073/pnas.0905620106

Wendt, J. W., & Hauser, S. (2013). An equivalent soil mass procedure for monitoring soil organic carbon in multiple soil layers. *European Journal of Soil Science*, *64*(1), 58–65. https://doi.org/10.1111/ejss.12002

West, E. J., & West, R. J. (2007). Growth and survival of the invasive alga, Caulerpa taxifolia, in different salinities and temperatures: Implications for

coastal lake management. *Hydrobiologia*, *577*(1), 87–94. https://doi.org/10.1007/s10750-006-0419-2

Whalen, S. C. (2005). Biogeochemistry of Methane Exchange between Natural Wetlands and the Atmosphere. *Environmental Engineering Science*, *22*(1), 73–94. https://doi.org/10.1089/ees.2005.22.73

Whiticar, M. J. (1999). Carbon and hydrogen isotope systematics of bacterial formation and oxidation of methane. *Chemical Geology*, *161*(1), 291–314. https://doi.org/10.1016/S0009-2541(99)00092-3

Williams, T. M. (1992). Diagenetic metal profiles in recent sediments of a scottish freshwater Loch. *Environmental Geology and Water Sciences*, *20*(2), 117–123. https://doi.org/10.1007/BF01737878

Worthington, T. A., Spalding, M., Landis, E., Maxwell, T. L., Navarro, A., Smart, L. S., & Murray, N. J. (2024). The distribution of global tidal marshes from Earth observation data. *Global Ecology and Biogeography*, *33*(8), e13852. https://doi.org/10.1111/geb.13852

Xie, M., Qian, L., Dong, H., Mei, W., Fu, X., Hu, Y., Yan, J., Sun, Y., Wu, P., Chen, X., & Wang, L. (2023). The high organic carbon accumulation in estuarine wetlands necessarily does not represent a high CO2 sequestration capacity. *Environment International*, *172*, 107762. https://doi.org/10.1016/j.envint.2023.107762

Xu, J., Zhuang, Q., Fu, Y., Huang, Y., Sun, Z., & Liu, Z. (2019). Spatial distribution, pollution levels, and source identification of heavy metals in wetlands of Suzhou Industrial Park, China. *Wetlands Ecology and Management*, *27*(5), 743–758. https://doi.org/10.1007/s11273-019-09691-2

Xue, D., Botte, J., De Baets, B., Accoe, F., Nestler, A., Taylor, P., Van Cleemput, O., Berglund, M., & Boeckx, P. (2009). Present limitations and future prospects of stable isotope methods for nitrate source identification in surface- and groundwater. *Water Research*, *43*(5), 1159–1170. https://doi.org/10.1016/j.watres.2008.12.048

Yamamuro, M. (2000). Chemical tracers of sediment organic matter origins in two coastal lagoons. *Journal of Marine Systems*, *26*(2), 127–134. https://doi.org/10.1016/S0924-7963(00)00049-X

Yamuza-Magdaleno, A., Jiménez-Ramos, R., Casal-Porras, I., Brun, F. G., & Egea, L. G. (2024). Long-term sediment organic carbon remineralization in different seagrass and macroalgae habitats: Implication for blue carbon

storage. *Frontiers in Marine Science*, *11*. https://doi.org/10.3389/fmars.2024.1370768

Yao, H., Montagna, P. A., Wetz, M. S., Staryk, C. J., & Hu, X. (2022). Subtropical estuarine carbon budget under various hydrologic extremes and implications on the lateral carbon exchange from tidal wetlands. *Water Research, 217*, 118436. https://doi.org/10.1016/j.watres.2022.118436

Yu, L., Huang, Y., Sun, F., & Sun, W. (2017). A synthesis of soil carbon and nitrogen recovery after wetland restoration and creation in the United States. *Scientific Reports*, *7*(1), 7966. https://doi.org/10.1038/s41598-017-08511-y

Yu, M., Rivera-Ocasio, E., Heartsill-Scalley, T., Davila-Casanova, D., Rios-López, N., & Gao, Q. (2019). Landscape-Level Consequences of Rising Sea-Level on Coastal Wetlands: Saltwater Intrusion Drives Displacement and Mortality in the Twenty-First Century. *Wetlands*, *39*(6), 1343–1355. https://doi.org/10.1007/s13157-019-01138-x

Zamora-López, A., Guerrero-Gómez, A., Torralva, M., Zamora-Marín, J. M., Guillén-Beltrán, A., López-Martínez de la Plaza, P., & Oliva-Paterna, F. J. (2022). Fish Assemblage Response to Eutrophic-Mediated Environmental Stress Events in the Mar Menor Coastal Lagoon (SE of Spain). *Biology and Life Sciences Forum*, *13*(1), 5. https://doi.org/10.3390/blsf2022013005

Zhang, H., Jiang, Y., Ding, M., & Xie, Z. (2017). Level, source identification, and risk analysis of heavy metal in surface sediments from river-lake ecosystems in the Poyang Lake, China. *Environmental Science and Pollution Research*, *24*(27), 21902–21916. https://doi.org/10.1007/s11356-017-9855-y

Zhang, J., Gan, S., Yang, P., Zhou, J., Huang, X., Chen, H., He, H., Saintilan, N., Sanders, C., & Wang, F. (2024). A global assessment of mangrove soil organic carbon sources and implications for blue carbon credit. *Nature Communications*, *15*. https://doi.org/10.1038/s41467-024-53413-z